

Universidade do Minho

Escola de Engenharia

Neryvaldo de Jesus Galvão Pereira

**The impact of human errors on the
performance to failure of concrete
bridges**

Doctoral Thesis

Doctoral Program in Civil Engineering

Work developed under the supervision of

Professor José Campos e Matos

Professor Luís Ferreira

Professor Rade Hajdin

DIREITOS DE AUTOR E CONDIÇÕES DE UTILIZAÇÃO DO TRABALHO POR TERCEIROS

Este é um trabalho académico que pode ser utilizado por terceiros desde que respeitadas as regras e boas práticas internacionalmente aceites, no que concerne aos direitos de autor e direitos conexos.

Assim, o presente trabalho pode ser utilizado nos termos previstos na licença abaixo indicada.

Caso o utilizador necessite de permissão para poder fazer um uso do trabalho em condições não previstas no licenciamento indicado, deverá contactar o autor, através do RepositóriUM da Universidade do Minho.

Licença concedida aos utilizadores deste trabalho



**Atribuição
CC BY**

<https://creativecommons.org/licenses/by/4.0/>

Acknowledgements

I have found myself in this place asking, whom should I acknowledge? And why should I acknowledge them? And these call for other questions, who am I at this point? And how have I come to be? Not really wishing to delight you with the true answers to the latter, I'll leave these open for you to ponder.

Frist and foremost, I would like to leave here my sincere appreciation to my supervisors for all the counselling, corrections, presented opportunities, enlightening discussions, and encouraging talks. Secondly, my co-author's support and fruitful collaborations. Furthermore, I would also like to thank: (i) those who have freely given their time when requested, namely, Arthur Slobbe, Blaise Girardin, Fernando Roseira, Herbert Friedl, Hugo Patricio, João Amado, José Barbosa, Luís Afonso, Renato Bastos, Paulo Fidalgo, Ricardo Leite and Tiago Rodrigues. (ii) Infrastructure Management Consultants for a wonderful period in Zurich (iii) the members of my research group: Carlos Santos, Edward Baron, Helder Sousa, João Fernandes, Mario Coelho and Monica Santamaria, and (iv) my remaining friends for all the laugh, and memorable days: Ailton Moreira, Anderson Bond, Angelo Nhaga, Bruno Carneiro, Davy Fonseca, Diana Neiva, Evelise Barbosa, Héder Sanches, HMSafterwork 😊, Juseny Moura, Mariana Bishop, Sérgio Fernandes, and Wilson de Carvalho. Finally, I would like to express gratitude to my family for their undying support, without which I would surely find myself living in the sorrowful dungeons of life.

This work was partially financed by (i) national funds through FCT - Foundation for Science and Technology, under grant agreement "PD/ BD/143003/2018" attributed to the PhD Candidate through the iRail Doctoral program; and (ii) FCT/MCTES through national funds (PIDDAC) under the R&D Unit Institute for Sustainability and Innovation in Structural Engineering (ISISE), under reference UIDB/04029/2020.

*Pah nhas tios Ermilinda e Aguinaldo que criam como ses fidjos
Pah mama e papa, pa tudo kês inxinam enquanto es staba pah perto
Pah dios k guiam e protejem*

"Si ka badu, ka ta birado – ditado krioulo"

*"Last but not least, I want to thank me.
I want to thank me for believing in me.
I want to thank me for doing all this hard work.
I want to thank me for having no days off.
I want to thank me for never quitting.
I want to thank me for always being a giver and try to give more than I receive.
I want to thank me for trying to do more right than wrong.
And I want to thank me for being me at all times".
by Snoop Dogg*

*Much more important than your work,
are the values and beliefs you stand for.
So, stay humble, share love and fight for the equality
of every man, woman and child
regardless of their religion, race or sexual orientation.
After all, mankind's greatest mistake, or should I say "human error"
has been its choice to hate instead of loving
by "Maybe you should google it 😊"*

Statement of integrity

I hereby declare having conducted this academic work with integrity. I confirm that I have not used plagiarism or any form of undue use of information or falsification of results along the process leading to its elaboration.

I further declare that I have fully acknowledged the Code of Ethical Conduct of the University of Minho.

Resumo

O colapso de pontes que tiveram lugar em todo o mundo nos últimos 50 anos destacou o erro humano como a principal causa do colapso de pontes. Dadas as implicações financeiras, sociais e psicológicas de tais eventos indesejados, a contribuição do erro humano no colapso de pontes deve ser investigada com o objetivo de compreender como é que a robustez e a segurança estrutural das pontes são afetadas pelos mesmos. A deterioração das pontes, leva à redução das margens de segurança, expondo muitas vezes deficiências causadas por erros de projeto e construção, realçando a importância do desenvolvimento de procedimentos de avaliação estrutural mais abrangentes, tendo em conta numerosas fontes de incertezas.

Apesar destes factos conhecidos existem poucos trabalhos disponíveis investigando questões tão relevantes. Neste sentido este trabalho aborda a identificação dos erros humanos em suas inúmeras formas, ou seja, erros de projeto e erros de construção, de acordo com opiniões de especialistas e eventos de colapso de pontes registados. Diferentes erros representam diferentes ameaças à segurança estrutural; como tal o risco relativo dos erros também é investigado. O real impacto dos erros humanos na segurança estrutural é investigado através de três pontes de betão armado, considerando a probabilidade de falha perante um conjunto de incertezas como principal indicador de desempenho. Tal investigação é realizada em duas etapas, uma onde os erros de projeto e construção são introduzidos em cenários onde se entende que eles estão presentes e outra onde a possibilidade de ocorrência de erros de construção é investigada considerando a probabilidade do erro humano e a magnitude do erro. Ocorrências únicas e múltiplas de erros também são discutidas.

Modelos de elementos finitos, considerada para fins de análise estrutural não linear, e modelos substitutos são introduzidos como a base das múltiplas análises de fiabilidade estrutural realizadas. Finalmente, a previsão da vida útil de pontes considerando a corrosão induzida por carbonatação e a redução da vida útil das pontes causada por erros de construção são questões também abordadas.

Palavras Chaves: Análise estrutural não linear, Deterioração de estruturas, Erros Humanos, Fiabilidade de estruturas, Modelos substitutos, Pontes de betão armado,

Abstract

The collapse of bridges that have taken place worldwide in the last 50 years has highlighted human error as the main cause of the collapse of bridges. Given the financial, social and phycological implications of such hazardous events, human errors' contribution to the collapse of bridges must be investigated, aiming to understand how their robustness and structural safety are affected. The ageing of bridges leads to safety margin reductions that often expose deficiencies caused by design and construction errors, underling the importance of developing more comprehensive frameworks that consider numerous sources of uncertainty for structural safety assessment purposes.

Despite these facts and known needs, few works facing such relevant concerns are available. Accordingly, human errors are identified in their numerous forms, i.e., design errors and construction errors, according to expert opinions and real-world bridge collapse events. Different errors represent different threats to structural safety; thus, their relative risk is also investigated. The actual impact of human errors on structural safety is investigated through one reinforced and two prestressed concrete bridges, using their probability of failure, given a group of uncertainties, as the main performance indicator. Such investigation is performed on two fronts, one where design and construction errors are introduced under scenarios where they are understood to be present, and another where the possibility of occurrence of construction errors is investigated considering probabilistic models to describe human error probabilities and error magnitudes. Single and multiple occurrences of errors are also discussed.

Finite element modelling, considered for non-linear structural analysis purposes, and surrogate models are introduced as the backbone of the multiple structural reliability analysis performed. Finally, the service life prediction of bridges considering carbonation-induced corrosion and the service life reduction of bridges due to construction errors are carefully addressed.

Keywords: Deterioration of structures, Human error, Non-linear structural analysis, Concrete bridges, Reliability of structures, Surrogate models.

Table of contents

Acknowledgements.....	iii
Resumo.....	v
Abstract.....	vi
Table of contents.....	vii
Acronyms.....	xi
List of figures.....	xiii
List of tables.....	xv
1. Introduction	1
1.1. Background and motivation	1
1.2. Aims and objectives	4
1.3. Scope	5
1.4. Outline and overview	8
1.5. Scientific contributions	9
2. Human error–induced risk in concrete bridge engineering.....	13
2.1. Introduction.....	14
2.2. Procurement errors	16
2.3. Design errors	17
2.3.1. Conceptual errors.....	17
2.3.2. Structural analysis and design errors.....	17
2.3.3. Detailing errors.....	18
2.4. Construction errors	19
2.4.1. Falsework execution errors.....	19
2.4.2. Material quality control errors.....	20
2.4.3. Logistics errors	20
2.5. Bridge collapses.....	21

2.6.	Design and construction errors investigation	22
2.6.1.	Delphi technique and survey	23
2.6.2.	Analytic hierarchy process	24
2.6.3.	Qualitative risk analysis.....	29
2.6.4.	Additional errors collected within the survey	31
2.6.5.	Investigation remarks.....	32
2.7.	Human error mitigation	34
2.7.1.	Quality management measures.....	34
2.7.2.	Risk mitigation.....	36
2.8.	Conclusions	38
3.	Human error impact on the structural safety of a prestressed concrete bridge	40
3.1.	Introduction.....	41
3.2.	Structural robustness	41
3.3.	Numerical modelling and non-linear analysis.....	43
3.3.1.	Case study description.....	43
3.3.2.	Numerical modelling.....	44
3.3.3.	Structural non-linear analysis	47
3.4.	Probabilistic based assessment.....	49
3.4.1.	Resistance uncertainties	49
3.4.2.	Sensitivity analysis.....	52
3.4.3.	Virgin reliability index	53
3.4.4.	Safety assessment.....	55
3.5.	Robustness analysis	56
3.5.1.	Modelling design and construction errors	56
3.5.2.	Impact on structural safety	59
3.6.	Conclusions	61

4.	Impact of construction errors on the structural safety of a post-tensioned concrete bridge.....	63
4.1.	Introduction.....	64
4.2.	Construction error models – a short review.....	65
4.2.1.	Human error probability.....	66
4.2.2.	Error magnitude	68
4.2.3.	HRA event tree	69
4.3.	Surrogate-based reliability analysis.....	70
4.4.	Case study.....	73
4.4.1.	Bridge description.....	73
4.4.2.	Numerical modelling.....	74
4.4.3.	Non-linear structural analysis	76
4.5.	Reliability assessment	77
4.5.1.	Resistance and loading uncertainties.....	77
4.5.2.	Safety evaluation	79
4.6.	Impact of construction errors.....	81
4.6.1.	Single error analysis – error magnitude PDFs only.....	82
4.6.2.	Detrimental and beneficial errors pairs – HEP and error magnitude PDFs.....	83
4.6.3.	HEP reduction	84
4.6.4.	Multiple occurrences of detrimental errors.....	86
4.7.	Conclusions	87
5.	Lifetime structural safety of a reinforced concrete bridge*	89
5.1.	Introduction.....	90
5.2.	Time invariant reliability assessment.....	91
5.2.1.	Theoretical background.....	91
5.2.2.	Deterioration models	92
5.2.3.	Construction error models	95

Table of contents

5.3.	Structural analysis	97
5.3.1.	Case study – description and digitalization	97
5.3.2.	Numerical modelling.....	99
5.3.3.	Load carrying capacity	101
5.4.	Structural safety	102
5.4.1.	Uncertainty characterization.....	102
5.4.2.	Initial structural safety.....	105
5.4.3.	Long-term structural safety	109
5.4.4.	Construction errors impact in structural safety.....	111
5.5.	Conclusions	112
6.	Conclusion.....	114
6.1.	Final remarks.....	114
6.2.	Future works	118
	References	120
	Appendix	132

Acronyms

AHP – Analytic Hierarchy Process

ALARP – As Low As Reasonably Possible

CI – Confidence Interval

CO – Consequences

COST – European Cooperation in Science and Technology

CoV – Coefficient of Variation

DE – Design Error

DIANA – Displacement Analysis

EM – Error Magnitude

EN – European Norm

IABSE – International Association for Bridge and Structural Engineering

ID – Identification Number

ISO – International Organization for Standardization

FEA – Finite Element Analysis

FEM – Finite Element Model

FIB – International Federation for Structural Concrete

FORM – First Order Reliability Method

HEP – Human Error Probability

HRA – Human Reliability Analysis

LM1 – Load Model 1

LM71 – Load Model 71

LQI – Life Quality Index

MATLAB – Matrix Laboratory

PDF – Probabilistic Distribution Function

PO – Probability of Occurrence

REBAP - Portuguese regulation for reinforced and prestressed concrete structures

RC – Reliability Class

RN – Random Number

RSA - Regulation for safety and load of structures

Acronyms

SIA – Swiss society of Engineers and Architects

SORM – Second Order Reliability Index

STR – Strength of Materials

TNO – The Netherlands organization

ULS – Ultimate Limit State

UQLab – Uncertainty Quantification Laboratory

List of figures

Figure 1.1 – Recorded failure numbers of bridges	3
Figure 2.1 – Main causes of failure of concrete bridges	14
Figure 2.2 – Human error clusters	15
Figure 2.3– Specific causes of failure of concrete bridges.....	16
Figure 2.4 – Design and construction error clusters	24
Figure 2.5 – Risk matrix of design errors.....	30
Figure 2.6 – Risk matrix of construction errors	30
Figure 2.7 – Risk reduction due to the mitigation actions.....	37
Figure 3.1 – Cavaco robustness index for a structural system of (a) lower, (b) medium and (c) higher robustness	42
Figure 3.2 – Case study longitudinal profile	44
Figure 3.3 – Transversal cross-section and reinforcement layout of (a) deck, (b) girders and (c) columns	44
Figure 3.4 – Geometry overview.....	45
Figure 3.5 – Materials constitutive models: (a) Concrete and (b) Steel Reinforcements	45
Figure 3.6 - Equivalent transversal cross-section loaded by load model 1	47
Figure 3.7 – Bending moment diagram for the maximum load factor.....	47
Figure 3.8 – Critical cross-section (a) strain – stress, (b) mid-span displacement – load factor, (c) curvature – bending moment curve and (d) cross-section over pier curvature – bending moment curve	48
Figure 3.9 – Random variables importance measure.....	53
Figure 3.10 – (a) Load-displacement (mm) curve of each generated sample and (b) Maximum load factor probabilistic distribution	54
Figure 3.11 – Structural safety reduction	60
Figure 4.1 – (a)PDFs of HEPs before inspection (orange) and after inspection (blue); (b) PDFs of error magnitudes	67
Figure 4.2 – HRA Event tree with some output results	70
Figure 4.3 – Case study; (a) picture (google maps view); (b) superstructure cross-section; (c) piers cross-section; and (d) prestressing cables layout and their minimum expected prestressing forces obtained from blueprints	74

Figure 4.4 – (a) Numerical model extruded geometry; (b) concrete constitutive model and (c) conventional and post-tensioning reinforcement constitutive model.....	75
Figure 4.5 – (a) Load-displacement curve (b) bending moment diagram distribution for maximum load factor	77
Figure 4.6 – (a) Load-displacement curve of multiple simulations and (b) histogram of the maximum carrying capacity	79
Figure 4.7– Probabilistic analysis convergence rate.....	81
Figure 4.8 – HEP effect on structural safety	85
Figure 5.1 – Ideal and faulty theoretical long-term performance of structures.....	90
Figure 5.2 – (a) Human error probability and (b) error magnitude PDFs.....	96
Figure 5.3 –Event tree for human reliability assessment.....	96
Figure 5.4 – (a) Longitudinal profile, (b) superstructure cross-section and (c) reinforcement detailing of the case study.....	98
Figure 5.5 – Digital mode of the Niederlenzerstrasse SBB overpass.....	98
Figure 5.6– Case study finite element model (DIANA FEA).....	99
Figure 5.7 – Load-displacement curve in section A.....	101
Figure 5.8 – Longitudinal bending moment diagram for the structure's maximum carrying capacity .	102
Figure 5.9 – Sensitivity analysis	103
Figure 5.10 – (a) Load-displacement curve (b) maximum carrying capacity generated based on 300 samples generated by the Latin hypercube sampling technique.....	104
Figure 5.11 – Active learning reliability analysis procedure (Adapted from Moustapha et al. [168])...	106
Figure 5.12 – Active learning convergence rate of (a) spatially correlated random variables and (b) spatially uncorrelated random variables in critical cross-sections	108
Figure 5.13 – Reliability index reduction as a function of the factored PDF of the live load (50-year reference period)	109
Figure 5.14 – (a) Lifetime structural safety (100-year reference period) (b) reinforcement cross-section loss given different current intensity scenarios.....	110
Figure 5.15 – Lifetime structural safety affected by construction errors.....	112

List of tables

Table 2.1 – List of design errors identified and analysed.....	27
Table 2.2 – List of construction errors identified and analysed	28
Table 2.3 – List of additional design errors collected within the survey	32
Table 2.4 – List of additional construction errors collected within the survey	32
Table 2.5 – Top five design and construction errors with the highest risk	33
Table 2.6 – Design supervision and construction works inspection levels according to Eurocode 0	36
Table 3.1 – Concrete main parameters.....	46
Table 3.2 – Reinforcement main parameters	46
Table 3.3 – Random variables considered for material and geometry probabilistic characterisation	50
Table 3.4 – Recommended minimum reliability indexes for ULSs	55
Table 3.5 – Errors leading to the damages considered for the robustness analysis.....	57
Table 3.6 – Damages magnitudes used for the robustness analysis.....	58
Table 3.7 – Robustness index results	60
Table 4.1 – Parameter for human performance models (construction).....	68
Table 4.2 – Concrete mechanical properties	76
Table 4.3 – Reinforcement mechanical properties.....	76
Table 4.4 – Probabilistic characterisation of materials, geometries and model uncertainty random variables.....	78
Table 4.5 – Probabilistic characterisation of permanent loads, live load and load model uncertainty random variable	79
Table 4.6 – Probabilistic analysis results.....	81
Table 4.7- Reliability index and failure probability due to the error magnitude PDFs.....	82
Table 4.8 – Probability of failure given HRA event tree.....	84
Table 4.9 – Dependency matrix	87
Table 4.10 – Structural failure probability due to multiple error occurrences.	87
Table 5.1 – Carbonation induced corrosion random variables.....	94
Table 5.2 – Construction error models parameters	95
Table 5.3 – Material mechanical properties.....	100
Table 5.4 – Abutment support stiffness.....	100
Table 5.5 – Structural resistance uncertainty characterization	103

List of tables

Table 5.6 – Probabilistic characterisation of permanent load, live load and load model uncertainty random variable	103
Table 5.7 – Maximum carrying capacity histogram overview	105
Table 5.8 – Structural reliability analysis obtained results	108

1. Introduction

Oscar Wilde once said: If you know exactly what you want to be in life, a teacher, a grocer, a judge or a soldier, you will become it. And that is your punishment. Actually, not knowing what you want to be in life, reinventing yourself every morning, not being a noun but being a verb, being moving in life and not being fixed in life is a privilege.

1.1. Background and motivation

The relevance of the transportation network for the exchange of goods and services, citizens' wellbeing, sustainable growth, competitiveness, and resilience of communities is well known. The transportation sector accounts for 5% and 7.7% of the gross domestic product of the European Union [1] and the United States [2], respectively. With respect to sustainability concerns, the transportation sector is responsible for 16.2% of global greenhouse gas emissions [3]. The European Commission is aiming to reduce CO₂ emissions by 60% by 2050 when compared to 1990 emission levels by (i) achieving a majority of intercity medium distances passengers travel by rail; (ii) tripling the size of the EU's high-speed rail network and (iii) attaining a 50% shift from freight journey with more than 300 km through roadways to other transport modes, since road freight and passengers transportation is responsible for 74.5% of the global CO₂ emissions of the transportation sector, while rail is responsible for only 1% of the emissions [4]. This comes as no surprise since the carbon footprint of travel per kilometre from railways is the lowest among all modes of transport, excluding cycling and walking [5]. Aiming to achieve a more reliable, sustainable and efficient transportation system, the European commission pledged a 23 billion euros investment for the transportation sector under the Connecting Europe Facility fund invested between 2014 and 2020. To put this number into perspective, the same fund pledged 4.67 billion euros to the energy sector. Such an initiative triggered an additional 50 billion euros in investment from the private and public sectors [6].

In most of the developed world, the ageing of the bridge stock is of some concern since many of them are approaching the estimated end of their service life, demanding their replacement, which usually

comes with considerable costs and environmental impact. Sustainability concerns make the proper management of the already built environment a vital goal of the United Nations Goal Agenda for 2030. Meaning that the lifespan of transportation assets should be confidently extended when proven to be the right course of action and reduced when proven otherwise, avoiding unnecessary expenses (environmental and financial) or unacceptable risks. Thereby, sophisticated computational models and numerical procedures must be used at their best. Simply put, current sustainability concerns due to climate change caused by greenhouse gas emissions, of which 3% and 7.2% come from the cement and the steel industry, respectively [3], demand the very best of our abilities when the design of new structures, and assessment of existing ones, are concerned.

The transportation network is very often disrupted by the unavailability of connections provided by bridges (i.e., roadway, railway, and footway), tunnels and retaining walls. Natural and human-made hazards usually trigger such unavailability, while human errors cripple structures, often making them unable to fulfil their intended use. Such structures play a crucial role in the transportation network, being responsible for tremendous consequences when wrongly managed. Several examples of bridge collapses can be found in the literature [7–9]. It is estimated that worldwide there is a stock of approximately 5.11 million bridges, 42 thousand tunnels and 26.39 million retaining walls. More specifically, it is estimated that there are 1.5, 0.83 and 0.62 million bridges in Europe, China and the US, respectively, according to Proske [10]. Of those 1.5 million bridges in Europe, one million are understood to be part of the roadways network, and the remaining half a million are part of the railway network, with 35% of the latter ageing over 100 years old [10,11]. According to the National Bridge Inventory of the US, 50% of their bridges are aged over 50 years, 14.7% are aged over 82 years, and 0.27% of them date back to 1900 [12].

An increasing trend with respect to the collapse of bridges has been reported by Syrkov [13,14], with more than 700 bridge collapses recorded between 1966 and 2020 (see Figure 1.1). From the period between 1996-2000 to 2016-2020, an increase of 640% is recorded, according to Syrkov [15]. Most of the data gathered are from Asia (32%), Europe (34%) and North America (27%). In 2004 Imhof [8] documented 347 bridge collapses between 1900 and 2004, with most of the data gathered being from Europe (37%), North America (34%) and Asia (12%). Regarding the collapse phase, 32% of the collapses occurred during the construction phase, and the remaining 68% were during the service phase. Similar numbers were reported by Syrkov [13,14], with 71% of the collapses taking place during the service phase and 21% taking place during the construction phase. Notwithstanding these numbers, one should note

that it is not unusual for the occurrence of collapses during the service phase to be caused by poor decision-making taken during the design and construction phase.

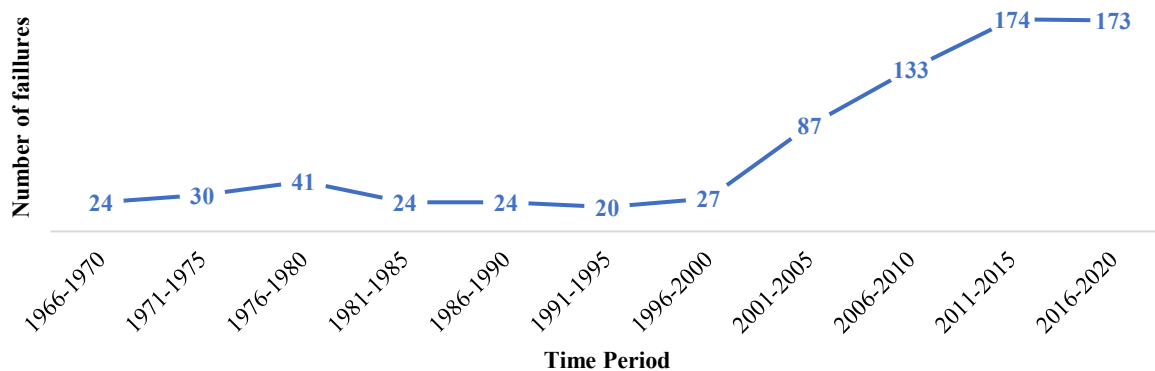


Figure 1.1 – Recorded failure numbers of bridges [15]

The collapse of bridges brings tremendous disruption to the network and great direct (fatalities, injuries, cost of rebuild) and indirect (i.e., disruption to the economy, environmental costs, political and social consequences) costs/consequences. The consequence of such collapses in human lives has been estimated to be 67 fatalities and 401 injuries yearly [10]. Additionally, 3070 fatalities and 4617 injuries have been reported by Syrkov [13,14], putting the yearly estimate around 56 fatalities and 86 injuries. Nonetheless, it is important to note that the 64-year period considered in this case is helping reduce the yearly estimate of the fatalities and injuries since most of the failures are recorded after the beginning of this century due to increasing data availability.

The increasing need for proper management of high capacity structures with precision and consistency, given challenges and increasing failure rates nowadays, has unfolded several projects within the international community (e.g., Horizon 2020 research projects such as SAFE-10-T and Safeway, as well as European Cooperation in Science and Technology (COST) Action TU – 1406 and 0601, among others) aiming the increase of structural safety for sustainable growth, addressing social and technical issues such as increasing traffic demands, advancing deterioration, operational and maintenance budget constraints, increasing occurrence of extreme events (natural and human-made) and also the less strict surveillance and quality assurance regarding the mass construction occurred in the sixties and seventies [16–18].

When the structural safety of civil engineering structures is concerned, some amount of failure is expected. In the genesis of structural design codes, due to sustainability, economic and productivity concerns, resources are expected to be properly allocated by breaking down engineering problems into the expected demand and the adequate capacity of the envisioned structure, as well as the uncertainties

allied to them. Thereafter, the engineering society decided that such matters should be tackled through a sphere of knowledge known as risk management, which aims to balance the probability of occurrence of hazardous events with their expected consequence and, in doing so, define what should be an acceptable and an unacceptable level of risk. Risk management might not be explicitly introduced in the design codes [19–22]. However, they are implicitly present, laying the foundation for a built environment that agrees with our limitations and expectations or, put another way, within the bounds of what is considered a reasonable level of risk. The ability to recover from hazardous events or restore functionalities is also a concern named “Resilience”. In many ways, these concerns depend very much on one’s ability to predict the future and one’s ability to put together the knowledge at hand, as well as the uncertainties associated with it, and recognize the unknowns. At present, there is no better way of doing so than uncertainty quantification, scenario analysis, predictive and numerical models, and structural reliability.

According to design standards [19,20,22], a structure shall be designed and executed in such a way, with an appropriate degree of reliability and robustness, that it will not be damaged to an extent disproportionate to triggering events such as explosion, impact and consequence of human errors. Aiming at the reduction of occurrence rate and consequence of bridge collapse, the reliability and robustness of these structures should be increased and properly assessed [23], as well as the identification of the sources of uncertainties and triggering events that may lead to their failure. The contribution of human error to the structural failure of engineering structures has been estimated in the past to be approximately 75% [24]. Meaning that in three out of every four failures recorded, human errors were considered to be the leading cause of failure. Recent estimations put it around 65% when the collapse of bridges is concerned [13,14]. Consequently, human errors are thoroughly addressed in this thesis.

1.2. Aims and objectives

This thesis aims to quantify the impact of human errors on the performance to failure or, put another way, on the structural reliability/structural safety of concrete bridges to better understand and adjust the risk linked to such sources of uncertainty. The accomplishment of such a central and general goal is attained by the fulfilment of the following objectives:

1. Establishment of a relevant, congruent, and broad-scope definition of human errors. The identification of design and construction errors in the day-to-day practice of bridge engineering, along with the development of a framework for the identification of the most relevant errors given a certain context through a risk-based qualitative assessment of errors.

2. Quantification of design and construction errors impact on the structural safety of bridges considering: (i) scenarios where it is understood that errors are present, and the severity of errors are measured as deviations from the expected outcome (i.e., the mean value of a certain parameter of interest); (ii) an initially and proportionally simplistic structural reliability analysis concept.
3. Quantification of the impact of construction errors on the structural safety of bridges considering human error probability models and error magnitude models that probabilistically characterize a specific group of errors. In doing so, the possibility of execution of a faulty structure is introduced in a more sophisticated structural reliability analysis procedure.
4. Service life estimation of an ideally executed structure and a faulty executed structure due to construction errors, considering corrosion as the leading deterioration mechanism.

The aims and objectives of this thesis led to the ascertainment and formulation of the following research questions:

1. Which are the main design and construction errors threatening the structural safety of concrete bridges?
2. What is the impact of recorded design and construction errors on the structural safety of concrete bridges?
3. What should be the expected impact of construction errors on the structural safety of concrete bridges, according to the likelihood of occurrence of an error and its severity?
4. How much is the long-term impact of construction errors on the structural safety of concrete bridges in terms of service life reduction?

1.3. Scope

The structural safety of bridges or any other structure depends on the constraint of the aleatoric and epistemic uncertainties associated with its capacity and the demands to which the structure will be subjected throughout its lifetime. Uncertainties can be clustered into the geometric, material, model, self-weight and live load uncertainties and human errors. The latter aims to encompass human fallibility in the execution of tasks, while the former comes from the limitations and simplifications of the mathematical models used to model real phenomena. For the design of new structures, such uncertainties are dealt with through characteristic values of concrete compressive strength and reinforcement-yielding strength, among others, partial safety factors given in semi-probabilistic design codes such as the Eurocode, and the inspection of construction works and supervision/review of design

calculations. Nonetheless, another way of dealing with numerous sources of uncertainty is structural reliability analysis. As a branch of engineering, structural reliability aims to quantify structures' probability of failure, taking into account numerous sources of uncertainties and scenarios probabilistically characterized, allowing the identification of potential weaknesses and vulnerabilities. It also encompasses the optimal allocation of resources so the structure can withstand loads and stresses over its lifetime, reducing the likelihood of failure or collapse and safeguarding the public from potential hazards.

Aiming the quantification of the impact of human errors on the performance to failure/structural safety of concrete bridges, engineering knowledge, statistical analysis and risk assessment techniques are employed. Under the scope of this work, a novel and more holistic approach aiming at quantifying the structural safety of concrete bridges is sought since human error is expected to be considered as an additional source of uncertainty in structural reliability analysis procedures. Consequently, the following intermediate steps are deemed to be necessary:

1. The identification of human errors in their numerous forms and those representing a higher risk to structural safety.
2. Estimation of the probability of failure of bridges considering conventional sources of uncertainties. Meaning that human error is initially neglected; This analysis is performed at two levels:
 - For the sake of simplicity, Normal (or Gaussian) probabilistic distribution functions are used for probabilistic characterization of the uncertainties used in the analysis allowing a more straightforward estimation of the probability of failure of the structure.
 - In the second stage, Lognormal, Gumbel and Gaussian probabilistic distribution functions are considered for probabilistic characterization of uncertainties, demanding a more complex but general procedure for the estimation of the probability of failure of structures.
3. Scenario analysis for the quantification of the impact of human errors on the structural safety (i.e., probability of failure) of bridges, with a gradual increase in the sophistication of the analysis according to the two preceding bullet points. As follows:
 - Modelling of design and construction errors as damages already present in the structure, i.e., neglecting the probability of occurrence of the damage caused by the error.
 - Modelling of construction errors as damages likely to be present in the structure, i.e., considering now the probability of occurrence of the error. Put another way, the

probability of the damage caused by the error being present is probabilistically considered in the analysis.

- Lastly, the structural safety decline (i.e., the increase in the probability of failure) over the structure's service life due to deterioration mechanisms (i.e., carbonation-induced corrosion and concrete compressive strength decline) together with construction errors are estimated, aiming the quantification of the impact of human errors on the service life of bridges.

Several examples of the contribution of human error to the collapse or partial collapse of structures can be found in the literature. Furthermore, among the different types of structural systems used for the structural design of bridges, i.e., suspension bridges, cable-stayed bridges, arch bridges, truss bridges, beam bridges, and floating bridges, numerous particularities of each type of bridge can raise distinct questions about possible errors and their relevance. The construction process and the base material used for the construction itself can also lead to distinct error types. As such, the scope of the work is narrowed to concrete beam bridges. Errors are present in the engineers' day-to-day activities and at the organizational level, often revealed by the inspection of construction works, review of design projects and when the end products of the design are tested after construction. Accordingly, a screening procedure for explicit identification of human errors in their numerous forms is required as a natural first step to take, aiming for the quantification of their impact on the structural safety of bridges. The Delphi Technique, Brainstorm meetings, Analytic hierarchy process and risk assessment techniques are utilized for such purposes.

Under the scope of this thesis, three concrete bridges are selected as case studies, namely a prestressed, post-tensioned and reinforced concrete bridge, since concrete beam bridges are the focus. These are 3-span beam bridges with total lengths ranging between 47.25 m and 63.80 m. Their maximum carrying capacity when longitudinal bending is concerned, assessed through 2D finite element models and non-linear structural analysis, is used as the leading parameters for structural reliability analysis – 2D beam elements are considered for finite element analysis aiming at reducing the computational costs of the analysis. Furthermore, parametric models built in DIANA FEA are used, given the flexibility it provides in modelling different types of errors and the built-in algorithms for structural analysis, thus, allowing the automation of the numerous analysis required for structural reliability purposes. Conventional methods such as Cornell's formulation (see Eq. (3.4)) and first- and second-order reliability methods make the consideration of event trees in the structural reliability analysis troublesome,

which are of major relevance for this work. For further reduction of computational costs and greater accuracy when structural reliability analysis is concerned, active learning techniques and surrogate models are combined, allowing further flexibility in the introduction of event trees used to probabilistically consider the probability of occurrence and the severity of an error in structural reliability calculations.

For reliability assessment and service life estimation purposes, threshold values such as target reliability indexes and target failure probabilities provided by structural design codes are considered. The overall loss of structural safety is measured by a robustness index and depicted by charts tracking the overall reduction of structural safety due to damages introduced by errors and deterioration mechanisms modelled as a function of time. Furthermore, numerous sensitivity analyses are performed to measure the sensitivity of the results based on a set of input parameters. The contribution of beneficial and detrimental errors are addressed, as well as the consequences of the occurrence of multiple errors.

1.4. Outline and overview

Given the described motivations, scope, and the pursuit of the aims and objectives detailed in the preceding subchapter, this thesis report is organized into the following six chapters:

1. **Introduction:** This chapter compiles the background and motivation of this thesis, its scope, as well as its aims and objectives: Furthermore, an outline and overview of the thesis reported are presented, and some additional scientific contributions are referred to.
2. **Human error–induced risk in concrete bridge engineering:** The second chapter of this thesis describes a group of identified design and construction errors and a survey developed for qualitative risk assessment of each of the errors previously identified. Additionally, some recent bridge collapses are presented, and human error mitigation measures are discussed.
DOI: [10.1061/\(ASCE\)CF.1943-5509.0001595](https://doi.org/10.1061/(ASCE)CF.1943-5509.0001595)
3. **Human error impact on the structural safety of a prestressed concrete bridge:** This chapter takes some of the errors identified in the preceding chapter to build a group of scenarios used for the reliability-based structural safety assessment of a prestressed concrete bridge using Cornell's formulation for reliability index estimation.
DOI: [10.1080/15732479.2021.1876105](https://doi.org/10.1080/15732479.2021.1876105)
4. **Impact of construction errors on the structural safety of a post-tensioned concrete bridge:** In chapter four, human error probability and human error magnitudes models of different errors are reviewed from the literature and considered for the structural safety assessment of a

post-tensioned concrete bridge. A more sophisticated procedure is considered, i.e., surrogate-assisted active learning strategies for structural reliability assessment.

DOI: [10.1016/J.ENGSTRUCT.2022.114650](https://doi.org/10.1016/J.ENGSTRUCT.2022.114650)

- 5. Lifetime structural safety of a reinforced concrete bridge:** The fifth chapter of this thesis addresses construction errors' long-term impact in the presence of carbonation-induced corrosion by forecasting the structural safety reduction of a reinforced concrete bridge over 120 years.

DOI: Under Review

- 6. Conclusion:** A summary of this thesis's main conclusions and original contributions are reviewed. Furthermore, some limitations and future development possibilities are enumerated.

A single literature review chapter is not provided since it is already comprised within each of the main chapters. Note that chapters 2, 3 and 4 have been published in peer-reviewed journals deserving of considerable reputation within the scientific community. Chapter 5 has also been compiled in a journal paper format for submission to a peer-reviewed journal. A more detailed summary of these chapters is given in the abstract at the beginning of each chapter. Note that the compiled papers in this report are presented as the best synergetic description of all the work developed during this PhD journey. Nonetheless, numerous additional publications with the participation of the PhD candidate can be found in the literature; some are presented in the appendix.

1.5. Scientific contributions

In addition to the contributions available in chapters 2, 3, 4 and 5, further relevant research work that also backs the maturity, continuous improvement, exchange of knowledge with peers, as well as the discovery of other subjects related to the main topic can be found in the following publications:

a) Journal Publications (in the Appendix)

- i. Matos JC, Moreira VN, Valente IB, Cruz PJS, Neves LC, **Galvão N**. Probabilistic-based assessment of existing steel-concrete composite bridges – Application to Sousa River Bridge. Eng Struct 2019;181:95–110. <https://doi.org/10.1016/j.engstruct.2018.12.006>.
- ii. Strauss A, Ivanković AM, Benko V, Matos J, Orcesi A, Wan-wendner R, et al (**Galvão N**). Round-Robin Modelling of the Load-bearing Capacity of Slender Columns by Using Classical and Advanced Non-linear Numerical and Analytical Prediction Tools. Struct Eng Int 2020;31:118–35. <https://doi.org/10.1080/10168664.2020.1740069> – ([Outstanding paper award](#)).

- iii. Strauss A, Hauser M, Täubling B, Ivanković AM, Skokandić D, Matos J, et al (**Galvão N**). Probabilistic and Semi-Probabilistic Analysis of Slender Columns Frequently Used in Structural Engineering. Appl Sci 2021;11:8009. <https://doi.org/10.3390/app11178009>.
- iv. Baron E, **Galvão N**, Docevska M, Matos J, Markovski G. Application of Quality Control Plan To Existing Bridges. Struct Infrastruct Eng 2021; in Press. <https://doi.org/10.1080/15732479.2021.1994618>.
- v. Eidsvig U, Santamaría M, **Galvão N**, Tanasic N, Piciullo L, Hajdin R, et al. Risk assessment of terrestrial transportation infrastructures exposed to extreme events. Infrastructures 2021;6:163. <https://doi.org/10.3390/infrastructures6110163>.

b) Chapters

- vi. Strauss A, **Galvão N**, Matos JC, Hauser M, Täubling B, Soliman M, et al. International Codes in the Prediction of Load-Bearing Capacity of Slender Columns. In: Matos JC, Lourenço PB, Oliveira D V., Branco J, Proske D, Silva RA, et al., editors. 18th Int. Probabilistic Work. (IPW 2020), vol. 153 LNCE, Springer; 2021, p. 457–68. https://doi.org/10.1007/978-3-030-73616-3_34.
- vii. Donolato T, **Pereira N**, Matos JC. Long-Term Evaluation of the Structural Reliability of an Existing Concrete Prestressed Bridge. In: Matos JC, Lourenço PB, Oliveira D V., Branco J, Proske D, Silva RA, et al., editors. 18th Int. Probabilistic Work. (IPW 2020), vol. 153 LNCE, Springer; 2021, p. 509–20. https://doi.org/10.1007/978-3-030-73616-3_38.

c) Conference Publications

- viii. Kušar M, **Galvão N**, Sein S. Regular bridge inspection data improvement using non-destructive testing. In: Caspeele R, Taerwe L, Frangopol D, editors. Life-Cycle Anal. Assess. Civ. Eng. Towar. an Integr. Vis. - Proc. 6th Int. Symp. Life-Cycle Civ. Eng. IALCCE 2018, Ghent, Belgium: 2019, p. 1793–7.
- ix. **Galvão N**, Campos e Matos J, Oliveira D, Santos C. Assessment of roadway bridges damaged by human errors using risk indicators and robustness index. In: Paulo B. Lourenço, Matos JC, Sousa H, editors. IABSE Symp. Guimaraes 2019 Towar. a Resilient Built Environ. Risk Asset Manag. - Rep., Guimarães, Portugal: 2019, p. 236–43.
- x. Mendoza C, Matos J, **Galvão N**, Viviescas Á. Reliability based performance assessment of a roadway bridge under seismic actions. In: Abu A, editor. IABSE Congr. – Resilient Technol. Sustain. Infrastruct., Christchurch, New Zealand: 2021, p. 212–9.
- xi. **Galvão N**, Sousa HS, Matos JC. Impact evaluation of human-made hazards on terrestrial transport infrastructure assets : modelling variables and failure modes. In: H.H. Snijder, Pauw B De, van Alphen SFC, Menegeot P, editors. IABSE Congr. Ghent 2021 - Struct. Eng. Futur. Soc. Needs Impact, Ghent, Belgium: IABSE; 2021, p. 1847–53.

d) Technical Reports

- xii. Hajdin R, Kusar M, Masovic S, Linneberg P, Amado J, Tanasić N (close collaborator: et al. **Galvão N**). Establishment of quality control plan - Cost Action TU1406. 2018. <https://doi.org/10.13140/RG.2.2.28730.03526>.
- xiii. **Galvão N**, Sousa H, Fernandes S, Pucci A, Matos J, Tanasić N, et al. Impact of human-made hazards (D2.2) - SAFEWAY: GIS-Based Infrastructure Management System for Optimized Response to Extreme Events of Terrestrial Transport Networks. vol. 1.0. 2019.

e) Oral Communication

- xiv. **Galvão N**. Assessment of roadway bridges damaged by human errors using risk indicators and robustness index. IABSE Symp. Towar. a Resilient Built Environ. Risk Asset Manag, Guimarães, Portugal: 2019.
- xv. **Galvão N**, Forensic structural engineering: a field of practice and research – The collapse of bridges and the lack of quality control procedures. Engineering New Zealand (Online). 2020.
- xvi. **Galvão N**, Impact evaluation of human-made hazards on terrestrial transport infrastructure assets: modelling variables and failure modes. IABSE Congr. Struct. Eng. Futur. Soc. Needs Impact, Ghent, Belgium (Online). 2021.

- xvii. **Galvão N**, Structural safety assessment of the Lenzburg overpass. SBB-CFF-FFS (Schweizerische Bundesbahnen – Chemins de fer fédéraux suisses – Ferrovie federali svizzere), Bern, Switzerland. 2022.
- xviii. **Galvão N**, The long-term structural safety of railway bridges: A case study in Switzerland. Institute for Sustainability and Innovation in Structural Engineering (ISISE) -day-out. Luso, Portugal. 2022.

2. Human error–induced risk in concrete bridge engineering

The problem with gender is that it prescribes who we should be rather than recognizing who we are.
by Chimamanda Ngozi Adichie

Neryvaldo Galvão, José C. Matos, Daniel V. Oliveira

Journal of Performance of Constructed Facilities

ASCE, Volume 35, Issue 4 – August 2021

[10.1061/\(ASCE\)CF.1943-5509.0001595](https://doi.org/10.1061/(ASCE)CF.1943-5509.0001595)

Abstract: Throughout the last century and in recent years, several bridge failures have taken place worldwide. Recent studies uncovered that the primary cause of these collapses was human errors in the design, construction, and operation phases. Regardless of this finding, there is still a considerable gap between this information and the known errors and the risk they represent for structural safety. Aiming for a better understanding of human errors, an identification procedure and a qualitative assessment of such errors considering risk-based indicators (probability of occurrence and consequence) were performed. Several brainstorming meetings with design and construction experts led to the identification of 49 relevant human errors, which were listed for further evaluation on a survey. Much more important than identifying and assessing these errors is identifying those that pose a greater threat to safety. Using a decision-making tool (i.e., analytical hierarchy process) to process all the information collected in the survey, the errors were ranked according to risk indicators. Furthermore, a qualitative risk assessment is performed, allowing the identification of the errors denoting a higher risk for structural safety, according to experts' opinions.

2.1. Introduction

Relying on the work developed by Syrkov [15] and further developed within task group 1.5 of the International Association for Bridge and Structural Engineering (IABSE), statistics on bridge failures will be briefly discussed. Such a database is probably the most relevant bridge failure database available (still under development), with more than 700 bridge failure incidents worldwide from 1966 to 2020 covering the leading causes of failure. The database encompasses mostly failures concerning the loss of equilibrium, complete collapse, partial collapse and near collapse. Examining the information provided by the database, it is concluded that the main source of uncertainties triggering a bridge collapse is human errors (see Figure 2.1). Design and construction errors are responsible for 31.8% of the collapses, while operation errors are responsible for 32.2%. A thorough discussion in the literature addressing human error as the main cause of the failure of structures, for some historical background, can be found in the literature [25,26].

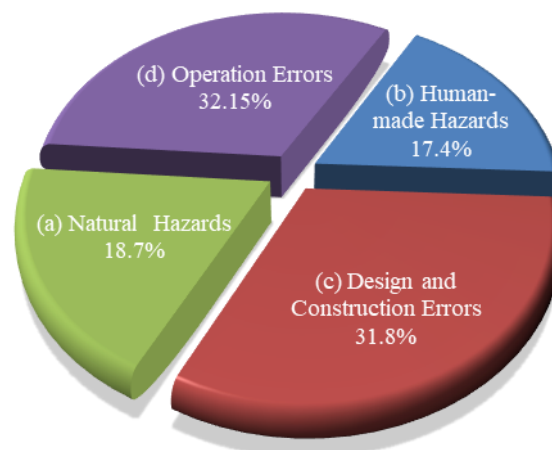


Figure 2.1 – Main causes of failure of concrete bridges [15]

Several definitions have been given to human errors in the literature. Nevertheless, due to its broad scope, a formal definition is required, leaning toward its boundaries definition to prevent misunderstandings with other definitions. Within the scope of this paper, human errors are any Procurement, Design, Construction and Operation errors (deviations out of the acceptable margins) that do not exceed the currently available engineering knowledge and have taken place due to poor work conditions, lack of knowledge, negligence, miss instruction and communication, greed, calculation errors, time and budget constraints, inadequate construction methods and lack of surveillance, among others. Such errors or uncertainties are not covered by the partial safety factors given in present-day semi-probabilistic standards. A similar understanding of what is understood by human errors is shared by Stewart and Melchers [27], Tylek et al. [28]. and Brehm and Hertle [29]. Also, aiming to explain the

boundaries of human errors, its clusters are schematically presented in Figure 2.2. Human errors and human-made hazards are two major components of the human factors field, with the former being the interaction of humans with a system as a technician and the latter the interaction of humans with the system as a user.

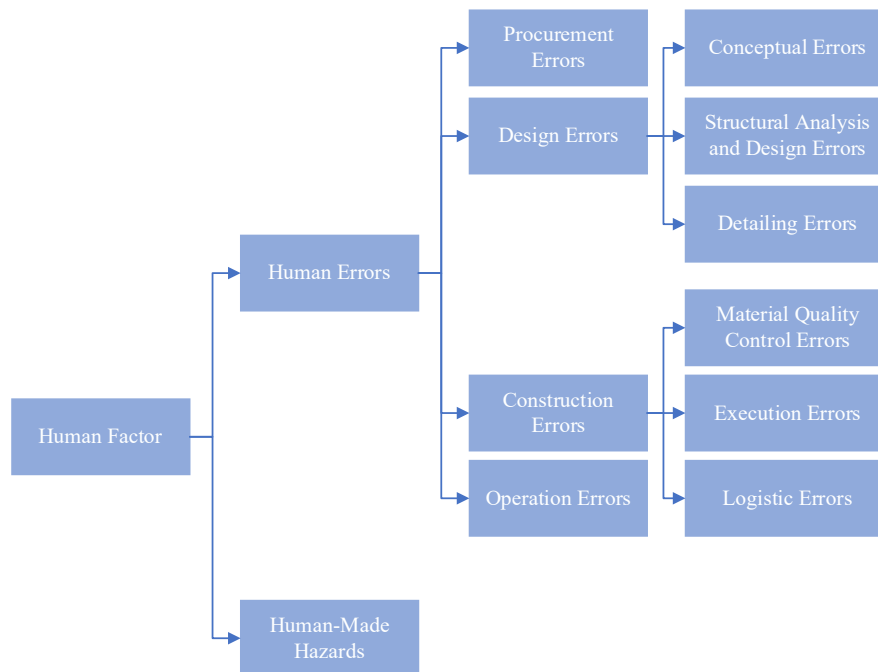


Figure 2.2 – Human error clusters

By performing a more exhaustive analysis of the database, aiming at a more detailed analysis of the causes of failure of concrete bridges, some relevant specific failure causes are presented in Figure 2.3. Each of these specific failures causes are linked to the main ones as follows: (a) Natural hazards (floods and wind effects); (b) Human-made hazards (ship collision, explosion, vehicle collisions, vandalism, and overloading by live load); (c) Design and construction errors (design defect, construction defect, design and construction defects and construction negligence); (d) Operation errors (corrosion, deterioration of reinforced concrete, and overloading by the live load (during maintenance works)). A similar classification of the causes of the collapse of bridges can be found in Deng et al. [30] and Imhof [8]. Some specific causes of failure, such as debris in the water, creep and shrinkage, temperature, normal corrosion, and freeze-thaw cycles with a small percentage, were gathered into the group named Others. One can observe from Figure 2.3 that flood is responsible for a considerable number of failures, and due to climate change, its influence is likely to increase due to increasing rainfall intensity [31]. More detailed research on flooding effects (namely scour) uncertainties can be found in Johnson et al. [32] and Manfreda et al. [33].

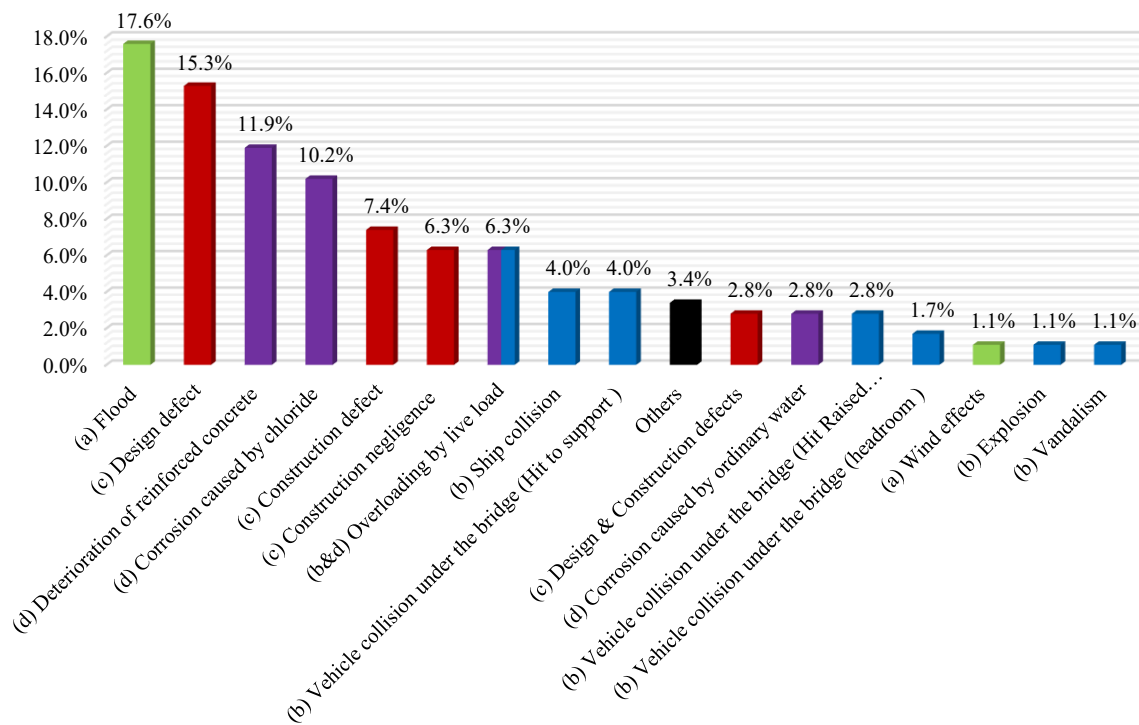


Figure 2.3– Specific causes of failure of concrete bridges

2.2. Procurement errors

The procurement phase is defined by the explanation of the overall idea of an undertaking, definition of execution deadlines suitable for the owner, forecast of the overall cost of the project and selection of the technical team (designer and contractor). The incorrect management of the procurement phase very often leads to poor decision-making from the owner, creating and stimulating several sources of the errors taking place in the design, construction and operation phases.

Given the highly aggressive labour market, companies from the construction industry sometimes face decisions where they are forced to assume execution time and financial costs beneath the needs for the proper fulfilment of the durability, safety or serviceability requirements. Hence, the technical expertise and technology required for successful design and execution are not always the key factor for the contractor or the designer's eligibility. The restricted execution time and limited resources usually lead to the simplification of complex tasks that typically require expertise and a detailed approach, leading very often to assumptions that do not correspond to reality or reliable execution strategies. Therefore, many of the errors that might occur in the later stages of a project are often the consequence of the procurement phase's primary mistakes. Quality control strategies are also features of the procurement phases that can greatly impact the identification and mitigation process of potential sources of errors. Thus, a balance between reasonable execution time, cost, quality control strategies and the selection of a qualified

technical team (enough experience) should be set as a strategy for human error mitigation in the long-term.

2.3. Design errors

2.3.1. Conceptual errors

The conceptual stage considers several essential aspects required for a successful design. Aspects such as the contextualization of the design project in time and space, considering the available engineering technology, adequate base material at disposal, maximum concrete strength manufactured with local raw materials, reachable technical and non-technical support, suitable structural system and construction procedure (according to geotechnical constraints) and required geotechnical characteristics. All these aspects influence the cost of the project and the complexity of execution, consequently providing a greater or lesser environment for human error occurrence [34]. Hence, a well-achieved conceptual design is also a mitigation strategy for human error–induced risk. Such considerations should demand even greater consideration when the project is of non-local or international nature since the designer and the contractor must get familiar with local needs and safety requirements.

A well-achieved conceptual design pays off in the long run with a good structural performance during its operation, minimization of the structure life cycle costs and robust performance under expected or even unexpected single or multiple hazards. Projects with a daring conceptual design with large spans, uncommon column and deck shapes, and other unique characteristics are more vulnerable to human errors, requiring utmost attention and mitigation measures. For conventional bridges, though, the conceptual design is a more standardized procedure because already established internal specifications dictate the material, span, and structural systems, among other features of the structure. Thus, a less error-prone design is to be expected. A good example of a well-achieved conceptual design leading to the reduction of a human-made hazard's probability of occurrence, is the consideration of an arch bridge instead of a common girder bridge with several piers to avoid vessel collisions on the piers. This example is given in a context where the bridge would span over a river/narrow sea with high traffic. The definition of a structural system compatible with the construction procedure or technique usually employed by contractors is also a good conceptual strategy aiming to reduce execution difficulties.

2.3.2. Structural analysis and design errors

These days, the international demand of the construction industry requires design corporations to be involved in numerous projects worldwide. Under this scenario, local standards must be used during the design very often, and the philosophy behind them may vary from one to another. The same standards

can occasionally be incomplete, leading to the need for the combination of different standards. Errors scenarios are drawn, mostly when the quantification of design loads is completed using a given standard where safety factors are less strict in the quantification of the design loads than in the resistance computation. Simultaneously, the resistance computation is performed according to a different standard where the philosophy behind it is the opposite. Consequently, the structural reliability due to these standards' combination will be below the target values established initially by both standards. Non-coherence between several international design codes was reported by Sykora et al. [35], where different target reliability values are recommended for the same case study.

Another common source of error is in the definition of the structure boundary conditions or the soil-structure interaction due to high uncertainties linked to soil behaviour when wrongly addressed. Foundation rotations, differential settlements, support condition stiffness, and geotechnical failure are issues that require careful evaluation from experts but are sometimes neglected, even though they are responsible for tremendous consequences. Other issues, such as mistaken allocation of the bearing devices and lack of maintenance leading to support conditions different from the initially designed, can lead to severe structural system malfunctioning. A common example used to demonstrate the importance of the previously mentioned matter is the development of second-order effects in bridges with long piers due to the development of friction forces between the deck and the malfunctioning bearing devices caused by deck thermal expansion or shrinkage. As the bearing device allows the deck to deform freely at the design stage, the second-order effects are typically not considered for strength computation.

During the construction and transportation of structural components, a structural element or the structural system itself goes through different static conditions that are often different from the final ones considered in the design. Therefore, the structural system or the element resistance might be tested in certain cross-sections not designed to support unexpected stresses. Precast and prestressed elements are often damaged by the failure of the decompression limit state caused by this error, leading to premature cracks. Nevertheless, more severe consequences such as element yielding or system collapse may also occur, especially when the construction technique demands static conditions that change during different assemble steps.

2.3.3. Detailing errors

All the information gathered and created by the designer is transferred to the main contractor through detailed drawings. Through the detailing phase, two stakeholders with different mindsets are deeply connected; hence, the information conveyance must be clear to avoid any misinterpretation of the high

volume of information being transferred. These are common characteristics of all linking and interface activities. As an interface or linking activity, detailing is considered a potential source of errors since it is susceptible to a mistaken interpretation of the given information, absence of specific information, and drawings mistakes, among other errors. As such, the detailing phase should be carefully managed, especially when the information being transferred is of great importance for structural safety.

During the structural analysis and design, several assumptions are made, and very often, these assumptions play a crucial role in the successful performance of a system. It is not uncommon to find detailing drawings where the detailing strategy does not agree with the standard recommendations for the previously considered design assumptions, leading to unpredicted behaviours. For instance, systems with some redistribution capabilities are usually proposed in seismic design. Thus, the connection between different structural elements is expected to have improved ductile behaviour; hence, specific detailing strategies should be used, so the structural analysis corresponds to the structure performance as built.

2.4. Construction errors

2.4.1. Falsework execution errors

Falsework or scaffold execution errors are referred to as being the most common errors and responsible for the worst consequences in the execution phase. They often lead to the complete demolition of concrete elements and a high number of fatalities and injuries. A flawed assessment of the falsework foundation, or no assessment at all going beyond the visual inspection, is a common problem. It is not unusual to find an execution plan where the collected data from piers or abutments foundation locations are used to check the falsework foundation resistance. This procedure may fail when the falseworks are needed in extended lengths because the foundation's geotechnical properties may vary along its length, especially if the given soil is heterogeneous, leading to soil properties assumptions entirely dissimilar to the real one. This mistaken assumption may well end up in substantial settlements, converted into large deflections, or even structural collapse. Another likely scenario of failure is the non-consideration of the reduction of soil resistance due to rainfall conditions. For this auxiliary structure, the area through which the load is transferred to the ground is usually small; thus, the soil stress limits should be carefully controlled. A common mistake here is the use of soil maximum load capacity as its resistance performance indicator, neglecting the importance of the area through which the load is transferred.

Movable falseworks require utmost attention when changing them from their current position to a new one since a constant change in their support condition is necessary. As such, no room for mistakes

is allowed, given the severe consequences that might take place. Collapses have taken place in several constructions using this technic due to miss coordination between the different involved parts and lack of proper surveillance and effective communication.

2.4.2. Material quality control errors

Nowadays, material quality control errors are becoming a less concerning issue due to the industry's rigorous standards adopted to avoid former misfortunes and for quality assurance purposes. Nevertheless, this was not a certainty during the last century. The exceptional registered occurrences are related to concrete quality specifications due to a mistaken evaluation of aggregates water content, alkali-aggregate reaction, wrongful quantification of the required admixtures, and miscalculations to fulfil specific concrete requirements (e.g., concrete strength and elasticity modulus, among others). It is also worth mentioning the deficient vibration of concrete in areas of difficult access due to the high density of passive and active reinforcement allowing the formation of voids, or excessive vibration leading to the segregation of concrete constituents. Additional deformation of concrete due to non-agreement between creep properties of employed concrete with those assumed in the design is an error to bear in mind. Concerning durability, it has been reported that the usage of the right or favourable cement type can double the service life of the structure [36]. In construction sites where more than one reinforcement class is available, it is vital to take these classes' incorrect usage as a potential risk. Additionally, proper storage condition of reinforcement to avoid early corrosion and ductility reduction is an important consideration to keep in mind, especially when a long-stored period is concerned. Also, a non-controlled concreting of mass concrete components leading to high temperature is an error that leads to deficient concrete with severe strength reduction.

2.4.3. Logistics errors

The construction phase requires massive management of human, equipment, and material resources. Thus, logistic errors are part of companies' daily work, and they must not be neglected. Some examples are as follows:

- Adoption of a concrete resistance class or other specification that is not available at an affordable distance from the construction site;
- Air pollution, underground water or soil contamination due to inadequate eco-friendly safety measures;

- Functional capabilities limitations of movable and fixed cranes in the construction site due to errors related to insufficient foundation preparation, limited action radius, allowed movable distance, and maximum transportation weight, among others;
- Absence of special licences for transportation of big precast elements through public roads or physical restrictions to transportation, which is a drawback that usually turns into large delays; and
- Inadequacy of the launching girders to the pier's geometry is a logistic error to keep in mind;

2.5. Bridge collapses

Particular major bridge collapses were recorded due to some of the errors highlighted in the previous section. Given their technical relevance, they are shortly described and discussed.

In early 2018, one of the towers of a concrete cable-stayed bridge under construction in Colombia (Chirajara) collapsed due to a design error. The same error also led to the demolition of the still-standing tower since it was also about to collapse, making any attempt at its strengthening or rehabilitation very problematic. Ten workers lost their lives during the incident, and another five were injured, requiring some medical support. An investigation of the incident headed by Modjeski and Masters concluded that the bridge collapse was caused by the failure of the prestressed transversal girder and the failure of the diamond tower lower diaphragm. The influence of the tower diaphragm, in its overall resistance, was overestimated at the design stage [37]. Other sources state that the prestressed transversal girder was insufficiently prestressed and that the main reinforcements of the tower diaphragm were placed in the wrong direction [38].

On March 2018, a pedestrian bridge under construction in the USA (Miami) collapsed due to a design error causing six deaths and eight injuries. It was reported by the Federal Highway Administration Office of Bridges and Structure that a design error led to the overestimation of the stresses that could be taken by the bridge. The cracks observed before the collapse were consistent with the design error. Lab tests were performed on the concrete samples to check their quality, proving that the concrete met the standard's requirements [39]. The bridge had structural design deficiencies that contributed to the collapse during one of the construction stages. The consultant hired by FIGG Bridge Engineers (the engineer of record) to conduct an independent peer review of its design did not check the structural integrity of the bridge for different construction stages. Consequently, the review was performed only for the final design stage, where all segments of the bridge were already in place and completed [40].

On August 2018, a cable-stayed bridge from the sixties, designed by Ricardo Morandi, collapsed in Italy (Genoa) during a heavy traffic day causing 43 deaths. The collapse was mainly triggered due to structural deterioration caused by advanced corrosion in one of the four cables. Despite this fact, the structure had an initial deficiency related to a lack of structural redundancy (absence of multiple load paths) or, consequently, lack of robustness because it had few crucial supports (four cables on each tower supporting the deck). The structure had another initial flaw that led to the crack of the protective concrete coat surrounding the stayed steel cable that left it unprotected, unchaining a premature corrosion process. An unneglectable piece of the puzzle is also the consequence of political decisions regarding public infrastructures when maintenance and restrictions applied to the structure are concerned. A good example of this last statement is the Morandi bridge since a political or owner decision neglecting the information given by experts also contributed to the bridge collapse [41]. The lack of structural robustness (disproportionate outcome due to any support failure) is here highlighted as a conceptual structural error once a different cable-stayed structural system with multiple load paths would avoid such a terrific ending. The high rate degradation of the southern cable is here seen as an error of operation since no maintenance action on the structure was taken before an obvious indication of high degradation that was prompted by a design error (protective concrete coat surrounding a highly tensioned element) from the early ages of the structures [42]. Three main groups of human errors led to this catastrophic ending: the conceptual error, the design error and the operation error. The occurrence of multiple errors, creating a sequence of events leading to a bridge collapse, is the typical scenario.

Despite today's efforts and the new standards for quality control that implicitly deals with human errors, these errors are still a major concern. It is also known that bridge quality control standards were less strict during the sixties, seventies and eighties when a high volume of bridges was built. Therefore, in the present days, it is important to consider human errors in infrastructure management procedures - in particular, when the error is expected to increase the deterioration rate of the structure since maintenance strategies and interventions are supported by predefined degradation rates (predictive models).

2.6. Design and construction errors investigation

The risk management process aims at the systematic use of available information within a carefully established and clearly defined context, to identify hazards and estimate the risk they pose to human beings, property, and the environment. Hence, three steps are initially required (i) Hazard identification, (ii) Probability of occurrence analysis, and (iii) Consequence analysis. The combination of the last two

provides the risk measure. Probability of occurrence and consequence analysis can be performed using a qualitative or a quantitative approach, but the latter is more complex and usually employed after the first one. A hazard is defined as any condition, circumstance or action that can undermine the structural system resistance features and may lead to malfunctioning or failure of the structure [16,43,44]. Within the scope of this paper, human errors are the leading hazard under assessment, with design and construction errors in concrete bridges being the focus subject. Therefore, the novelty of this research lies in the identification of design and construction errors that are carefully addressed according to expert judgement.

2.6.1. Delphi technique and survey

For hazard identification purposes, the Delphi technique is employed here. The Delphi technique is defined in ISO 31010 [45] as "a procedure to obtain a reliable consensus of opinion from a group of experts through a standardized procedure". Experts are expected to express their opinions independently and anonymously while having access to the other expert's views as the procedure goes on. Accordingly, six experts (20 years of average work experience) were selected and questioned about the most common and troubling design and construction errors in concrete bridge engineering they encountered during their professional careers. The experts were asked to keep in mind a standard roadway overpass with three spans of 68 m (18 m + 27.8 m + 18 m, which is the most common type in the Portuguese road transportation network). This request aimed to narrow the discussion around conventional bridges, avoiding particular structural types such as suspension, cable-stayed and large-span arch bridges. Nevertheless, the content of the information provided by the experts exceeded, to a small extent, such expectations. The expert views converged to a group of 20 design and 29 construction errors (see Table 2.1 and Table 2.2, respectively), clustered according to Figure 2.4. The concerns expressed in the preceding chapters are also a summary of the experts' thoughts.

Following the detailed discussion around design and construction errors and listing of such errors by experts (i.e., hazard Identification), the second and third steps of the risk analysis are achieved through a survey addressed to experts aiming the qualitative assessment of the probability of occurrence and consequence of such errors according to five categorical levels. The experts were also encouraged to suggest additional errors important to be considered. The survey was carried out by e-mail through the COST Action TU 1406 network and to additional Portuguese civil engineers. The answers provided by the participants were analysed using a multi-criteria decision-making tool named the analytic hierarchy process (AHP) and a risk matrix. Twenty-four participants, with professional experience ranging between

5 and 40 years, answered the survey call. Half were from Portugal, and the other half were from other European countries. Half of them were design engineers, and the other half were construction site engineers, but some of them had experience in both fields. Other relevant surveys dating from a few decades ago can be found in the literature [46,47].

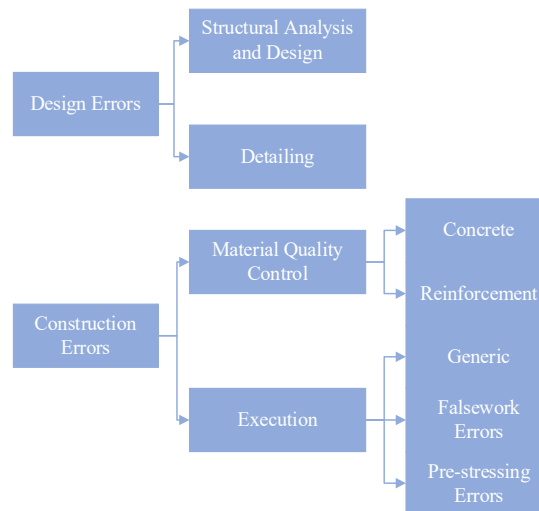


Figure 2.4 – Design and construction error clusters

2.6.2. Analytic hierarchy process

The AHP is a multi-criteria decision-making tool [48] that considers pair-wise comparisons of alternatives and criteria to prioritize such alternatives or criteria. It is supported by qualitative or quantitative inputs comparing different objects/subjects. Such comparison is numerically represented by a matrix comparing alternative i with alternative j . The AHP is typically implemented in three main steps: (i) decomposition; (ii) comparative judgment; (iii) synthesis of priorities [49]. The decomposition is the particularization of the problem into different choices or possible solutions, which in this paper are the design and construction errors listed in the survey. The comparative judgment is performed by the survey participants where the probability of occurrence (PO) and consequence (CO) of each of the errors are categorized into five levels (see Figure 2.5 and Figure 2.6). The comparative judgement is then transformed into a comparison matrix that will allow the synthesis of priorities through the matrix eigenvectors, leading to the ranking of the errors according to their probability of occurrence and consequence, given the input of the survey participants.

The AHP is implemented through a MATLAB script developed according to Goepel's methodology [50,51], aiming at a more automatized procedure to analyse the information collected through the survey. Such methodology is being widely used by the research community (e.g., Kifokeris et al. [52]) given its simplicity, straightforward tutorials and Excel templates available in Goepel [50]. The methodology is summarized into the following consecutive steps:

1. The pair-wise comparison is summarized in a square comparison matrix, rating the probability of occurrence and consequence of each error using a qualitative typical 5-point Likert scale ranging from one to nine or from one to the inverse of 9 (i.e., 1-3-5-7-9 and 1-1/3-1/5-1/7-1/9). One is used when errors are similarly likely to occur, or similar consequences are to be expected, and nine is used when an error is much more likely to occur than another one, or a much greater consequence is expected from one error to the other. The inverse numbers are used when the error is less likely to occur, or a minor consequence should be expected when compared to another error. The comparison matrices of each participant were all considered consistent.
2. The consolidation of each expert input is achieved by an aggregated square comparison matrix, considering the weighted geometric mean method according to Eq. (2.1), where $a_{ij(k)}$ is the comparison performed according to the Likert scale comparing error i to error j by expert k ; and w_k is the expert weighting factor defined according to its years of experience as follows: i) 1.0 for 5 to 10 years of experience; ii) 1.5 for 10 to 20 years; iii) 1.75 for 20 to 30 years; iv) 2.0 for 30 to 40 years.

$$C_{ij} = \exp \frac{\sum_{k=1}^K w_k \ln a_{ij(k)}}{\sum_{k=1}^K w_k} \quad (2.1)$$

3. In order to quantify the agreement or homogeneity between different experts' input, a consensus index is computed, ranging the consensus between experts' opinions from 0% (no agreement) to 100% (perfect agreement). Finding a reasonable rate of this index is crucial to support the claim of a satisfactory convergence in the identification of relative priorities of the errors. The consensus or group judgement dispersion is derived from the consensus index S^* , computed according to Eq. (2.2),

$$S^* = \frac{\left[\frac{M - \exp(H_{\alpha \min})}{\exp(H_{\gamma \max})} \right]}{\left[\frac{1 - \exp(H_{\alpha \min})}{\exp(H_{\gamma \max})} \right]} \quad \text{where } M = \frac{1}{\exp(H_{\beta})} \quad (2.2)$$

where H_{β} Shannon entropy beta measures the variations of priorities distribution among experts, given by Eq. (2.3). Which is dependent on Shannon entropy alpha H_{α} and gamma H_{γ} . The first one measures the average individual expert priority distribution among the errors, computed for all K experts, and the second one measures the group aggregated priorities. The Shannon entropy alpha and gamma are computed according to Eq. (2.4), where p_{ik} is the normalized priority value of the i th error according to the k th expert, given by Eq. (2.5). The absolute priority

values r_i are computed according to the row geometric mean method, as shown in Eq. (2.6)

where N is the total number of errors.

$$H_\beta = H_\alpha - H_\gamma \quad (2.3)$$

$$H_\alpha = \frac{1}{K} \sum_{k=1}^K \sum_{i=1}^N -p_{ik} \ln p_{ik} \quad \& \quad H_\gamma = \sum_{k=1}^K -\bar{p}_k \ln \bar{p}_k \quad \text{where} \quad \bar{p}_k = \frac{1}{N} \sum_{i=1}^N p_{ik} \quad (2.4)$$

$$p_i = \frac{r_i}{\sum_{i=1}^N r_i} \quad (2.5)$$

$$r_i = \exp \left[\frac{1}{N} \sum_{j=1}^N \ln(a_{ij}) \right] \quad (2.6)$$

Subsequently, the minimum Shannon alpha entropy $H_{\alpha min}$ and the maximum Shannon gamma entropy $H_{\gamma max}$ must be computed by applying Eq. (2.7) and Eq. (2.8), respectively, where $c_{max} = 9$ is the maximum value of importance rating used according to the 5-point Likert scale to build the pair-wise comparison matrix in step 1.

$$H_{\alpha min} = -\frac{c_{max}}{z} \ln \left(\frac{c_{max}}{z} \right) - (N-1) \frac{1}{z} \ln \left(\frac{1}{z} \right) \quad \text{with} \quad z = N + c_{max} - 1 \quad (2.7)$$

$$H_{\gamma max} = (N-K) \left(-\frac{1}{z} \right) \ln \left(\frac{1}{z} \right) - \frac{u}{z} \ln \left(\frac{1}{K} \frac{u}{z} \right) \quad \text{with} \quad u = K + c_{max} - 1 \quad (2.8)$$

4. Priority values are obtained by computing the eigenvector of the pair-wise comparison square matrix. The prioritization or ranking of the errors is displayed in the last two columns of Table 2.1 and Table 2.2 for each risk indicator, that is, the probability of occurrence (PO) and consequence (CO). Relative ranking position numbers are used, where the number one is attributed to the error that is more likely to occur or the error expected to have the highest consequences, while the maximum number is assigned to the error that represents the lowest probability of occurrence or the lowest consequence.

Table 2.1 – List of design errors identified and analysed

Errors Cluster	ID	List of Errors	Rankings	
			PO	CO
Structural Analysis and Design Errors	1	Error due to a non-conservative arrangement between design and load regulations with different backgrounds, leading to a less reliable structure	16	17
	2	Errors in regulations interpretation	9	20
	3	Error in live loads quantification due to lack of data	13	14
	4	Error in dead load quantification	20	1
	5	Error in the definition of the most significant load combinations	11	7
	6	Error in defining the gravity centre for highly compressed elements, or in defining load eccentricity	18	11
	7	Error in defining a cross-section shear centre (torsion effects)	7	18
	8	Error in the quantification of the effects of deck deformation due to creep, shrinkage and temperature variation, in columns (second-order effects)	1	16
	9	Error in defining the buckling length of an element	12	10
	10	Error in defining/describing the location of prestressing tendons	15	8
	11	Error in the decompression limit state calculation	14	19
	12	Error in defining the prestressing hyperstatic effects	3	15
	13	Error in defining the soil-structure interaction (boundary conditions and differential settlements)	2	12
	14	Error due to lack of consideration of different support conditions that a bridge or an element will be subjected to through the construction process	5	2
	15	Error in modelling the connections between structural elements (e.g., deck, beams and columns)	8	5
Detailing Errors	16	Error due to the lack of consistency between the design assumptions and the detailing rules	4	9
	17	Error in reinforcement cross-section area	17	3
	18	Error in reinforcement spacing (flexural and shear reinforcement)	10	4
	19	Error in concrete and reinforcement classes indication	19	6
	20	Error in defining the quota of implantation	6	13

The consensus index obtained according to the AHP was 87% among the design engineers and 73% among the construction site engineers. Thus, expert opinions did not disperse too much. The awareness and resemblance of the design engineer's assessment of the design errors are higher than those provided for the construction site engineers for the construction errors. Given that the designer's daily activities go through a more standardized procedure, a higher consensus index for the design engineers is a reasonable observation.

Table 2.2 – List of construction errors identified and analysed

Errors Cluster	ID	List of Errors	Rankings	
			PO	CO
Material Quality Control Errors	Concrete	1 Errors leading to alkali-aggregate reaction	19	15
		2 Error in the quantification of cement hydration heat	18	22
		3 Error in the evaluation of aggregates humidity	13	28
		4 Error due to poor concrete workmanship leading to concrete with characteristics and properties different from the requested	22	13
	Reinforcement	5 Errors leading to reinforcement corrosion	10	25
		6 Error using a wrong reinforcement class especially when different reinforcement classes are also used in construction	29	23
		7 Error in the production of reinforcement cross-section area	26	14
Execution Errors	Generic Errors	8 Error due to wrong positioning of supports	15	12
		9 Error due to expansion joints deficiency and wrongly positioned	3	19
		10 Error due to wrong interpretation of the design project	21	8
		11 Error in topographic implantation	14	16
		12 Error due to wrong concrete vibration	20	27
		13 Error in the reinforcement covering	2	18
		14 Error in the longitudinal shape due to shrinkage and creep effects not correctly computed in the design phase	9	26
		15 Error due to consideration of support conditions different from those defined in the design phase	23	24
		16 Error due to the establishment of wrong final boundary conditions	25	20
		17 Error due to wrong evaluation of the foundation soil properties	5	4
		18 Error due to geometric imperfections (inclination and cross-section imperfection)	11	29
	Falsework Execution Errors	19 Error due to poor evaluation of the falsework foundation soil properties, and variation of these properties after rainfall	1	3
		20 Error due to poor preparation of the falsework foundation using gravel material and/or poor positioning of the timber elements that support the falsework	8	10
		21 Error due to deficiency in the continuous falsework bracing, leading to global instability	4	1
		22 Error due to a deficient maintenance plan leading to poor falsework material quality	12	7
		23 Error in the falsework clamping elements (connectors and couplers)	6	6
		24 Error in movable falsework due to non-controlled hyperstaticity reduction to perform his movement	16	2
		25 Error in the assessment of the formwork and falsework deformability properties	7	17
	Prestressing Errors	26 Error due to wrong positioning of formwork ties	17	21
		27 Error due to insufficient prestressing	28	5
		28 Error due to over-loss of prestressing	24	11
		29 Error due to insufficient curing of concrete subjected to prestressing forces leading to a deficient bond between the concrete and the prestressed cables	27	9

The input of each expert was weighted according to their years of experience. For instance, the input of a structural engineer with additional professional experience should have more influence on the outcome than the contribution of a junior engineer. As it is very difficult to quantify the influence of professional experience in this matter, there is no way to validate the weighting factors adopted in Eq. (2.1) without performing a major study of the topic. However, it is known that a senior engineer is more likely to make a better decision than a junior engineer due to the accumulated expertise; therefore, the weighting factor was increased with the years of experience.

2.6.3. Qualitative risk analysis

Once the design and construction error rankings are established according to the probability of occurrence and consequence, it is of paramount importance to characterize the relationship between these two for qualitative estimation of the risk. Hence, the risk matrix approach is employed [44]. It is commonly used to rank hazardous events according to their significance, to screen out insignificant events, or to evaluate the need for risk reduction of some events.

The loss of information concerning the qualitative levels assigned to the errors by the experts is one of the AHP handicaps. In other words, the priority list or ranking is set with a great cost since the qualitative level of each one of the errors becomes unknown during the AHP procedure. The loss of such information renders difficult the qualitative assessment of the error with a risk matrix. To overcome this drawback and accomplish a broader analysis of the information provided by the survey participants, the qualitative levels assigned to each risk indicator are obtained for each error using a weighted geometric mean method to aggregate the participant's inputs. Figure 2.5 and Figure 2.6 show the qualitative risk matrices of the design and construction errors, respectively, and their distribution according to their likelihood and expected consequences, using their identification number (ID) provided in Table 2.1 and Table 2.2. The prioritization information obtained by the AHP is also considered inside each matrix cell.

Risk = PO x CO		Impact or Consequences (CO)				
		Very Low	Low	Average	High	Very High
		1	2	5	10	20
Probability of Occurrence (PO)	Very High	5				
	High	4				
	Average	3			8 12 13 16 20	14
	Low	2		11	2 3 9 10 15 18	17
	Very Low	1			1 6 19	4

Figure 2.5 – Risk matrix of design errors

Risk = PO x CO		Impact or Consequences (CO)				
		Very Low	Low	Average	High	Very High
		1	2	5	10	20
Probability of Occurrence (PO)	Very High	5				
	High	4				
	Average	3		9	13	19
	Low	2		14 18 3 5 12 15 16	11 20 22 25 26 27 28 29	17 21 23 24
	Very Low	1		6		

Figure 2.6 – Risk matrix of construction errors

Making use of the information provided by the AHP and risk matrix, comprehensive risk classification of the errors was achieved. For exemplification purposes, let one take the errors with ID7 ($PO_{\text{Ranking}} \rightarrow 7$ and $CO_{\text{Ranking}} \rightarrow 18$) and ID8 ($PO_{\text{Ranking}} \rightarrow 1$ and $CO_{\text{Ranking}} \rightarrow 16$) from the design risk matrix. They are

both within the high-risk group ($40 \geq Risk \geq 25$), but if the AHP ranking information is taken into account, the error with ID8 can be highlighted as the one representing greater risk because it has a higher ranking position than the error with ID7. Therefore, the wrong definition of a cross-section shear centre (design error ID7) represents a lower risk than a wrong quantification of the effects of deck deformation due to creep, shrinkage and temperature variation in columns, leading to unexpected second-order effects (design error ID8). Using this same procedure, a further distinction between the risk of the different errors within the same cell is possible. Nonetheless, the risk of errors can be easily categorised into five different risk levels.

Based on Epaarachchi and Stewart [53], the error magnitude is the size of the error as a percentage of the correct outcome; in other words, it is the parameter that describes the severity of the error. It is a vital characteristic of an error, here neglected. The severity of an error is always associated with its consequence but is not the ultimate factor. For instance, the consequence of error with ID8 increases with the slenderness of the column; therefore, the same error with the same magnitude (equal relative deviation from its correct value) might have entirely different consequences for different structural systems or components. Subsequently, it is important to consider the magnitude of the error in a detailed structural analysis, mainly if the error is understood as being of paramount importance for risk management. Some research work addressing error magnitude can be found in the literature [53–56]. Nevertheless, such analysis is beyond the scope of this paper, which addresses a general approach for the categorization of errors according to five risk levels considering their probability of occurrence and expected consequences.

An essential characteristic of the risk matrix used here is that it enhances the influence of the consequence over the probability of occurrence in terms of risk rating. Such a risk matrix was chosen for this research because it is directly connected with the risk management of civil engineering activities. Dissimilar risk matrices can be found in the literature [44]. However, in civil engineering, the consequence should be enhanced over the probability of occurrence of an event in risk quantification.

2.6.4. Additional errors collected within the survey

Besides the errors listed above, the inquired experts reported a series of other errors (see Table 2.3 and Table 2.4). They were not considered in the risk analysis since different experts independently reported them; thus, insufficient information for the analysis was available. Nevertheless, it is important to make them available in the literature for further research.

Table 2.3 – List of additional design errors collected within the survey

Errors Cluster		List of Errors
Structural Analysis and Design Errors		Error due to low design experience
		Error due to accelerated design programmes to meet deadlines and design budgets
		Error due to incorrect application and understanding of partial prestressing
		Error due to incorrect use of structural analysis software
		Errors of data entry in structural software (e.g., material strength, boundary and nodal constraints, self-weight, elasticity modulus. etc.)
		Error due to non-validation of automatic computation of complex numerical models with simpler models
		Error due to hydrostatic effects negligence in the structural analysis
		Error due to the project non-verification by authorized and qualified design reviewers
Detailing Errors		Lack of experience with good detailing practices (mainly in steel structures)
		Error due to drawings misinterpretation due to lack of experience and awareness
		Error due to the use of general details drawings from existing projects
		Error due to lack of coherence between shear reinforcement detailing and different details

Table 2.4 – List of additional construction errors collected within the survey

Errors Cluster		List of Errors
Material Quality Control Errors	Concrete	Error due to non-attendance of quality control expert inspectors to the construction site
		Error due to lack of protective measures in very high and low-temperature work sites
	Reinforcement	Error due to non-attendance of quality control expert inspectors to the construction site
		Error due to non-conformity of steel reinforcement bars with standards
Execution Errors	Generic Errors	Clashing of reinforcement (particularly for precast elements)
		Error in the execution of the abutment's embankments
		Error due to deficiency in the execution of the approach slabs
		Errors or deficiencies caused by interrupted concreting because of equipment malfunctioning or delays of the concreting mixer trucks
		Error due to non-controlled concreting of mass concrete elements leading to high temperatures in the concrete core (spread foot of abutments and piers, and pile cap, among others)
	Falsework Execution Errors	Errors due to the inexistence of checklist or check procedures for execution quality control
		Errors caused by changes in the assembly technique and material concerning the execution project
		Errors due to the usage of uncertified materials
		Errors caused by the absence of the rainwater drainage system or any other protective measure

2.6.5. Investigation remarks

Looking at the risk matrices (see Figure 2.5 and Figure 2.6), three errors stand out in the critical zone ($Risk \geq 50$), one in design errors risk matrix (ID 14) and two in the construction errors risk matrix (ID 19 & 21). The error with ID 14, described as the lack of consideration of different support conditions through which the element or the structural system will be subjected during the construction procedure for validation of the design calculation, is identified as the error that might represent the highest risk in

the design phase, within the context described in this paper. Coincidentally, it is the main cause of the Miami bridge collapse described in the “Bridge collapses” section that took place in March 2018. The construction errors found in the critical zone are both concerning falseworks. One is related to the continuous bracing required for the global stability of the falsework. The other is associated with the poor assessment of the foundation soil properties supporting the falsework, neglecting water influence in such properties. Such negligence is common since the falsework is just a temporary structure, and further investigation addressing such an issue is usually not performed.

Table 2.5 – Top five design and construction errors with the highest risk

Design Errors	Construction Errors
Error due to lack of consideration of different support conditions that a bridge or an element will be subjected to through the construction process (ID 14)	Error due to deficiency in the continuous falsework bracing leading to global instability (ID 21)
Error in reinforcement cross-section area detailing (ID 17)	Error due to poor evaluation of the falsework foundation soil properties, and variation of these properties after rainfall; (ID 19)
Error due to lack of consistency between the design assumptions and the detailing rules (ID 16)	Error in movable falseworks due to non-controlled hyperstaticity reduction needed to perform his movement (ID 24)
Error in the definition of the soil-structure interaction (e.g., boundary conditions and differential settlements) (ID 13)	Error due to wrong evaluation of the foundation soil properties (ID 17)
Error in modelling the connections between structural elements (e.g., deck, beams and columns) (ID 15)	Error in the falsework clamping elements (connectors and couplers) (ID 23)

For summary purposes, the top five design and construction errors are listed in Table 2.5, according to the investigation described in this paper (AHP and Qualitative risk analysis). Many errors related to falsework/scaffolding take the lead in the risk analysis, along with the soil properties and support conditions. During the brainstorming meetings, the malfunctioning of structures was primarily linked to these errors because they support whatever is going to be built and hence have remarkable consequences. Detailing of reinforcement and lack of consistency between the design assumptions and detailing rules are two detailing errors that are among the ones representing the highest risk.

The design error identified as the most frequent error is the incorrect quantification of the effects of deck deformation due to creep, shrinkage and temperature variation in columns, causing and amplifying second-order effects (ID 8). On the other hand, the least frequent error is the mistaken dead load quantification (ID 4). Within the construction phase, reinforcement covering errors (ID 13) are the second most frequent errors, followed by expansion joints deficiency (ID 9).

2.7. Human error mitigation

Mitigation measures against human errors exhibit a vast scope due to the multidisciplinary partners playing different roles in this matter. The political decisions, economic constraints, cultural and environmental influences, missing technological advancements of the sector, engineers' qualifications, and type of structural systems and geometric shapes used make it very difficult to provide specific mitigation measures without bringing forth a long discussion that goes beyond the scope of this work. Nonetheless, a thorough discussion addressing measures against errors in the building process, provided by Matousek [57], can be found in the literature.

The increase of awareness of design and construction errors and the discussion around the subject and their risks is a mitigation strategy itself because the mitigation of known potential hazards and their risks are part of engineers' daily challenges.

A few common mitigation measures were pointed out by the experts consulted within the scope of this research, namely the use of different design software for outputs validation, critical interpretation of the outputs by expert engineers, self-made computation sheets for validation of the software outputs, the careful appointment of the project surveillance team and serious investigation of the geological and geotechnical properties of the foundation soil.

In civil engineering, the uniqueness of each construction project and its details make it challenging to approach the problem in terms of production automation. However, with artificial intelligence, there might be a greater influence of technology in the construction sector for human error mitigation. Today, contractors are continuously gathering data on accidents taking place on construction sites, so machine learning can be used to find underlying patterns in the collected data and prevent accidents [58–60]. Nevertheless, other technological advancements are already playing an important role in this matter through technologies such as Building Information Modelling Technology, 3D printing, Virtual Reality and Augmented reality [61]. From the economic point of view, investments in such innovative technologies are compensated because a problem found during the design phase that costs 1\$ to fix will cost 20\$ to fix during the construction phase and 60\$ to fix during the operation phase [58].

2.7.1. Quality management measures

Basic design, execution and maintainability requirements are the foundation of design codes such as the Eurocodes. Accordingly, the fulfilment of requirements such as structural safety, serviceability, traffic safety and durability, must be assured by the designer and the contractor, for all relevant load cases and traffic demands for an indicative design working life of 100 years, according to the current codes.

Therefore, quality management strategies for quality control and quality assurance should be employed to reduce or avoid design and construction errors, so the newly constructed bridges are handed over to the owner fulfilling the code's requirements. Such codes are Eurocode 0 [19], Eurocode 1 [62], EN 13670 [63], and ISO 22966 [45], among others, whose main goal is standardization for quality assurance in bridge design and execution.

The Eurocode 0 [19] provides quality management measures aiming at the reduction of errors during the design and execution of structures so that the structures can meet certain reliability levels. For quality management purposes, three design supervision levels and three inspection levels for construction works are proposed according to the reliability classes and consequence classes defined in Eurocode 0 [19] (see Table 2.6). Similar measures are proposed by Melchers and Beck [64]. The FIB [65] proposed as-built documentation that describes the actually constructed structure, including the results of the initial inspection and direct input parameters required for maintainability purposes. The recommended structural reliability classes, measured by a target reliability index (β_T), are defined according to the expected consequence (life loss, material damage, and functionality losses, among others) of failure of a structure. Hence, three consequence classes are correlated to three reliability classes. The target reliability index stands for the minimum nominal probability of failure that should be assured by the employed design and construction procedures. Nevertheless, Eurocode 0 [19] states that "the actual frequency of failure is significantly dependent upon human errors, which are not considered in partial factor design". Thus, the target reliability index does not necessarily provide an indication of the actual frequency of structural failure since they stand for reliability classes of structures designed and built according to the codes, not necessarily as built.

As stated previously, the design codes do not take into account human errors in the definition of the threshold value provided for reliability classes since such errors are expected to be eliminated by design supervision and construction inspection, even though this is not always the case. Nonetheless, several attempts targeting the numerical quantification of the impact of human errors on structural safety can be found in the literature, namely, sensitivity analysis aiming to quantify the impact of different errors in structural safety reduction [55,56]. Further research seeking the probabilistic characterization of errors' magnitude through probability distribution functions is also available [61,64,66]. Nevertheless, additional investigation is required.

Table 2.6 – Design supervision and construction works inspection levels according to Eurocode 0 [19]

Reliability Class (RC)*	Examples of buildings and civil engineering works [22]	Design supervision levels	Inspection Levels
RC3 ($\beta_T = 4.3$)	Major bridges and public buildings where consequences of failure are high (e.g., fewer than 500 fatalities)	Third-party checking: Check performed by an organisation different from that which has prepared the design	Third-party inspection
RC 2 ($\beta_T = 3.8$)	Typical bridges, residential, office buildings and public buildings where consequences of failure are medium (e.g., fewer than 50 fatalities)	Checking by different persons than those originally responsible and in accordance with the procedure of the organization	Inspection in accordance with the procedures of the organisation
RC 1 ($\beta_T = 3.3$)	Agricultural buildings where people do not normally enter (e.g., storage buildings), greenhouse	Self-checking: Checking performed by the person who has prepared the design	Self-inspection

*Target reliability levels established for ultimate limit states for 50 years reference period.

On the organization level, Terwel and Jansen [67] reported that internal factors regarding interactions between project partners (e.g., agencies, contractors, consultants, designers, owners, reviewers and inspection team) were the ones with the greatest impact on structural safety. Such factors are (i) allocation of responsibility, (ii) coordination and control mechanisms, (iii) communication and collaboration, (iv) safety culture, and (v) risk management, among others. External factors such as the economic and political landscape are also important factors to keep in mind. Each organization manages each of these factors according to its internal specification standards and code procedure to tackle human interaction, which is the weakest link in the structural design and construction process.

2.7.2. Risk mitigation

The risk analysis is usually followed by a risk evaluation, where the risk of the assessed hazard is compared with acceptance criteria, which sometimes are hard to define and can vary for different industries and societies. The establishment of such acceptance criteria aims to direct proper mitigation actions to specific hazards, seeking risk levels as low as reasonably practicable (ALARP) [68]. The ALARP concept is directly related to the acceptance criteria; thus, it groups the risk of a hazard into three categories, the critical region, the ALARP region and the acceptable region. A hazardous event considered to be present in the critical region cannot be accepted, so it must be reduced at all costs. The ALARP region is characterized by a risk reduction principle targeting the avoidance of a gross disproportion between the risk reduction costs and the obtained risk reduction. Thus, a risk reduction measure must be efficiently employed so the costs are minimized and the risk reduction is maximized. [69]. For risks within the acceptable region, mitigation is unnecessary, but it is worth mentioning that many of these hazards can lead to unexpected accidents due to their accumulation or long-term effect. In this paper,

according to the qualitative analysis performed, the critical, ALARP and acceptable regions are identified respectively by the " $Risk \geq 50$ ", " $40 \geq Risk \geq 5$ " and " $Risk \leq 4$ ", respectively, see also Figure 2.5 and Figure 2.6.

As discussed above, the critical zone of the risk matrix usually encompasses risks that must be mitigated at all costs. Consequently, two mitigation actions were suggested by experts for "error due to poor evaluation of the falsework foundation soil properties, and variation of these properties with rainfall" (ID 19, see Table 5); see also Figure 2.6:

Mitigation Action 1: Quantification of the soil plastic properties in order to consider further resistance reduction due to rainfall conditions and to better predict the soil's maximum bearing capacity.

Mitigation Action 2: Adoption of a new construction technique (i.e., launching girder) to avoid continuous loading of the soil by the falsework structure.

A theoretical curve for risk reduction and its cost is depicted in Figure 2.7. However, for more precise results, a quantitative risk analysis should be performed. With the first mitigation action, the uncertainty concerning the soil properties is decreased; therefore, a risk reduction at a reduced cost can be achieved. A significant risk reduction can be achieved by Mitigation action two because the adoption of a new construction technique would significantly reduce the error probability of occurrence. However, this mitigation action demands a higher cost than the previous one, because the acquisition or renting cost of a launching girder is considerable.

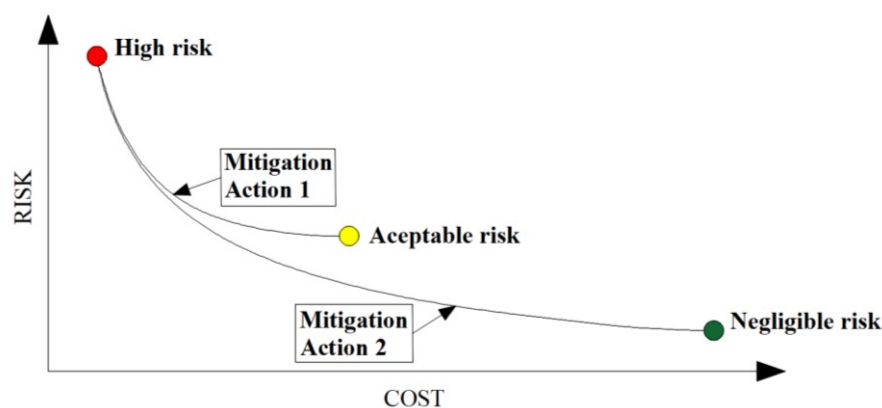


Figure 2.7 – Risk reduction due to the mitigation actions

2.8. Conclusions

Design and construction errors are responsible for about 32% of bridge collapses recorded worldwide; hence, they must be carefully addressed. Given the numerous multidisciplinary activities required for the materialization of any idealized engineering structure into its physical equivalent and the human uncertainties in executing such activities, a screening procedure and assessment of the most important sources of errors are demanded. This work provides a framework for such investigation with conclusive outcomes that allow the design and the construction engineers conceiving the structure to focus their attention on the most relevant errors, and the inspection and the design supervision team to perform enhanced surveillance of the construction works and peer-review of design calculations. The framework for the management of human errors risks implemented in this research work is summarized according to the following consecutive steps:

- a) An initial screening procedure aiming at the identification of the most concerning errors threatening the structural safety of similar structures according to recorded and well-documented failure or collapse cases;
- b) Brainstorming meeting with experts aiming at the identification of errors concerning the ongoing project or any other structural system under assessment;
- c) Qualitative risk assessment of the initially identified errors by a carefully selected group of experts;
- d) Prioritization of the errors according to their expected probability of occurrence and consequence leading to the identification of the risk they represent, according to experts' judgement; and
- e) Definition of mitigation strategies for errors denoting greater risk and benchmark of their benefits with their costs aiming at the implementation of the most efficient ones;

A qualitative categorization of design and construction errors has been performed, considering a qualitative risk assessment of such errors by experts through a survey. Different error risk groups are defined, employing risk matrix and AHP, allowing the prioritization of errors according to their probability of occurrence, consequence and risk. Therefore, a more efficient risk mitigation strategy can be implemented for errors that denote a higher risk for structural safety or construction works, besides overall supervision of the errors that denote lower risks according to standards recommendations. Focusing on the most relevant errors, risk reduction techniques should be effectively implemented, and structural safety easily assured. Errors concerning geotechnical and falsework malfunctioning and the system supporting condition changes throughout different construction stages, as well as reinforcement detailing, are highlighted as the errors with the highest risk.

Furthermore, the impact of three design errors (ID = 4, 13, 17) was numerically assessed in [55] considering a prestressed concrete overpass. Their impact on structural safety reduction was in accordance with the results obtained with the Analytic Hierarchy Process. Their relative consequence, as ranked in Table 2.1, was confirmed. Nevertheless, this was not the case for the consequence of two construction errors (ID = 4, 27) also numerically assessed in the same paper.

Some design and construction errors go undetected or not reported due to legal implications, but they are usually uncovered after failure. Some errors are detected in existing structures given the structural system underperformance, visible deterioration and deficiencies, non-destructive tests and monitoring systems, but still, many of them go undetected. Thus, the assessment of existing structures should employ strategies for the identification of design and construction errors that are likely to lead to the underperformance of the structural system, service life reduction or even structural collapse.

3. Human error impact on the structural safety of a prestressed concrete bridge

"Be a bush if you can't be a tree. If you can't be a highway, just be a trail. If you can't be a sun, be a star. For it isn't by size that you win or you fail. Be the best of whatever you are."
by Martin Luther King Jr.

Neryvaldo Galvão, José C. Matos, Daniel V. Oliveira, Rade Hajdin

Structure and Infrastructure Engineering

Taylor & Francis, Volume 18, Issue 6 –2022

[10.1080/15732479.2021.1876105](https://doi.org/10.1080/15732479.2021.1876105)

Abstract: The economic and social losses due to increasing bridge collapses over the years have underlined the importance of the development of more robust bridge structural systems when exposed to harmful events, such as natural hazards, human-made hazards and human errors. Natural and human-made hazards are usually explicitly addressed in the numerous works available in the literature, but when it comes to human errors, very few studies can be found. It is worth mentioning that human errors have been identified as one of the main causes of bridge failures. Consequently, the main goal of this paper is the assessment of human errors' impact on the robustness and safety of a prestressed concrete bridge through a probabilistic-based approach. Uncertainties concerning the numerical model, material strength, geometry and loading condition are used as key input parameters for the probabilistic assessment. Considering the structural system performance in its early days (i.e., virgin reliability index), the human error impact on structural safety is measured according to the structural system performance reduction given different errors with different magnitudes. Therefore, the structural system's ability to maintain acceptable levels of performance, given such errors, is assessed.

3.1. Introduction

Recent studies have shown that human errors are one of the main causes of failure of high-capacity structures, namely, roadway, railway and footway bridges, when failures during the construction and service phase are concerned [7,8,15]. Therefore, the enhancement of the assessment procedures for the proper safety management of such systems should incorporate the impact evaluation of human errors on the short- and long-term behaviour of structures. The development of an integrated framework, considering deterioration rates, design and construction errors in the robustness assessment of structures, will allow greater accuracy when forecasting their behaviour during their service life, also leading to a better understanding of how the robustness of a structural system can be affected by those factors.

Robustness is defined within the scope of this paper as “the ability of a structure to withstand events like fire, explosions, impact or the consequences of human error, without being damaged to an extent disproportionate to the original cause” [19]. As such, the novelty of this research lies in the quantification of the structural safety reduction given deviations of ideal design properties/characteristics of a structural system due to human errors, considering a probabilistic-based approach to quantify the structural system robustness when exposed to such errors. The structural safety reduction due to damages triggered by human errors will be measured through a robustness index.

3.2. Structural robustness

The robustness concept is here implemented in order to track the structural system performance reduction, from its optimal or flawless design (virgin reliability index) to decreased safety levels due to different errors and increasing their magnitude. A robustness index presented elsewhere [70] is used here to measure the overall performance reduction of each of the deficiencies caused by human errors.

One of the fundamental requirements concerning a structural system's performance is its robustness features, meaning that a structural system should be robust enough to avoid cascading failures or serious performance reduction triggered by extraordinary and unforeseen events like natural hazards, human errors and human-made hazards. Several measurements of robustness can be found in the literature, e.g., Risk-based [71], reliability-based [72,73] and deterministic-based (residual influence factor, and reserve strength ration, among others) [74]. In the literature, such measures are mostly dealing with sudden events, but they are not restricted to them. Cavaco et al. [75] suggested a robustness index aiming to avoid the lack of sensitivity of some of the previously mentioned measures of robustness that do not take into account the gradual development of damages caused by, for instance, increasing

corrosion. Such characteristic makes it suitable for an analysis where gradual safety reduction is concerned since it establishes robustness as a function of damage intensity.

The proposed index for this paper (Cavaco index) is established based on the area of a normalised performance function $f(x)$ that describes the system performance between a normalised damage magnitude, given according to Eq. (3.1). The normalisation of the performance function is based on the highest performance level of the system. Within this approach, the performance function itself can be set based on a deterministic, probabilistic or risk-based formulation.

The performance of the system will, further on, be measured by the reliability index reduction as a function of design and construction errors increasing magnitude. Since the partial safety factors available in current semi-probabilistic standards do not consider human error uncertainties in the design and construction phase, a probabilistic approach is an important step in this framework since it will allow the benchmarking of current safety levels of the structures, bearing some deficiencies triggered by human errors, with safety threshold's values (target reliability index) established within the engineering community.

According to different types of damage, the system can display different levels of robustness (see Figure 3.1). Within this work, the performance function for robustness quantification will be set based on the reduction of the structural system virgin reliability index with increasing error magnitude.

$$I_R = \int_{D=0}^{D=1} f(x) dx \quad (3.1)$$

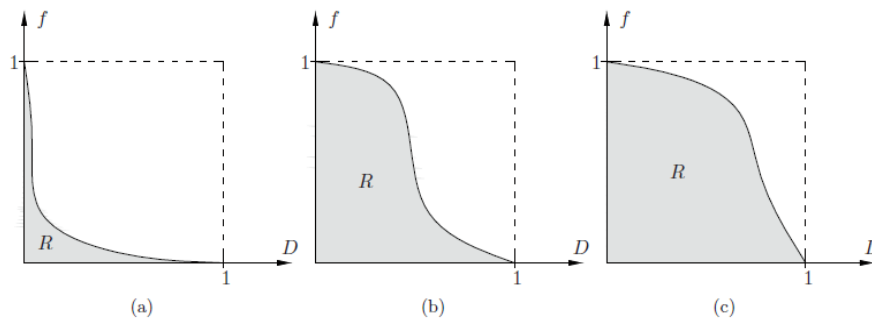


Figure 3.1 – Cavaco robustness index for a structural system of (a) lower, (b) medium and (c) higher robustness [76]

3.3. Numerical modelling and non-linear analysis

A prestressed concrete bridge is introduced, modelled and analysed to assess further the impact of different design and construction errors, carefully selected from the literature [77]. Bearing in mind the large diversity of design and construction errors that can, to a short or large extent, damage a structural system, a parametric model was suggested aiming for easy control of the model's main properties so that errors could be modelled and assessed further on. Aiming the characterisation of the structural system performance a 2D finite element model is developed in DIANA FEA [78] using phased analysis and non-linear material constitutive models in order to compute its maximum load-carrying capacity.

3.3.1. Case study description

The case study is a 3-span overpass with an overall length of 67.80 m (Figure 3.2). The deck transversal cross-section is shaped by three “I” shape precast and prestressed girders plus a cast-in-situ concrete slab in its spans (Figure 3.3a – left side). Over the piers, the deck is shaped by the concrete slab coupled with pier caps (Figure 3.3a – right side). The prestressed concrete structure was mainly designed according to Portuguese regulations for reinforced and prestressed concrete structures. However, when the regulation is omissive, the Eurocode is employed.

The in-situ cast elements (i.e., slab, pier caps, bearing beams and piers) were cast with a C30/37 concrete. The girders were precast with a C45/55 concrete and prestressed with pre-tensioned strands (i.e., Y 1860 S7 15.2) spread in their lower and upper flanges in three different layers, with an additional layer in the girders of the middle span (Figure 3.3b). The case study was designed under the exposure class XC4 from Eurocode 2 [79]. The continuity of the deck over the piers is only ensured by the conventional steel reinforcements (i.e., S500 NR SD) found in the in-situ cast slab and the precast girders. With 15 m height, the piers of the overpass are supported by a deep spread foot foundation placed more than 3 m below the road platform. The piers cross-section is displayed in Figure 3.3c.

For the construction works, two main static systems were set; thus, two construction phases are considered for the structural analysis; one where the prestressed girders are simply supported over the piers and abutments; and another where the slab and the pier caps are cast together and connected to the girders. In the first phase, no hyperstatic forces are immediately developed due to the prestress forces since the girders are pre-tensioned. Although not considered in this study, long-term effects are expected to lead to the development of hyperstatic forces due to the differential loading of the deck components and creep effects. During the second phase, the deck becomes rigidly connected to the piers through the pier caps. The deck, shaped by the girders connected through dowels to the slab, is supported over the

abutment by bearing devices supporting the bearing beams with 1.75 m height (opposing to 3.0 m height of the pier caps) that is handing over the loads in the deck to the bearing devices.

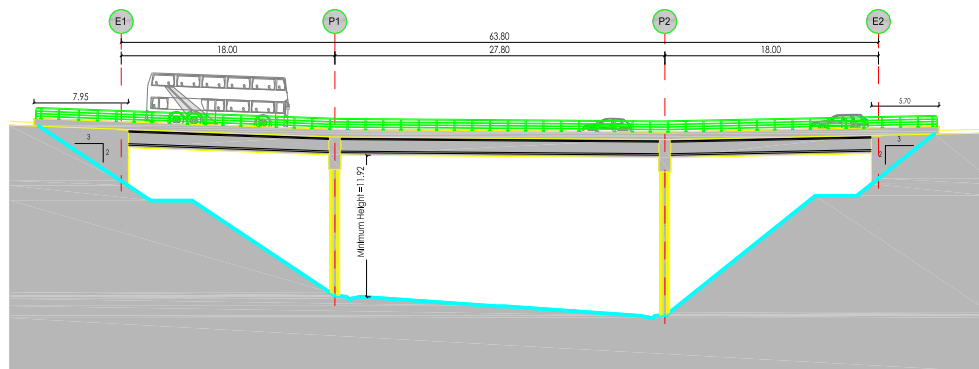


Figure 3.2 – Case study longitudinal profile [80]

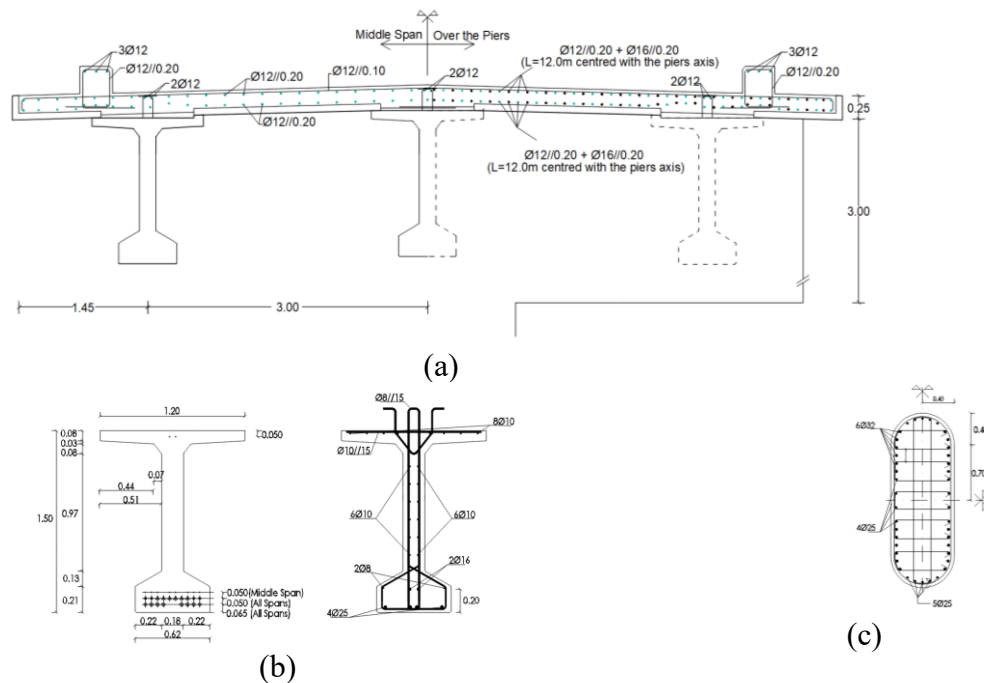


Figure 3.3 – Transversal cross-section and reinforcement layout of (a) deck, (b) girders and (c) columns (measurement unit: meters) [80]

3.3.2. Numerical modelling

The numerical model was developed following the structural design plans and drawings of the case study. Within this work, a two-dimensional class-II beam element with two nodes and three degrees of freedom per node plus an additional elongation variable is considered for prestressing effects. The beam element basic variables are the translation u_x (length), u_y (height) and the rotation ϕ_z , plus the additional variable Δu_x (representing the relative elongation of the beam element). Such an element encompasses numerical integration along its axis and the defined transversal cross-section (see Figure 3.4 and Figure 3.6), but it does not consider shear deformations. Accordingly, this numerical element is commonly used

for material and geometric non-linear analysis of straight elements [81]. More sophisticated numerical elements are available; however, their high computational cost was considered not suitable for the number of required analyses within the probabilistic calculations. A mesh optimisation procedure was considered in order to optimise the numerical model computational costs.

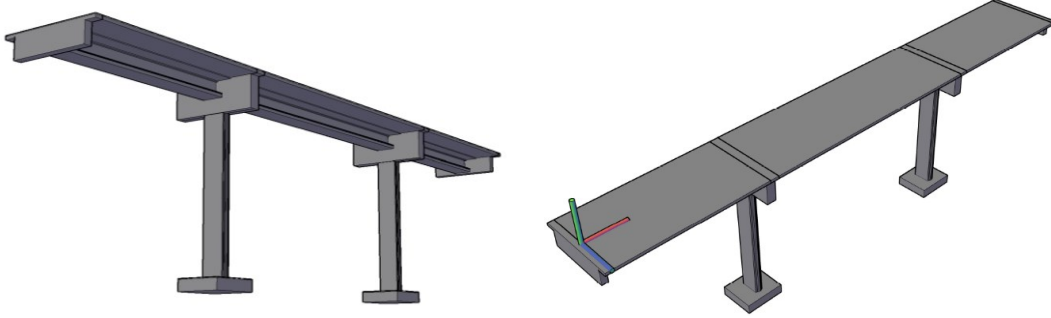


Figure 3.4 – Geometry overview

The non-linear material models of concrete and steel reinforcement were taken from Eurocode 2 [79,82]. The concrete constitutive model (Figure 3.5a) is characterised by the tensile strength f_{ctm} , compressive strength f_c for a compressive strain ϵ_{c1} , elasticity modulus E_{cm} and a maximum compressive strain ϵ_{cu} . The steel reinforcement constitutive model (Figure 3.5b) is characterised by the elastic stress limit $f_{sp,\theta}$ for a elastic strain limit $\epsilon_{sp,\theta}$, maximum stress level $f_{sy,\theta}$, elasticity modulus $E_{s,\theta}$, yielding strain $\epsilon_{sy,\theta}$, and a maximum strain $\epsilon_{st,\theta}$.

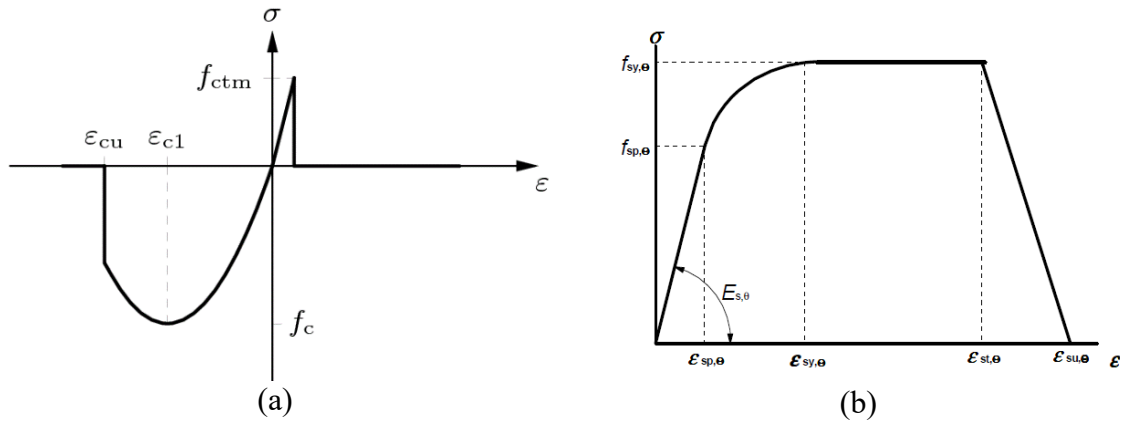


Figure 3.5 – Materials constitutive models: (a) Concrete and (b) Steel Reinforcements [83]

Given the different types of concrete and reinforcements used to build the model, each of the main parameters necessary to describe their behaviour are summarised in Table 3.1 and Table 3.2. Mean values are used here in the first deterministic analysis since the design verification is not the main goal of this work. Such values are available in Eurocode 2 [79] and the Probabilistic model code [84]. For the reinforcements, an elastic-plastic behaviour was considered ($f_{sp} = f_{sy}$).

Table 3.1 – Concrete main parameters

	E_{cm} (Gpa)	f_{ctm} (Mpa)	f_{cm} (Mpa)	ϵ_{c1} (‰)	ϵ_{cu} (‰)
C30/37	33	2.9	38	2.2	3.5
C45/55	36	3.8	53	2.4	3.5

Table 3.2 – Reinforcement main parameters

	A500 NR SD	Y 1860 S7 15.2mm
ϵ_{sp} (‰)	2.8	6.45
ϵ_{sy} (‰)	20.0	20.0
ϵ_{st} (‰)	150.0	50.0
ϵ_{su} (‰)	200.0	100.0
E_s (Gpa)	200.0	195
f_{sp} (Mpa)	560.0	1644.24
f_{sy} (Mpa)	560.0	1644.24

The structural system is assessed considering dead loads, prestressing forces and live loads, applied in two different phases. The prestressing forces and most of the structure self-weight (in-situ slab and precast girders) are applied during the first stage, where the deck was considered simply supported over the three spans. The remaining dead loads (bituminous pavement, guardrails, and sidewalks, among others) and the live load are applied at the second stage, where the deck is considered rigidly connected to the piers, therefore, changing the load distribution configuration.

Normally, there are different types of live loads acting on the structure, namely road and pedestrian traffic, wind, temperature, snow and others. Nevertheless, for common short and medium-span bridges, road traffic and their dynamic effects are the relevant ones. Road traffic loads may vary between different bridges depending on their composition (e.g., percentage of lorries), density (e.g., the average number of vehicles per year), condition (e.g., jam frequency), extremely likely weights of vehicles and their axle loads, and, if relevant, the influence of road signs restricting carrying capacity [62]. Therefore, the quantification of the volume and intensity of traffic using measurements from Weight-in-Motion systems would allow a real estimation of the loads the bridge is subjected to.

However, for this investigation, the traffic load was estimated according to the load model (LM1) from Eurocode 1, considering the provided characteristic axle load (Q_k) and the distributed load (q_k) given in Figure 3.6. Such values correspond to a probability of exceedance of 5% (or 95th percentile) in 50 years, assuming a normal probabilistic distribution function (PDF) with a coefficient of variation (CoV) equal to 15%, as recommended by Matos et al. [85]. Based on these assumptions, the axle load and distributed load mean values were defined. The LM1 already takes into account dynamic amplification effects [62].

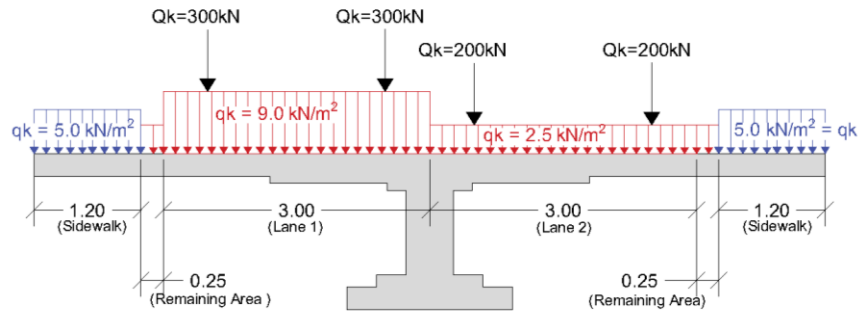


Figure 3.6 - Equivalent transversal cross-section loaded by load model 1

In order to determine the critical location of the load, two main cross-sections were considered, namely the larger span middle cross-section (for the sagging moment) and the cross-section over the piers (for the hogging moment). After computing the load-bearing capacity of the structure for both cross-sections, considering their respective critical loading positions, it was found that the middle span cross-section was the critical one since the structure failed for a lower load factor.

3.3.3. Structural non-linear analysis

The structural system analysis was detailed in Figure 3.7 and Figure 3.8 till the concrete crushing (3.5%) in the upper layer of the critical section (according to the stress-strain curve displayed in Figure 3.8a) after reaching the deck plastic bearing capacity, i.e., after the development of a plastic hinge in the critical section (middle span middle cross-section - Figure 3.8c) and the cross-section over the piers. Nevertheless, the full rotation capacity of the cross-sections over the piers was not fully explored (Figure 3.8d). In summary, the maximum carrying capacity of the bridge was determined by the longitudinal redistribution capacity of the bridge deck.

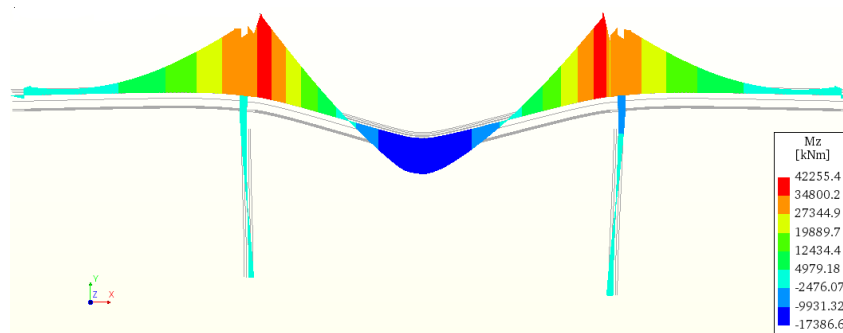


Figure 3.7 – Bending moment diagram for the maximum load factor

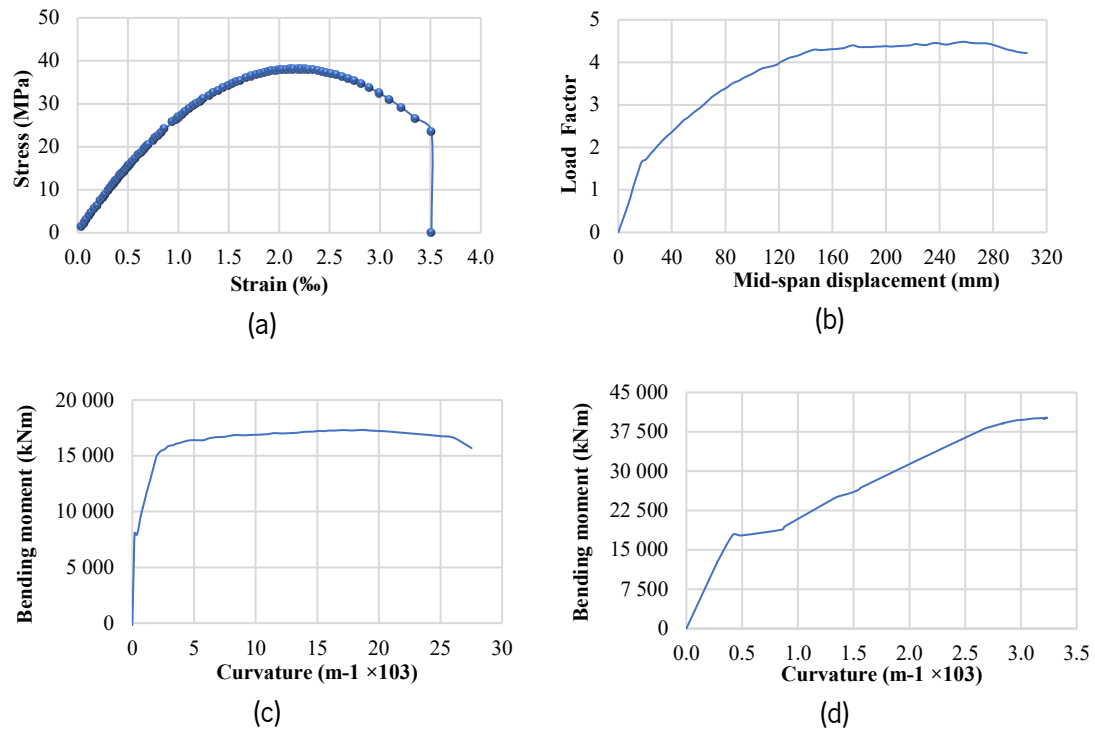


Figure 3.8 – Critical cross-section (a) strain – stress, (b) mid-span displacement – load factor, (c) curvature – bending moment curve and (d) cross-section over pier curvature – bending moment curve

The load-displacement curve (Figure 3.8b) shows a stiffness reduction close to a load factor of 1.71 due to concrete cracking in the critical cross-section for a bending moment of 8068.79 kNm. The cracking of the concrete takes place given the occurrence of tensile strains greater than concrete tensile strength (f_{ctm}), according to Figure 3.5a. Such stiffness reduction is followed by further reductions till the yielding of the reinforcement in the same cross-section and the cross-sections over the piers. The maximum bearing capacity of the structure occurs for a load factor of 4.48, which is equivalent to an increase of the LM1 by 4.5 times. The critical section's maximum bending capacity is recorded at 17386.6 kNm, according to the bending moment diagram and moment-curvature curve displayed in Figure 3.7 and Figure 3.8c), respectively. Thus, the structural system carrying capacity can be characterised by the computed maximum load factor when the deck failure due to bending is concerned, and the failure is governed by the strength of the materials in its ultimate limit state (ULS: STR).

Furthermore, it is important to emphasise the fact that a conventional cross-section analysis where the structural capacity is characterised by the critical section plastic moment, neglecting the structural system redistribution features, would lead to an underestimation of the system bearing capacity in approximately 20%. Meaning that the redistribution capacity of the structural system plays a significant role in its carrying capacity since after the plastic capacity of the critical cross-section (Figure 3.8c) is

reached, the load factor is further increased from 3.6 to 4.5 given the redistribution to the cross-section over the piers (Figure 3.8d).

3.4. Probabilistic based assessment

Numerical models are developed considering decisive parameters for a reliable prediction of systems performance; models shaped by sub-models such as (a) action models, (b) geometrical models, (c) material models and (d) mechanical models [84,86]. Nevertheless, such models are a mathematical or physical, simplified idealisation of the real phenomenon. Therefore, successful attempts to model reality bring uncertainties inherent to the limitations of models and accepted or required simplifications.

Having characterised the case study through deterministic models, important uncertainties (i.e., aleatoric and epistemic) inherent to the models should now be considered for a probabilistic characterisation of the system response and its safety levels by means of reliability index or probability of failure.

3.4.1. Resistance uncertainties

During the design stage, some uncertainties are treated in design codes by characteristic values and partial safety factors (semi-probabilistic approach). Some other uncertainties are dealt with by using quality control measures, design checks and construction supervision to reduce and avoid human performance uncertainties. In order to perform a probabilistic analysis, uncertainties must be considered through well-characterised random variables considering the available information in the literature and experimental data. Therefore, in order to assure a reliable statistical characterisation of the structure's ultimate load-bearing capacity, the following resistance uncertainties are characterised: (i) geometric uncertainties (ii) material uncertainties and (iii) model uncertainties. At a further stage, (iv) human errors will be introduced.

Geometric uncertainties, usually considered due to expected geometric imperfections to take place during the construction or production of a structural element, are also relevant. Imperfections in manufactured concrete elements are understood as being the deviations of the design values of the shape and dimension of cross-sections, positioning of reinforcements (e.g., stirrups spacing and longitudinal reinforcement), horizontality and verticality of concrete elements and alignments or spatial positioning of columns and girders. Such deviations should fall within the acceptable aleatory space (or tolerances) established by quality control standards; otherwise, such uncertainty should be considered a construction error (human errors). Several factors affect the statistical parameters that characterise this source of uncertainty, namely, type of structural element (slab bridge, I-girder bridge, box girder), construction

process (precast, in-situ, launching girders), quality control for execution, and time constraints, among others. For the probabilistic assessment proposed here, the deck slab thickness is assumed as a random variable with a CoV of 3.5%, as recommended in the Probabilistic Model Code [87]. The reinforcement cross-section area is also addressed with a CoV of 2% [84].

The material properties of a structural system can vary randomly in space and time; however, time is not explicitly addressed. Concerning spatial variability, the strength of a material in one segment of the structure is likely to be different from a different segment of the same structure within the acceptable and standardized random field. Any material is usually characterised by a constitutive law (e.g., elastoplastic model or non-linear model, among others) and random variables (e.g., strength and modulus of elasticity) that define the mathematical model. Here, the following random variables are considered for concrete material uncertainty: i) compressive strength, f_{cm} ; ii) tensile strength, f_{ctm} ; and iii) modulus of elasticity, E_{cm} . For the conventional and prestressed reinforcement, the yielding (f_{sy}) and strength (f_{sp}) are considered according to the statistical properties presented in Table 3.3.

Table 3.3 – Random variables considered for material and geometry probabilistic characterisation

ID	Description	Random Variables	Notation	Mean Values	CoV	PDF	Reference
1	C30/37	Compressive strength	f_{cm}	38 MPa	12%	Normal	[87]
2		Tensile strength	f_{ctm}	2.9 MPa	20%	Normal	[84,87]
3		Modulus of elasticity	E_{cm}	33 GPa	8%	Normal	[87])
4		Deck slab thickness	e	25 cm	3,5%	Normal	[89]
5	C45/55	Compressive strength	f_{cm}	53 MPa	9%	Normal	[87]
6		Tensile strength	f_{ctm}	3.8 MPa	20%	Normal	[79,87]
7		Modulus of elasticity	E_{cm}	36 GPa	8%	Normal	[87]
8	S500B	Yielding stress and strength	f_{sy} e f_p	560 MPa	5.4%	Normal	[84]
9		Reinforcement cross-section area	A_s	–	2%	Normal	[84]
10	S1670/1860	Yielding stress and strength	f_{sy} e f_p	1644 MPa	2.5%	Normal	[84,87]
11		Prestress tension	σ_p	1087 MPa	1.5%	Normal	[87]
12	C30/37 and C45/55	Concrete self-weight	γ_c	25.8 kN/m ³	8%	Normal	[84,87]

Model uncertainties address the so-called epistemic uncertainties since it takes into account the numerical model accuracy in predicting a real phenomenon. Two types of model uncertainty can be found, specifically, the uncertainty concerning the accuracy of an equation in predicting experimental data

(e.g., the idealised stress-strain relationship of the material) and the uncertainty concerning how a structural model (e.g., wire, shell and solid elements) can predict the structural behaviour [90]. Recommended values and PDF for model uncertainty for a more or less standard structural finite element model can be found in the Probabilistic Model Code [84]. In general, such uncertainty can be introduced as follow, according to Eq. (3.2),

$$R = \theta_R \cdot f(f_{cm}, A_s, f_{sy} \dots A_c, d) \quad (3.2)$$

where R is the parameter that measures the resistance of the structure, θ_R represents the model uncertainty probabilistic distribution, f is the resistance analytical model or numerical model, and $f_{cm}, A_s, f_{sy}, A_c, d$ are the resistance critical random variables.

Considering that the model function f is frequently not 100% accurate, the outcome R is predicted with an error even if the values of the basic random variables are known. Thus, the real outcome can be computed by introducing the variable θ_R , which accounts for the resistance model function f deviation from the real outcome R , due to negligence of 3D effects, simplification of connections, inhomogeneities, etc. The model uncertainty θ_R PDF considered for this work, bearing in mind the case study static bending resistance, is a lognormal distribution function of mean value 1.2 with a CoV of 15%, as recommended in the Probabilistic Model Code [84]. However, different values are recommended by other authors in Sykora et al. [91] and Holický et al. [92] (mean value $\cong 1.0$ and a CoV = 10%), Melchers and Beck [64] (mean value = 1.02 and a CoV in the range 3%-4.6%) and Nowak [93] (mean value = 1.01 and CoV = 6%). Given the numerous material and finite element models available to numerically assess the flexural capacity of a structure, a scatter in model uncertainties statistical parameters is to be expected since it is dependent on the model itself.

Uncertainties due to the correct or erroneous performance of a task by a human or uncertainties related to the knowledge and experience of an engineer [54] are imperative to be considered when safety is a concern, considering that experts have underlined human errors as being responsible for a considerable number of failures [7,14]. Within the scope of this work, design and construction errors' impact on structural safety will be further addressed in chapter 3.5. Design and construction errors are usually mitigated or minimised through design checks and construction supervision, respectively. These are commonly used quality control techniques for assurance of uncertainty reduction.

From the probabilistic point of view, a human error has taken place when the recorded value or occurrence goes beyond the acceptable deviations allowed by the regulations. These are the incidents

with deviations greater than those that would fall within the PDF with the mean value and CoV given for a certain random variable; see also Table 3.3. The deviation might have a positive or negative effect on the resistance of the structure. Within this work, unfavourable effects are mostly investigated. Discussion regarding the development of human error probabilistic models can be found in De Haan et al.[94], Lind [95], Nessim and Jordaan [96], Stewart [97,98] and Stewart and Melchers [99] and Vrouwenvelder et al. [100].

3.4.2. Sensitivity analysis

A probabilistic analysis is usually preceded by a sensitive analysis aiming at the reduction of the number of random variables initially selected according to expert judgement. This preceding analysis is essential to reduce probabilistic computational costs, which are very much dependent on the number of random variables under consideration. The sensitivity analysis aims at the quantification of each random variable influence in the structural response or output parameter of interest. The importance of each random variable can be computed according to Eq. (3.3),

$$b_k = \sum_{i=1}^n \frac{|\Delta y_{i,k}|}{y_{m,k}} / \frac{\Delta x_{i,k}}{x_{m,k}} \cdot COV[\%] \quad (3.3)$$

where b_k measures the importance of the random variable k , $\Delta y_{i,k}$ quantifies the structural response (i.e., maximum load factor) variation given a deviation $\Delta x_{i,k}$ to the random variable k mean value $x_{m,k}$. $y_{m,k}$, is the average response, and n is the total number of deviations given to the random variable. The importance measure is standardized using its highest computed value.

The computed importance measure of each random variable is graphically displayed in Figure 3.9 according to their identification number (ID). A threshold value of 10% is used to classify the random variables as being essential or nonessential for the probabilistic analysis [85]. Therefore, the following random variables were considered for further investigation: i) yielding stress and strength of the conventional reinforcement (ID = 8); ii) reinforcement cross-section area (ID = 9); iii) yielding stress and strength of the prestressed reinforcement (ID = 10); iv) girder's concrete compressive strength (ID = 5); v) deck slab thickness (ID = 4); and vi) slab's concrete compressive strength (ID = 1).

The random variable with the highest importance measure was the yielding stress of the conventional reinforcement, as reported in the literature for ductile structures [85,101,102]. Nonetheless, one must keep in mind that the ratio between the conventional reinforcement and prestressed reinforcement cross-section area is an important factor to be taken into account since such ratio, in the deck transversal cross-section close to the piers is 3.39 and in the critical cross-section is 1.89.

Consequently, it is reasonable to expect a greater importance factor for the yielding strength of conventional reinforcement than the yielding strength of prestressed reinforcement.

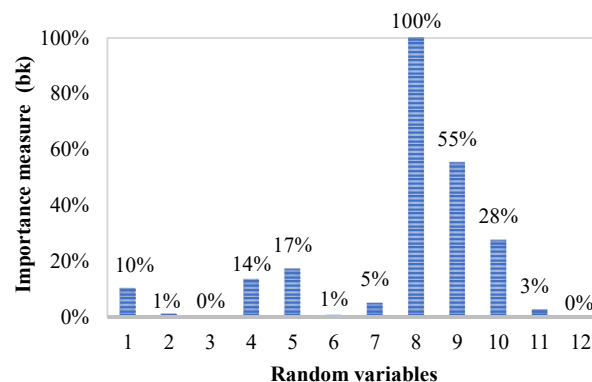


Figure 3.9 – Random variables importance measure

3.4.3. Virgin reliability index

After a careful selection of the relevant random variables, a probabilistic analysis is performed to explicitly investigate and quantify the uncertainties effects in structural safety by means of a virgin reliability index β . The virgin reliability term was introduced by Hajdin et al.[17] and also discussed by Hajdin [103]. This safety measure will be computed according to Eq. (3.4).

The computation of the reliability index requires the characterisation of the PDF of the structural system resistance in its ultimate limit state. Employing the LHS technique [104–106] to reduce the number of required simulations to achieve a reliable estimation of the mean value and CoV of the resistance curve, 100 samples of the numerical model were generated. The number of simulations considered shall provide estimations with an average error of 10% and uncertainty of 1%, according to Schuyler's rule [107].

Each one of the generated models is analysed using DIANA FEA to extract their maximum load-bearing capacity measured through load factors. The model uncertainty was considered afterwards. Note should be made to the fact that the random variables were considered to be statistically independent, or not correlated, since the selected random variables from the sensitivity analysis, aiming probabilistic computational costs reduction, lead to non-consideration of the statistically dependent variables, such as concrete compressive and tensile strength, and modulus of elasticity. The outputs of this procedure are displayed in Figure 3.10a, where the load-displacement curve of each sample can be observed, as well as in Figure 3.10b, where the histogram of the maximum load factors and the normal PDF is used to fit the data. The goodness-of-fit is confirmed by the Kolmogorov Smirnov test [56,64].

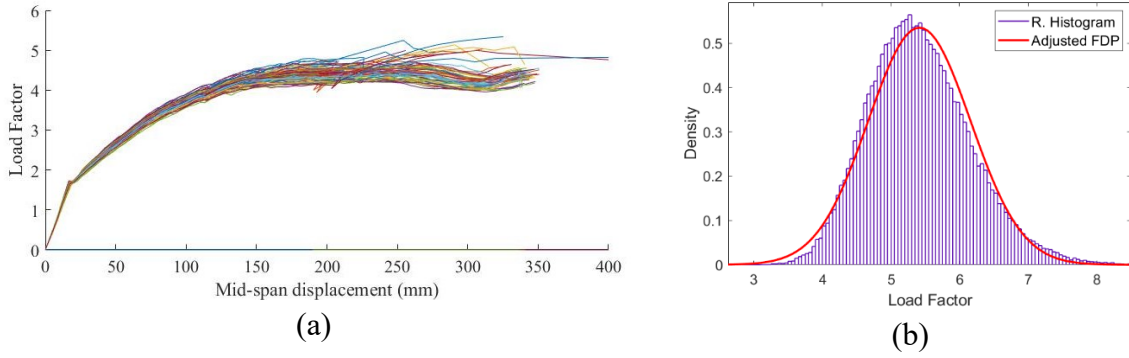


Figure 3.10 – (a) Load-displacement (mm) curve of each generated sample and (b) Maximum load factor probabilistic distribution

Considering that the resistance distribution is defined by means of load factors of the defined live load, a resistance PDF with a mean value (μ_R) of 5.41 and standard deviation (σ_R) of 0.746 was achieved. Thus, the load distribution can be defined by a distribution curve with a mean value (μ_s) equal to one and a standard deviation (σ_s) of 0.15, since the resistance is quantified as a function of the LM1. Hence, the limit state function can be defined as $G = R - S = 0$ where the failure of the system takes place for $R < S$ or $G < 0$.

The reference period for which the load is assessed (50 years) is of seldom relevance since it determines the reference period for which the reliability index is calculated (e.g., annual reliability or lifetime reliability) [19,20]. Thus, the reliability index is computed for the considered reference period according to:

$$\beta = \frac{\mu_R - \mu_s}{\sqrt{\sigma_R^2 + \sigma_s^2}} = \frac{5.41 - 1}{\sqrt{0.746^2 + 0.15^2}} = 5.80 \rightarrow P_f = 3.41 \times 10^{-9} \quad (3.4)$$

Nonetheless, Eq. (3.4) provides an exact solution only when the random variables are normally distributed and uncorrelated. Additionally, the limit state function must be defined as a linear function where $G = R - S$. Thus, some limitations are associated with such an approach since such restrictions are not always the real characteristic of the problem at hand but rather a simplification of the problem. More sophisticated techniques can be used, such as approximation or gradient methods (i.e., FORM and SORM), simulation-based methods (i.e., monte Carlo simulation, importance sampling, and subset simulation, among others), or metamodel-based methods (e.g., response surface, kriging, and artificial neural networks, among others) where computationally less expensive models than real numerical model are generated [108]. Either way, one must keep in mind the limitation of each method and choose the

suitable one for the problem at hand, benchmarking the accuracy of the solution, the required computational effort and the adequacy of the method to the problem.

3.4.4. Safety assessment

In structural design codes and international standards, structural safety is guaranteed by designing the structural system components so their reliability levels, measured by the reliability index, are greater than the target reliability (β_T) index, according to Eq. (3.5):

$$\beta \geq \beta_T \quad (3.5)$$

Such threshold values are established based on economic optimisation procedures (cost of consequence, cost of safety, reference period), and acceptance criteria defined according to countries' life quality index (LQI). These threshold values for the design of new structures differ from the target values for the assessment of existing structures, even though this is not the case for many countries. The motivation for such difference relies on the fact that more detailed information is available for existing structures (reduced uncertainties), and the cost of safety is relatively higher than the cost for the same safety improvement during the design phase. Less restrictive target values are recommended in ISO 13822 [21] for existing structures. Since the case study was modelled as designed (not as-built), design target values are considered.

According to Eurocode 0 [19], the minimum values for safety target values for ULSs are given for 50 years reference period and a 1-year reference period (see Table 3.4). More detailed information for reliability target values is given in Probabilistic Model Code [20] and ISO 2394 [22], where different consequence levels are associated with the cost of safety measures for a reference period of 1 year. The consequence of an unforeseen failure of the structure under assessment is considered to be medium according to consequence classes provided in Eurocode 0, which stands for a reliability class 2 (RC2). Therefore, the suitable target reliability index considered here is 3.8.

Table 3.4 – Recommended minimum reliability indexes for ULSs [19]

Reliability Class	Minimum values for β	
	1 Year Reference period	50 Years Reference period
RC3	5.2	4.3
RC2	4.7	3.8
RC1	4.2	3.3

In semi-probabilistic structural design codes such as Eurocodes [19], the target reliability index and therefore, the partial safety factors are set for structural components. However, structural systems designed accordingly may exhibit reliability levels beyond their components due to internal redundancies

(redistribution capability) of the structural system. Such features of the structural system were considered for the computation of the reliability index given in Eq (3.4). The failure of individual components is often linked to significantly lower consequences when compared to system failure. Therefore, some considerations should be made for the adaptation of target values for system reliability. In Sykora et al. [35], it is recommended to increase the target reliability index in 0.5 when the reliability of a system or its key component is verified. Therefore, the target reliability index is increased to 4.3, which is lower than the computed reliability index. As a result, safety is verified.

Notwithstanding the importance of defining a target reliability level, it should be noted that target reliability levels do not necessarily reflect the actual frequency of failure since such frequency is significantly dependent upon human errors, which are not covered by the target reliability values nor by the partial safety factors provided in design codes. Nonetheless, such inconvenience is tackled in Eurocode 0 [19] through quality control measures aiming at the reduction of errors in the design and in the execution of the structure. In the design phase, to ensure the structural design is performed according to standards' safety guidelines, and in execution, to ensure the as-built structure provides the designed resistance, design supervision levels and inspection levels for execution are provided in Eurocode 0 [19] with specific recommendations for each of the reliability classes given in Table 3.4.

3.5. Robustness analysis

The virgin reliability index computed considering the case study as designed doesn't necessarily represent the reliability of the structure as-built, due to execution errors that are likely to take place during the construction phase. Therefore, this section is dedicated to the assessment of the impact of different errors with increasing magnitude on structural safety. Here the robustness analysis intends to quantify the structural ability to sustain damages, i.e., to quantify performance reduction given some deficiencies introduced to the structure by design or construction errors. Errors are considered as being the cause of structural damage, and damages are the effect of errors in the structural system or a structural element; therefore, this two will be used interchangeably. Nonetheless, the performance measure to be considered is the reliability index, and the performance function should be carefully defined so a complete safety reduction spectrum can be drawn. The robustness index will be computed according to Eq. (3.1) [75].

3.5.1. Modelling design and construction errors

The design and construction errors selected for the robustness analysis were retrieved from Galvão et al. [109], where the most common design errors (DE) and construction errors (CE) are listed for the type of bridge under study in this work. Three main criteria are used to select the errors described in Table 3.5,

namely; i) the ease of modelling the damage caused by the error; ii) the adaptability of the error to the case study; iii) the risk associated with each error. The risk of each error is qualitatively assessed by Galvão et al. [109], considering two indicators, namely, the likelihood of occurrence and consequence. Ideally, a construction report (neglecting legal implications) identifying the magnitude and the exact location of the damages caused by the errors should be considered.

Currently, few studies can be found on error types, frequency and their magnitude in the design and construction process. Given the quality control procedures usually employed, petty errors (common errors) are likely to be eliminated. On the other hand, black swan errors (highly improbable errors) are the most dangerous and usually take place due to a very unlikely sequence of events. Nonetheless, the approach proposed here is adequate for petty errors, which are of moderate interest since they do not endanger structural safety immediately unless an accumulation of such errors has taken place.

Concerning the error in dead load quantification, a decimal mistake when introducing loads in structural analysis software followed by non-verification of the reaction forces is a possible error scenario. The verification of the reaction forces is a common procedure in the design phase used to ensure the loads were correctly introduced and considered for structural design. Mistaken detailing drawings of reinforcement are common scenarios leading to the misplacement of reinforcements. Consequently, deficient reinforced structural components are built without complying with the safety requirements demanded by a successfully performed structural design.

Table 3.5 – Errors leading to the damages considered for the robustness analysis

Damages	Errors leading to damages under analysis	Error type
1	Error in dead load quantification	DE
2	Error in the definition of the reinforcement cross-section area	DE
3	Error in the definition of the soil-structure interaction	DE
4	Error due to insufficient prestressing force	CE
5	Error due to poor concrete workmanship and manufacturing leading to concrete with characteristics and properties different from the ordered	CE

Regarding the soil-structure interaction, several uncertainties are associated with soil behaviour when wrongly addressed. Foundation rotations, differential settlements, support condition stiffness and geotechnical failure, are issues that require careful evaluation from experts but sometimes are not thoroughly addressed, leading to deviations from the assumptions considered during the design. The insufficient prestressing of cables caused by mistaken measurement of the forces applied to the cables due to mechanical deficiency of the prestressing equipment or anchorage is a possible error scenario.

Factors such as water-cement ratio, concrete vibration, curing of concrete, and temperature, among others, might influence the strength of the concrete. Thus, if wrongly addressed, the concrete strength is deeply affected.

To model the damages caused by the errors, Table 3.6 identifies the numerical parameter suitable for each damage scenario. The damages were modelled mostly deterministically since it is very hard to characterise them probabilistically. However, when the damage is modelled through random variables used during the probabilistic analysis, the uncertainty inherent to the variable (e.g., geometric or material uncertainty) is kept, avoiding uncertainty reduction by decreasing the number of random variables used in the numerical model. Thus, the damages are modelled by deviating the mean value of the random variable.

Table 3.6 – Damages magnitudes used for the robustness analysis

Damages	Numerical parameters	Damage magnitude			
Damage 1	$G_{k1} = 98.97 \text{ kN/m}$	$1.15 G_k$	$1.45 G_k$	$1.75 G_k$	$2.00 G_k$
	$G_{k2} = 56.16 \text{ kN/m}$				
Damage 2	$A_{s1 \text{ y sup}} = 54.3 \text{ cm}^2$	$0.85 A_s$	$0.55 A_s$	$0.25 A_s$	$0.0 A_s$
	$A_{s1 \text{ inf}} = 49.8 \text{ cm}^2$				
	$A_{s2 \text{ y sup}} = 142.7 \text{ cm}^2$				
	$A_{s2 \text{ inf}} = 138.2 \text{ cm}^2$				
Damage 3	d_s	5 cm	10 cm	15 cm	20 cm
Damage 4	$\sigma_{p1} = 1046.25 \text{ MPa}$	$0.85 \sigma_p$	$0.55 \sigma_p$	$0.25 \sigma_p$	$0.0 \sigma_p$
	$\sigma_{p2} = 1087.05 \text{ MPa}$				
Damage 5	$f_{cm, C30/37} = 38 \text{ MPa}$	$0.85 f_{cm}$	$0.55 f_{cm}$	$0.3 f_{cm}$	$0.2 f_{cm}$
	$f_{cm, C45/55} = 53 \text{ MPa}$				
Multiple Damages	$G_{k1} \text{ e } G_{k2}$	$1.15 G_k$	$1.45 G_k$	$1.55 G_k$	
	d_s	5 cm	10 cm	11 cm	
	$f_{cm, C45/55} \text{ and } f_{cm, C30/37}$	$0.85 f_{cm}$	$0.55 f_{cm}$	$0.45 f_{cm}$	

The damage 1 was simulated by increasing the dead load employed, during the cast of in-situ elements (self-weight, G_{k1}) and applied afterwards (remaining permanent loads; G_{k2}). Despite the consideration of equal percentage deviation in G_{k1} and G_{k2} , an equal absolute deviation in G_{k1} should have a greater impact on safety reduction because the deck is simply supported when the G_{k1} is applied, concentrating most of the sagging moment in the critical cross-section, which is not the case for G_{k2} . The damage 2 was introduced by reducing the reinforcement area (A_s) in the critical cross-sections (i.e., maximum hogging and sagging moments). However, only the slab reinforcement was reduced since the likelihood for error occurrence is greater on the construction site when compared to precast elements (e.g., precast girders). Note should be made to the fact that the tensile reinforcement area reduction in precast girders would have a greater impact on resistance reduction. The damage 3 was modelled by

introducing differential settlements (d_s) on the structural system columns, incremented linearly with the self-weight loading, adding additional sagging moment to the pier where the settlement is applied and residual hogging moment to the other pier.

The insufficient prestress (σ_{p2}) of the prestressed reinforcement, labelled as damage 4, is modelled by reducing the prestressing stress applied to the girders. It is important to highlight that the prestressed tendons area was maintained. The concrete quality is assessed here, bearing in mind its compressive strength (f_{cm}). As it is well known, bridge collapse is often preceded by more than one design or construction error, unless a very serious error has taken place. Hence, the analysis should also encompass the accumulation of different errors. Hence, a multiple damages scenario caused by multiple errors is also considered.

The damages caused by errors can take a wide range of magnitude. It is very difficult to justify the magnitude of an error if it has not been measured. Nevertheless, investigations published in Froderberg and Thelandersson [54] addressing human errors reported column loads differed by a factor of three for vertical loads and a factor of two for horizontal loads, considering the lowest and highest suggested value obtained from a round-robin investigation considering 16 independent structural engineers engaged on the design of specific columns (vertical loads) and shear walls (horizontal loads). Therefore, for the robustness analysis proposed, the magnitudes of the errors are varied, between what is here considered as a minor and major magnitude. Such consideration aims to provide an overall view of the structural system sensitivity to the magnitude of such errors within the range of absolute values displayed in Table 3.6. Nonetheless, with proper design supervision and construction supervision, gross errors are less likely to occur when compared to minor errors.

3.5.2. Impact on structural safety

The structural safety reduction, measured by the reliability index, is tracked in Figure 3.11 for each of the errors mentioned above. A similar study has been developed by Nowak and Collins [56]. The overall safety reduction is measured by means of the robustness index described in chapter 3.2, and according to Eq. (3.6),

$$I_R = \int_0^{45\%} f_\beta(D) dD \quad \text{and} \quad I_R = \int_{0\%}^{100\%} f_\beta(D) dD \quad (3.6)$$

where I_R is the robustness index (normalised area of the chart), f_β is the performance function of the reliability index normalised by the virgin reliability index, and D is the damage magnitude normalised by the highest absolute value of the damage. By performance function, is meant the reliability index reduction

given the damage, as displayed in Figure 3.11. The robustness index quantified for each of the damages is displayed in Table 3.7 and ranked (R_k) for two damage limits, namely, 45% and 100%.

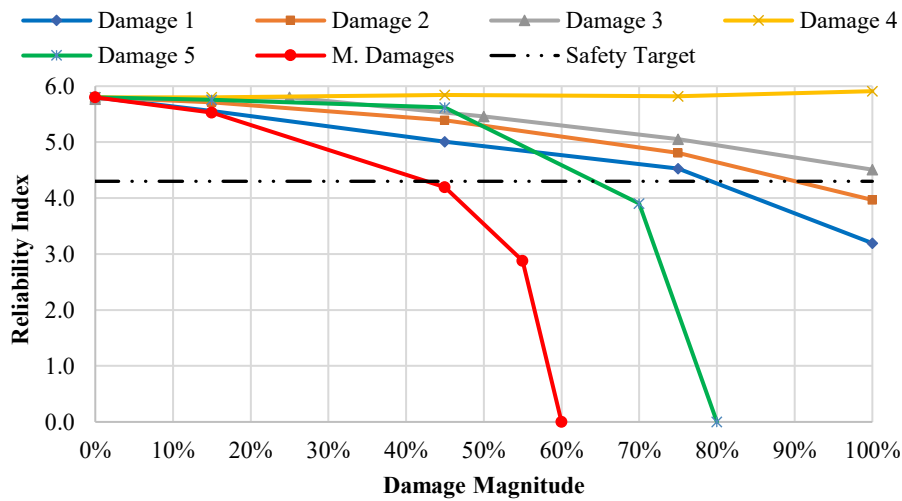


Figure 3.11 – Structural safety reduction

Table 3.7 – Robustness index results

	$I_R^{100\%}$	$R_k^{100\%}$	$I_R^{45\%}$	$R_k^{45\%}$
Damage 1	83.3%	2	93.4%	1
Damage 2	88.9%	3	96.9%	2
Damage 3	92.5%	4	98.4%	3
Damage 4	99.4%	5	99.0%	5
Damage 5	68.2%	1	98.6%	4
Multiple Damages	47.1%		88.4%	

The errors triggering damage 1, 2 and 3 show a more or less linear impact in structural safety reduction, being damage 1 the worst-case scenario among the three, followed by damage 2 and damage 3. The damage 4 has demonstrated a negligible impact on structural safety; however, attention should be called to the fact that the same would not occur for serviceability limit states regarding, crack width and decompression. These would mainly affect the durability or in other words, increase the deterioration rate of the structural system. Hence, the impact of design and execution errors in other limit states should be investigated, especially when durability is concerned.

Examining the robustness index computed for the 45% mark is concluded that damage 1, with a robustness index of 93.4%, has the highest impact on structural safety reduction than all the other damages. Nonetheless, for the 100% mark, among the damages under analysis, the concrete strength reduction (Damage 5) has proven to be the one with the greatest impact on safety reduction. It has exhibited a far higher non-linear behaviour than the others, with a huge drop after the 45% mark, with the

robustness index dropping from 98.6% when considering the 45% mark to 68.2% when considering the maximum damage magnitude (i.e., 100%). Nevertheless, if one considers its impact for magnitudes lower than 45%, the safety reduction when benchmarked with the other errors is less meaningful.

The structural safety reduction quantified for damage 5, modelled by concrete strength reduction, might suggest some incoherence with the results provided in the sensitivity analysis since, in chapter 3.4.2, the results show that the structural system is not very sensitive to the variation of such parameter as a random variable. Nevertheless, one should keep in mind that when human error is addressed the threshold limits established by the PDF of a certain random variable are removed since they are not valid anymore. Thus, the range of values that might be taken by the concrete strength was decreased, beyond the range allowed by the random variable PDF, according to Table 3.5. This more expressive reduction of the concrete strength when modelling damage 5, as shown that after a certain concrete strength reduction, the structural safety is greatly affected. Such observation underlines the importance of the approach employed for structural safety assessment considering human errors, given that a less broad-range approach would lead to deceiving conclusions.

The multiple damages scenario, considering just three errors, indicates a considerable reduction in structural safety with a robustness index of 88.4%, for the 45% mark, and 47.1%, for the 100% mark. Although this is the most realistic and frequent scenario, here it is considered that the errors take place with equal magnitude. One needs not say that this is a very unlikely scenario. Therefore, the investigation of multiple damage scenarios considering the interaction of different damage magnitudes should be further assessed, as well as other possible combinations, correlation and occurrence of more than just three simultaneous errors.

3.6. Conclusions

Quality management is a must to guarantee the reliable performance of any system. In the construction industry, human errors have led to numerous system failures during the construction and operation of the structures despite the efforts to eliminate them, aiming for the assurance of safety levels demanded by a successfully performed design, according to guidelines of design codes and safety standards. Nevertheless, the complete elimination of errors is not possible. Therefore, the quantification of their effects in the short and long term should bring some value to the engineering community, allowing more effective mitigation measures to be employed, thus leading to the anticipation of unexpected failures.

In compliance with such challenges, this paper provides an investigation of design and construction errors' influence on the safety of a prestressed concrete overpass, using a probabilistic non-linear finite

element analysis to quantify the system safety by means of a reliability index. The overall influence of the errors is measured by a robustness indicator. The structural analysis is accomplished by the finite element software DIANA FEA. The probabilistic analysis aiming the characterisation of the structural system resistance probabilistic distribution function encompasses geometric, material and model uncertainties, using a variance reduction technique named Latin Hypercube sampling technique that was preceded by a sensitivity analysis aiming the characterisation of the importance of each random variable on the load-bearing capacity of the case study. The procedure elaborated here allows the quantification of the gap between the safety level of the structure as designed and as-built. Such information is relevant when the period of time for which the system will perform safely is of concern since the initial safety margin can be early reduced by human errors.

The errors demonstrated different patterns in safety reduction. Therefore, the robustness of the structural system is dependent on the type of error threatening the structural safety, with one specific error modelled by the concrete strength, showing a non-linear and significant impact on safety reduction when compared to the remaining errors. The accumulation of errors, modelled by a multiple damages scenario, shows how the target reliability was able to be crossed close to the 45% mark. Such a scenario is the most realistic one since it is commonly reported more than one error as being responsible for structural failures. In time, considering that gross errors have not taken place, even petty errors introducing small damages to the structural system might play a key role in structural safety assurance since the safety margin is usually decreased by deterioration and increasing demand.

4. Impact of construction errors on the structural safety of a post-tensioned concrete bridge

"When the impulse to share becomes obligatory, when personal boundaries are no longer respected, when only the shared space of togetherness is acknowledged and private space is denied, fusion replaces intimacy and possession co-opts love."
by Esther Perel

Neryvaldo Galvão, José C. Matos, Rade Hajdin, Luís Ferreira, Mark G. Stewart

Engineering Structures

Elsevier, Volume 267, 15 September 2022

[10.1016/J.ENGSTRUCT.2022.114650](https://doi.org/10.1016/J.ENGSTRUCT.2022.114650)

Abstract: The ageing of bridge stock in developed countries worldwide and the increasing number of recorded bridge collapses have underlined the need for more sophisticated and comprehensive assessment procedures concerning the safety and serviceability of structures. In many recent failures, construction errors or deficiencies have contributed to the unfortunate outcome either by depleting the safety margin or speeding up the deterioration rate of structures. This research aims to quantify the impact of construction errors on the structural safety of a bridge considering corresponding models available in the literature that probabilistically characterise the occurrence rate and severity of some of these errors. The nominal probability of failure of structures, neglecting construction errors, is typically computed in numerous works in the literature. Therefore, the novelty of this paper lies in the consideration of an additional source of uncertainty (i.e., construction errors) combined with sophisticated numerical methods leading to a more refined estimation of the probability of failure of structures. Accordingly, some benchmark results focussing on error-free and error-included scenarios are established, providing useful information to close the gap between the nominal and the actual probability of failure of a railway bridge.

4.1. Introduction

According to current standards [19,65], recently designed and constructed structures should be accompanied by comprehensive as-built or birth certificate documentation. Such documents should include inspection results of the construction process, performed quality control measures, verified design assumptions, and adopted construction techniques, among other relevant information for regular maintenance not available on the design reports or blueprints [110]. Throughout the sixties and the seventies, a period of mass construction, quality control requirements were less demanding than nowadays. That was also a time when digitalisation was in its infancy and available for very few, if any, in the construction industry, making access to this information tedious or even impossible. Regarding the quality assurance throughout the lifespan of the structure, the absence of this information (i.e., as-built, birth certificate reports and documented deviations from design) adds further uncertainties. Such additional sources of uncertainty are likely to lead to unrealistic conventional safety and serviceability reliability assessment. Conventional reliability assessment as defined here doesn't explicitly consider construction errors as a source of uncertainty. Furthermore, the initial margin of safety of such structures has likely suffered some decline due to deterioration and/or load increase since many of these structures already operate in the second half of their designed service life, becoming more sensitive to hidden defects. It is of no relevance whether these defects remained undetected or detected, but the corresponding documentation is lost [52,111,112].

Bridge collapses typically arouse the interest of engineers and researchers since they offer a unique opportunity to investigate the causes of the collapse, determine the underlying triggering event and gain new insights into structural behaviour. Depending on the source, construction errors during the construction phase are responsible, at least to some degree, for 6-17% of the overall bridge collapses [7,14,113–115]. This percentage depends on the considered definition of human errors [109]. While the contribution of construction errors in the overall collapse of bridges has been roughly estimated, their impact on the structural safety reduction of still-standing structures has not been thoroughly investigated. As such, this paper aims the introduction of construction error models in the reliability assessment of bridges.

Regarding the collapse of the Polcevera viaduct (a.k.a Morandi bridge), whose cause is still under investigation, Calvi et al. [116,117] suggest that the failure of one of the four stays attached to the collapsed pylon is the probable cause of the collapse. It seems, however, that the stay's failure is caused by advanced local corrosion of the tendons enabled by the poor grouting on the cables. Thus, an initial

construction error and insufficient quality control during construction might have played a role in the bridge's collapse. A more overwhelming contribution of construction errors to the collapse of bridges was recently reported by Pujol et al. [38]. The insufficient prestressing of the main transversal girder and placement of the main reinforcement of the pylon diaphragm in the wrong direction led to the failure of a concrete cable-stayed bridge during its construction. Deviations from the initial design during the construction phase have also been reported to contribute to the collapse of the Xiaoshan ramp bridge [118].

The need for quality assurance to avoid, identify, and mitigate the consequences of design and construction errors is a well-known requirement within the engineering community and design standards [119]. In design standards, a sufficiently low failure rate as a basis for design checks is assumed, considering unavoidable uncertainties in the design and construction process [7,19,109]. This failure rate is called the nominal failure rate, and the unavoidable uncertainties can be regarded as acceptable deviations. If these deviations were the only ones, the actual failure rate would be the same as the nominal failure rate. However, this is not the case due to human errors.

Consequently, this paper seeks to consider construction errors in the reliability assessment of a post-tensioned concrete railway bridge. The outcomes of this paper should help establish some results relevant for possible consideration of construction errors in the definition of partial safety factors and future revisions of design and assessment codes.

4.2. Construction error models – a short review

The discrepancy between the actual and the nominal failure rate is attributed to human errors [19,95] and actions that are not, or not with sufficient intensity, covered by the codes of practice. However, in the nuclear power plant industry, when safety is concerned, human errors are explicitly considered through a well-established human reliability analysis (HRA) procedure supported by event tree techniques and Monte Carlo simulation. The HRA allows the modelling of a process by subdividing it into consecutive macro and micro tasks providing the ability to model errors in the performance of a task (i.e., error of commission) or model the consequence of non-performance of a task (i.e., error of omission) [120].

A construction error is described within this work as a deviation of a certain structural parameter, from its design value, beyond the acceptable tolerances assumed by standards. Stewart [24,120] developed an HRA event tree seeking to model construction errors' influence on the failure probability of a typical reinforced concrete beam. The HRA model incorporated tasks directly related to the flexural strength of a beam, such as the (a) longitudinal reinforcement area, (b) effective depth of the tensile

reinforcement, (c) beam width and (d) quality of the concrete mix. Considering general guidelines provided by Swain and Guttman [121] and experts' opinions collected in carefully elaborated surveys, the probabilistic appraisal of human error probabilities (HEP) and error magnitudes was possible (see Table 4.1). Different HEPs are provided (i.e., before and after inspection) based on the assumption that after the inspection of finished construction works, leading to the identification of errors, corrective measures are put in place to eliminate such errors.

Design errors are also relevant sources of uncertainty addressed by Stewart and Melchers [98,99,122,123]. Stewart [98] investigated construction and design errors' impact on structural safety reduction and concluded that construction errors were more detrimental to structural safety reduction. Nonetheless, this might not be the case for specific structures or situations. Either way, they are both relevant and should be treated as such. However, the focus of this work is construction errors. Additional work relevant for some historical background is the work developed by Ellingwood [124], where a thorough review of the status of design and construction errors in structural safety studies of the time is provided, and some simplified mathematical tools are summarized. A discussion addressing the difficulty of consideration of errors in design standards is also presented.

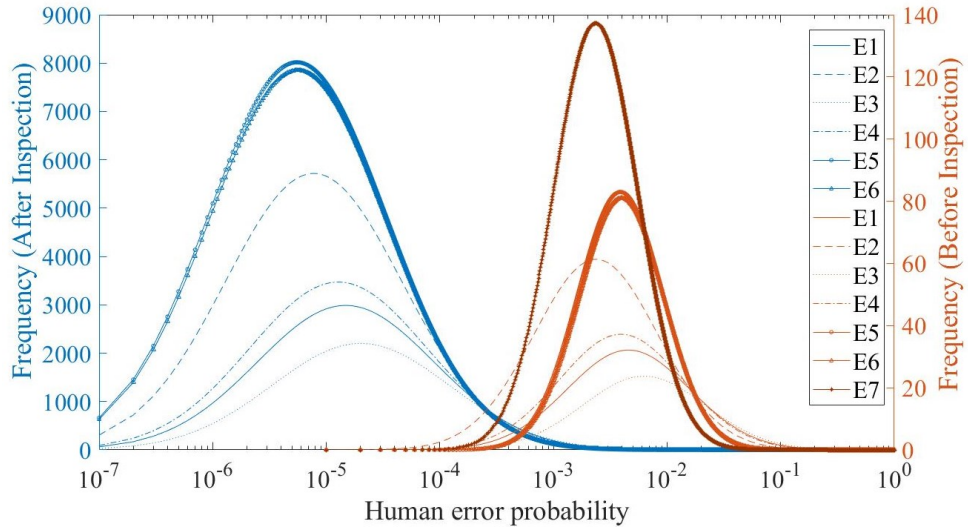
4.2.1. Human error probability

The HEP is defined by the number of times the error has been observed, provided a total number of performed inspections. Within this paper, one must highlight that the provided HEP models are exclusively limited to the rate of occurrence of construction errors. According to Swain and Guttman [121], a lognormal probabilistic distribution function (PDF) should be used to model HEP, mainly because tasks performed by experienced individuals are expected to accumulate error rates at the lower error end of a distribution, i.e., close to zero; thus, skewing the density function towards zero. The lognormal PDF is chosen in HRA to model operator errors in nuclear power plants.

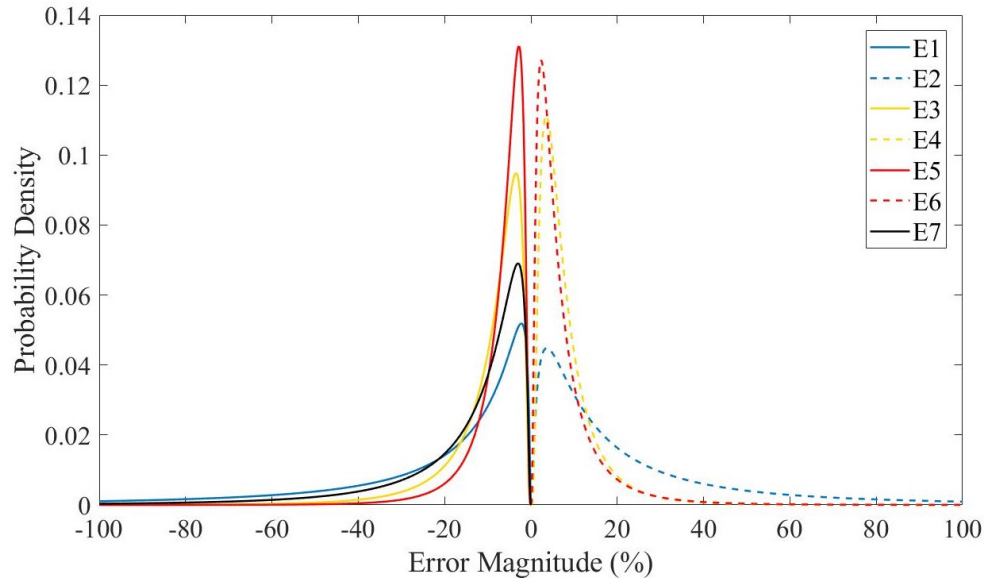
For the definition of any PDF, a mean value and a measure of the dispersion of the random variable (i.e., variance or standard deviation) must be proposed. The HEP dispersion is a consequence of different personal skills and traits, the work environment, the task itself, and many other factors that might affect the performance of a task. Consequently, Stewart [98,120] proposed the median estimate parameter based on expert judgments collected through a survey disseminated to construction experts and the dispersion parameter set according to guidelines for operator tasks in the nuclear power plants industry. Such parameters are presented in Table 4.1, where, \tilde{m}_0 is the median and EF_0 is an error factor used to compute the standard deviation σ_0 of the HEP distribution through Eq. (4.1). The EF_0 is the square

root of the ratio between the 90th and 10th percentile values of the PDF of the HEP. In other words, it is a measure that allows one to specify the dispersion of the bounds of a distribution.

$$\sigma_0 = \frac{\ln(EF_0)}{1.2817} \quad (4.1)$$



(a)



(b)

Figure 4.1 – (a)PDFs of HEPs before inspection (orange) and after inspection (blue); (b) PDFs of error magnitudes

The HEP PDFs of selected construction errors are given in Figure 4.1a. For each error, HEPs before and after the inspection is provided. The influence of inspection and subsequent implementation of corrective measures in the HEP PDFs is evident, with the mean value decreasing by several orders of magnitude for the same error despite the increase in the dispersion of the distribution. The previous statement is true except for E7 (i.e., inadequate concrete mix) since the HEP is maintained after the

inspection. Such exception is mainly because visual inspections are considered to take place, making unfeasible the assessment of the compliance of the concrete strength.

Table 4.1 – Parameter for human performance models (construction) [120]

Error type	Before Inspection		After Inspection		λ_{BE}	λ_{UB}
	\tilde{m}_0	EF_0	\tilde{m}_i	EF_i		
E1 Reduced area of reinforcement	0.0218	5	3.73×10^{-4}	10	-14.30	-82.22
E2 Increased area of reinforcement	0.0114	5	1.95×10^{-4}	10	15.16	69.22
E3 Decreased effective depth	0.0296	5	5.06×10^{-4}	10	-7.10	-21.14
E4 Increased effective depth	0.0188	5	3.21×10^{-4}	10	6.27	16.60
E5 Decreased beam width	0.0081	3	1.39×10^{-4}	10	-5.24	-14.54
E6 Increases beam width	0.0083	3	1.42×10^{-4}	10	5.22	16.52
E7 Inadequate concrete mix	0.0049	3	0.0049	3	-9.58	-38.1

4.2.2. Error magnitude

The error magnitude m_e is here defined as the percentage deviation from the designed outcome of a construction process according to Eq. (4.2). In short, m_e is the severity of the error,

$$m_e = \frac{z - z_m}{z_m} \times 100\% \quad (4.2)$$

where z_m is the designed outcome, and z is the measured or estimated actual outcome. Two types of error are considered to model the error magnitude: an error of commission and an error of omission. An error of commission is a deviation with the error magnitude ranging from 0% to 99% from the designed outcome. The error of omission is the failure to execute a process (i.e., $m_e = -100\%$). For instance, if a complete layer of reinforcement is missing, an error of omission has taken place. On the other hand, if a few bars of reinforcement are missing in a deployed layer of reinforcement, an error of commission has taken place. Simply put, an error of commission is the wrongful performance of a task, while an error of omission is the failure to perform a task. In addition, errors can be detrimental or beneficial to the structure's resistance; thus, both positive and negative percentage deviations must be considered.

An error of omission might be more frequent for some types of error than others; nevertheless, one can state with reasonable confidence that they are less frequent and likely to be revealed during the inspection process and corrected afterwards. The proposed PDF for the error magnitude is also a lognormal distribution defined according to the provided median estimate λ_{BE} and the 90th percentile upper bound estimate λ_{UB} of the PDF (see Table 4.1). The standard deviation of the error magnitude PDF σ_{me} is computed through Eq. (4.3).

$$\sigma_{me} = \frac{\ln\left(\frac{\lambda_{UB}}{\lambda_{BE}}\right)}{1.2817} \quad (4.3)$$

The lognormal distributions obtained because of the detrimental and beneficial errors are displayed in Figure 4.1b. The possible range of deviations for beneficial errors can exceed 100%; however, this is very unlikely. On the other hand, error magnitudes for detrimental errors are limited to error magnitudes not greater than -100% (i.e., error of omission) [24,120].

4.2.3. HRA event tree

Stewart [120] proposed an event tree (see Figure 4.2) to combine the realisations of the HEPs and error magnitudes according to their respective PDFs described in 4.2.1 and 4.2.2. Later on, Epaarachchi and Stewart [53] also considered such an event tree to discuss construction errors' impact on multi-story reinforced concrete buildings. The proposed event tree allows the simulation of construction outcomes within the expected range of deviation allowed by construction tolerances and the simulation of construction outcomes outside of such acceptable ranges of deviation (i.e., detrimental, and beneficial errors).

Error-free and error-included realisations are allowed by the event tree, and their rate of occurrence is dependent on the HEP PDFs considered and the realisation of a random number (RN_i) with a uniform distribution. Simply stated, the rate of occurrence of a detrimental error in the overall number of generated samples is given by the number of times the realisations of RN_i is lower than the realisation of the considered HEP. The size of the deviation from the nominal value X_{nom} (i.e., mean value) is given by the detrimental and beneficial error magnitude PDF (i.e., EM_{i,d} or EM_{i,b}, respectively). Furthermore, it is important to highlight that the realisations of HEPs, EMs and RN_i, are all independently generated according to their respective PDF. Accordingly, the probability of failure of the structure is computed considering these main two branches of the event tree, namely, error-free and error-included realisations, where the error rate is given by the number of times the realisation of RN_i, with a uniform PDF between 0 and 1, is lower than HEP_{i,d} and HEP_{i,d} + HEP_{i,b} (see Figure 4.2). The i, d and c indexes are respectively the ith number from the sample vector obtained from the PDFs of the dth detrimental error (i.e., E1, E3, E5 and E7) and bth beneficial error (i.e., E2, E4 and E6).

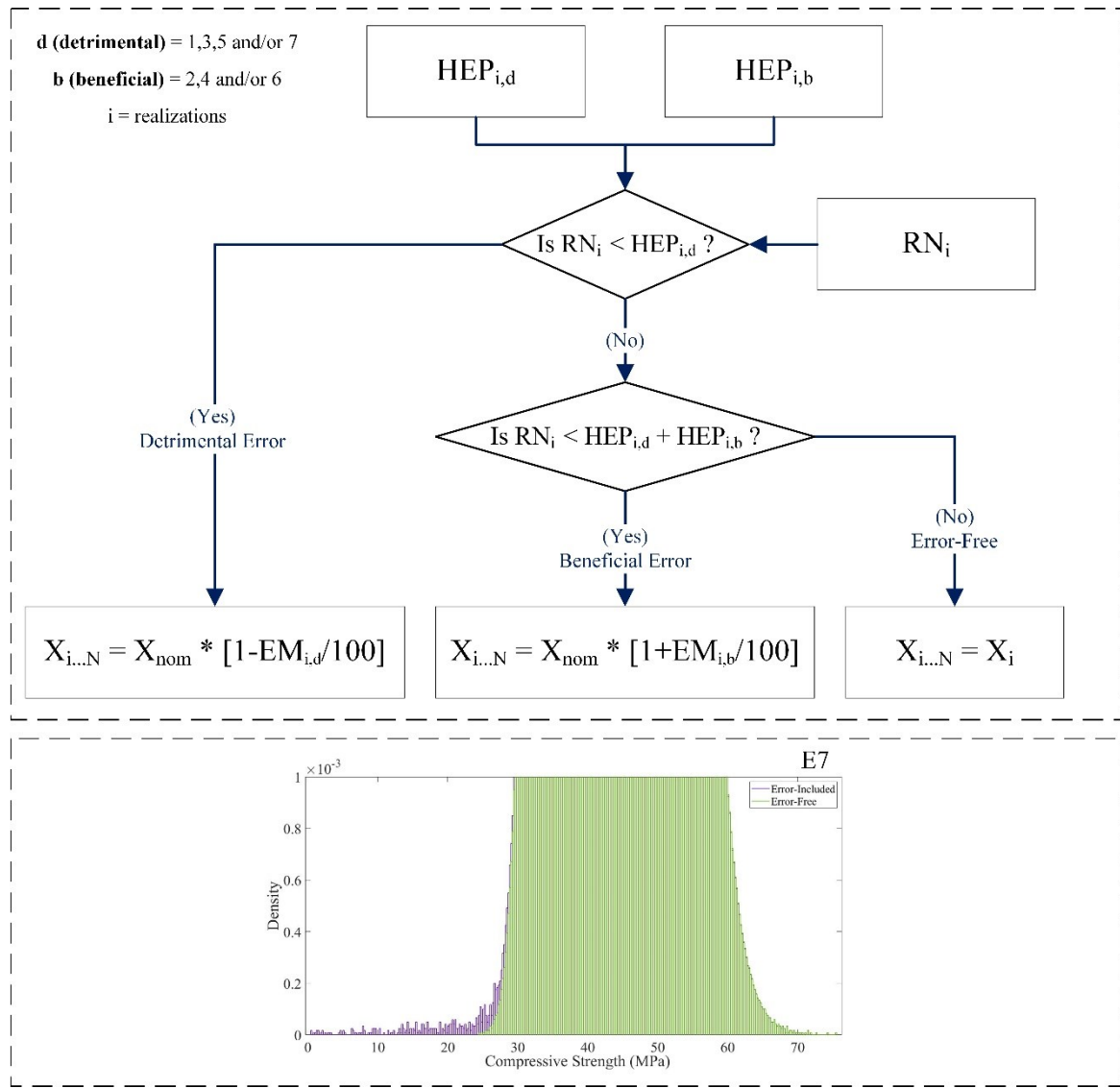


Figure 4.2 – HRA Event tree with some output results

For illustration purposes, the influence of the E7 models (i.e., inadequate concrete mix) in the PDF of the concrete compressive strength is presented in Figure 4.2. One should note that the PDF is truncated for a probability density of 1×10^{-3} , aiming to emphasise the main differences between the tail of the error-free and the error-included PDF. Further elaboration on the HRA event tree is presented in 4.6.

4.3. Surrogate-based reliability analysis

Reliability analysis using finite element models (FEM) can be computationally expensive, particularly for simulation-based approaches where each run requires full FEM analysis. Therefore, surrogate models have been extensively used because they allow the replacement of an expensive numerical model (i.e., FEM) for a far less computationally demanding model that can predict the output of interest with sufficient accuracy for reliability analysis. Surrogate models are the result of supervised machine learning techniques that map the relationship between a set of input and output parameters. Considering that

$G(X)$ is the performance function set to assess the violation of a limit state equation (i.e., $G(X) \leq 0$), the probability of failure can be computed as follows in Eq. (4.4),

$$P_f = P[G(X) \leq 0] = \int_{G(X) \leq 0} f_X(X) dx \quad (4.4)$$

where $f_X(X)$ is the joint density function of the random variables X considered to estimate the resistance and loading of the system. Thus, if the safe and the failure domain can be easily drawn by verifying the performance function $G(X)$, the failure probability can be estimated. Accordingly, for a less expensive approximation of $G(X)$ surrogate models have been introduced.

Several surrogate modelling techniques can be found in the literature, e.g., kriging, polynomial chaos expansion, neural networks, support vector machine, and response surface, among others [125–127]. Nevertheless, for the current investigation, a kriging-based surrogate model was selected to approximate the performance function of the case study under assessment. Kriging is a controlled learning procedure that seeks to solve a stochastic problem where the output of interest is the realisation of a gaussian process, i.e., a stochastic process where a finite combination of its random variables has a normal PDF. The prediction given by the surrogate model for the experimental design samples (i.e., initial samples used to train the surrogate) interpolates the exactly known solution (i.e., the observation from the true numerical model). A kriging-based surrogate model is generally described by the following Eq. (4.5) [128,129],

$$M^k(X) = \rho^T f(X) + \sigma^2 Z(X, w) \quad (4.5)$$

where, $M^k(X)$ is the model output given by the realisation of a gaussian process indexed by the random variable X , ρ^T is a vector of regression coefficients of possible arbitrary base functions $f(X)$ (e.g., polynomial and quadratic, among others). The first term of the equation provides the deterministic approximation of the output of interest in the vicinity of its mean value. $Z(X, w)$ and σ^2 , are the zero-mean and unit-variance stochastic Gaussian process and the constant that represents the variance of the gaussian process, respectively.

Notwithstanding the increased efficiency afforded by a surrogate model, a surrogate-based reliability analysis can be further improved by an active learning technique that allows the approximation of the performance function in the vicinity of the limit state equation $G(X) = 0$ using a learning function in a process known as the enrichment procedure [129–131]. Such a procedure is used in a loop until a

convergence criterion is satisfied. The stability of the reliability index (i.e., the convergence criteria) is verified in Eq. (4.6) as follows,

$$\frac{|\beta^j - \beta^{j-1}|}{\beta^j} \leq \epsilon_\beta \quad (4.6)$$

where β^j and β^{j-1} are the reliability index of the j^{th} and its preceding iteration, respectively. The threshold value ϵ_β considered in this work is 0.02.

To estimate the probability of failure the subset simulation is chosen. The subset simulation technique is an efficient and robust simulation-based technique that allows the estimation of very low probabilities of failures. Such sampling technique is supported by the definition of a sequence of failure domains ($D_1 \supset D_2 \supset D_3 \dots D_i$) where the final intersection of all the failure domains will equal the actual probability of failure of the numerical problem ($D_f = \bigcap_{k=1}^i D_k$). A group of decreasing threshold values $t_1 > t_2 > t_3 \dots t_i = 0$ determines a set of different limit state equations (i.e., $G(X) \leq t_i$) that define the domains (D_i) in such a way that the probability of each event related to D_i (i.e., $P(D_i)$) is close to a pre-established probability P_0 (i.e., $P(D_i) \approx P_0$ where $0 < P_0 \leq 0.5$). Henceforth, the probability of failure of a defined sequence of failure domains is estimated through the multiplicand of conditional probabilities ($D_{j+1}|D_j$), according to Eq. (4.7) [132,133]:

$$P_f = P\left(\bigcap_{k=1}^i D_k\right) = P(D_1) \prod_{j=1}^{i-1} P(D_{j+1}|D_j) \quad (4.7)$$

For evaluation of the quality of the surrogate model in the approximation of the expensive numerical model, the leave-one-output cross-validation error (ϵ_{LOO}) given in Eq. (4.8) is used as the error measure,

$$\epsilon_{LOO} = \frac{1}{N} \left(\frac{\sum_{i=1}^N [G(x_i) - Y_{val}(x_i)]^2}{Var[G]} \right) \quad (4.8)$$

where $G(x_i)$ is the output of the accurate model (i.e., FEM) and $Y_{val}(x_i)$ is the surrogate model output for the realisations x_i of the random variables, both computed based on a validation sample. $Var(G)$ is the variance of all the known values of $G(x_i)$.

4.4. Case study

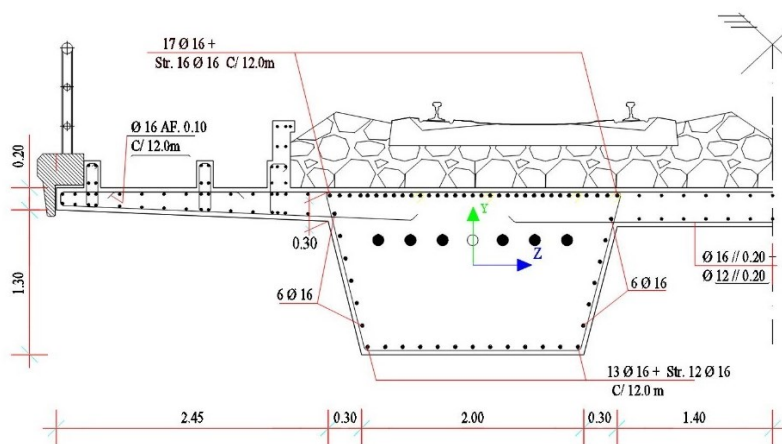
4.4.1. Bridge description

A post-tensioned concrete railway bridge is introduced to investigate the construction errors' impact on structural safety. The case study is a three-span post-tensioned concrete overpass of 52 m in length constructed in Pinheiro, Portugal, in 2010. The outward spans are 15 m, while the middle span has 22 m in length (see Figure 4.3a). Two solid V ribs attached to a concrete slab shape the superstructure, each supporting a rail track. The ribs are 2 m and 2.6 m in width, in their bottom and top sections, respectively, attached to a standard concrete slab of 12.9 m in width and 0.35 m thick (see Figure 4.3b). The superstructure has a total height of 1.5 m, and the ribs are spaced by 5.4 m. The superstructure is monolithically connected to two piers with 9.73 m in height, and it is supported over the abutments by elastomeric bearing devices through transversal girders. The piers' foundation contains piles of more than 31 m, connected by rigid pile caps that support the piers. The piers' cross-section is displayed in Figure 4.3c. The overpass was designed according to the Portuguese regulation for reinforced and prestressed concrete structures (REBAP) and the regulation for safety and load of structures (RSA), using a static live load model equivalent to the load model 71 (LM71) of Eurocode 1 [62] and considering 40 mm minimum concrete cover given the exposure conditions.

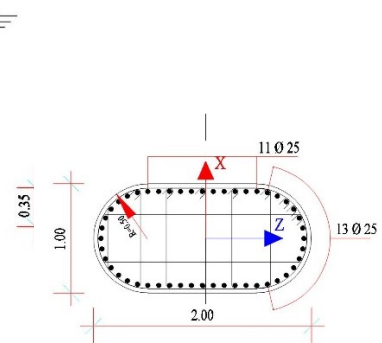
The bridge superstructure was built using a C35/45 concrete, while the piers were executed with a C30/37 concrete. The structure was reinforced by S500-A steel reinforcement and post-tensioned by a low relaxation (i.e., class 2) bonded reinforcement Y 1860 S22 15 mm. All its elements were cast in situ, using falseworks as temporary supports. The superstructure is prestressed by six cables per rib in its length, with varying heights (see Figure 4.3d). Each cable is made of 22 strands of 1.5 cm² of area. The expected immediate and time-dependent losses of the applied post-tensioning forces were estimated to be between 22% to 27%. The estimated long-term post-tensioning forces are available in Figure 4.3d.



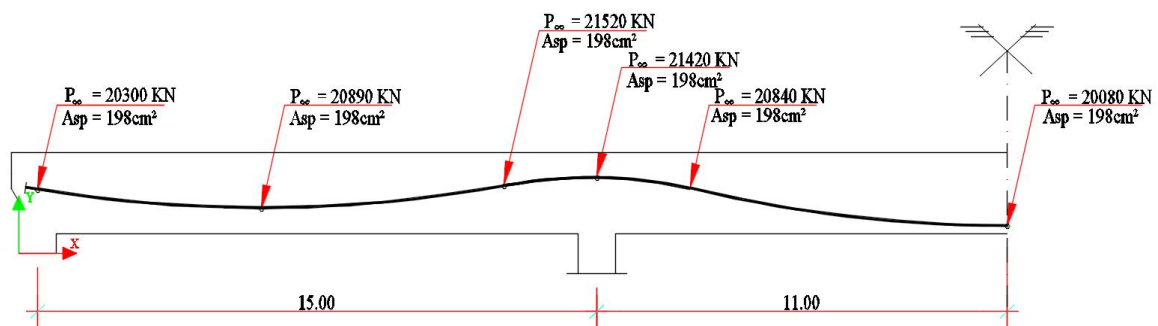
(a)



(b)



(c)



(d)

Figure 4.3 – Case study, (a) picture (google maps view); (b) superstructure cross-section, (c) piers cross-section; and (d) prestressing cables layout and their minimum expected prestressing forces obtained from blueprints (Adapted from:[134])

4.4.2. Numerical modelling

For non-linear structural analysis purposes, half of the bridge is modelled using two-dimensional FEM in DIANA FEA software [81,83,135]. The model aims to characterise the maximum carrying capacity of the structural system (i.e., ultimate limit state (ULS)) when bending is concerned. The superstructure and piers were modelled by a fully numerically integrated (in its axis and cross-section) class III-Mindlin-Reissner beam element of 0.25 *m*, with three nodes and three degrees of freedom per node (i.e., u_x , u_y and ϕ_z). Equivalent cross-sections were used to model the superstructure cross-section and the piers.

The superstructure was modelled with seven layers (see Figure 4.4a), each with five integration points in its height, while the piers are modelled with a simpler cross-section. For integration purposes, the composite Simpson rule was employed.

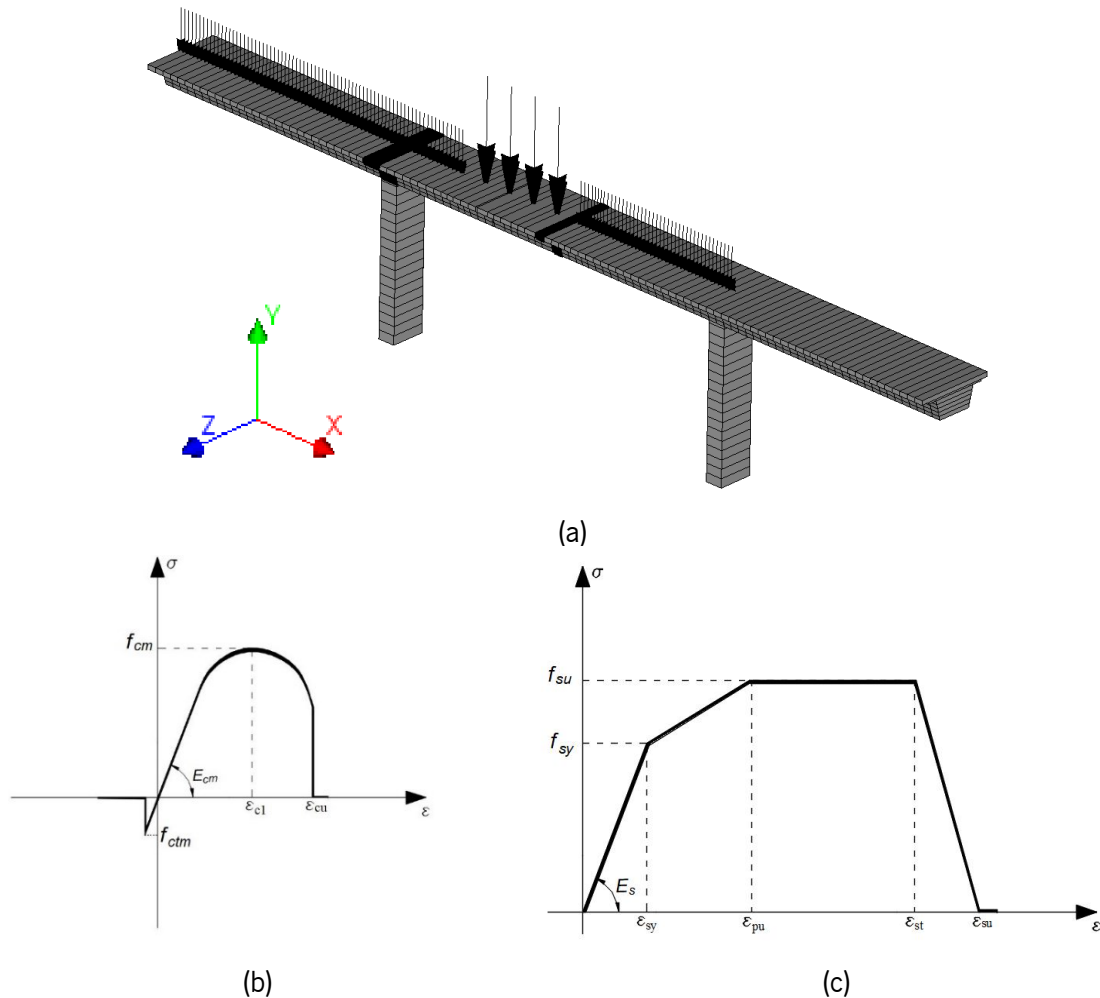


Figure 4.4 – (a) Numerical model extruded geometry; (b) concrete constitutive model and (c) conventional and post-tensioning reinforcement constitutive model

A fixed total strain-based crack model was considered to depict the non-linear behaviour of concrete, as recommended by Hendriks et al. [136]. The concrete was modelled by the constitutive model in Figure 4.4b, while the conventional and post-tensioned reinforcement behaviour was modelled by the constitutive model in Figure 4.4c. For post-tensioning of the superstructure, the prestressing reinforcements were considered initially unbonded as the superstructure was being loaded by its self-weight and the post-tensioning forces, followed by a bonded phase when applying the remaining permanent and live load. The material mechanical properties used for the preliminary deterministic structural analysis discussed in 4.4.3 are provided in Table 4.2 and Table 4.3.

The self-weight of the reinforced concrete structure was estimated considering 25 kN/m³ of weight, leading to a total self-weight of 116.3 kN/m. The total remaining permanent load comprising, namely; (i) the ballast, (ii) sleepers, (iii) rails, (iv) precast covers, (v) precast slabs, (vi) ballast protection, (vii) cornices, (viii) guardrails and (ix) cables' gallery filling, was approximated around 72.8 kN/m. The rail traffic static vertical loads were modelled according to the LM71 [62]. Nevertheless, for the structural analysis results presented in 4.4.3, mean values of LM71 are considered, bearing in mind that the provided characteristic values equal the 98th percentile of a Gumbel PDF with a coefficient of variation (CoV) of 10%, considering a 50-year reference period (see Table 4.5).

Table 4.2 – Concrete mechanical properties

	E_{cm} (GPa)	f_{ctm} (MPa)	f_{cm} (MPa)	ϵ_{st} (‰)	ϵ_{cu} (‰)
C30/37	33	2.9	38	2.2	3.5
C35/45	34	3.2	43	2.3	3.5

Table 4.3 – Reinforcement mechanical properties

	S 500-A	Y 1860 S22 15mm
ϵ_{sy} (‰)	2.8	8.22
ϵ_{pu} (‰)	25.0	20.0
ϵ_{st} (‰)	50.0	50.0
ϵ_{su} (‰)	100.0	100.0
E_s (GPa)	200.0	200.0
f_{sy} (MPa)	560.0	1644.0
f_{pu} (MPa)	580.0	1934.0

The case study was designed and assessed considering an alpha factor equal to 1.0. The dynamic amplification effects caused by the speed of the moving load, irregularities of the track, vehicle imperfections, spacing of axle loads, and suspension characteristics of the vehicles, among other reasons, were considered through a dynamic amplification factor of 1.21, assuming a track under standard maintenance [62]. Provided the adequate structural system influence line, the LM71 was positioned to maximise its effects on the superstructure cross-section over one of the piers (see Figure 4.4a). Such a cross-section was proven to be the critical one when longitudinal bending is concerned.

4.4.3. Non-linear structural analysis

For non-linear structural analysis, an incremental-iterative loading procedure based on the Modified Newton Raphson iteration scheme and force control incremental procedure was implemented using energy and force norm as convergence criteria. Accordingly, the maximum carrying capacity of the structural system when longitudinal bending is concerned, and the failure is characterised by the material's strength (i.e., ULS: STR), was estimated to be approximately 6.7 times the mean value of LM71, according to Figure 4.5a. The Figure 4.5a displays the load-displacement curve of the middle span cross-section highlighted in Figure 4.4a. Further analysis considering the 5% quantile values and design

values (using resistance partial safety factors of Eurocode 2 [79]) of the concrete compressive strength, and conventional and post-tensioning reinforcement yielding strength, was also performed, aiming to assess the structural system carrying capacity for such deviations. The remaining parameters were kept with their mean values. In summary, the data shows an 8.96% and 24.78% reduction in the system carrying capacity for the 5% quantile and the design values, respectively.

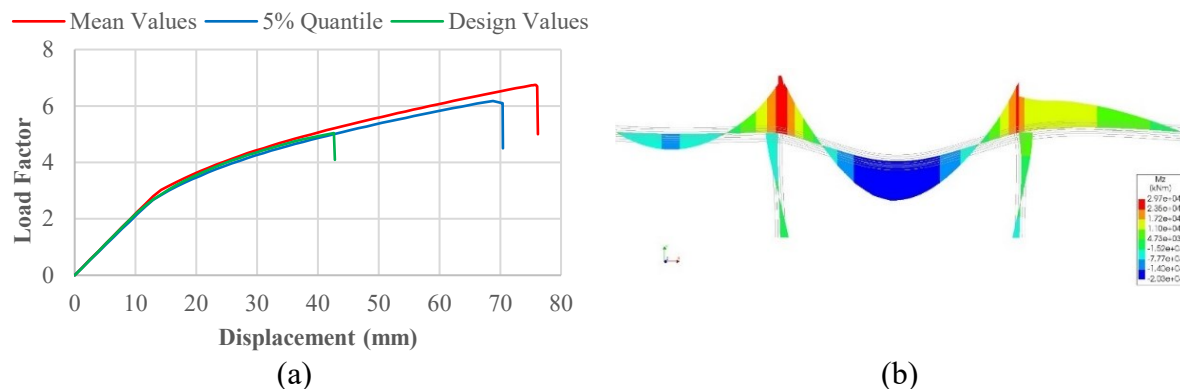


Figure 4.5 – (a) Load-displacement curve (b) bending moment diagram distribution for maximum load factor

The maximum carrying capacity is attained after reinforcement yielding and bending moment redistribution due to concrete crushing in the lowest fibre of the superstructure cross-section over the pier when the concrete reaches its ultimate compressive strain of 3.5%. The maximum bending moment capacity of the superstructure cross-section over the piers is estimated to be 28528 kNm (see Figure 4.5b).

4.5. Reliability assessment

4.5.1. Resistance and loading uncertainties

Structural safety is often assessed using structural reliability analysis to evaluate failure probability given uncertainties in the assumption of the loading and resistance. However, human error is also an important source of uncertainty, neglected too often in such analysis, despite being addressed through quality control measures. In this section, a conventional structural reliability assessment (i.e., neglecting construction errors) is performed. In the subsequent section, construction errors probabilistically characterised in section 4.2 are introduced as an additional source of uncertainty through an HRA event tree in a more comprehensive reliability analysis procedure. Based on the literature [84,87,89,101,137–141], stochastic models for resistance and loading, as well as the correlation coefficients given in the footnotes, used in the reliability analysis are given in Table 4.4 and Table 4.5, respectively.

Bridges designed according to Eurocode 2 [142] should be executed according to EN13670 [63] with careful attention to the construction tolerances allowed by the standard and workmanship

recommendations. The range of values allowed by the PDF of the random variables and the construction tolerances provided by the standards are reasonable benchmarks that can be used to determine the boundaries between acceptable and unavoidable random variations and construction errors. Nonetheless, the density function associated with the ranges of acceptable random variations must not be neglected.

Table 4.4 – Probabilistic characterisation of materials, geometries and model uncertainty random variables

ID	Random Variables	Notation	Mean Values	CoV	PDF	Reference	
1	C35/45	Compressive strength	f_{cm}	43 MPa	12%	Lognormal	[101]
2		Tensile strength ¹	f_{ctm}	3.2 MPa	20%	Lognormal	[87,101]
3		Modulus of elasticity ²	E_{cm}	34 GPa	8%	Normal	[87]
4		Slab thickness	t	25.5 cm	3.5%	Normal	[89]
5	S500A	Yielding stress	f_{sy}	560 MPa	5.4%	Lognormal	[84]
6		Ultimate Strength ³	f_{su}	580 MPa	6.9%	Lognormal	[84]
7		Area ^{4,5}	A_s	–	2%	Normal	[84]
8		Effective Depth ⁶	d_s^*	Nom.*1.4 Nom.*1.0	15% 3.3%	Lognormal	[89] [137]
9	S1670/1860	Yielding stress	f_{py}	1644. MPa	2.5%	Normal	[84]
10		Ultimate Strength ⁷	f_{pu}	1934 MPa	2.5%	Normal	[84]
11		Prestressing force (t=∞) ⁸	F_{∞}	20300-21520 kN	9.0%	Normal	[84]
12		Area ⁷	A_p	–	1.2%	Normal	[89]
13	Resistance model uncertainty		θ_R	1.00	17%	Lognormal	[138]

¹ $f_{cm} - f_{ctm} \rightarrow$ Correlation coefficient (ρ)=0.7; ² $f_{cm} - E_{cm} \rightarrow \rho=0.9$; ³ $f_{su} - f_{sy} \rightarrow \rho=0.85$; ⁴ $A_s - f_{su} \rightarrow \rho=0.5$; ⁵ $A_s - f_{sy} \rightarrow \rho=0.35$; ⁶The effective depth is measured from the top layer of the bridge superstructure; ⁷The correlations valid for conventional reinforcement properties are also valid for the prestressing reinforcement; ⁸The prestressing force applied to the different tendons are considered fully correlated coefficient.

Using DIANA FEA software in combination with UQLab sampling algorithms [143,144], an initial investigation of the unavoidable uncertainty impact on the maximum carrying capacity of the case study was performed. The variability of the maximum carrying capacity of the structure, measured as a load factor of the mean value of LM71, caused by the stochastic models summarised in Table 4.4 and Table 4.5 (apart from the resistance θ_R and live load θ_S model uncertainty as well as live load uncertainty) is displayed in Figure 4.6a and Figure 4.6b, considering 400 samples generated through the Latin hypercube sampling technique. In summary, the PDF of $R(X)$ in Eq. (4.9) is roughly estimated by the histogram given in Figure 4.6b. The variability of the maximum carrying capacity of the structure, defined by the histogram in Figure 4.6b, has a mean value of 6.52 and a standard deviation of 0.28. The 2% and 98% quantile values of the histogram are 5.89 and 7.02, respectively.

Table 4.5 – Probabilistic characterisation of permanent loads, live load and load model uncertainty random variable

ID	Random Variables	Notation	Mean Values	CoV	PDF	Reference
1	Self-weight load ^{1,2}	DL	25.8 kN/m ³	7.1%	Normal	[101]
2	Additional load ^{1,3}	AL	72.8 kN/m	11%	Normal	[101]
3	Live load model uncertainty	θ_S	1.0	15%	Normal	[139]
4	Lifetime (50-year peak) Live load model 71 ^{4,5}	LM71	198.5 kN (63.2 kN/m)	10%	Gumbel	[140,141]

¹Model uncertainty included ²Correlated with slab thickness ($\rho = 0.5$) ³Sleepers, rails, railings, etc. ⁴Characteristic value provided by EC corresponded to the 98th percentile. ⁵50-year reference period.

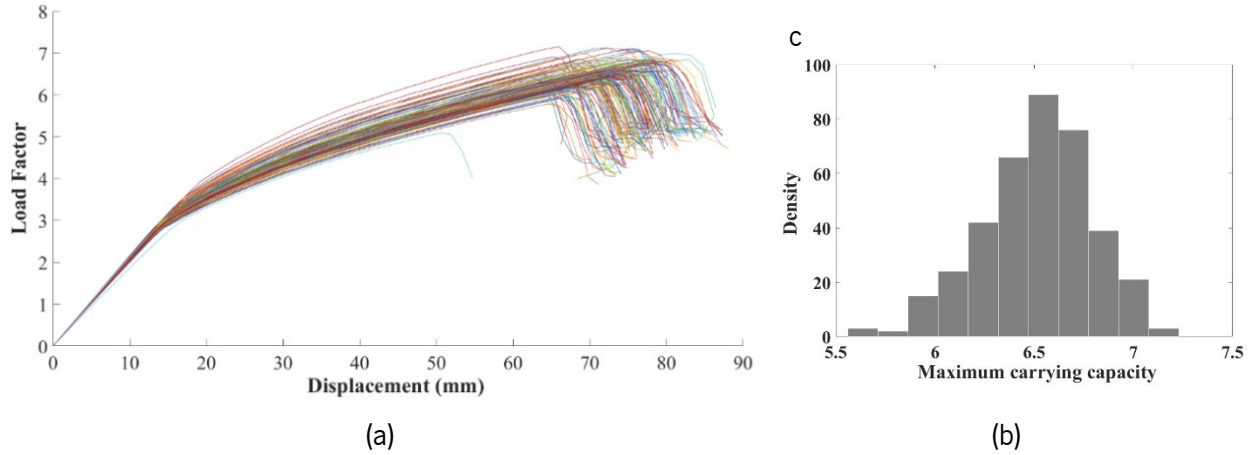


Figure 4.6 – (a) Load-displacement curve of multiple simulations and (b) histogram of the maximum carrying capacity

4.5.2. Safety evaluation

For reliability assessment, the limit state equation $G(X) = 0$ (see Eq. (4.9)) is defined as the boundaries between the failure and the safe domain necessary for failure probability evaluation. Thus, the safe and the failure domain are defined by $G(X) > 0$ and $G(X) \leq 0$, respectively:

$$G(X) = \theta_R \times R(X) - 1.21 \times S \times \theta_S = 0 \quad (4.9)$$

where, $R(X)$ is the load-carrying capacity defined as a factored mean value of LM71 (roughly estimated in Figure 4.6b) given a group of random variables (X) selected based on a sensitivity analysis (see [55,85]), θ_R is the resistance model uncertainty, 1.21 is the considered dynamic amplification factor, S is the load parameters that represent the LM71 with a unitary mean value and the same CoV given to LM71, and θ_S is the live load model uncertainty. One should highlight that $R(X)$ represents the remaining load-carrying capacity of the structural system in the presence of permanent loads.

Employing a surrogate-based reliability analysis approach for reliability analysis as described in section 4.3, by coupling the UQLab [128,130] algorithms for kriging-based surrogate modelling and active learning techniques (based on U learning functions) with DIANA FEA [135] to predict the output of interest $R(X)$, the probability of structural failure, as well as its confidence interval (CI), are estimated. Initially, 30 experimental design samples were generated followed by a 2-point enrichment procedure considered

to refine the surrogate model in the vicinity of the limit state function. The enrichment procedure ends when the stopping criteria defined in Eq. (4.6) is fulfilled for two consecutive steps. Furthermore, the subset simulation technique was used to estimate the lifetime (50 years) probability of structural failure.

The convergence rate in the computation of the failure probability for each incremental evaluation of the FEM or each generated enrichment sample is displayed in Figure 4.7. After 118 FEM evaluations, the lifetime probability of structural failure was estimated as $P_f = 3.62 \times 10^{-13}$ with a CoV of 4.6%, putting the structural reliability index between 7.16 and 7.19 (see Table 4.6). The quality of the surrogate model was assessed according to Eq. (4.8), yielding a leave one output cross-validation error $\epsilon_{Loo} = 3.18 \times 10^{-4}$, which is a reasonable result, according to Blatman and Sudret [145].

The recommended minimum target reliability index for a ULS of structural members of structures belonging to a reliability class 2, considering a 50-year reference period, is 3.8 according to Eurocode 0 [19] and Ghasemi and Nowak [146]. Moreover, according to Sykora et al. [35], a 0.5 increment to the target reliability index was considered since the analysis presented here is performed at the system level. Nonetheless, one should state that this further increment is conservative and further investigation to search for a less conservative target reliability index is recommended.

From the structural reliability assessment point of view, safety is assured ($\beta > \beta_T$) due to the high-reliability index value obtained, which is higher than the target reliability index of $\beta_T = 4.3$. The high-reliability index value is mainly due to the redistribution capability of the structural system in the longitudinal direction.

Despite the relevance of the approach used to estimate the variability of the maximum carrying capacity of the structure (see Figure 4.6) as well as the structure reliability index, one must recognise its limitation. The stochastic models introduced in this analysis were fully correlated throughout the numerical model. To overcome this limitation, random fields should be introduced in the analysis. Nonetheless, one cannot stress enough the increase in computational costs that this approach demands. A simplistic approach for considering the spatial variability of stochastic models would be to allow the independent realisation of the random variables in the cross-sections highlighted in Figure 4.4a. This would mostly require duplication of most of the stochastic models given in Table 4.4, which of course, comes with additional computational costs.

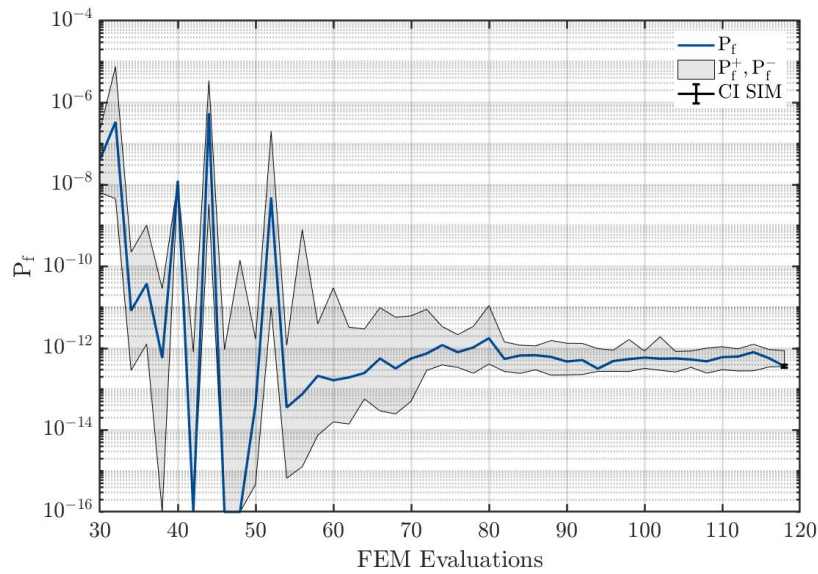


Figure 4.7– Probabilistic analysis convergence rate

Table 4.6 – Probabilistic analysis results

Method	β [CI]	CoV	P_f [CI]	FEM Evaluations
AK-SS-U	7.17 [7.16 – 7.19]	4.6%	3.62×10^{-13} [3.29×10^{-13} – 3.94×10^{-13}]	118

4.6. Impact of construction errors

Following the evaluation provided by a conventional framework for reliability assessment (i.e., human errors excluded), the construction error PDFs introduced in 4.2 are here considered as an additional source of uncertainty aiming to probabilistically assess the impact of human errors during construction on the structural safety of the post-tensioned concrete bridge. In a preceding study, Galvão et al. [55] had deterministically evaluated the impact of some construction and design errors on the structural safety of a prestressed concrete roadway bridge considering error magnitudes. Here, construction errors are modelled as possible occurrences and not as already observed or identified errors.

The analysis performed in this section is summarised as follows; in subsection 4.6.1, each error, detrimental or beneficial, is independently introduced considering only their respective error magnitude PDF, i.e., disregarding the HEP PDFs (see Table 4.7). Subsection 4.6.2 encompass the implementation of the HRA event tree (see Figure 4.2) for combinations of detrimental and beneficial errors (e.g., E3+E4, among others – see Table 4.8). A sensitivity analysis concerning HEP reduction is performed in 4.6.3 (see Figure 4.8). In 4.6.4, the HRA event is implemented by combining two or more detrimental errors (e.g., E1+E7, E1+E3+E4, among others – see Table 4.10). Note that here multiple error occurrences address the possibility of the occurrence of multiple errors.

The construction errors models are introduced in the surrogate-based reliability analysis procedure through the HRA event tree proposed by Stewart [120]. In short, for each beneficial, detrimental and combination of detrimental errors, a surrogate model is set to assess the performance function $G(X)$ and, subsequently, the probability of failure.

Notwithstanding the significant computational cost reduction achieved by the defined surrogates of the FEM, further reduction of the computational costs was necessary. The computational cost reduction to a realistic timeframe was achieved through the vectorisation of the MATLAB script used to model the HRA event tree and the script used to invoke UQLab's algorithms for reliability analysis [132]. Vectorisation is a computer programming technique that allows the application of operations or functions to the whole vector or matrix instead of applying them to their individual elements. This allows one to reduce the computational costs (i.e., increase computational speed) of a script in several orders of magnitude (i.e., three to four orders of magnitude) [147].

4.6.1. Single error analysis – error magnitude PDFs only

The influence of the error magnitude PDFs alone on the structural failure probability was initially assessed. Succinctly, the rate of occurrence of the errors is set to 1.0, meaning that construction errors will occur. In other words, for every run, a deviation to the input of interest is introduced according to the error magnitude model of each construction error, independently. Furthermore, each error magnitude PDF, detrimental or beneficial, is directly linked to a structural failure probability. The results of this analysis are reviewed in the second column of Table 4.7.

Table 4.7- Reliability index and failure probability due to the error magnitude PDFs

Error models	Reliability index (Probability of failure)		
	No bounds	m_e bounds	With bounds
E1	3.01 (1.31×10^{-03})	0% - 50%	6.13 (4.35×10^{-10})
E2	7.20 (3.07×10^{-13})	-	-
E3	6.97 (1.62×10^{-12})	0% - 50%	7.09 (6.89×10^{-13})
E4	7.08 (7.24×10^{-13})	-	-
E5	4.40 (5.30×10^{-06})	0% - 30%	7.00 (1.27×10^{-12})
E6	7.15 (3.89×10^{-13})	-	-
E7	1.81 (3.54×10^{-02})	0% - 50%	6.72 (9.41×10^{-12})

The beneficial error magnitude PDFs (i.e., E2, E4, E6) had little influence on the structural failure probability, sometimes decreasing the structural reliability slightly. Given the very low initial failure probability of the system, this slight decrease in structural reliability is caused by some inaccuracy or instability in the computation of very low probabilities of failure. One can conclude that the beneficial error models did not improve failure probability in this case study. On the other hand, the detrimental error

magnitude PDFs, namely, E1, E5 and E7, significantly impacted the structural failure probability, being E7 the error whose error magnitude PDF had the largest impact on safety reduction.

The error magnitude PDF of E1 (i.e., reduced area of post-tensioning reinforcement) introduced a considerable reduction in structural safety, reducing the initial reliability index from 7.17 to 3.01. With respect to E3, little impact on safety reduction is observed since it was modelled as the effective height of conventional tensile reinforcement; however, the post-tensioning reinforcement is responsible for most of the carrying capacity of the structure. The E5, modelled as width decrease of the different layers of the superstructure's rib, leads to a reliability index of 4.11. Finally, the concrete compressive strength reduction (i.e., E7) was the most detrimental error leading to a reliability index of 1.81, caused mainly by the extension added to the tail of its PDF (see PDF in Figure 4.2). Furthermore, the strength reduction affects all layers of the critical cross-sections of the superstructure, i.e., spatial variability of the concrete strength was not considered. Further investigations through random fields are recommended to address this shortcoming.

Despite being carefully defined, the error magnitude PDFs produce values that one may argue as unrealistic or would rarely go undetected and not be mitigated during the construction process—especially those more sensitive to human eyes, i.e., geometry-related errors. For instance, one might find it hard to believe that a complete layer of reinforcement would go missing during the construction of a bridge, which is the case when a realisation with an error magnitude of -100% for E1 (i.e., reduced area of post-tensioning reinforcement) is concerned. Nonetheless, one can also argue that gross errors that sometimes sound unrealistic may have a non-zero likelihood of occurrence [54]. Either way, the range of the values produced by the detrimental error magnitudes PDFs is restricted to more feasible ranges, using bounds displayed in the third column of Table 4.7. The obtained results considering such constrained PDFs are presented in the last column of Table 4.7, showing a less significant decrease in structural safety. This was already expected since, with the bounds, the largest deviations previously introduced by the original error magnitude PDFs are removed from the analysis; thus, no significant change to the tail of the original PDF of the random variables affected by the error is introduced. The truncated PDFs still lead to an integral of the distribution equal to one.

4.6.2. Detrimental and beneficial errors pairs – HEP and error magnitude PDFs

Considering now the HRA event tree displayed in Figure 4.2, the failure probabilities of the case study are summarised in Table 4.8 according to the displayed combination of detrimental and beneficial errors. Meaning that the occurrence of either beneficial or detrimental errors is allowed in the probabilistic

analysis as described in the HRA event tree in 4.2.3. The failure probabilities given by the different HEP PDFs (i.e., before and after inspection – see Figure 4.1a) differ in one order of magnitude (see Table 4.8) for the errors concerning the post-tensioning reinforcement area (i.e., E1+E2) and the superstructure's rib width (i.e., E5+E6). However, for the concrete compressive strength associated error (i.e., E7), the results are the same since visual inspection works are not expected to have any influence on error detection and, therefore, any influence on the reduction of its HEPs. The models addressing the effective height of the tensile reinforcement (i.e., E3 and E4) have a low impact on safety reduction, as already demonstrated in Table 4.7 and discussed in 4.6.1. The concrete compressive strength-related error is identified as the error with the highest impact on safety reduction.

Table 4.8 – Probability of failure given HRA event tree

Error models	Reliability index (Probability of failure)	
	After inspection	Before inspection
E1 + E2	4.55 (2.74×10^{-06})	3.86 (5.72×10^{-05})
E3 + E4	7.15 (4.45×10^{-13})	7.15 (4.32×10^{-13})
E5 + E6	5.78 (3.79×10^{-09})	5.29 (6.18×10^{-08})
E7	3.49 (2.52×10^{-04})	3.49 (2.52×10^{-04})

In summary, for a certain range of reduction introduced by the error magnitude PDF to the parameter of interest at a given rate (i.e., number of times $RN_i < HEP_{i,d}$), failure develops into a more likely scenario. For instance, if the strength of the concrete is lower than the required strength to sustain its self-weight and other permanent loads, failure is inevitable since $G(X)$ will assume a negative value. Consequently, the frequency of occurrence of such an event will increase the probability of failure of the structure, especially when the discrepancy between the probability of failure of the error-free scenario and such an event is several orders of magnitude.

4.6.3. HEP reduction

The HEP PDFs considered in 4.6.2 might not adequately mirror today's reality. Considering the latest progress in the quality control and standardization of the construction process, especially in the bridge engineering field, the decrease of the previously introduced HEPs is a reasonable consideration that should be investigated. Furthermore, HEPs are also dependent on the skills of the construction worker, internal framework for quality control, socially established frameworks for quality assurance, and risk tolerance, among other factors. As such, scenarios considering the reduction of the HEP are analysed aiming to assess the increase of structural safety due to the decrease of HEPs caused by more effective implementation of quality control strategies. This is accomplished by shifting the mean value of HEP

PDFs. Accordingly, Figure 4.8 summarises the results of such analysis for the errors with the highest impact on safety reduction, i.e., E1+E2 and E7.

The increase and decrease of the mean values of the HEP PDFs by one order of magnitude at a time demonstrated a similar trend, for E1+E2 and E7, in the reduction and increase of safety. Despite not being very evident, one can note a slight tendency for a plateau when the mean values of the HEPs models are approaching the lower end of the chart. Therefore, the impact of construction errors on safety reduction, as modelled in this work, can be constrained if the error rate is ensured to be low enough. Not surprisingly, this is what quality management measures and standards suggest. Meaning, that structural safety can only be assured if efficient quality control measures are in place to constrain the rate of occurrence of errors and by correcting those that have been identified.

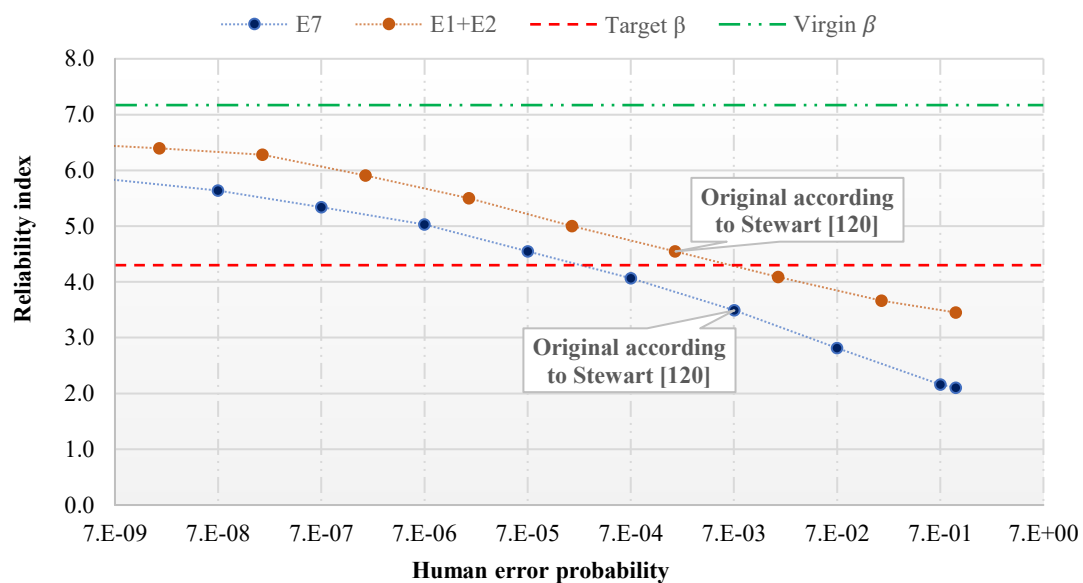


Figure 4.8 – HEP effect on structural safety

The original E7 PDF proposed by Stewart [120] put the structure reliability index below the target safety level, while the original E1+E2 models put the structural reliability index slightly above the target safety level (see Figure 4.8). Nonetheless, from Figure 4.8, it is noticeable that the assurance of a structural safety level close to the virgin reliability index (i.e., $\beta = 7.17$) demands a HEP PDF with a mean value way lower than 7.0×10^{-09} for both errors, especially for E7. The virgin reliability index notion, introduced by Hajdin et al. [17,103] and computed in 4.5.2, refer to the reliability index of the undamaged (i.e., the absence of deterioration process or construction errors) state of the bridge. The results displayed in Figure 4.8 suggest that the computed virgin reliability index would be hard to ensure if the construction error models were to be taken into account since, after reduction of the HEPs' mean value in several order of magnitudes, the computed reliability index was still below the virgin reliability index. Furthermore,

in real life, a HEP PDF with a mean value below 7.0×10^{-9} seems to be hard to achieve through quality control procedures. One should keep in mind that the analysis is also dependent on the PDFs of the error magnitude and the importance of the parameters affected by them on structural safety.

4.6.4. Multiple occurrences of detrimental errors

The impact of errors in structural safety should encompass the consideration of the simultaneous occurrence of different errors. Some dependency between the occurrence of different errors is assumed. Such dependency is based on the assumption that one should assume an error-prone realisation for multiple occurrences of errors if a first error has occurred. Therefore, in the HRA event tree, if an error has been recorded is likely that multiple errors (i.e., the simultaneous occurrence of more than one error) will follow in the same realisation. The rate of occurrence of multiple errors and their dependency is provided by the common RN_i used for d^{th} verifications in "Is $RN_i < HEP_{i,d}?$ " (see Figure 4.2) for different errors. Consequently, for realisations where RN_i takes a very low number, more than one detrimental error is likely to follow because the condition in "Is $RN_i < HEP_{i,d}?$ " will likely be true for more than one detrimental error. The simultaneous occurrence of errors was considered most relevant for detrimental errors. This is mainly because beneficial errors were not considered relevant for the improvement of structural safety (see 4.6.1).

Keeping in mind that there is a maximum of 4 possible detrimental errors per simulation (scenario with results in the last two columns of Table 4.10), the realisations where one and multiple errors have taken place can be summarised as follow: (i) the rate of occurrence of at least one error is 1.22%, (ii) the rate of occurrence of at least two errors is 0.36%, (iii) the rate of occurrence of at least three errors is 0.076% and (iv) the rate of occurrence of four errors is 0.013%.

Furthermore, as intermediate simulation results, the dependency between two errors is summarised in Table 4.9. The dependency is here understood as the probability of occurrence of one error given the occurrence of another error (e.g., $P(E_1|E_3)$). Thus, Table 4.9 should be read as the probability of occurrence of the error in the row given the occurrence of the error in the column. To put the obtained numbers in practical terms, the computed dependency of the errors can be seen as of low, moderate and high dependency if the obtained conditional probabilities are approximately 0.06, 0.15 and 0.51, respectively [148,149].

Table 4.9 – Dependency matrix

	E1	E3	E5	E7
E1	1.00	0.17	0.30	0.14
E3	0.24	1.00	0.35	0.17
E5	0.12	0.10	1.00	0.07
E7	0.56	0.48	0.70	1.00

Table 4.10 – Structural failure probability due to multiple error occurrences.

Two-Errors	Reliability index	Three-Errors	Reliability index	Four-errors	Reliability index
E1+E3	4.64 (1.76×10^{-06})	E1+E3+E5	4.62 (1.90×10^{-06})	E1+E3+E5+E7	3.54 (1.98×10^{-04})
E1+E5	3.97 (3.67×10^{-05})	E1+E3+E7	3.56 (1.85×10^{-04})		-
E1+E7	3.52 (2.19×10^{-04})	E1+E5+E7	3.51 (2.22×10^{-04})	-	-
E3+E5	5.85 (2.50×10^{-09})	-	-	-	-
E3+E7	3.52 (2.15×10^{-04})	-	-	-	-
E5+E7	3.50 (2.37×10^{-04})	-	-	-	-

The impact of multiple errors in structural safety reduction was summarised in Table 4.10. To assess the influence of the combination of errors in the performance function (i.e., $G(X)$) for realisations where multiple errors were verified, different surrogates were created for the combinations provided in Table 4.10. Outputs of the analysis demonstrate that the combination itself did not introduce additional safety reduction since the results show that the probability of failure of the structure is dominated by the most detrimental error in the combination. Simply put, the overall failure probability of the combination will be approximately the failure probability computed for the most detrimental error in the combination. For instance, for combinations where E7 has been introduced, the system failure probability for any combination will be around 2.52×10^{-04} ($\beta=3.49$). A failure probability that was already obtained in 4.6.2. Such observation is true because of the difference in the impact of the different errors in safety reduction.

4.7. Conclusions

Construction errors are too often neglected when structural safety is concerned. Hence, this work's novelty lies in considering construction errors as an additional source of uncertainty in a surrogate-based structural reliability analysis procedure leading to the quantification of their impact on structural safety reduction. Bearing in mind the assumptions, scenarios, results and the discussion introduced in this work, the following conclusions are drawn:

1. Detrimental and beneficial errors have an asymmetric impact on structural safety. While detrimental errors can decrease structural safety significantly, conservative errors will not increase structural safety considerably. That being said, one needs to state that this does not mean one cannot increase structural safety with strategic decisions.
2. Structural safety levels obtained when neglecting construction errors are hard to assure when construction errors as an additional source of uncertainty are introduced in the analysis, even when human error probabilities are significantly reduced. Simply put, the results suggest that the actual probability of failure of the case study is limited to a certain upper threshold due to construction errors. A system can only be as reliable as the quality control procedure or as good as the efficiency of the error identification and mitigation procedure employed; nonetheless, these can not be improved endlessly.
3. The combination of multiple errors does not reduce structural safety beyond the safety reduction already introduced by the most detrimental error in the combination. Meaning that, in the end, safety reduction due to construction error can be mostly modelled considering single error occurrence scenarios.

The ageing of bridges brings with it a margin of safety reduction and additional uncertainties that must be dealt with. Additionally, execution quality is something infrastructure management institutions and engineers should be concerned with, as well as the compliance of available blueprints with the executed structure back in the day. Therefore, a screening procedure for possible construction errors or construction deficiencies identification is highly recommended when structural safety management is concerned. Furthermore, design errors not addressed in this work should also be investigated despite being part of a more standardized procedure and thus less susceptible to errors.

The combination of construction error models, non-linear FEM and surrogate-based reliability analysis led to the establishment of relevant benchmark results when construction errors are concerned. Such benchmarks are absent in the literature and are important for an improved understanding of the overall impact of construction errors on the structural safety of bridges.

5. Lifetime structural safety of a reinforced concrete bridge*

"Dreams without goals are just dreams, and they will ultimately fuel disappointment. On the road to achieving your dreams, you must apply discipline and consistency. Because without commitment, you will never start, but more importantly, without consistency, you will never finish."
by Denzel Washington

Neryvaldo Galvão, Rade Hajdin, Aleksandar Trifunović, José C. Matos,

Structural Safety

Under review

Abstract: Construction errors have seldomly been considered when the structural safety quantification of structures is concerned, and even less so when it comes to reliability-based service life estimation of bridges. Given the multiple reports of the collapse of bridges due to construction errors, its consideration as an additional source of uncertainty is of utmost importance to close the gap between the nominal probability of failure suggested by the codes and the actual probability of failure of structures. The foundations to cover such a research gap are laid in this paper, considering non-linear finite element modelling and surrogate-based reliability analysis techniques coupled with active learning techniques. In addition to construction errors, carbonation-induced corrosion and concrete ageing are considered for service life estimation. In summary, two key scenarios are analysed, one where construction errors are neglected as a source of uncertainty and another one where the possibility of a faulty executed structure due to construction error is introduced, leading to the quantification of service life reduction of a case study due to construction errors.

*This section, as presented here, is likely to suffer multiple changes during the peer-review process required for journal publication.

5.1. Introduction

The service life of bridges depends on numerous factors such as initial margin of safety, deterioration rate, maintenance, load increase, construction errors and proper use, among other factors [13,109,113,115]. Many of these factors have been, up to a certain extent and in some way or another, discussed in the literature and considered for service life prediction of bridges [150–153]. However, despite the awareness of construction errors' relevance for structural safety, it is too often neglected when service life prediction or structural safety assessment is concerned. Furthermore, the combination of construction errors with deterioration models for service life prediction has not - to the best of authors' knowledge – been treated in the literature. Consequently, this work aims to tackle this gap in the literature.

The consequences of human errors (e.g., procurement, design, construction and operation errors [109]) can be clustered in three main groups, namely: (i) sharp reduction of structural safety due to a gross error leading to collapses during the construction phase or during the first years of operation (e.g., Florida pedestrian bridge collapse [40,154,155], and Chirajara bridge collapse [38]); (ii) structural safety reduction in the long run due to errors, impairing some functionalities and/or leading to premature deterioration of the structure and poor management, leading consequently to the reduction of the service life of the structures in many years (e.g., Morandi bridge [116,117]); and (iii) trivial reduction in structural safety due to negligible errors. The second group is the focus of this work, and it is summarized in Figure 5.1, where the disconnect between the ideal performance of structures is put against the performance of a faulty structure. One should note that the initial performance level, i.e., P_1 and P_2 (see Figure 5.1), does not necessarily differ. Former studies have similarly argued that structural safety should be quantitatively expressed considering a pair of probabilities of failure; where one, is the result of structural reliability theories disregarding gross errors, and the other one a result of the consideration of gross errors in the analysis [156].

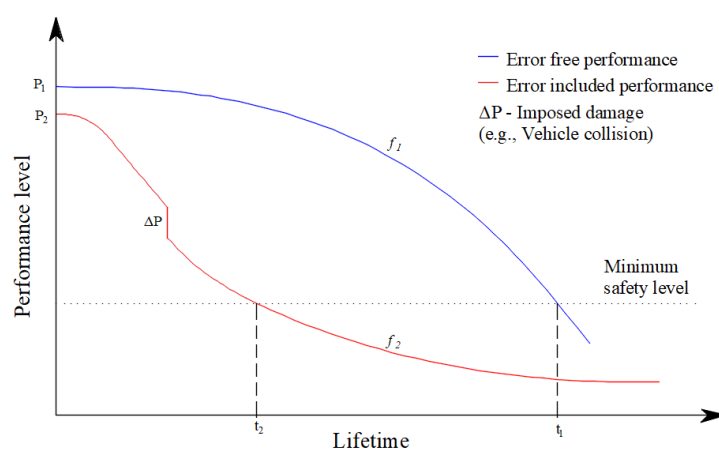


Figure 5.1 – Ideal and faulty theoretical long-term performance of structures

For the long-term performance assessment of a bridge, a case study is introduced, and its longitudinal carrying capacity is assessed through a non-linear structural analysis. The performance parameter considered for the long-term performance assessment is the reliability index. As such, structural reliability analysis techniques are employed, namely, surrogate-based reliability techniques used to replace the expensive finite element model (FEM) used for non-linear structural analysis. Moreover, active learning techniques are also used for a strategic selection of samples to train the surrogate. Deterioration mechanisms such as corrosion and ageing of concrete are initially considered to estimate the end of service life of an ideally executed structure. Later, the possibility of a faulty executed structure due to construction error is introduced in the analysis for the service life prediction of the structure.

5.2. Time invariant reliability assessment

5.2.1. Theoretical background

Civil engineering structures, as well as numerous engineering marvels, are subject to stochastic processes during their lifetime. Stochastic processes are time-dependent or time-variant random variables that characterize the capacity of the structure $R(t)$ or the combination of actions $S(t)$ which act upon the structure over its lifetime. The structural capacity is time-dependent mostly due to deterioration processes such as corrosion, fatigue, etc., or imposed damages (i.e., vehicle collision, earthquakes, etc.). The actions are also time-dependent due to the natural variability of live loads [20,64]. Accordingly, the structural failure probability of a structural system at time t (i.e., $P_f(t)$) is given by the integral in Eq. (5.1),

$$P_f(t) = P(G[X(t)] \leq 0) = \int_{G[X(t)] \leq 0} f_X [X(t)] dx \quad (5.1)$$

where $G[X(t)] = R(t) - S(t)$ is the limit state function that takes as input the realization of the stochastic processes at time t characterized by the matrix $X(t)$ and the joint density function $f_X [X(t)]$. However, the computation of $P_f(t)$ alone can be quite deceiving, excluding stationary processes, since it does not take into account the preceding loading history up to t ; therefore, possible failure events prior to the time t [157]. Thus, the full history of the random process up to time t , bounded by a time interval known as the reference period $T \in [0 \rightarrow t]$, should be considered, requiring one to solve the stochastic problem using, for instance, the first-passage probability problem. Nonetheless, this calls for a good understanding of sophisticated concepts about stochastic processes which on its own is not enough when dealing with complex problems (i.e., high dimensional problems and numerical representation of the

system) [158,159]. Hence, the problem is often simplified into the so-called time-invariant reliability or time-integrated approach, considered to be a good approximation of the actual problem [64,75].

In time-invariant reliability analysis, the stochastic processes are transformed into random variables for the selected reference time period (i.e., removing their explicit time dependency). In this transformation, the live loads are modelled by extreme value distributions (i.e., $S_{max}(T)$) i.e., the probability of an extreme occurrence with some given intensity over the specified reference period T . Moreover, for practical reasons, the structural capacity is often considered to be time-invariant. Hence, the limit state function becomes,

$$G(X) = R_i - S_{max}(T) \quad (5.2)$$

where R_i is the time-invariant capacity of the structure over the reference period T . Nonetheless, to model structural deterioration over the lifetime of the structure, the capacity R_i must be updated as a function of a deterioration process [160,161]. One should note that the problem, as represented in Eq. (5.2), can lead to conservative failure probabilities estimation when comparing $S_{max}(T)$ with the deteriorated capacity R_i since the peak realizations of the demand can take place when the structure is in a fairly good state [20,64,157]. The transformation from the time-variant to a time-invariant reliability problem is often convenient since the latter can be solved by more simplistic approaches available in the literature (i.e., FORM, Monte Carlo Simulation, etc), as discussed in 5.4.2. Nonetheless, it is important to understand the background of the time-invariant approach and its limitations as a consequence of a simplification of the time-variant approach.

5.2.2. Deterioration models

When reinforced concrete structures are concerned, reinforcement corrosion during the structure's lifetime is of interest since structural safety can be reduced if the damage process reaches critical levels. Corrosion is an electrochemical process where the electrons move from the anode (i.e., reinforcement bars) to the cathode (i.e., concrete cover) region affecting the initial chemical composition of the bars that in combination with water and oxygen, produce oxides of increased volume. These oxides are responsible for concrete cover spalling and loss of reinforcement cross-section area. The reinforcement corrosion is mainly triggered by concrete carbonation or chloride ingress. The former is triggered by sufficient penetration of CO_2 present in the atmosphere into the reinforced cross-section through the concrete cover, leading to a reduction of the high alkalinity of concrete (i.e., $\text{pH} > 12.6$) followed by the destruction of the protective layer formed around the reinforcement during concrete curing [75,162,163].

The concrete alkalinity reduction and the destruction of the protective reinforcement layer accelerate the electrochemical corrosion process in three orders of magnitudes, separating the initiation phase (i.e., the depassivation of reinforcement) from the propagation phase (i.e., active corrosion) [75,162,163]. Each phase is modelled according to *fib* [65,162]. The carbonation depth x_c at time t in years (i.e., $x_c(t)$) can be computed according to Eq. (5.3), based on Fick's first law of diffusion,

$$x_c(t) = \sqrt{2 \cdot k_e \cdot k_c \cdot (k_t \cdot R_{ACC,0}^{-1} + \varepsilon_t) \cdot C_s \cdot \sqrt{t} \cdot W(t)} \quad (5.3)$$

$$W(t) = \left(\frac{t_0}{t}\right)^{\frac{(\rho_{SR} \cdot ToW)^{b_w}}{2}} \quad (5.4)$$

$$k_e = \left[\frac{1 - \left(\frac{RH_{real}}{100}\right)^{5.0}}{1 - \left(\frac{RH_{ref}}{100}\right)^{5.0}} \right]^{2.5} \quad (5.5)$$

$$k_c = \left(\frac{t_c}{7}\right)^{b_c} \quad (5.6)$$

$$g = a - x_c(t) \quad (5.7)$$

where k_e is an environmental function, k_c is an execution transfer parameter, k_t is a regression parameter, $R_{ACC,0}^{-1}$ is the inverse effective carbonation resistance of concrete, ε_t is an error term, C_s is the CO_2 concentration, and $W(t)$ is a weather function given as a function of time t in years. Further details of the introduced random variables in Eq. (5.3), (5.4), (5.5), (5.6) and (5.7), and their probabilistic distribution function (PDF) are summarized in Table 5.1. The carbonation depth $x_c(t)$ is modelled against the concrete cover a , leading to the establishment of the Eq. (5.7) as the limit function g for probabilistic characterization of the initiation phase (i.e., the probability that carbonation reaches reinforcement), considered to be over when a cumulative failure probability of 9.68×10^{-2} (i.e., $\beta = 1.3$) over the years is attained [162]. Note that such a target value is used to separate the initiation phase from the propagation phase.

Table 5.1 – Carbonation induced corrosion random variables ([162,164])

Random Variables	Notation	Mean Values	CoV	PDF
Real relative humidity	RH_{real}	77.6%	14%	Beta
Reference relative humidity	RH_{ref}	65%		Constant
	b_c	-0.567	4.23%	Gaussian
Curing time	t_c	4 days		
Factor for natural carbonation	k_t	1.25	28%	Gaussian
Accelerated carbonation	$R_{acc,0}^{-1}$	$9.8 \times 10^{-11+}$ (3092) ⁺	41.8%	Gaussian
Error Term	ε_t	$1 \times 10^{-11+}$ (315.5) ⁺	0.15	Gaussian
CO ₂ Concentration	C_s	8.2×10^{-4} [kg/m ³]	12.2%	Gaussian
Time of wetness	ToW	0.26		Constant
Exponent of regression	b_w	0.446	36.5%	Gaussian
Probability of driving rain	ρ_{SR}	1		Constant
Time of reference	t_0	0.0767 years		Constant
Concrete cover	a	130 mm/ 40mm	32%	Lognormal
Current intensity	i_{corr}	1.0 – 3.0 $\mu A/cm^2$	20%	Gaussian

⁺(m²/s)/(kg/m³) + (mm²/years)/(kg/m³)

The propagation phase is characterized by the actual occurrence of corrosion of the reinforcement triggering the effects of corrosion, namely the loss of the reinforcement cross-section area, bond reduction and the embrittlement of the reinforcement. The reinforcement cross-section loss is modelled according to Eq. (5.8),

$$x_{corr}(t) = \int_{t_{ini}}^t V_{corr}(t) \cdot dt \quad (5.8)$$

where $x_{corr}(t)$ is the loss of steel radius and $V_{corr}(t) = 1.16 \cdot 10^{-3} \cdot i_{corr}$ (cm/year) is the degradation rate in the radial direction of the reinforcement given as a function of the corrosion current intensity i_{corr} ($\mu A/cm^2$) [165].

Besides the loss of reinforcement cross-section area, corrosion brings with it two additional unpleasant effects, namely, the reduction of the yielding f_{sy} and ultimate f_{su} strength of the reinforcement, and the ductility reduction ε_{st} of the reinforcement due to the notch effect, caused mostly by the imperfections developed throughout the reinforcement bars [161,163,166,167]. These are modelled, respectively, according to Eq. (5.9), (5.10), and (5.11) as a function of the average percentage

loss of reinforcement cross-section area η_s (i.e., based on Eq. (5.8)) and their uncorroded properties (i.e., f_{sy0} , f_{su0} and ε_{st0}) [166]. The ductility loss is particularly of additional relevance when bending moment redistribution is concerned (i.e., structural system-level analysis) since it is very much dependent on the ductility of the reinforcement.

$$f_{sy}(\eta_s) = (1 - 1.435 \times 10^{-2} \eta_s) \cdot f_{sy0} \quad (5.9)$$

$$f_{su}(\eta_s) = (1 - 1.253 \times 10^{-2} \eta_s) \cdot f_{su0} \quad (5.10)$$

$$\varepsilon_{st}(\eta_s) = (e^{-2.05 \times 10^{-2} \eta_s}) \cdot \varepsilon_{st0} \quad (5.11)$$

The concrete itself can be affected by numerous deterioration mechanisms such as sulphate attack, acid attack, freezing-thaw cycles, and expansive aggregate reactions, among others. According to Wang et al.[161], concrete ageing is also addressed in this work. The concrete strength deterioration is modelled as a function of time t in years according to Eq. (5.12) and (5.13) considering two main parameters, i.e., concrete mean compressive strength f_{cm0} at 28 days and the standard deviation σ_0 of its PDF. Nonetheless, comprehensive work in this field is missing.

$$f_{cm}(t) = (1.3781^{-0.0187[\ln(t)-1.7282]^2}) \cdot f_{cm0} \quad (5.12)$$

$$\sigma(t) = (0.0347t + 0.9772) \cdot \sigma_0 \quad (5.13)$$

5.2.3. Construction error models

Some of the construction error models introduced by Stewart [120] are introduced here to further support the lifetime structural safety assessment. These models are also discussed in more detail by Galvão et al. [168] and Epaarachchi and Stewart [53]. Key parameters for the definition of the PDF of the Human error probability (HEP) and Error magnitude (EM) models are introduced in Table 5.2, namely, the median \tilde{m}_i and the error factor EF_i used to compute the standard deviation estimation of the HEP PDF. Additionally, the median estimate λ_{BE} and the upper bound estimate (i.e., 90th percentile) λ_{UB} of the EM models are also provided. The lognormal PDF of the HEP models and the EM models are displayed in Figure 5.2a and Figure 5.2b. These are important since they provide a sense of the range of values being considered, as well as their frequency.

Table 5.2 – Construction error models parameters [120]

Error type	After Inspection		λ_{BE}	λ_{UB}
	\tilde{m}_i	EF_i		
E1 Reduced area of reinforcement	3.73×10^{-4}	10	-14.30	-82.22
E2 Increased area of reinforcement	1.95×10^{-4}	10	15.16	69.22
E7 Inadequate concrete mix	0.0049	3	-9.58	-38.1

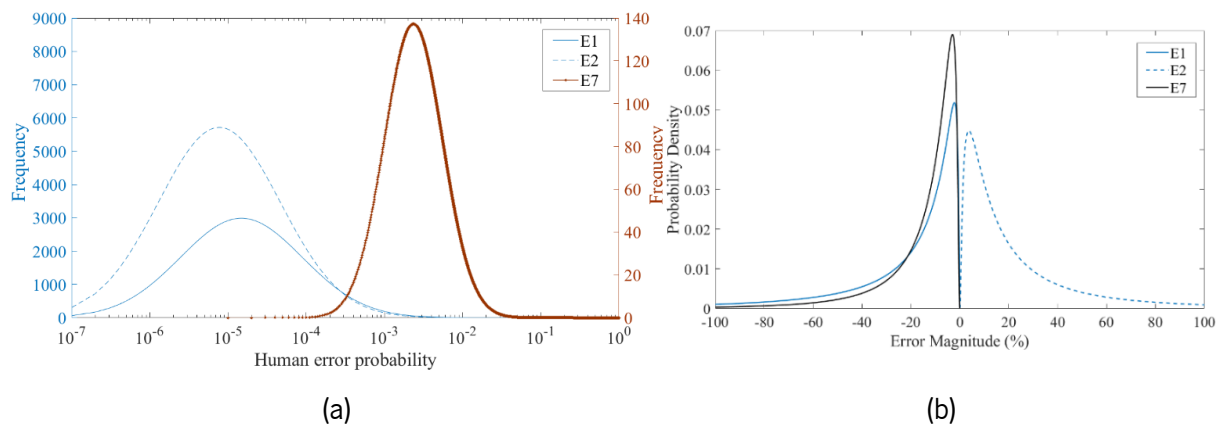


Figure 5.2 – (a) Human error probability and (b) error magnitude PDFs

The HEP models and EM models are introduced in the reliability analysis through the event tree displayed in Figure 5.3, where RN_i stands for a random variable with a uniform PDF with values ranging between one and zero; X_{nom} addresses the average occurrence of the random variables being affected by the construction errors, and these are the reinforcement cross-section and the concrete compressive strength.

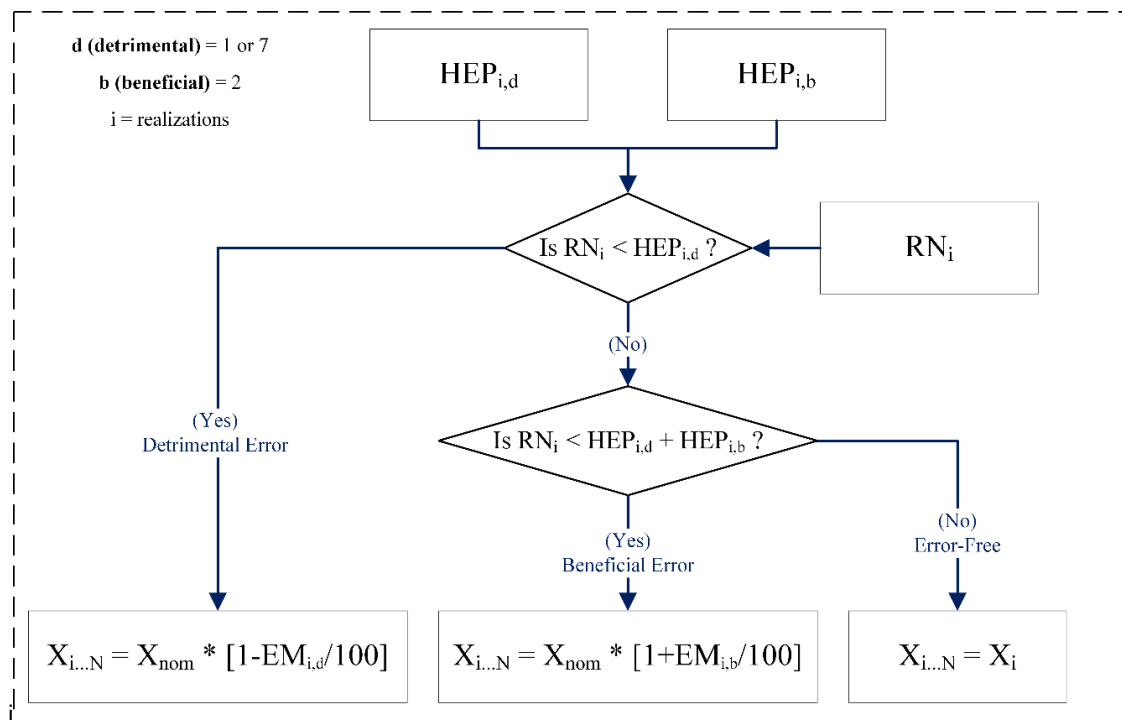


Figure 5.3 –Event tree for human reliability assessment

5.3. Structural analysis

5.3.1. Case study – description and digitalization

A case study provided by the Swiss Federal Railways (SBB) is introduced to support the developed research work. The case study is the new Niederlenzerstrasse SBB overpass built in 2009 in Lenzburg to integrate the existing railway connection between Zurich and Bern. It is a three-span cast-in-place reinforced concrete bridge with a total length of 47.28 m which is monolithically connected to the abutments and two piers. The outward and the central spans are 13 m and 21 m long, respectively. The overpass is formed by two piers, each made of two circular columns with 1 m in diameter grounded on the cap of drilled piles (see Figure 5.4a). The superstructure cross-section displayed in Figure 5.4b has 7.0 m in width and 1.35 m in height. The overpass is longitudinally reinforced mostly with 22 mm and 50 mm bars of class S500B, according to Figure 5.4c. The 50 mm bars are only used in the superstructure as additional reinforcement in the middle span and over the piers cross-section, i.e., section A (with 17 m in length) and section B (with 7 m in length) represented in Figure 5.4a. The resistance class of the employed concrete is C30/37, and its exposure class is XC4. The overpass was designed according to the current Swiss society of Engineers and Architects (SIA) standards.

A digitalization campaign for characterization purposes of the condition state of the bridge, as well as its geometry, was performed using an unmanned aerial vehicle. The digital model of the bridge as it was standing in March of 2022 was created through photogrammetry (see Figure 5.5). The results of this photogrammetry-assisted inspection indicated that there are no advanced deterioration processes on the bridge and that its geometry is in agreement with the blueprints. The digital model will be used by the stakeholder (i.e., SBB) as a reference model to track the appearance and evolution of future deterioration processes through different 3D snapshots of the bridge to be built throughout its years of operation. The highest potential for the application of digital bridge models is certainly in bridge management. The greatest challenges for the seamless implementation of digital models in practice lie in the process of data collection and data post-processing, where the identification of structural elements and damage characterization has a pivotal role. It is expected that the perpetual advancements in machine learning, artificial intelligence and other cutting-edge technologies will significantly improve the speed of data collection and foster data post-processing, enabling the widespread use of digital models.

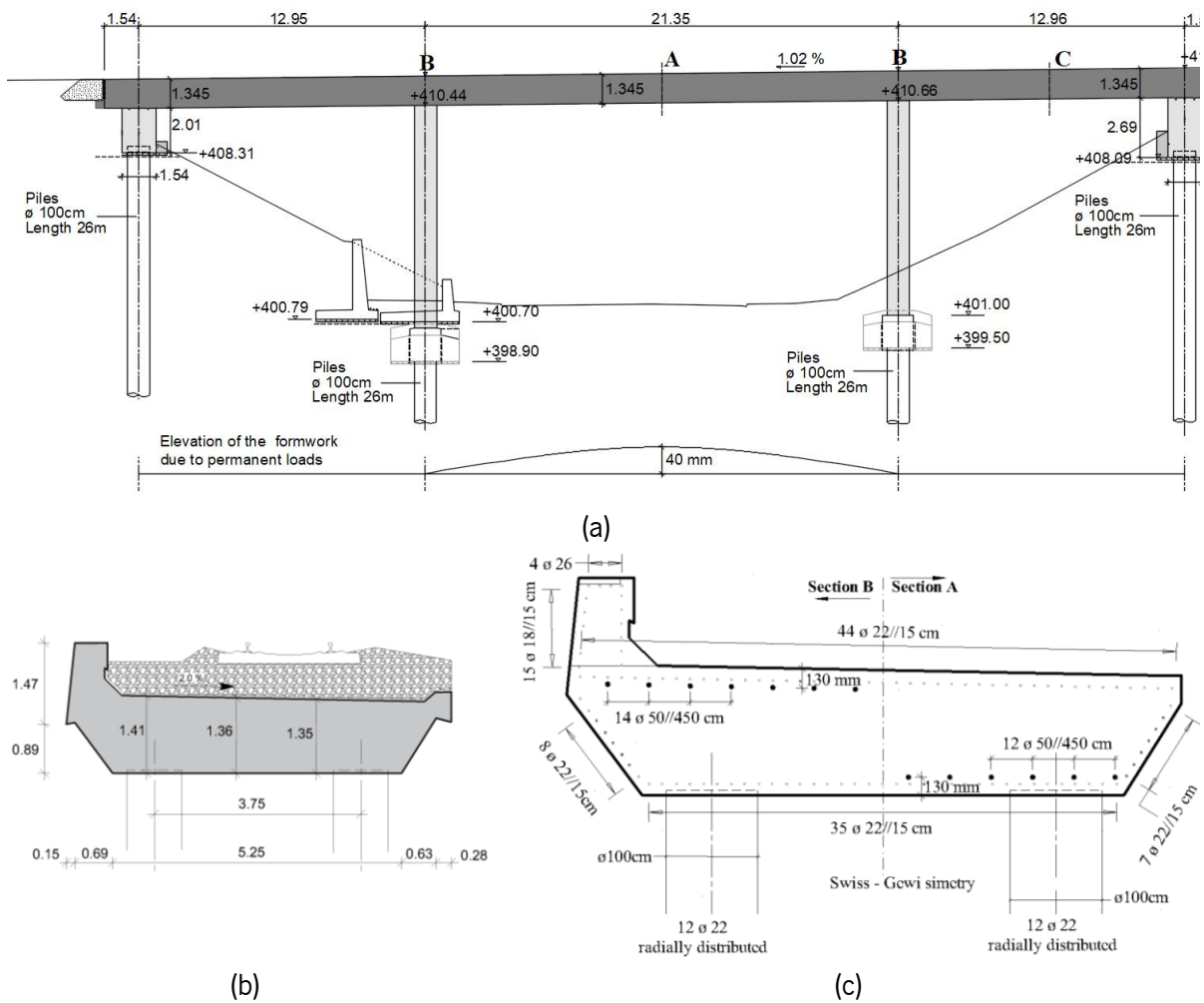


Figure 5.4 – (a) Longitudinal profile, (b) superstructure cross-section and (c) reinforcement detailing of the case study



Figure 5.5 – Digital model of the Niederlenzerstrasse SBB overpass

5.3.2. Numerical modelling

For structural analysis purposes, a 2D FEM using beam elements is created in DIANA FEA software. A class III-Mindlin-Reissner beam element of 0.15 m with two nodes and three degrees of freedom per node is used (i.e., u_x , u_y , and ϕ_z). The model's main usage is the characterization of the maximum carrying capacity of the structure when longitudinal bending is concerned. As such, an equivalent transversal cross-section of the superstructure and piers, with 8 and 9 layers, respectively, is defined to model the structure. For numerical integration purposes, the Gauss rule is considered, and 5 integration points are added for each layer. The concrete was modelled with a fixed total strain-based model. The Eurocode constitutive model, according to the properties given in Table 5.3, was introduced to model the reinforcement and the concrete stress-strain relationship.

The supports of the overpass were modelled through springs whose stiffness was defined according to the geotechnical conditions of the site and the foundation structure. The stiffness in the horizontal direction was estimated at around 125.94 MN/m for pier one and 115.56 MN/m for pier two (see Figure 5.6). The rotational stiffness is set to be 1230.7 MNm/rad for pier one and 1166.66 MNm/rad for the other one. The abutment horizontal translation stiffness was modelled by employing multiple springs with increasing stiffness according to their depth, as detailed in Table 5.4. The depth of each spring is given as a function of its distance from the centre of gravity of the superstructure.

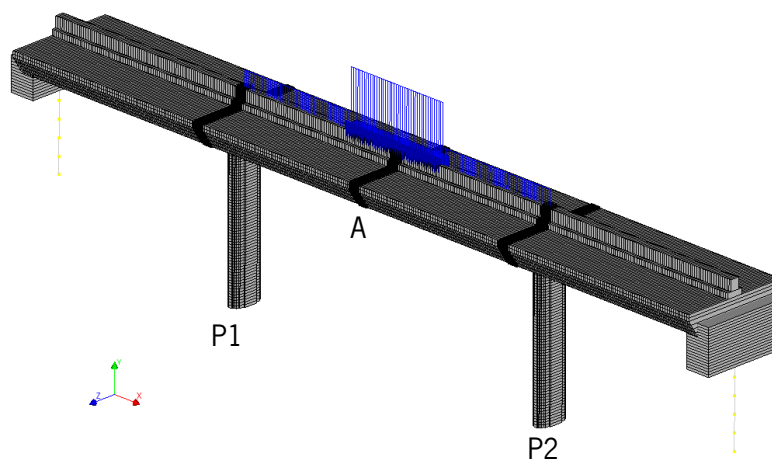


Figure 5.6– Case study finite element model (DIANA FEA)

Table 5.3 – Material mechanical properties

Material Properties	S 500-B	Material Properties	C30/37
ε_{sy} (‰)	2.8	-	-
ε_{su} (‰)	50.0	-	-
ε_{st} (‰)	150.0	ε_{ci} (‰)	2.0
ε_{su} (‰)	200.0	ε_{cu} (‰)	3.0
E_s (GPa)	205	E_{cm} (GPa)	33.0
f_{sy} (MPa)	560.0	f_{cm} (MPa)	38.0
f_{su} (MPa)	580.0	f_{ctm} (MPa)	2.9

Table 5.4 – Abutment support stiffness

Depth	Abutment 1	Depth	Abutment 2
-3.79 m	57 KN/m	-4.49 m	84 KN/m
-4.79 m	96 KN/m	-5.49 m	117 KN/m
-5.79 m	153 KN/m	-6.49 m	171 KN/m
-6.79 m	189 KN/m	-7.49 m	171 KN/m
-7.79 m	219 KN/m	-8.49 m	258 KN/m

The reinforced concrete specific weight was set to 25 KN/m³, leading to a uniform distributed load on the deck of 229.2 KN/m. The remaining permanent load added by the ballast, the track, the sealing protective layers and the protective wall is added as a uniform distributed load of 90.8 KN/m. The selected load model (LM) recommended by SIA to model the rail traffic is the LM71 from Eurocode 1 [62]. The tandem system of LM71 is introduced as a uniform distributed load over a length of 6.40 m. For an initial deterministic analysis, the live load is positioned as displayed in Figure 5.6 with its mean values (i.e., $Q_k = 198.5 \text{ KN}$ and $q_k = 63.2 \text{ KN/m}$) defined as a function of the characteristics values of LM71, considering a Gumbel distribution with a coefficient of variation (CoV) of 10%, according to the bias (λ) provided by Eq. (5.14) [140,169–171]. Simulation-based approaches were used to confirm the estimated values given by Eq. (5.14),

$$\lambda = \frac{1 + \left(\frac{\pi}{CoV\sqrt{6}} - \gamma \right)^{-1} \gamma}{1 + \left(\frac{\pi}{CoV\sqrt{6}} - \gamma \right)^{-1} s_p(\tau)} = 0.794 \quad (5.14)$$

where $s_p(\tau)$ is the Gumbel standard extremal variate given by $-\ln(-\ln(1 - p(\tau)))$. $p(\tau)$ is the exceedance probability of the characteristic value within the 50-year reference period (τ). γ is 0.5772, and it stands for the Euler constant. The characteristic values amount to the 98th percentile of the PDF over a reference period of 50 years. Additionally, the bridge was designed with a dynamic amplification factor of 1.16 and an alpha factor of 1.33 for further adjustments of the characteristic values of the live load.

5.3.3. Load carrying capacity

The structural system carrying capacity is quantified as a function of the load factor of the mean value of the live load, given that the failure is characterized by the strength of materials in their ultimate limit state (i.e., ULS: STR). An incremental interactive procedure based on force control and a modified Newton-Raphson iteration scheme was employed to solve the non-linear problem.

The maximum carrying capacity of the structural system is estimated at around 6.67 times the mean values of the live load (see Figure 5.7). This is attained when the concrete upper fibre of the middle span cross-section (i.e., section A, see Figure 5.6) reaches 3.0 ‰, where right after there is a bump in the load-displacement curve followed by the yielding of the reinforcement in the middle span cross-section and later the yielding of the reinforcement over the piers. The initial bump right after the maximum carrying capacity is mostly caused by the rib in the upper part of the cross-section. The final bump in the load-displacement curve is triggered by the concrete crushing of the lower fibre of the cross-section over the piers. The middle span cross-section yielded capacity is approximately 30.7 MNm, while the yielded capacity of the cross-section over the piers is approximately 33.9 MNm. Nonetheless, the peak capacity of the middle span cross-section, right before the concrete crushing in the upper layer of the rib, is approximately 39.4 MNm, as displayed in Figure 5.8, which represents the bending moment diagram at the structure's maximum carrying capacity.

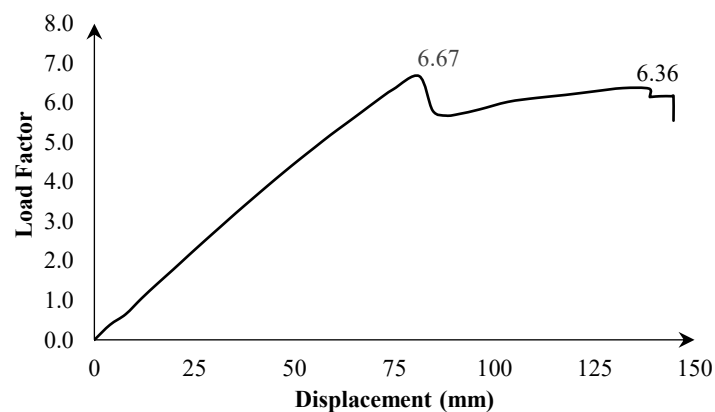


Figure 5.7 – Load-displacement curve in section A

For conventional reinforced concrete, the crack limitation is verified for the quasi-permanent combination, which considers just the self-weight and additional permanent loads with a partial safety factor of 1.0. Consequently, concrete cracking happens with just 10% of the live load. Accordingly, the stiffness reduction due to concrete cracking is barely noticeable in the load-displacement curve since it occurs at an earlier stage (see Figure 5.7). For prestressed or post-tensioned reinforced concrete

structures, such stiffness reduction is evident since the decompression limit state puts stricter requirements in place.

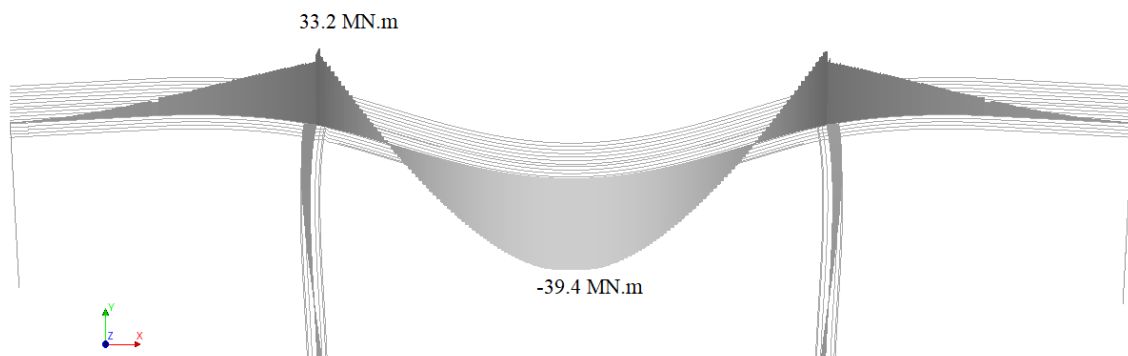


Figure 5.8 – Longitudinal bending moment diagram for the structure's maximum carrying capacity

5.4. Structural safety

5.4.1. Uncertainty characterization

The quantification of the impact of uncertainties in the overall ability of structures to fulfil their intended use during a given reference period provided a certain safety target is a common procedure for structural safety assessment. Simply put, given the careful probabilistic characterization of the variability of relevant input parameters, the procedure aims to assess how likely it is that the output parameter of interest is in agreement with the intended use of the structure. The aforementioned procedure is regularly named structural reliability assessment, and it fundamentally answers one important question; How safe is the structure? Or, put another way, how certain can one be about the structure's safety?

The capacity and demand associated uncertainties, and their correlations, are summarised in Table 5.5 and Table 5.6 according to the provided references. The correlation coefficients considered are obtained from the same references. With respect to the case study's structural carrying capacity, a sensitivity analysis based on Sobol indices, also known as ANOVA, is performed. The results are summarized in Figure 5.9, highlighting the most relevant random variables for the maximum carrying capacity of the system. Those are mainly the reinforcement yielding and ultimate strength, concrete compressive strength, and young modulus.

Table 5.5 – Structural resistance uncertainty characterization

ID	Random Variables	Notation	Mean Values	CoV	PDF	Reference	
1	C30/37	Compressive strength	f_{cm}	38 MPa	14%	Lognormal	[87,172]
2		Tensile strength ¹	f_{ctm}	2.9 MPa	21%	Lognormal	[87,172]
3		Young Modulus ²	E_{cm}	33 GPa	8%	Gaussian	[87]
4		Deck height	t	1.36 m	2.0%	Gaussian	[89]
5		Ultimate strain	ε_{cu}	3.84 ‰	15%	Lognormal	[84]
6	B500B	Yielding stress	f_{sy}	560 MPa	5.4%	Lognormal	[84]
7		Ultimate Strength ³	f_{su}	580 MPa	6.9%	Lognormal	[84]
8		Area ^{4,5}	A_s	–	2%	Gaussian	[84]
9		Peak Strain ^{6,7,8}	ε_{st}	0.17	9%	Lognormal	[84,173]
10		Effective Depth ⁹	d_s	Nom.*1.4 Nom.*1.0	15% 3.3%	Lognormal	[89] [137]
11	Resistance model uncertainty		θ_R	1.00	17%	Lognormal	[138]

¹ $f_{cm} - f_{ctm} \rightarrow$ Correlation coefficient (ρ)=0.7; ² $f_{cm} - E_{cm} \rightarrow \rho=0.9$; ³ $f_{sy} - f_{su} \rightarrow \rho=0.85$; ⁴ $A_s - f_{sy} \rightarrow \rho=0.5$; ⁵ $A_s - f_{su} \rightarrow \rho=0.35$; ⁶ $f_{sy} - \varepsilon_{st} \rightarrow \rho=-0.50$; ⁷ $f_{su} - \varepsilon_{st} \rightarrow \rho=-0.55$; ⁸Characteristic values defined as 10% quantile value according to EC2 Table C.1; ⁹The nominal (Nom.) effective depth is measured from the top layer of the bridge superstructure;

Table 5.6 – Probabilistic characterisation of permanent load, live load and load model uncertainty random variable

ID	Random Variables	Notation	Mean Values	CoV	PDF	Reference
1	Self-weight load ^{1,5}	Sw	25.8 kN/m ³	7.1%	Gaussian	[101,139]
2	Additional Permanent load ^{1,2}	AL	–	11%	Gaussian	[101,139]
3	Live load model uncertainty	θ_S	1.0	15%	Gaussian	[139]
4	Lifetime (50-year peak) Live load model 71 ^{3,4}	LM71	198.5 kN (63.2 kN/m)	10%	Gumbel	[141,169]

¹Model uncertainty included ²Sleepers, rails, railings, etc. ³Characteristic value provided by EC corresponded to the 98th percentile. ⁴50-year reference period. ⁵Correlated with slab thickness ($\rho=0.5$)

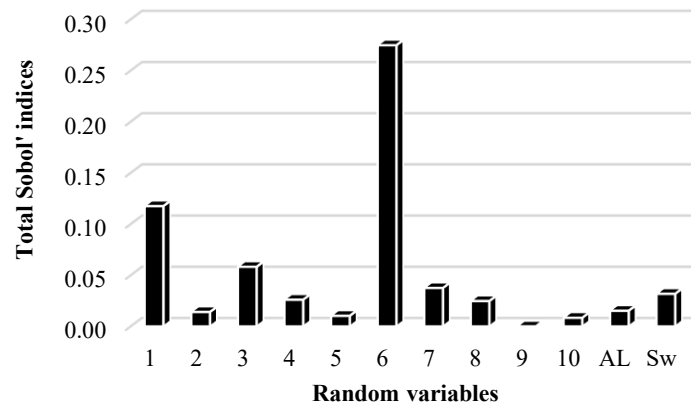


Figure 5.9 – Sensitivity analysis

The variability of the maximum carrying capacity of the system is summarised in Figure 5.10, assuming two modelling strategies named “spatially correlated” and “spatially uncorrelated”. The former considers that the realization of the different random variables takes the exact same value throughout the structure. Meaning, for instance, that the concrete strength in sections A and B (see Figure 5.4a) takes the same realization in the same FEM simulation. This approach is quite often used, aiming to reduce the computational burden required when more sophisticated approaches such as random fields are implemented. With random fields, this shortcoming is addressed since it allows the realization of different occurrences of the same random variable in space. With the spatially uncorrelated strategy, aiming to allow spatial variability for the random variables and avoid large computational burdens, the realizations of the most relevant random variables are allowed to take different values within the FEM model in its most relevant cross-sections highlighted in black in Figure 5.6. In each of these three sections, the most relevant random variables assume different realizations during the same FEM simulation.

The results of the analysis are summarized in the load-displacement curve in Figure 5.10a and the histogram of the maximum load factors (i.e., the maximum carrying capacity of each FEM simulation) in Figure 5.10b. The results show a concentration of the maximum carrying capacity towards the mean value of the histogram of the spatially uncorrelated case when compared with the spatially correlated case (see Figure 5.10b). This is also evident from the results summarized in Table 5.7, showing a reduction of the CoV for the spatially uncorrelated case. Additionally, the 5% and 95% quantile and the minimum and maximum occurrences for the spatially uncorrelated case are inside the same intervals observed for the spatially correlated case.

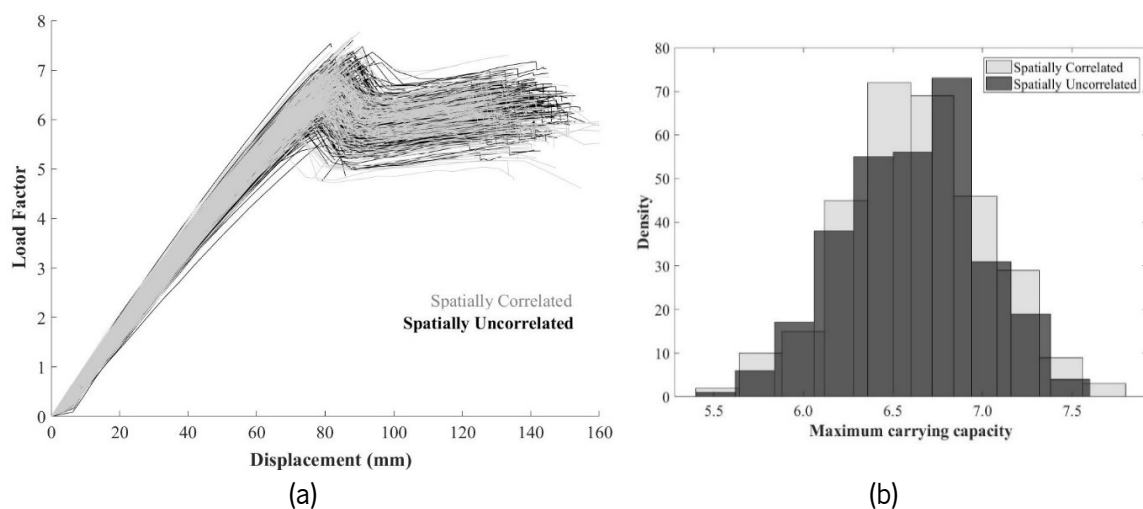


Figure 5.10 – (a) Load-displacement curve (b) maximum carrying capacity generated based on 300 samples generated by the Latin hypercube sampling technique

Table 5.7 – Maximum carrying capacity histogram overview

	Mean values	CoV	Quantile [5%-95%]	Min-Max
Spatially correlated	6.62	6.04%	5.94 - 7.29	5.46 - 7.77
Spatially uncorrelated	6.61	5.75%	5.96 - 7.22	5.48 - 7.60

5.4.2. Initial structural safety

For structural safety quantification, the reliability index is considered. For the estimation of such an index, several techniques are available in the literature. Well-known methods present in several standards and in the literature are the so-called gradient-based techniques, i.e., first-order reliability methods (FORM) and second-order reliability methods (SORM). Moreover, simulation-based techniques such as Monte Carlo simulation, Importance sampling, and Latin hypercube sampling, among others, are also well-known techniques. Nonetheless, neither of them is directly implemented in this work, given their drawbacks. The former (i.e., FORM and SORM) are too often used with some disregard for their limitations. Those are mainly their constrained ability to only approximate accurately first and second-order limit state functions. The latter (i.e., simulation-based techniques) are prohibitive when FEM are considered for structural reliability analysis since millions of simulations are very often required, especially when low failure probabilities are expected.

To overcome the limitations of the aforementioned methods, a kriging-based surrogate technique is implemented [126,127]. The main advantages of surrogate-based techniques are their ability to replace computationally expensive numerical models, such as FEM, with a computationally cheap and accurate approximation function. Furthermore, active learning techniques are often put in place to select specific samples, usually in the vicinity of the limit state equation, to train the surrogate. This allows one to train the surrogate in the vicinity of the limit state equation, which is the region of most interest when structural reliability or failure probabilities are concerned. This refinement process is known as the enrichment procedure. Surrogate models such as kriging, polynomial chaos expansion, and polynomial chaos kriging can approximate very complex limit state functions allowing one to bypass the limitations of FORM and SORM. Once the surrogate has been built, simulation-based techniques are used to estimate the structure failure probability since the surrogate is computationally cheap. The full procedure described in this paragraph is known as Active learning structural reliability analysis, and it is summarised in Figure 5.11. It was implemented using a Matlab-based software named UQLab. For further details, the reader is directed to UQLab user manuals [130,143,144,174,175].

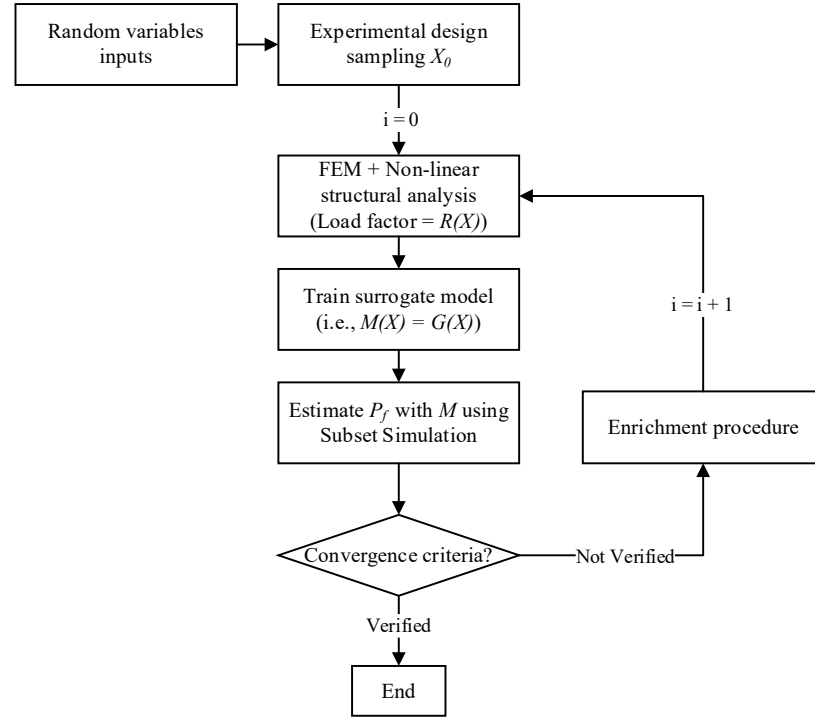


Figure 5.11 – Active learning reliability analysis procedure (Adapted from Moustapha et al. [175])

The limit state equation considered for the structural reliability analysis is presented in Eq. (5.15) where θ_R and θ_S are the resistance and load model uncertainties, respectively. $R(X)$ is the remaining carrying capacity of the structure, given its self-weight and additional permanent loads, estimated with FEM through a non-linear structural analysis procedure. S is the live load random variable characterized by a unitarian mean value and the CoV of LM71. The failure and the safe domain are respectively given by $G(X) \leq 0$ and $G(X) > 0$, as such the structural failure probability P_f is given by Eq. (5.16) where $f_x(X)$ is the joint density function of the random variables matrix X . The dynamic amplification factor (i.e., 1.16) was modelled as a deterministic factor; nevertheless, it can be taken as a random variable. One should highlight that for cases where the maximum load-carrying capacity is reached after the yielding of the reinforcement, the dynamic amplification factor is expected to suffer some reduction. Thus, further investigation to better understand and quantify such reduction is recommended.

$$G(X) = \theta_R \times R(X) - 1.16 \times S \times \theta_S = 0 \quad (5.15)$$

$$P_f = P[G(X) \leq 0] = \int_{G(X) \leq 0} f_x(X) dx \quad (5.16)$$

Two reference periods were considered for structural failure probability estimation, namely 50-year and 100-year. Thus, for the 100-year reference period analysis, the live load PDF function is changed by adjusting the exceedance probability of the characteristic value according to Eq. (5.17) [169,170],

$$[1 - p(1)]^n = 1 - p(n) \quad (5.17)$$

where $p(1) = 4.04 \times 10^{-4}$ is the annual exceedance probability of the live load characteristic value and $p(n)$ is the exceedance probability of the live load characteristic value over a reference period of n years. For a reference period of 100 years, the obtained exceedance probability $p(100)$ is 3.96%.

The performed structural reliability analysis is summarized in Table 5.8 and Figure 5.12. The structural reliability index for the spatially correlated and spatially uncorrelated cases discussed in 5.4.1 are respectively 7.08 and 7.13. The spatially uncorrelated case leads to a higher structural reliability index, meaning that the spatially correlated case is a more conservative approach. Note that the density of the lower tail of the histogram in Figure 5.10b, where the random variables were considered spatially uncorrelated, is thinner than in the other case, which translates to lower occurrences of the lower tail of the histogram. This, as well as the quantile and minimum values of the histogram summarized in Table 5.7, helps explain the structural reliability index increase for this case. Nonetheless, one must note that the observed difference is negligible for risk-informed decision-makers. Additionally, the results of the analysis considering a reference period of 100 years are also summarized in Table 5.8. The increased reference period leads to an increase in the exceedance probability of the characteristic value of the live load to 4%. Naturally, there is a decrease in the reliability index for the 100-year reference period when compared to the 50-year reference period. The obtained reliability indexes are respectively 6.96 and 7.08 (see Table 5.8).

In structural reliability assessment, safety is assured through a target reliability index β_T established according to the expected degree of consequence due to failure, cost of improvement of safety and considered reference period [19,20]. For a 50-year reference period, the Eurocode recommends a β_T of 3.8 for a structure like the case study under assessment. Nonetheless, this recommendation is a for section level assessment. For an assessment at the structural system level a conservative β_T of 4.3 is recommended by Sykora et al. [35,55] for a 50-year reference period. For different reference periods the β_T can be adjusted according to Eq. (5.18),

$$\Phi(\beta_T) = [\Phi(\beta_1)]^{t_n} \quad (5.18)$$

where β_T is the target reliability index given as a function of a reference period of t_n years and β_1 is the target reliability index for a 1-year reference period. Consequently, for a 100-year reference period a β_T of 4.14 is recommended. Given that $\beta > \beta_T$, structural safety is assured.

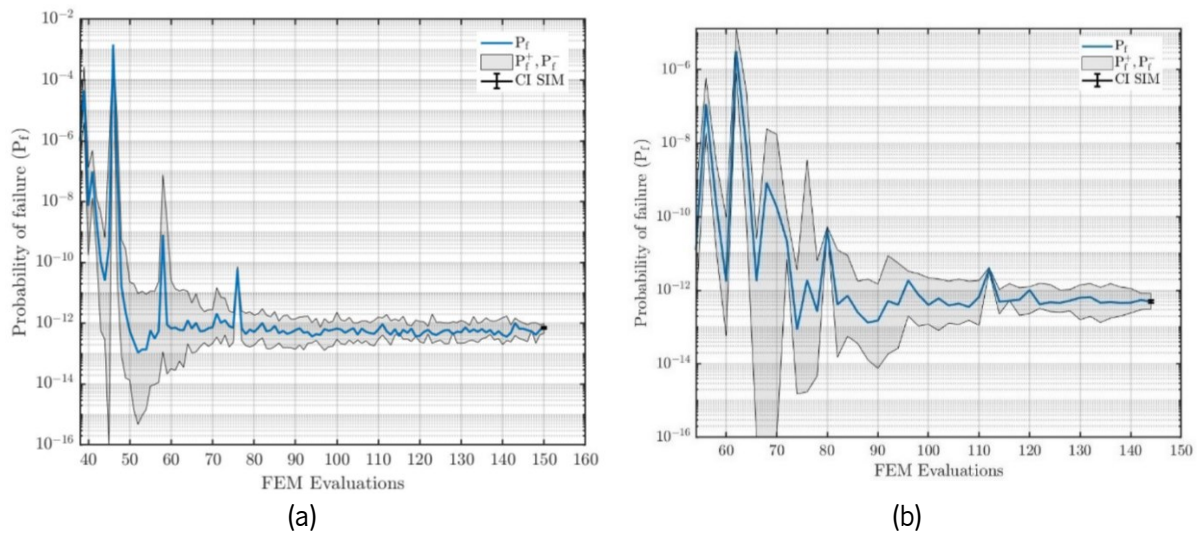


Figure 5.12 – Active learning convergence rate of (a) spatially correlated random variables and (b) spatially uncorrelated random variables in critical cross-sections

In practice, the owner often requires either the decrease or the increase of the magnitude of the allowed live load on specific bridges or road paths. Accordingly, the structural reliability reduction or increase as a function of a load factor applied to the PDF of the live load is investigated in Figure 5.13. The analysis presented here assumes that the CoV of the PDF of the live load is maintained at 10%. Consequently, the load factor presented in Figure 5.13 is equally valid for the mean value and the 98% quantile value (i.e., the characteristic value) of the PDF of the live load. Hence, when bending is concerned and structural system redistribution capabilities are taken into account, the live load characteristics value taken into account for design can be increased up to 2 times and still respect the target safety level proposed by design codes. Nevertheless, less ductile failure modes such as shear failure in its ULS should be investigated since such an increase of the live load might lead to reliability indexes below the target safety level.

Table 5.8 – Structural reliability analysis obtained results

Correlation	Reference Period	Method	β [CI]	CoV	P_f [CI]	FEM Evaluations
Spatially correlated	50 years ex.P (2%)	AK-SS-U	7.08 [7.07 – 7.09]	4.5%	7.08×10^{-13} [$6.46 \times 10^{-13} - 7.71 \times 10^{-13}$]	150
Spatially uncorrelated	50 years ex.P (2%)	AK-SS-U	7.13 [7.12 – 7.14]	4.6%	4.96×10^{-13} [$4.52 \times 10^{-13} - 5.41 \times 10^{-13}$]	144
Spatially correlated	100 years ex.P (4%)	AK-SS-U	6.96 [6.95 – 6.97]	4.4%	1.73×10^{-12} [$1.58 \times 10^{-12} - 1.88 \times 10^{-12}$]	320

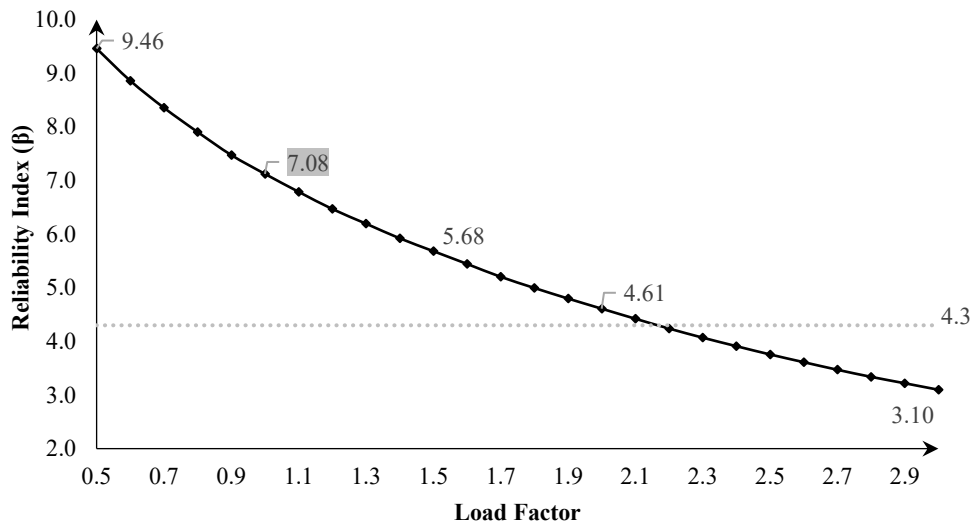


Figure 5.13 – Reliability index reduction as a function of the factored PDF of the live load (50-year reference period)

5.4.3. Long-term structural safety

Having estimated the initial structural safety of the bridge as designed, the long-term structural safety decrease is investigated according to the models introduced in 5.2.2. The bridge is a railroad bridge located in a landlocked country, making carbonation-induced corrosion the most likely scenario.

The corrosion initiation due to carbonation was forecasted, with a certain probability, in 26 years and 62 years after the construction for the 22 mm bars with a concrete cover of 40 mm and the 50 mm bars with a concrete cover of 130 mm (see Figure 5.4c), respectively. The corrosion initiation was estimated considering a low probability of violation of the limit function given in Eq. (5.7). Note that the carbonation initiation model itself, introduced in 5.2.2, considers an increase in the concentration of CO_2 in the atmosphere due to climate change. However, a concentration increase of 1.5 ppm/year is considered the base assumption, and last year according to statista.com [176] an increase of 2.21 ppm was recorded from 2020 to 2021. The propagation phase was investigated considering three current intensity scenarios of 1.0, 2.0 and 3.0 $\mu\text{A}/\text{cm}^2$ (see Figure 5.14a). The reinforcement uniform cross-section loss modelled for the 22 mm and 50 mm bars on the deck (see Figure 5.4c) as a function of time is presented in Figure 5.14b, according to the different current intensity scenarios considered in the analysis. The long-term structural safety assessment is performed considering a reference period of 100 years. Therefore, the exceedance probability of the characteristic value of the live load is adjusted to 4% according to Eq. (5.17), as well as the target safety level $\beta_T = 4.14$, according to Eq. (5.18).

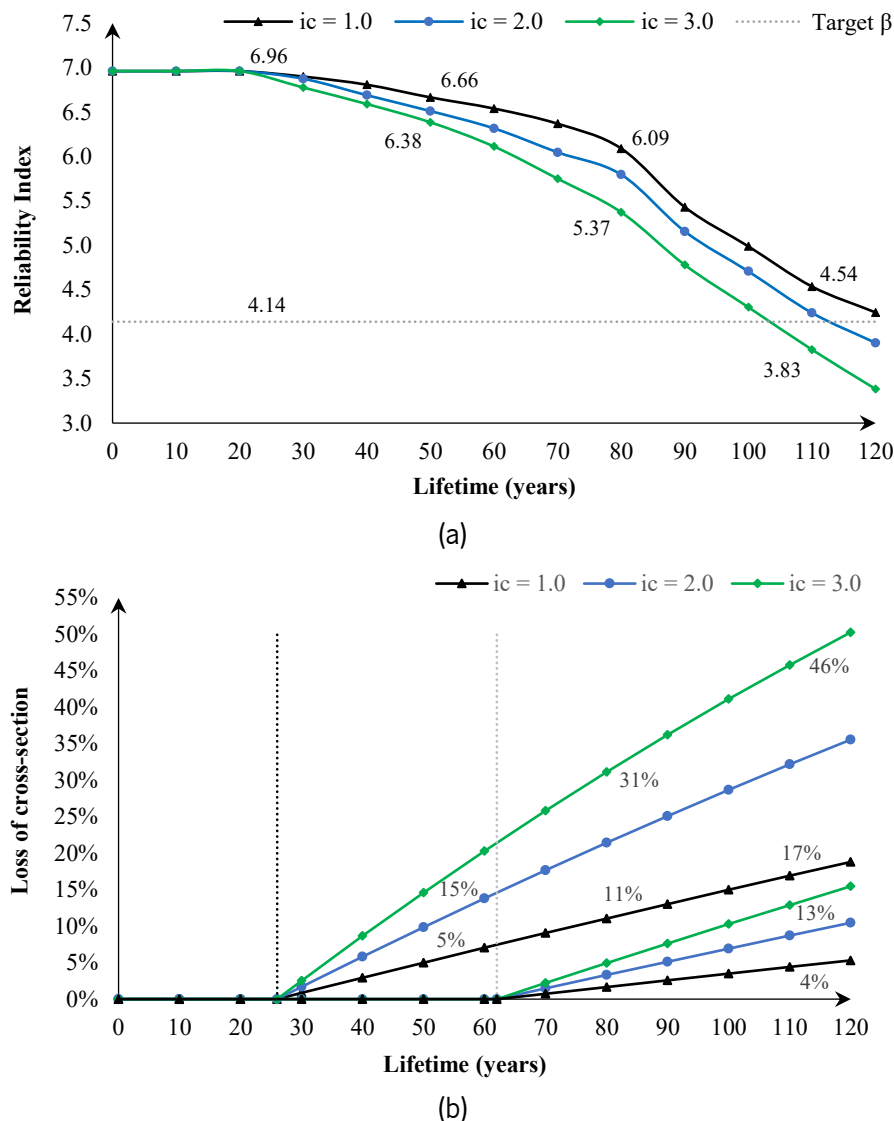


Figure 5.14 – (a) Lifetime structural safety (100-year reference period) (b) reinforcement cross-section loss given different current intensity scenarios

The results displayed in Figure 5.14a put the end of the service life of the overpass between 100 and 120 years, depending on the current intensity scenario considered, given that corrosion initiates at the estimated time. One should note the sources of uncertainties and deterioration mechanisms that were not considered, e.g., fatigue, creep, reinforcement bond loss, traffic increase, climate change (e.g., temperature increase), human-made hazards (e.g., vehicle collision) and construction errors. Furthermore, the uncertainties associated with corrosion are partially modelled. For instance, there is an increase of uncertainty with corrosion propagation in time, evident in Imperatore et al. [166] and Zhang et al. [167], which were not probabilistically modelled in the literature and, thus, not taken into account in this work. However, part of it is captured by the deterioration model introduced in 5.2.2.

5.4.4. Construction errors impact in structural safety

The service life reduction of structures due to construction errors is a known fact or somewhat expected; nonetheless, the actual reduction is yet to be estimated. It goes without saying that the service life of structures depends on numerous factors that are hard to quantify numerically at once since several players are usually involved. Some errors can be mitigated with corrective or maintenance works, and some constraints on the demand side can also be put in place, according to the identified damage triggered by the error, aiming to limit its overall short and long-term consequences. Notwithstanding these neglected factors and difficulties, the quantification of construction errors' impact on the service life reduction of bridges should not be discouraged.

Construction errors are here addressed as an additional source of uncertainty quantified by HEP and EM PDFs introduced in 5.2.2. They are added to the structural reliability analysis framework through the event tree in Figure 5.3, where the occurrence of detrimental and beneficial errors is a conceivable outcome. Two construction errors are investigated: inadequate concrete mix and wrongful placement of reinforcement. Multiple error occurrences are neglected here since Galvão et al. [168] concluded that the combination of errors does not contribute significantly to structural safety decline beyond the most detrimental error in the combination. As such, each construction error is investigated separately.

The wrongful placement of reinforcement as a construction error is modelled through the cross-section area of the longitudinal reinforcement surrounding the most relevant sections highlighted in Figure 5.4a. Moreover, four independent random variables were considered to model the longitudinal reinforcement; namely, the lower longitudinal reinforcement of the deck (i.e., 35 \varnothing 22 and 12 \varnothing 50) and the upper longitudinal reinforcement of the deck (i.e., 44 \varnothing 22 and 14 \varnothing 50) – see Figure 5.4c. Consequently, aiming to keep this independence in the realization of these different reinforcements, four independent EM PDFs were used to model the wrongful placement of reinforcement as a construction error.

Construction errors' impact on structural safety and service life reduction is summarized in Figure 5.15. Note that the error-free scenario used as a reference in Figure 5.15 is the one representing the corrosion scenario with a current intensity of 2.0 $\mu\text{A}/\text{cm}^2$ in Figure 5.14a. The wrongful placement of reinforcement (i.e., E1+E2) as an additional source of uncertainty leads to an initial structural reliability index drop from 6.96 to 5.81. In terms of probability of failure, this means that the structure is 1000 times more likely to fail. The service life of the bridge, limited by the target reliability index given for a reference period of 100 years for a ULS, is reduced by 30 years due to the construction error E1+E2.

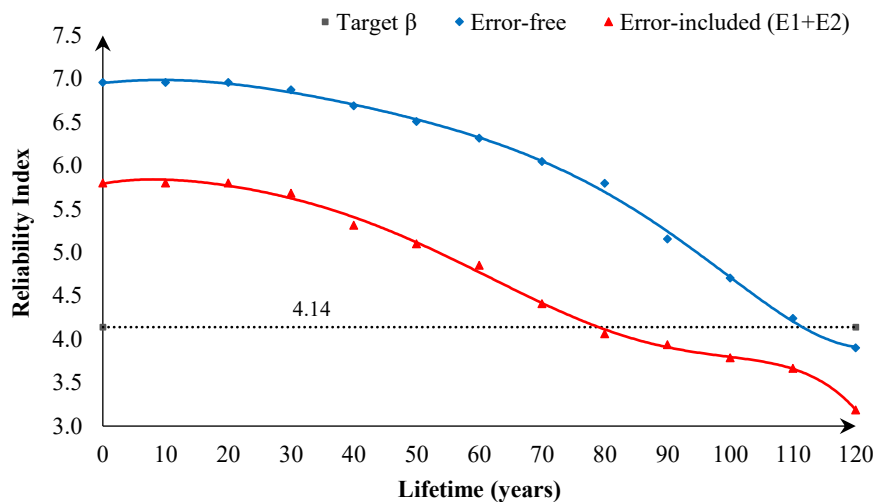


Figure 5.15 – Lifetime structural safety affected by construction errors

5.5. Conclusions

Structural safety is significantly dependent upon human errors in their many forms. Notwithstanding the evident difficulties of consideration of human error in the structural reliability analysis framework, construction errors' impact on structural safety and service life reduction of a case study is here investigated. Finite element models, replaced by a computationally less expensive surrogate model combined with an active learning technique, form the backbone of the structural reliability analysis results introduced in this work. Furthermore, carbonation-induced corrosion and concrete strength reduction are introduced as deterioration mechanisms impacting the carrying capacity of the structure.

In line with the assumptions, scenarios, discussion and accomplished outcomes, the subsequent conclusions are drawn:

1. The end of the service life of the bridge when longitudinal bending maximum carrying capacity is concerned is estimated between 100 and 120 years for different corrosion intensity scenarios investigated.
2. Construction errors as an additional source of uncertainty will increase the initial probability of failure of the structure by three orders of magnitude. Put another way, as the current state-of-the-art allows it to be estimated, the as-built structure might be 1000 times more likely to fail than the initially designed structure.
3. The service life of the case study is reduced by 30 years due to a given likelihood of wrong full placement of reinforcement (i.e., E1+E2); with an initially estimated service life of 110 years being reduced to 80 years.

The longitudinal bending capacity is investigated as the leading effect of the loads in this work. However, other effects, such as shear, torsion and buckling, with different failure modes should be investigated for service life prediction considering deterioration and construction errors.

6. Conclusion

"I asked for strength, and God gave me difficulties to make me strong. I asked for wisdom, and God gave me problems to solve. I asked for courage, and God gave me dangers to overcome. I asked for love, and God gave me troubled people to help. My prayers were answered."
by Inayat Khan

6.1. Final remarks

Human error is an additional source of uncertainty not explicitly taken into account by the design codes. The contribution of human errors to the structural collapse of bridges, alongside its impact on structural safety decline, has fostered the endeavours described in this thesis report. Aiming to clarify the short- and long-term contribution of human error to the structural safety of concrete bridges, this work thoroughly identifies a broad scope of design and construction errors in the daily practices of engineers. Experts' knowledge is carefully harnessed for identification, qualitative assessment and mitigation of construction and design errors, as well as for prioritization of errors through analytic hierarchy process techniques.

Moreover, prestressed, post-tensioned and reinforced concrete bridges are thoroughly described and analysed, considering sophisticated numerical computation techniques available in the literature for structural reliability assessment. Sophisticated algorithms for non-linear structural analysis of finite element models and machine learning techniques, i.e., polynomial chaos kriging surrogate models and active learning techniques, were brought together. Multiple scenarios analysis is presented according to experts' recommendations and the literature. In an early stage, construction and design errors are analysed, neglecting their likelihood of occurrence and addressing only their severity/magnitude, considering deviations solely in their expected value (i.e., mean value). Such deviations are addressed as damages present in the structure due to design and construction errors. In a later stage, construction errors as an additional source of uncertainty are introduced in the analysis, considering human error probability and error magnitude probabilistic models contemplating their beneficial and detrimental

contribution to the structural safety of bridges. Additionally, the direct impact of visual inspection of construction works on the structural safety of bridges is also inferred, considering error rates identified before and after inspection works. The contributions of a single error and simultaneous occurrences of multiple errors to the structural safety decline of bridges are also delivered.

The service life of a bridge is estimated considering carbonation-induced corrosion and concrete strength deterioration, together with multiple sources of uncertainty concerning corrosion initiation and corrosion propagation. Finally, deterioration and construction error models are brought together to quantify the long-term impact of construction errors on the service life reduction of bridges.

This thesis's original contribution to the current state-of-the-art is presented in the concluding section of each preceding chapter, forming the backbone of this thesis report. Nonetheless, these are summarized into the following key consecutive contributions:

1. Identification of numerous design and construction errors and highlighting of those denoting the highest risk for the structural safety of concrete bridges by qualitatively assessing their probability of occurrence and expected consequences. Additionally, a framework for human error investigation is presented and suggested for design codes, seeking to complement the design supervision and inspection levels proposed for structures demanding the highest reliability class. (Chapter 2)
2. The structural reliability of a prestressed concrete bridge as affected by damages introduced by a group of carefully selected errors is thoroughly investigated, demonstrating how different damages and their combination can impair the structural safety (a.k.a robustness) of a bridge. (Chapter 3)
3. When the maximum longitudinal flexural capacity is concerned, the reliability of structures is limited by an upper ceiling given by construction errors. By consideration of construction errors in structural reliability analysis, the safety levels obtained when these were neglected were never attained, even though human error probabilities were brought close to one in a billion occurrences. Additionally, structural reliability is much more sensitive to detrimental errors than beneficial errors since results indicate that beneficial changes to random variables had negligible influence on the increase of the reliability index. On the other hand, detrimental changes to random variables considerably influenced the decrease in the reliability index. (Chapter 4)
4. The long-term impact of construction errors on the service life of a reinforced concrete bridge is estimated to be approximately a 30-year reduction in service life. Such estimation is attained by

bringing together construction error models and deterioration models for the first time in structural reliability analysis. Furthermore, in its worst form (collapse excluded), the short-term impact is estimated to be an increase in the probability of failure between three to six orders of magnitude. (Chapter 5)

Moreover, according to the discussion presented in this report, additional contributions to state-of-the-art can be broken down into the following bullet points:

- Human error is defined as any Procurement, Design, Construction and Operation errors (deviations out of the acceptable margins) that do not exceed the currently available engineering knowledge and have taken place due to poor working conditions, lack of knowledge, negligence, miss instruction and communication, greed, calculation errors, time and budget constraints, inadequate construction methods, and lack of surveillance, among others. Human errors and human-made hazards are two major components within the human factors field, and those are distinguished by the fact that the former tackles the interaction of humans with a system as a technician and the latter the interaction of humans with the system as a user.
- The design errors considered to pose a greater threat to the structural safety of concrete bridges are (i) Errors due to a lack of consideration of different support conditions that a bridge or an element will be subjected to through the construction process and (ii) Error in reinforcement cross-section area detailing.
- The construction errors considered to pose a greater threat to the structural safety of concrete bridges are (i) Error due to deficiency in the continuous falsework bracing leading to global instability and (ii) Error due to poor evaluation of the falsework foundation soil properties, and variation of these properties after rainfall.
- The structural safety of a 3-span girder bridge, measured by reliability indexes when longitudinal bending is concerned, and redistribution capabilities are taken into account, is estimated to be between 7.08 – 7.17 when designed according to the Portuguese regulation for Reinforced and Prestressed Concrete Structures (REBAP) or the standards of the Swiss Society of Engineers and Architects (SIA).
- Structural safety is much more dependent on the likelihood of the occurrence of a single serious error than it is on the likelihood of the occurrence of multiple errors. The investigation demonstrates that structural safety can hardly be decreased beyond the safety levels already attained because of the worst single error considered when combined with less meaningful errors.

This is true when such errors are addressed as likely scenarios, i.e., their likelihood of occurrence is addressed in the analysis. On the other hand, multiple identified concerning damages (i.e., they are understood to be present on the structure) caused by errors can be devastating to structural safety.

- Given different current intensities, to define corrosion scenarios of a reinforced concrete bridge, the service life is estimated to be between 100 and 120 years when longitudinal bending is concerned. A reliability index is used as the measure of performance, and a target reliability index as the threshold value.
- The number of structural reliability indexes computed in this work demonstrates the reduction of the computational costs of a finite element model-based structural reliability analysis allowed by surrogate models and active learning techniques. Such results are proof of the increasing feasibility of structural reliability analysis since they are becoming less time-consuming with computer science advancements; thus, more attractive to the engineering community, year after year.

The legal implication of an error or a mistake is mostly feared by technicians, as well as design and construction companies, leading very often to some internal conflict when deciding about reporting them. It's reasonable to assume such a conflict, given the feelings of shame and fear of possible self-centred consequences associated with their own mistakes, especially if gross errors are concerned. Accordingly, some legal protection seeking to encourage the exposure of major errors should be considered, keeping in mind that this would lead to earlier identification of the problem and avoidance of major consequences in the future. This should be the case, especially for structures of major relevance for society and extended expected service life (e.g., major bridges, dams, and skyscrapers).

An official document highlighting the differences between the structure as built and as designed should be available for management of the structural system performance over its service life. Structures like bridges are very much taken for granted because of their long service life. Very often, these structures are put under the management of engineers from different generations. Thus, it's important to provide the next generation with built heritage in good health and very detailed, relevant and structured information (e.g., 2D drawings, 3D models, BIM, Digital Twins and detailed reports, among others) so they can better decide and track the service life of structures when their time comes. Consequently, they will inherit and enjoy a built environment in great shape and not one falling apart, avoiding the need for future CO₂ emissions.

6.2. Future works

Despite the contributions provided within the scope of this doctoral thesis, there are still many questions that remain unanswered. According to the expertise accumulated and the attained overall view of the current state-of-the-art, the following points are suggested for further development:

- There are some sophisticated human reliability assessment techniques (e.g., THERP, CREAM, NARA and SPAR-H, among others) investigated by NASA [177] that could be used for additional quantitative assessment of human error probabilities within the civil engineering industry. Moreover, errors of operation should be investigated since they are responsible for a significant number of failures.
- In the literature, a limited number of structural reliability-oriented works addressing shear, torsion and buckling effects can be found. Hence, additional research in this regard should be established to better understand the current safety margin or reliability index produced by the codes and most commonly used numerical models. Furthermore, there is little information about model uncertainties of the numerical models (i.e., beam, shell and solid elements) best suited to model such load effects.
- Service limit state functions (e.g., maximum displacement and decompression limit states, among others) have been somewhat neglected. Nonetheless, its consideration for structural serviceability quantification coupled with construction error models is encouraged, as well as the consideration of deterioration models to track the reduction of the serviceability margins over time.
- Fatigue as a deterioration mechanism is of considerable relevance for service life prediction of structures, especially in the presence of corrosion, as suggested by some works in the literature [167]. Consequently, a fatigue-oriented service life estimation is the natural subsequent step that should be later combined with the corrosion of reinforcement. Taking into account, of course, all the relevant sources of uncertainties through structural reliability analysis.
- The increase of CO₂ concentration in the atmosphere and the rising temperature impact on corrosion models should be thoroughly investigated, aiming to predict the service life reduction of our structures due to such changes. The increasing frequency of extreme weather events must not be overlooked.
- Spatial variability of random variables through random fields is another subject for expansion, bringing together the latest advancements in the topic.

- Bayesian updating seeking to take into account posterior information concerning the current state of the bridge is also a step forward that must be encouraged. Structural health monitoring information is also a plus, paving the way for a more refined digital twin of the assets. Additionally, weigh-in-motion data should be used to update the load model used for structural reliability analysis.

References

"Education is the great engine of personal development. It is through education that the daughter of a peasant can become a doctor; that the son of a mine worker can become the head of the mine; that a child of farm workers can become the president of a great nation."
by Nelson Mandela

- [1] European Commission. Transport sector economic analysis. EU Sci Hub 2021:1–4. https://joint-research-centre.ec.europa.eu/scientific-activities-z/transport-sector-economic-analysis_en (accessed August 8, 2022).
- [2] Bureau of Transportation Statistics. Transportation Economic Trends: Contribution of Transportation - Final Demand. US Dep Transp 2022. <https://data.bts.gov/stories/s/pgc3-e7j9> (accessed August 8, 2022).
- [3] Ritchie H, Roser M. Emissions by sector - Our World in Data. Univ Oxford 2020. <https://ourworldindata.org/emissions-by-sector> (accessed July 4, 2022).
- [4] Ritchie H, Roser M, Rosado P. Transport - Our World in Data 2020. <https://ourworldindata.org/transport#citation> (accessed August 8, 2022).
- [5] Ritchie H. Which form of transport has the smallest carbon footprint? - Our World in Data. CO2 Greenh Gas Emiss 2020. <https://ourworldindata.org/travel-carbon-footprint> (accessed August 8, 2022).
- [6] European Commission. European Commission - Connecting Europe Facility (CEF). Eur Comm 2021. https://ec.europa.eu/info/strategy/eu-budget/performance-and-reporting/programme-performance-overview/connecting-europe-facility-performance_en (accessed August 8, 2022).
- [7] Scheer J. Failed Bridges - Case Studies, Causes and Consequences. Hannover: Ernst&Sohn; 2010. <https://doi.org/10.1002/9783433600634>.
- [8] Imhof D. PhD Thesis: Risk Assessment of Existing Bridge Structures. University of Cambridge, 2004.
- [9] Cavaco ES. PhD Thesis: Robustness of corroded reinforced concrete structures. University of Lisbon, 2013.
- [10] Proske D. Estimation of the Global Health Burden of Structural Collapse. 18th Int. Probabilistic Work., Springer Nature; 2021, p. 327–40. https://doi.org/10.1007/978-3-030-73616-3_24.

-
- [11] Casas JR. The bridges of the future or the future of bridges? *Front Built Environ* 2015;1:3. <https://doi.org/10.3389/fbuil.2015.00003>.
 - [12] Federal Highway Administration (FHWA). Tables of Frequently Requested NBI Information - National Bridge Inventory - Bridge Inspection - Safety - Bridges & Structures - Federal Highway Administration 2021. <https://www.fhwa.dot.gov/bridge/britab.cfm> (accessed August 9, 2022).
 - [13] Milic I, Ivankovic AM, Syrkov A, Skokandic D. Bridge failures, forensic structural engineering and recommendations for design of robust structures. *Gradjevinar* 2021;73:717–36. <https://doi.org/10.14256/JCE.3234.2021>.
 - [14] Syrkov A, Høj NP. Bridge failures analysis as a risk mitigating tool. *IABSE Symp. Towar. a Resilient Built Environ. - Risk Asset Manag.*, Guimarães, Portugal: 2019, p. 304–10.
 - [15] Syrkov A. Review of bridge collapses worldwide 1966 - 2018. *IABSE Work. Ignorance, Uncertain. Hum. errors Struct. Eng.*, Helsinki, Finland: 2017.
 - [16] Canisius TDG, Barker JB, Diamantidis D, Ellingwood BR, Faber M, Holicky M, et al. *Structural Robustness Design for Practising Engineers*. 2011.
 - [17] Hajdin R, Kusar M, Masovic S, Linneberg P, Amado J, Tanasić N. Establishment of quality control plan - COST Action TU1406. 2018. <https://doi.org/10.13140/RG.2.2.28730.03526>.
 - [18] Galvão N, Sousa H, Fernandes S, Pucci A, Matos J, Tanasić N, et al. Impact of human-made hazards (D2.2) - SAFEWAY: GIS-Based Infrastructure Management System for Optimized Response to Extreme Events of Terrestrial Transport Networks. vol. 1.0. 2019.
 - [19] European Committee for Standardization (CEN). EN 1990, Eurocode 0: Basis of structural design. Brussels, Belgium: 2002.
 - [20] Joint Committee on Structural Safety (JCSS). Probabilistic Model Code - Part 1: Basis of design. 2001.
 - [21] International Organization for Standardization (ISO). ISO 13822, Bases for design of Structures – Assessment of Existing Structures. Switzerland: 2010.
 - [22] International Organization for Standardization (ISO). ISO 2394, General Principles on Reliability for Structures. Switzerland: 2015.
 - [23] Starossek U, Haberland M. Disproportionate Collapse: Terminology and Procedures. *J Perform Constr Facil* 2010;24:519–28. [https://doi.org/10.1061/\(asce\)cf.1943-5509.0000138](https://doi.org/10.1061/(asce)cf.1943-5509.0000138).
 - [24] Stewart MG. Modeling Human Performance in Reinforced Concrete Beam Construction. *J Constr Eng Manag* 1993;119:6–22. [https://doi.org/10.1061/\(asce\)0733-9364\(1993\)119:1\(6\)](https://doi.org/10.1061/(asce)0733-9364(1993)119:1(6)).
 - [25] Hadipriono FC. Analysis of Events in Recent Structural Failures. *J Struct Eng* 1985;111:1468–81. [https://doi.org/10.1061/\(asce\)0733-9445\(1985\)111:7\(1468\)](https://doi.org/10.1061/(asce)0733-9445(1985)111:7(1468)).
 - [26] Blockley DI. Analysis of Structural Failures. *Proc Inst Civ Eng* 1977;62:51–74. <https://doi.org/10.1680/iicep.1977.3259>.
 - [27] Stewart MG, Melchers RE. Simulation of human error in a design loading task. *Struct Saf* 1988;5:285–97. [https://doi.org/10.1016/0167-4730\(88\)90029-X](https://doi.org/10.1016/0167-4730(88)90029-X).
-

-
- [28] Tylek I, Kuchta K, Rawska-Skotniczny A. Human Errors in the Design and Execution of Steel Structures—A Case Study. *Struct Eng Int* 2017;27:370–9. <https://doi.org/10.2749/101686617X14881937385287>.
 - [29] Brehm E, Hertle R. Failure Identification: Procedural Causes and Corresponding Responsibilities. *Struct Eng Int* 2017;27:402–8. <https://doi.org/10.2749/101686617X14881937385160>.
 - [30] Deng L, Wang W, Yu Y. State-of-The-Art Review on the Causes and Mechanisms of Bridge Collapse. *J Perform Constr Facil* 2016;30:04015005. [https://doi.org/10.1061/\(ASCE\)CF.1943-5509.0000731](https://doi.org/10.1061/(ASCE)CF.1943-5509.0000731).
 - [31] Chen TT. Factors in Bridge Failure, Inspection, and Maintenance. *J Perform Constr Facil* 2017;31:04017070. [https://doi.org/10.1061/\(ASCE\)CF.1943-5509.0001042](https://doi.org/10.1061/(ASCE)CF.1943-5509.0001042).
 - [32] Johnson PA, Clopper PE, Zevenbergen LW, Lagasse PF. Quantifying Uncertainty and Reliability in Bridge Scour Estimations. *J Hydraul Eng* 2015;141:04015013. [https://doi.org/10.1061/\(asce\)hy.1943-7900.0001017](https://doi.org/10.1061/(asce)hy.1943-7900.0001017).
 - [33] Manfreda S, Link O, Pizarro A. A theoretically derived probability distribution of scour. *Water (Switzerland)* 2018;10:1520. <https://doi.org/10.3390/w10111520>.
 - [34] Fröderberg M. Conceptual Design Strategy: Appraisal of Practitioner Approaches. *Struct Eng Int* 2015;25:151–8. <https://doi.org/10.2749/101686614x14043795570615>.
 - [35] Sykora M, Diamantidis D, Holicky M, Jung K. Target reliability for existing structures considering economic and societal aspects. *Struct Infrastruct Eng* 2017;13:181–94. <https://doi.org/10.1080/15732479.2016.1198394>.
 - [36] Zambon I, Anja V, Strauss A, Matos J. Use of chloride ingress model for condition assessment in bridge management. *J Croat Assoc Civ Eng* 2019;71:359–73. <https://doi.org/10.14256/JCE.2411.2018>.
 - [37] Bridge Design Engineering. Report published on fatal Colombian bridge collapse 2018. <https://www.bridgeweb.com/Report-published-on-fatal-Colombian-bridge-collapse/4659> (accessed September 18, 2020).
 - [38] Pujol S, Kreger ME, Monical JD, Schultz AE. Investigation of the Collapse of the Chirajara. *Concr Int* 2019;41:29–37.
 - [39] NTSB. Miami bridge that collapsed and killed 6 had design errors 2018. <https://eu.usatoday.com/story/news/2018/11/15/ntsb-miami-bridge-collapse-design-errors/2012020002/> (accessed September 6, 2020).
 - [40] Ayub M. Investigation of March 15, 2018 Pedestrian Bridge Collapse at Florida International Univesity, Miami, Florida. Washington, D.C: 2019.
 - [41] The New York Times. Genoa Bridge Collapse: The Road to Tragedy 2018. <https://www.nytimes.com/interactive/2018/09/06/world/europe/genoa-italy-bridge.html> (accessed September 6, 2020).
 - [42] Morgese M, Ansari F, Domaneschi M, Cimellaro GP. Post-collapse analysis of Morandi's Polcevera viaduct in Genoa Italy. *J Civ Struct Heal Monit* 2020;10:69–85. <https://doi.org/10.1007/s13349-019-00370-7>.
-

-
- [43] Faber MHJ. Risk Assessment in Engineering: Principles, System Representation & Risk Criteria. 2008.
 - [44] Rausand M. Risk assessment: Theory, Methods, and Applications. New Jersey: John Wiley & Sons; 2011.
 - [45] International Organization for Standardization (ISO). IEC/ISO 31010, Risk management - Risk assessment techniques. 1.0. Geneva, Switzerland: International Electrotechnical Commission (IEC); 2009.
 - [46] John Fraczek. ACI Survey of Concrete Structure Errors. *Concr Int* 1979;1:14–20.
 - [47] Allen DE. Errors in concrete structures. *Can J Civ Eng* 1979;6:465–7. <https://doi.org/10.1139/cjce-1979-030465>.
 - [48] Saaty TL, Vargas LG. Decision Making with the Analytic Network Process. 2nd ed. Boston, MA, USA: Springer; 2013. <https://doi.org/10.1007/978-1-4614-7279-7>.
 - [49] Thompson PD, Patidar V, Labi S, Sinha K, Hyman WA, Shirolé A. Multi-objective optimization for bridge management. *Proc. 3rd Int. Conf. Bridg. Maintenance, Saf. Manag. - Bridg. Maintenance, Safety, Manag. Life-Cycle Perform. Cost*, Porto, Portugal: 2006, p. 735–6. <https://doi.org/10.1201/b18175-311>.
 - [50] Goepel KD. Implementing the Analytic Hierarchy Process as a Standard Method for Multi-Criteria Decision Making In Corporate Enterprises – A New AHP Excel Template with Multiple Inputs. *Proc. Int. Symp. Anal. Hierarchy Process*, Kuala Lumpur, Malaysia: 2013, p. 1–10. <https://doi.org/10.13033/ISAHP.Y2013.047>.
 - [51] Goepel KD. Implementation of an Online software tool for the Analytic Hierarchy Process (AHP-OS). *Int J Anal Hierarchy Process* 2018;10:469–87. <https://doi.org/10.13033/isahp.y2018.029>.
 - [52] Kifokeris D, e Matos JAC, Xenidis Y, Bragança L. Bridge quality appraisal methodology: Application in a reinforced concrete overpass roadway bridge. *J Infrastruct Syst* 2018;24:04018034. [https://doi.org/10.1061/\(ASCE\)IS.1943-555X.0000455](https://doi.org/10.1061/(ASCE)IS.1943-555X.0000455).
 - [53] Epaarachchi DC, Stewart MG. Human Error and Reliability of Multistory Reinforced-Concrete Building Construction. *J Perform Constr Facil* 2004;18:12–20. [https://doi.org/10.1061/\(ASCE\)0887-3828\(2004\)18:1\(12\)](https://doi.org/10.1061/(ASCE)0887-3828(2004)18:1(12)).
 - [54] Fröderberg M, Thelandersson S. Uncertainty caused variability in preliminary structural design of buildings. *Struct Saf* 2014;52:183–93. <https://doi.org/10.1016/j.strusafe.2014.02.001>.
 - [55] Galvão N, Matos JC, Oliveira D V, Hajdin R. Human error impact in structural safety of a reinforced concrete bridge. *Struct Infrastruct Eng* 2022;18:836–50. <https://doi.org/10.1080/15732479.2021.1876105>.
 - [56] Nowak AS, Collins KR. Reliability of structures. 2nd ed. Thomas Casson; 2000.
 - [57] Matousek M. Measures against errors in the building process (Translation No. 2067, National Research Council of Canada, Ottawa, Canada/1983). Zurich, Switzerland: 1983.
 - [58] engineering .com. How Machine Learning is Improving Construction 2019. <https://www.engineering.com/BIM/ArticleID/19317/How-Machine-Learning-is-Improving-Construction.aspx> (accessed August 10, 2020).
-

-
- [59] Maskin entreprenoren. AI to prevent fatalities | Machine contractor. MaskinentreprenorenSe 2020. <https://maskinentreprenoren.se/ai-ska-hindra-dodliga-olyckor/> (accessed September 27, 2020).
 - [60] Kifokeris D, Xenidis Y. Risk source-based constructability appraisal using supervised machine learning. *Autom Constr* 2019;104:341–59. <https://doi.org/10.1016/j.autcon.2019.04.012>.
 - [61] Qeshmy DE, Makdisi J, Da Silva EHDR, Angelisa J. Managing human errors: Augmented reality systems as a tool in the quality journey. *Procedia Manuf* 2019;28:24–30. <https://doi.org/10.1016/j.promfg.2018.12.005>.
 - [62] European Committee for Standardization (CEN). EN 1991-2, Eurocode 1: Actions on structures - Part 2: Traffic loads on bridges. Brussels, Belgium: 2003.
 - [63] European Committee for Standardization (CEN). EN 13670, Execution of concrete structures. Brussels, Belgium: 2007.
 - [64] Melchers R., Beck AT. Structural Reliability Analysis and Prediction. 3rd Editio. New York.: John Wiley & Sons Ltd.,; 2018.
 - [65] International Federation for Structural Concrete (FIB). Model Code for Concrete Structures. Lausanne, Switzerland: Ernst&Sohn; 2010.
 - [66] Haan J. Human Error in Structural Engineering The design of a Human Reliability Assessment method for Structural Engineering. 2012.
 - [67] Terwel KC, Jansen SJT. Critical Factors for Structural Safety in the Design and Construction Phase. *J Perform Constr Facil* 2015;29:04014068. [https://doi.org/10.1061/\(asce\)cf.1943-5509.0000560](https://doi.org/10.1061/(asce)cf.1943-5509.0000560).
 - [68] Jones-Lee M, Aven T. ALARP - What does it really mean? *Reliab Eng Syst Saf* 2011;96:877–82. <https://doi.org/10.1016/j.ress.2011.02.006>.
 - [69] Aven T. Risk assessment and risk management: Review of recent advances on their foundation. *Eur J Oper Res* 2016;253:1–13. <https://doi.org/10.1016/j.ejor.2015.12.023>.
 - [70] Cavaco E, Neves LAC, Casas JR. Reliability-based approach to the robustness of corroded reinforced concrete structures. *Struct Concr* 2017;18:316–25. <https://doi.org/10.1002/suco.201600084>.
 - [71] Baker JW, Schubert M, Faber MH. On the assessment of robustness. *Struct Saf* 2008;30:253–67. <https://doi.org/10.1016/j.strusafe.2006.11.004>.
 - [72] Biondini F, Restelli S. Damage propagation and structural robustness. *Life-Cycle Civ. Eng. - Proc. 1st Int. Symp. Life-Cycle Civ. Eng. IALCCE '08*, Varenna, Italy: 2008, p. 131–6. <https://doi.org/10.1201/9780203885307.ch14>.
 - [73] Frangopol DM, Curley JP. Effects of damage and redundancy on structural reliability. *ASCE* 1987;113:1533–49. [https://doi.org/https://doi.org/10.1061/\(ASCE\)0733-9445\(1987\)113:7\(1533\)](https://doi.org/10.1061/(ASCE)0733-9445(1987)113:7(1533)).
 - [74] International Organization for Standardization (ISO). ISO 19902, Petroleum and natural gas industries - Fixed steel offshore structures. 1st ed. 2007.
-

- [75] Cavaco ES, Neves LAC, Casas JR. On the robustness to corrosion in the life cycle assessment of an existing reinforced concrete bridge. *Struct Infrastruct Eng* 2017;22:137–50. <https://doi.org/10.1080/15732479.2017.1333128>.
- [76] Cavaco E, Casas JR, Neves LC, Huespe A. Robustness of corroded reinforced concrete structures: a structural performance approach. *Struct Infrastruct Eng* 2013;9:42–58. <https://doi.org/10.1080/15732479.2010.515597>.
- [77] Galvão N, Matos J, Oliveira D, Fernandes J. Human errors and corresponding risks in reinforced concrete bridges. *IABSE Conf. Kuala Lumpur 2018 Eng. Dev. World - Rep.*, Kuala Lumpur, Malaysia: 2018, p. 323–9.
- [78] TNO DIANA. User's Manual - Theory. Release 10. Delft, The Netherlands: 2016.
- [79] European Committee for Standardization (CEN). EN 1992-1-1, Eurocode 2: Design of concrete structures - Part 1-1: General rules and rules for buildings. Brussels, Belgium: 2004.
- [80] Ascendi. Execution Project - Discriptive Memory ANCX.E.PS8.170.M (Internal Reference). Porto, Portugal: 2011.
- [81] TNO DIANA. User's Manual - Element Library. Release 10. Delft, The Netherlands: 2020.
- [82] European Committee for Standardization (CEN). EN 1992-1-2, Eurocode 2: Design of concrete structures - Part 1-2: General rules Structural fire design. Brussels, Belgium: 2010.
- [83] TNO DIANA. User's Manual - Material Library. Release 10. Delft, The Netherlands: 2020.
- [84] Joint Committee on Structural Safety (JCSS). Probabilistic Model Code - Part 3: Material properties. 2000.
- [85] Matos JC, Moreira VN, Valente IB, Cruz PJS, Neves LC, Galvão N. Probabilistic-based assessment of existing steel-concrete composite bridges – Application to Sousa River Bridge. *Eng Struct* 2019;181:95–110. <https://doi.org/10.1016/j.engstruct.2018.12.006>.
- [86] Joint Committee on Structural Safety (JCSS). Probabilistic Model Code - Part 2: Load Models. 2001.
- [87] Wiśniewski DF, Cruz PJS, Henriques AAR, Simões RAD. Probabilistic models for mechanical properties of concrete, reinforcing steel and pre-stressing steel. *Struct Infrastruct Eng* 2012;8:111–23. <https://doi.org/10.1080/15732470903363164>.
- [88] Wisniewski DF. Safety Formats for the Assessment of Concrete Bridges. Guimarães Univ Minho 2007.
- [89] Casas JR, Wisniewski D. Safety requirements and probabilistic models of resistance in the assessment of existing railway bridges. *Struct Infrastruct Eng* 2013;9:529–45. <https://doi.org/10.1080/15732479.2011.581673>.
- [90] Bulleit WM. Uncertainty in Structural Engineering. *Pract Period Struct Des Constr* 2008;13:24–30. [https://doi.org/10.1061/\(asce\)1084-0680\(2008\)13:1\(24\)](https://doi.org/10.1061/(asce)1084-0680(2008)13:1(24)).
- [91] Sykora M, Krejsa JK, Mlcoch J, Prieto M, Tanner P. Uncertainty in shear resistance models of reinforced concrete beams according to fib MC2010. *Struct Concr* 2018;19:284–95. <https://doi.org/10.1002/suco.201700169>.

-
- [92] Holický M, Retief J V, Sýkora M. Assessment of model uncertainties for structural resistance. Probabilistic Eng Mech 2016;45:188–97. <https://doi.org/10.1016/j.probengmech.2015.09.008>.
- [93] Nowak AS. Calibration of LRFD bridge design code. 1999.
- [94] Haan J De, Terwel KC, Al-Jibouri S. Design of a Human Reliability Assessment model for Structural Engineering. Eur. Saf. Reliab. Conf. ESREL 2013, Safety, Reliab. risk Anal. beyond Horiz., 2013.
- [95] Lind NC. Models of human error in structural reliability. Struct Saf 1982;1:167–75. [https://doi.org/10.1016/0167-4730\(82\)90023-6](https://doi.org/10.1016/0167-4730(82)90023-6).
- [96] Nessim MA, Jordaan IJ. Models for human error in structural reliability. J Struct Eng 1985;111:1358–76. [https://doi.org/10.1061/\(ASCE\)0733-9445\(1985\)111:6\(1358\)](https://doi.org/10.1061/(ASCE)0733-9445(1985)111:6(1358)).
- [97] Stewart M. Simulation of human error in reinforced concrete design. Res Eng Des 1992;4:51–60. <https://doi.org/10.1007/BF02032392>.
- [98] Stewart M. Structural reliability and error control in reinforced concrete design and construction. Struct Saf 1993;12:277–92. [https://doi.org/10.1016/0167-4730\(93\)90057-8](https://doi.org/10.1016/0167-4730(93)90057-8).
- [99] Stewart M, Melchers R. Error control in member design. Struct Saf 1989;6:11–24. [https://doi.org/10.1016/0167-4730\(89\)90004-0](https://doi.org/10.1016/0167-4730(89)90004-0).
- [100] Vrouwenvelder T, Holický M, Sykora M. Modelling of human error. Jt. Work. COST Actions TU0601 E55, Ljubljana, Slovenia: 2009, p. 55–64.
- [101] Wisniewski DF, Casas JR, Ghosn M. Simplified probabilistic non-linear assessment of existing railway bridges. Struct Infrastruct Eng 2009;5:439–53. <https://doi.org/10.1080/15732470701639906>.
- [102] Nowak AS, Yamani AS, Tabsh SW. Probabilistic models for resistance of concrete bridge girders. ACI Struct J 1994;91:269–76. <https://doi.org/10.14359/4354>.
- [103] Hajdin R. Managing existing bridges - on the brink of an exciting future. Maintenance, Safety, Risk, Manag. Life-Cycle Perform. Bridg. - Proc. 9th Int. Conf. Bridg. Maintenance, Saf. Manag. IABMAS, 2018.
- [104] Shields MD, Teferra K, Hapij A, Daddazio RP. Refined Stratified Sampling for efficient Monte Carlo based uncertainty quantification. Reliab Eng Syst Saf 2015;142:310–25. <https://doi.org/10.1016/j.ress.2015.05.023>.
- [105] Olsson A, Sandberg G, Dahlblom O. On Latin hypercube sampling for structural reliability analysis. Struct Saf 2003;25:47–68. [https://doi.org/10.1016/S0167-4730\(02\)00039-5](https://doi.org/10.1016/S0167-4730(02)00039-5).
- [106] Sallaberry CJ, Helton JC, Hora SC. Extension of Latin hypercube samples with correlated variables. Reliab Eng Syst Saf 2008;93:1047–59. <https://doi.org/10.1016/j.ress.2007.04.005>.
- [107] Boussabaine HA, Kirkham RJ. Whole Life-Cycle Costing: Risk and Risk Responses. Oxford: 2008. <https://doi.org/10.1002/9780470759172>.
- [108] Guimarães H, Matos JC, Henriques AA. An innovative adaptive sparse response surface method for structural reliability analysis. Struct Saf 2018;73:12–28. <https://doi.org/10.1016/j.strusafe.2018.02.001>.
-

-
- [109] Galvão N, Matos J, Oliveira D V. Human Errors induced risk in reinforced concrete bridge engineering. *J Perform Constr Facil* 2021;35:04021026. [https://doi.org/10.1061/\(ASCE\)CF.1943-5509.0001595](https://doi.org/10.1061/(ASCE)CF.1943-5509.0001595).
- [110] Hajdin R, Casas JR, Campos e Matos J. Inspection of Existing Bridges – Moving on from condition rating. IABSE Symp. Towar. a Resilient Built Environ. Risk Asset Manag., Guimarães, Portugal: IABSE; 2019, p. 940–7. <https://doi.org/10.2749/guimaraes.2019.0940>.
- [111] Darmawan MS, Stewart MG. Spatial time-dependent reliability analysis of corroding pretensioned prestressed concrete bridge girders. *Struct Saf* 2007;29:16–31. <https://doi.org/10.1016/j.strusafe.2005.11.002>.
- [112] Biondini F, Frangopol DM. Time-variant redundancy and failure times of deteriorating concrete structures considering multiple limit states. *Struct Infrastruct Eng* 2017;13:94–106. <https://doi.org/10.1080/15732479.2016.1198403>.
- [113] Garg RK, Chandra S, Kumar A. Analysis of bridge failures in India from 1977 to 2017. *Struct Infrastruct Eng* 2020. <https://doi.org/10.1080/15732479.2020.1832539>.
- [114] Schaap HS, Caner A. Bridge collapses in Turkey: causes and remedies. *Struct Infrastruct Eng* 2020;18:295–312. <https://doi.org/10.1080/15732479.2020.1867198>.
- [115] Wardhana K, Hadipriono FC. Analysis of recent bridge failures in the United States. *J Perform Constr Facil* 2003;17:144–50. [https://doi.org/10.1061/\(ASCE\)0887-3828\(2003\)17:3\(144\)](https://doi.org/10.1061/(ASCE)0887-3828(2003)17:3(144)).
- [116] Calvi GM, Moratti M, O'Reilly GJ, Scattarreggia N, Monteiro R, Malomo D, et al. Once upon a Time in Italy: The Tale of the Morandi Bridge. *Struct Eng Int* 2019;29:198–217. <https://doi.org/10.1080/10168664.2018.1558033>.
- [117] Malomo D, Scattarreggia N, Orgnoni A, Pinho R, Moratti M, Calvi GM. Numerical Study on the Collapse of the Morandi Bridge. *J Perform Constr Facil* 2020;34:04020044. [https://doi.org/10.1061/\(asce\)cf.1943-5509.0001428](https://doi.org/10.1061/(asce)cf.1943-5509.0001428).
- [118] Peng W, Tang Z, Wang D, Cao X, Dai F, Taciroglu E. A forensic investigation of the Xiaoshan ramp bridge collapse. *Eng Struct* 2020;224:111203. <https://doi.org/10.1016/j.engstruct.2020.111203>.
- [119] Proske D. Bridge Collapse Frequencies versus Failure Probabilities. Cham: Springer Cham; 2018. <https://doi.org/10.1007/978-3-319-73833-8>.
- [120] Stewart MG. A human reliability analysis of reinforced concrete beam construction. *Civ Eng Syst* 1992;9:227–50. <https://doi.org/10.1080/02630259208970651>.
- [121] Swain AD, Guttman HE. Handbook of reliability analysis with emphasis on nuclear plant applications. Washington, D.C.: 1983.
- [122] Stewart MG. Human error in steel beam design. *Civ Eng Syst* 1990;7:94–101. <https://doi.org/10.1080/02630259008970576>.
- [123] Stewart MG, Melchers RE. Decision model for overview checking of engineering designs. *Int J Ind Ergon* 1989;4:19–27. [https://doi.org/10.1016/0169-8141\(89\)90046-2](https://doi.org/10.1016/0169-8141(89)90046-2).
- [124] Ellingwood BR. Design and construction error effects on structural reliability. *J Struct Eng* 1987;113:409–22. [https://doi.org/doi:10.1061/\(ASCE\)0733-9445\(1987\)113:2\(409\)](https://doi.org/doi:10.1061/(ASCE)0733-9445(1987)113:2(409)).
-

- [125] Bhattacharyya B. Uncertainty quantification and reliability analysis by an adaptive sparse Bayesian inference based PCE model. *Eng Comput* 2022;38:1437–58. <https://doi.org/10.1007/s00366-021-01291-0>.
- [126] Teixeira R, Martinez-Pastor B, Nogal M, O'Connor A. Reliability analysis using a multi-metamodel complement-basis approach. *Reliab Eng Syst Saf* 2021;205:107248. <https://doi.org/10.1016/j.ress.2020.107248>.
- [127] Teixeira R, Nogal M, O'Connor A. Adaptive approaches in metamodel-based reliability analysis: A review. *Struct Saf* 2021;89:102019 Contents. <https://doi.org/10.1016/j.strusafe.2020.102019>.
- [128] Lataniotis C, Wicaksono D, Marelli S, Sudret B. UQLab user manual - Kriging (Gaussian process modeling), Report # UQLab-V1.4-105. Zurich, Switzerland: 2021.
- [129] Echard B, Gayton N, Lemaire M. AK-MCS: An active learning reliability method combining Kriging and Monte Carlo Simulation. *Struct Saf* 2011;33:145–54. <https://doi.org/10.1016/j.strusafe.2011.01.002>.
- [130] M. Moustapha, S. Marelli and BS. UQLab user manual - Active learning reliability, Report UQLab-V1.4-117. Zurich, Switzerland: 2021.
- [131] Marelli S, Sudret B. An active-learning algorithm that combines sparse polynomial chaos expansions and bootstrap for structural reliability analysis. *Struct Saf* 2018;75:67–74. <https://doi.org/10.1016/j.strusafe.2018.06.003>.
- [132] Marelli S, Schobi R, Sudret B. UQLab user manual - Structural Reliability (Rare Event Estimation), Report # UQLab-V1.4-107. Zurich, Switzerland: 2021.
- [133] Schneider R, Thöns S, Straub D. Reliability analysis and updating of deteriorating systems with subset simulation. *Struct Saf* 2017;64:20–36. <https://doi.org/10.1016/j.strusafe.2016.09.002>.
- [134] Infraestruturas de Portugal. Case study II blue prints (Internal Reference). Lisboa, Portugal: 2006.
- [135] TNO DIANA. User 's Manual - Analysis Procedures. Release 10. Delft, The Netherlands: 2020.
- [136] Hendriks MAN, de Boer A, Belletti B. Guidelines for nonlinear finite element analysis of concrete structures - RTD:1016-1:2017. 2017.
- [137] Wisniewski D, Casas JR, Henriques AA, Cruz PJS. Probability-based assessment of existing concrete bridges-stochastic resistance models and applications. *Struct Eng Int* 2009;19:203–10. <https://doi.org/10.2749/101686609788220268>.
- [138] Danish Road Directorate. Reliability-Based Classification of The Load Carrying Capacity of Existing Bridges. Denmark: Danish Road Directorate (DRD); 2004.
- [139] O'Connor A, Pedersen C, Gustavsson L, Enevoldsen I. Probability-based assessment and optimised maintenance management of a large riveted truss railway bridge. *Struct Eng Int* 2009;19:375–82. <https://doi.org/10.2749/101686609789847136>.
- [140] Honfi D, Mårtensson A, Thelandersson S. Reliability of beams according to Eurocodes in serviceability limit state. *Eng Struct* 2012;35:48–54. <https://doi.org/10.1016/j.engstruct.2011.11.003>.

- [141] Moreira VN, Matos JC, Oliveira D V. Probabilistic-based assessment of a masonry arch bridge considering inferential procedures. *Eng Struct* 2017;134:61–73. <https://doi.org/10.1016/j.engstruct.2016.11.067>.
- [142] European Committee for Standardization (CEN). EN 1992-2, Eurocode 2: Design of concrete structures - Part 2: Concrete bridges - Design and detailing rules. Brussels, Belgium: 2005.
- [143] Moustapha M, Marelli S, Sudret B. UQLab user manual – The UQLINK module, Report #UQLab-V1.4-110. Zurich, Switzerland: 2021.
- [144] Lataniotis C, Torre E, Marelli S, Sudret B. UQLab user manual – The Input module, Report # UQLab-V1.4-102. Zurich, Switzerland: 2021.
- [145] Blatman G, Sudret B. Adaptive sparse polynomial chaos expansion based on least angle regression. *J Comput Phys* 2011;230:2345–67. <https://doi.org/10.1016/j.jcp.2010.12.021>.
- [146] Ghasemi SH, Nowak AS. Target reliability for bridges with consideration of ultimate limit state. *Eng Struct* 2017;152:226–37. <https://doi.org/10.1016/j.engstruct.2017.09.012>.
- [147] Lataniotis C, Marelli S, Sudret B. UQLab user manual – The Model module, Report # UQLab-V1.4-103. Zurich, Switzerland: 2021.
- [148] Stewart MG, Ginger JD, Henderson DJ, Ryan PC. Fragility and climate impact assessment of contemporary housing roof sheeting failure due to extreme wind. *Eng Struct* 2018;171:464–75. <https://doi.org/10.1016/j.engstruct.2018.05.125>.
- [149] Kirwin B. A guide to practical human reliability assessment. London, UK: Taylor & Francis; 1994.
- [150] Baron E, Galvão N, Docevska M, Matos J, Markovski G. Application of Quality Control Plan To Existing Bridges. *Struct Infrastruct Eng* 2021;in Press. <https://doi.org/10.1080/15732479.2021.1994618>.
- [151] Siqi W, Liye Z, Han S, Jinsheng D. Time-dependent robustness-based condition assessment of RC bridges subjected to corrosion. *Structures* 2021;34:4500–10. <https://doi.org/10.1016/j.istruc.2021.10.061>.
- [152] Sajedi S, Huang Q, Gandomi AH, Kiani B. Reliability-Based Multiobjective Design Optimization of Reinforced Concrete Bridges Considering Corrosion Effect. *ASCE-ASME J Risk Uncertain Eng Syst Part A Civ Eng* 2017;3:04016015. <https://doi.org/10.1061/ajrua6.0000896>.
- [153] Tu B, Dong Y, Fang Z. Time-Dependent Reliability and Redundancy of Corroded Prestressed Concrete Bridges at Material, Component, and System Levels. *J Bridg Eng* 2019;24:04019085. [https://doi.org/10.1061/\(asce\)be.1943-5592.0001461](https://doi.org/10.1061/(asce)be.1943-5592.0001461).
- [154] Cao R, El-Tawil S, Agrawal AK. Miami Pedestrian Bridge Collapse: Computational Forensic Analysis. *J Bridg Eng* 2020;25:04019134. [https://doi.org/10.1061/\(asce\)be.1943-5592.0001532](https://doi.org/10.1061/(asce)be.1943-5592.0001532).
- [155] Zhou X, Di J, Tu X. Investigation of collapse of Florida International University (FIU) pedestrian bridge. *Eng Struct* 2019;200:109733. <https://doi.org/10.1016/j.engstruct.2019.109733>.
- [156] Ditlevsen O. Fundamental postulate in structural safety. *J Eng Mech* 1983;109:1096–102. [https://doi.org/10.1061/\(asce\)0733-9399\(1983\)109:4\(1096\)](https://doi.org/10.1061/(asce)0733-9399(1983)109:4(1096)).

- [157] Straub D, Schneider R, Bismut E, Kim HJ. Reliability analysis of deteriorating structural systems. *Struct Saf* 2020;82:101877. <https://doi.org/10.1016/j.strusafe.2019.101877>.
- [158] Hawchar L, El Soueidy CP, Schoefs F. Principal component analysis and polynomial chaos expansion for time-variant reliability problems. *Reliab Eng Syst Saf* 2017;167:406–16. <https://doi.org/10.1016/j.ress.2017.06.024>.
- [159] Wang C, Li Q, Ellingwood BR. Time-dependent reliability of ageing structures: an approximate approach. *Struct Infrastruct Eng* 2016;12:1566–72. <https://doi.org/10.1080/15732479.2016.1151447>.
- [160] Guo T, Chen Z, Liu T, Han D. Time-dependent reliability of strengthened PSC box-girder bridge using phased and incremental static analyses. *Eng Struct* 2016;117:358–71. <https://doi.org/10.1016/j.engstruct.2016.03.011>.
- [161] Wang X, Mao X, Frangopol DM, Dong Y, Wang H, Tao P, et al. Full-scale experimental and numerical investigation on the ductility, plastic redistribution, and redundancy of deteriorated concrete bridges. *Eng Struct* 2021;234:111930. <https://doi.org/10.1016/j.engstruct.2021.111930>.
- [162] International Federation for Structural Concrete (FIB). Bulletin 34: Model Code for Service Life Design. Lausanne, Switzerland: 2006.
- [163] Du YG, Clark LA, Chan AHC. Residual capacity of corroded reinforcing bars. *Mag Concr Res* 2005;57:135–47. <https://doi.org/10.1680/macr.2005.57.3.135>.
- [164] Hackl J, Kohler J. Reliability assessment of deteriorating reinforced concrete structures by representing the coupled effect of corrosion initiation and progression by Bayesian networks. *Struct Saf* 2016;62:12–23. <https://doi.org/10.1016/j.strusafe.2016.05.005>.
- [165] International Federation for Structural Concrete (FIB). Bulletin 59: Condition control and assessment of reinforced concrete structures. 2011.
- [166] Imperatore S, Rinaldi Z, Drago C. Degradation relationships for the mechanical properties of corroded steel rebars. *Constr Build Mater* 2017;148:219–30. <https://doi.org/10.1016/j.conbuildmat.2017.04.209>.
- [167] Zhang W, Song X, Gu X, Li S. Tensile and fatigue behavior of corroded rebars. *Constr Build Mater* 2012;34:409–17. <https://doi.org/10.1016/j.conbuildmat.2012.02.071>.
- [168] Galvão N, Matos J, Hajdin R, Ferreira L, Stewart MG. Impact of construction errors on the structural safety of a post-tensioned reinforced concrete bridge. *Eng Struct* 2022;267:114650. <https://doi.org/10.1016/J.engstruct.2022.114650>.
- [169] Melhem MM, Caprani CC, Stewart MG, Ng A. Bridge Assessment Beyond the AS 5100 Deterministic Methodology. Sydney, Australia: Austroads Ltd; 2020.
- [170] Caprani CC, Melhem MM, Siamphukdee K. Reliability analysis of a Super-T prestressed concrete girder at serviceability limit state to AS 5100:2017. *Aust J Struct Eng* 2017;18:60–72. <https://doi.org/10.1080/13287982.2017.1332843>.
- [171] OBrien EJ, Schmidt F, Hajializadeh D, Zhou XY, Enright B, Caprani CC, et al. A review of probabilistic methods of assessment of load effects in bridges. *Struct Saf* 2015;53:44–56. <https://doi.org/10.1016/j.strusafe.2015.01.002>.

- [172] Swiss society of Engineers and Architects (SIA). SIA 262:2003 - Concrete Structures. Zurich, Switzerland: 2003.
- [173] Slobbe A, Rózsás Á, Allaix DL, Bigaj-van Vliet A. On the value of a reliability-based nonlinear finite element analysis approach in the assessment of concrete structures. *Struct Concr* 2020;21:32–47. <https://doi.org/10.1002/suco.201800344>.
- [174] Schobi R, Marelli S, Sudret B. UQLab user manual – Polynomial chaos Kriging, Report # UQLab-V1.4-109. Zurich, Switzerland: 2021.
- [175] Moustapha M, Sudret B, Marelli S. Active learning for structural reliability: Survey, general framework and benchmark. *Struct Saf* 2022;96:102174. <https://doi.org/10.1016/j.strusafe.2021.102174>.
- [176] Atmospheric CO2 concentrations worldwide 1959-2021 | Statista 2021. <https://www.statista.com/statistics/1091926/atmospheric-concentration-of-co2-historic/> (accessed June 1, 2022).
- [177] Chandler T, Chang J, Mosleb A, J. M, Boring R, Gertman D. Human Reliability Analysis Methods: Selection Guidance for NASA. 2006.

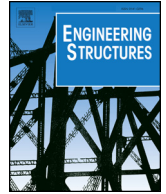
"It ain't what you don't know that gets you into trouble. It's what you know for sure that just ain't so"
By Mark Twain

Appendix

"Poor leadership paired with good management is simply a faster journey to the wrong destination."
by Stephen Covey

In the Appendix, additional journal publications are presented as published by the respective journals. These publications were incremental steps necessary to explore ideas and concepts very much needed for the achievement of the overall goals of this thesis project. These were published under the following titles:

- i. Probabilistic-based assessment of existing steel-concrete composite bridges – Application to Sousa River Bridge. DOI: <https://doi.org/10.1016/j.engstruct.2018.12.006>.
- ii. Round-Robin Modelling of the Load-bearing Capacity of Slender Columns by Using Classical and Advanced Non-linear Numerical and Analytical Prediction Tools. <https://doi.org/10.1080/10168664.2020.1740069>
- iii. Probabilistic and Semi-Probabilistic Analysis of Slender Columns Frequently Used in Structural Engineering. <https://doi.org/10.3390/app11178009>
- iv. Application of Quality Control Plan To Existing Bridges. <https://doi.org/10.1080/15732479.2021.1994618>
- v. Risk assessment of terrestrial transportation infrastructures exposed to extreme events. <https://doi.org/10.3390/infrastructures6110163>



Probabilistic-based assessment of existing steel-concrete composite bridges – Application to Sousa River Bridge

José C. Matos^{1,*}, Vicente N. Moreira¹, Isabel B. Valente¹, Paulo J.S. Cruz², Luís C. Neves³, Neryvaldo Galvão¹

ISISE, Department of Civil Engineering, University of Minho, Guimarães, Portugal

ARTICLE INFO

Keywords:

Probabilistic-based assessment
Uncertainty sources
Steel-concrete composite bridges
Existing structures
Bayesian inference
Model identification

ABSTRACT

This paper presents a framework to assess the safety of existing structures, combining deterministic model identification and reliability assessment techniques, considering both load-test and complementary laboratory test results. Firstly, the proposed framework, as well as the most significant uncertainty sources are presented. Then, the developed model identification procedure is described. Reliability methods are then used to compute structural safety, considering the updated model from model identification. Data acquisition, such as that collected by monitoring, non-destructive or material characterization tests, is a standard procedure during safety assessment analysis. Hence, Bayesian inference is introduced into the developed framework, in order to update and reduce the statistical uncertainty. Lastly, the application of this framework to a case study is presented. The example analyzed is a steel and concrete composite bridge. The load test, the developed numerical model and the obtained results are discussed in detail. The use of model identification allows the development of more reliable structural models, while Bayesian updating leads to a significant reduction in uncertainty. The combination of both methods allows for a more accurate assessment of structural safety.

1. Introduction

Structural assessment comprises all activities required to evaluate the condition of structures for future use, namely their safety. Several authors have used probabilistic-based procedures to assess the safety of existing structures, having shown that conclusions can be dramatically different from those obtained by using existing codes [1–6]. When assessing an existing structure, the available information regarding materials and geometry is usually limited. In order to overcome this drawback, model identification techniques may be used to estimate structural parameters based on measured performance, such as deflections. More recently, Bayesian inference was introduced to improve the quality of the probabilistic models for both resistance and effect of loadings, by using data collected from the structure under analysis [7,8].

In this work, a probabilistic-based structural assessment framework, combining deterministic model identification and reliability assessment, is presented and tested on a composite steel-concrete bridge

subjected to a performance load test. In the first step, a sensitivity analysis is used to identify the most influential parameters on the overall structural response at both service and ultimate loading conditions. Then, these parameters are found considering a model identification algorithm, which consists in an optimization procedure minimizing the difference between observed performance (e.g. vertical displacements collected during the load tests) and performance predicted using a non-linear numerical model. A convergence criterion which addresses the expected accuracy of experimental and numerical results, is considered [9]. This procedure yields a set of near optimal solutions, from which the best model is selected considering the probability of each solution occurring based on previous knowledge, followed by an engineering judgment procedure. A reliability assessment algorithm is then applied, considering the selected model. In some circumstances, complementary tests are developed to increase the reliability of the estimation of input parameters. An updated resistance probability density function (PDF) is computed through the use of a Bayesian inference procedure, and considering obtained data from

* Corresponding author.

E-mail addresses: jmatos@civil.uminho.pt (J.C. Matos), isabelv@civil.uminho.pt (I.B. Valente), pcruz@arquitectura.uminho.pt (P.J.S. Cruz), luís.neves@nottingham.ac.uk (L.C. Neves), neryvlado.galvao17@live.com (N. Galvão).

¹ ISISE, Department of Civil Engineering, University of Minho, Campos de Azurém, 4800-058 Guimarães, Portugal.

² Lab2PT, School of Architecture, University of Minho, Campos de Azurém, 4800-058 Guimarães, Portugal.

³ Resilience Engineering Research Group, University of Nottingham, NTEC Building, NG7 2RD, UK.

performed complementary tests. The proposed framework is applied to the assessment of a steel-composite bridge built in Portugal.

2. Framework

The proposed safety assessment framework comprises two steps. Initially, a deterministic analysis is used to quantify the numerical model critical parameters, based on the combination of the results obtained by nonlinear finite element method (NL-FEM) models and data obtained with experimental tests and inspection or monitoring assignments. This procedure, denoted as model identification, searches for mean values of the mechanical and geometrical properties of the structure, which is fundamental to define the probabilistic distributions of structural parameters that will be used in the reliability assessment of the structure.

The model identification procedure can be computationally expensive due to the need to evaluate a large number of NL-FEM models. To minimize the impact of this, a sensitivity analysis is used to identify the critical parameters, minimizing the complexity of the model identification procedure [10,11]. This analysis consists of evaluating the fitness function variation with each input parameter [12]. An importance measure, b_k , is obtained for each parameter as,

$$b_k = \sum_{i=1}^n (\Delta y_{i,k} / y_{m,k}) / (\Delta x_{i,k} / x_{m,k}) \cdot CV_k \quad [\%] \quad (1)$$

where b_k is the importance measure of parameter k , $\Delta y_{i,k}$ is the variation in structural response parameter, $\Delta x_{i,k}$ is the variation of input parameter around its average value $x_{m,k}$, $y_{m,k}$ is the average response, n is the number of data points to be considered on the computation procedure and CV is the coefficient of variation of the assessed parameter. For the assessed model parameter importance measure, it is added or subtracted a standard deviation value to its mean value, keeping the remaining parameters values with their mean values. Then, each set of assessed parameter values is analyzed through structural analysis software, being then applied Eq. (1) to obtain the parameter importance measure. After this procedure is applied to all model parameters, obtained importance measure values are normalized with respect to the highest one.

2.1. Model identification

Most likely values for critical parameters are evaluated using an optimization procedure, minimizing the difference between numerical and experimental data as:

$$f = \sum_{i=1}^n |y_i^{num} - y_i^{exp}| / \max(y^{exp}) \cdot 1/n \quad [\%] \quad (2)$$

where y_i^{exp} and y_i^{num} are the numerical and experimental result i , and n is the number of comparing points to be used in the algorithm, which usually corresponds to the maximum number of measurements at the real structure. If more than one measurement is made, independently of being the same type or not, then the standardized values should be added and divided by the total number of measurements, in order to obtain a final standardized value. As such, by normalizing the value of each parameter, it is possible to use different transducers, measuring different parameters in any section of the structure and load case (LC).

In order to limit the probability of overfitting, optimization is conducted, not to find the best solution, but a group of solutions associated with a fitness under a given threshold. It is assumed that when computing the difference between numerical and experimental data, results associated with a fitness below the expected amplitude of errors are considered as optimal. The threshold value, ε , is calculated using the law of propagation of uncertainty [9], combining both measurement and modelling errors. Among different optimization methods, evolutionary strategies [13] have shown to be the most efficient and robust in

this type of problem [12].

2.1.1. Quantification of error

When using a model identification procedure, two sources of errors should be considered: related to experimental measurements (difference between real and measured quantities in a single measurement) and numerical analysis (difference between the response of a given model and that of an ideal model which accurately represents the structural behavior). Consequently, when computing the difference between numerical and experimental data, results should be considered not as deterministic but as a range of values, following a Uniform PDF [9]. Based on the law of propagation of uncertainty [9] and assuming independent between error sources, the total error, u , can be estimated as a combination of measurement and modelling errors:

$$u = \sqrt{\sum_{i=1}^n (\partial f / \partial x_i)^2 \cdot u(x_i)^2} \quad (3)$$

where $u(x_i)$ is the error associated with each source of uncertainty and $\partial f / \partial x$ is the partial derivative of the fitness function in order to each component x . The partial derivative, in relation to each term, can be determined as $\partial f / \partial y^{num} = \partial f / \partial y^{exp} = 1 / \max(y^{exp})$. Once the expected error is computed, it is used: (1) to define the convergence criteria for the optimization algorithm; and (2) to define potential solutions. The optimization algorithm is considered converged if the improvement in the fitness of solutions between two generations, i.e., the convergence criterion, Δf , is smaller than a threshold value, ε , as defined by Eq. (4),

$$\Delta f = |f_{i+n} - f_i| \leq \varepsilon \quad (4)$$

with f_i and f_{i+n} , respectively, the fitness function values for generation i and $i + n$, and n the defined gap between two generations. In this case, a threshold value, ε , is a measure of accuracy, and it is considered to be equal to the total error, u , defined by Eq. (3).

2.1.2. Expert judgment procedure

Global optimization algorithms, as evolutionary strategies [13], when incorporated in model identification, result in a population of optimal or near optimal models. A decision regarding which of these set of parameters is the most accurate must be made using either experience or more robust algorithms. However, even in this latter case, an expert judgment criterion might be necessary. In this work, the used algorithm is based on the principle that the most suitable model is that which assessed parameter values are close to initial mean values, unless some accidental situation is detected. Therefore, the likelihood of each model, f_d , is computed through:

$$f_d = \prod_{i=1}^n f(x_{id}) \quad (5)$$

where x_{id} is the value of the assessed parameter i , and $f(x_{id})$ is the PDF value for this parameter, assuming a PDF from bibliography [14] or based in experience. Then the product of all PDF values, for all assessed parameters, and for all extracted models, is computed (f_d). The updated model, from proposed model identification procedure, is that which presents the highest value. Herein, expert judgment is used, in combination with the likelihood of each model, to identify and select the most likely model [12].

2.2. Probabilistic-based assessment

In the second step of the proposed algorithm, reliability analysis is used to evaluate, from a probabilistic point of view, the structural safety condition through the computation of the reliability index or, the corresponding failure probability. Accordingly, the previously updated numerical model is converted into a probabilistic model by considering the randomness in model parameters. The use of gradient-based methods, like FORM, in conjunction with NL-FEM is complex, while

simulation methods are simpler and robust, but computationally expensive. Variance reduction simulation techniques allow a significant reduction in the required number of simulations to compute a specific variance value. One of these techniques is the Latin Hypercube Sampling (LHS) [15]. Herein, Latin Hypercube Sampling (LHS) [15], with an in-built Iman and Conover correlation method [16], in order to consider structural parameters correlation, is used to sample numerical models. Then, for the set of obtained failure load factors, a distribution fitting procedure was performed, being obtained the resistance curve (R).

In safety assessment, a comparison between resistance, R , and loading, S , distributions is performed [17]. Accordingly, the failure probability, p_f , corresponds to the case in which the structural resistance is lower than the applied load. In this situation, the limit function may be defined by $Z(R,S) = R - S$. The correspondent reliability index, β , is given by $\beta = -\Phi^{-1}(p_f)$, being Φ^{-1} the inverse cumulative distribution function for a standard Normal distribution.

Bayesian methods provide tools to incorporate external information into data analysis process, with the aim of reducing the statistical uncertainty. As more data is collected, Bayesian analysis is used to update the prior into a posterior distribution. The Bayes theorem, which weights the prior information with evidence provided by new data, is the basic tool for the updating procedure. This way, the reliability index is continuously updated. The structural safety assessment [14,18] consists of computing the obtained reliability index and comparing it to a target value, β_{target} , proposed by existing standards [12].

3. Case study

The Sousa River Bridge, a composite steel-concrete bridge built in 2010, on highway A43, Gondomar to Aguiar de Sousa (IC24), in Portugal (Fig. 1a), is analyzed herein. The bridge presents a total length of 202 m between abutments – from 6 + 722.50 km to 6 + 924.50 km – divided in four spans of 44 m and an extreme span, near abutment A2, of 26 m, as shown in Fig. 1b. This bridge consists of two adjacent and independent structures, with an identical typology. The continuous deck is composed of a precast reinforced concrete slab supported on two longitudinal steel welded I-beams, as shown in Fig. 1c. The longitudinal girders present a constant height of 2.0 m, with exception of the extreme span in which height varies with the deck inclination.

Transversally, these girders are fixed by stringers, evenly spaced of 5.5 m in each 44 m span, and of 5.2 m in the extreme span (Fig. 2a and b). These stringers are composed of IPE600 laminated steel profiles that are welded to half IPE600 steel profiles for connection with the longitudinal beams. These half profiles are welded to the longitudinal girder flanges. The reinforced concrete slab, the metallic girders and the stringers constitute a transversal and rigid framework.

Nelson headed studs [19], welded to the top flange of metallic girders, are used to connect concrete slabs and steel girders. To improve web stability, vertical steel plates were placed at thirds of the distance between stringers, in the regions that are close to the supports, see Fig. 2. In both columns and abutments, symmetrical interior web plates were included. Over the supports, the IPE600 stringers are replaced by welded rectangular hollow sections, as represented in Fig. 2a and b. The reinforced concrete columns have a maximum height of 35.0 m (average of 25.0 m). A constant I-section is adopted, with maximum dimensions 2.50 m \times 4.80 m. The abutments are independent from the rest of the structure, as expansion joints allowing longitudinal movement due to temperature and other environmental effects, were introduced in the bridge ends (Fig. 1b). The pavement is bituminous, with 20 mm thickness of regularization and a 30 mm thickness wear layer. C30/37 concrete [20] was used for bridge foundations, abutments and columns, and C40/50 concrete [20] was used for precast slabs and cast *in-situ* concrete. S500 NR SD steel [21] was used for reinforcement bars and S355 steel [21] was used for steel profiles. S355J0 is used in plates with a thickness lower than 50 mm, S355J2 is used for plates with a

thickness between 50 and 75 mm, S355K2 for plates with a thickness between 75 and 90 mm and S355ML for plates between 90 and 110 mm. For laminated steel profiles, S355J0 is used. An elasticity modulus of 210 GPa (reinforcing steel, $E_{s,b}$ and steel profile, $E_{s,p}$, modulus of elasticity) was considered for all steel materials. The headed studs are produced of S235 J2 G3 + C450 steel [19], with a yield strength (f_y) of 350 MPa, a ultimate limit strength (f_u) of 450 MPa and a limit strain (ϵ_{lim}) of 18%.

3.1. Load test

3.1.1. Description

In order to evaluate the bridge behavior before entering in service, a load test was carried out twenty eight days after the last concrete casting [22]. Both vertical displacement and temperature were measured during the test through an automatic data acquisition system. Load-tests took place between the 9:18am and 12:31 pm, being the overall load-test time of 3 h and 14 min. The temperature was measured at both inferior and superior faces of the deck, using PT100 resistive detectors. All transducers are electric based and were tested and calibrated in laboratory, before the load test. The vertical displacement measurements were measured with reference to the ground level, using invar wires, and linear variable differential transformers (LVDTs). These transducers present a precision of 0.05 mm (maximum value) for a measurement field of ± 25 mm (full scale), corresponding to a linearity of 0.10%. Fig. 3a shows the location of all sensors. A frequency of 10 Hz was designed for registering the vertical displacement data. Two displacement transducers were installed in span A1 – C1, designated by VD1 and VD2, and other two at span C1 – C2, denoted as VD3 and VD4 (Fig. 3a). The load was applied using four identical vehicles (with four axles), each vehicle loaded with sand in order to obtain a total weight close to 32 tons. The two front axles support 40% (20% each – 6.4 ton) of the load, while the two rear axles support 60% (30% each – 9.6 ton) of the total weight [23–26].

Three different load cases (LC) are considered, as represented in Fig. 3b: (1) LC1: maximum displacement in span A1 – C1; (2) LC2: maximum displacement in span C1 – C2 and rotation at C1; and (3) LC3: maximum rotation at C2. In each situation, the vehicles are immobilized on the bridge deck for 5 min, eliminating any dynamic effects while avoiding environmental effects (temperature, humidity). The temperature effects may be neglected, as it was verified that during the test the temperature was kept almost constant, significantly limiting its impact on obtained results [22].

3.1.2. Experimental results

The results gathered on the unloaded bridge are used to control the temperature effect on the structure and in the monitoring system along the test. The temperature effects may be neglected, as it was verified that during the test the temperature was kept almost constant, significantly limiting its impact on obtained results [22]. The vertical displacements registered are shown in Table 1. The maximum vertical displacement was registered at the extreme span A1 – C1. Since all spans have the same geometry, the small rotation stiffness of the abutment makes this span critical in terms of vertical displacements.

3.2. Numerical analysis

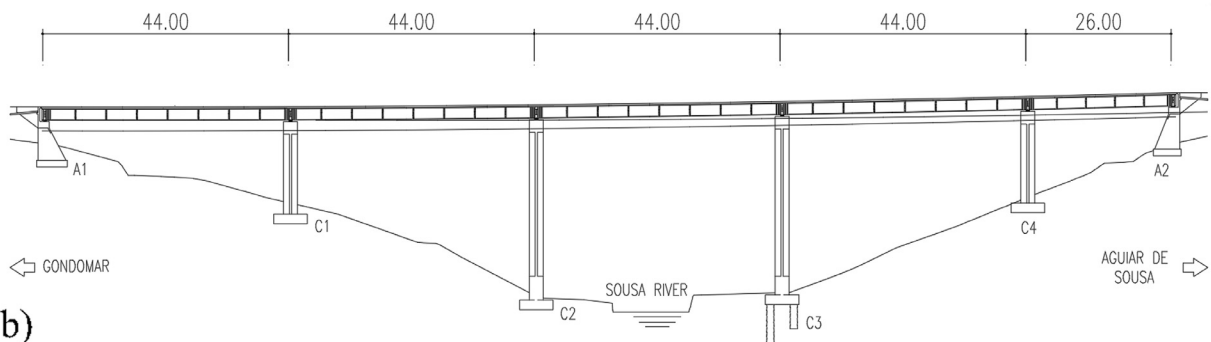
3.2.1. Numerical model

In order to evaluate the bridge performance, a numerical model was developed using ATENA® nonlinear structural analysis software [27]. The bridge is modelled using a 2D plane stress model elements. Vertical displacements are restricted at all supports, while deformation of piers is modelled using linear springs.

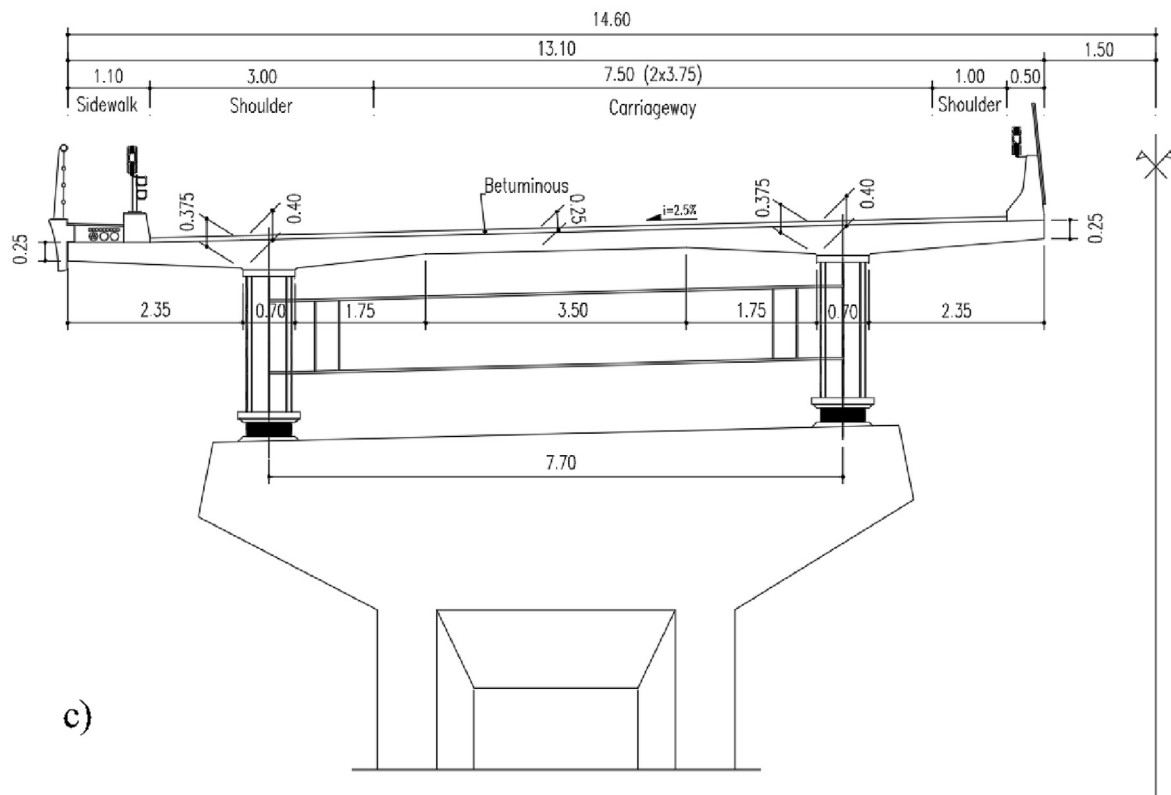
The precast slab presents a non-uniform geometry (Fig. 1c). This non-uniformity is considered in the numerical model by introducing several concrete layers. As the number of layers increase, the model's



a)



b)



c)

Fig. 1. Sousa River Bridge: (a) overview [22]; (b) side view (m) [28]; (c) transversal profile (m) [28].

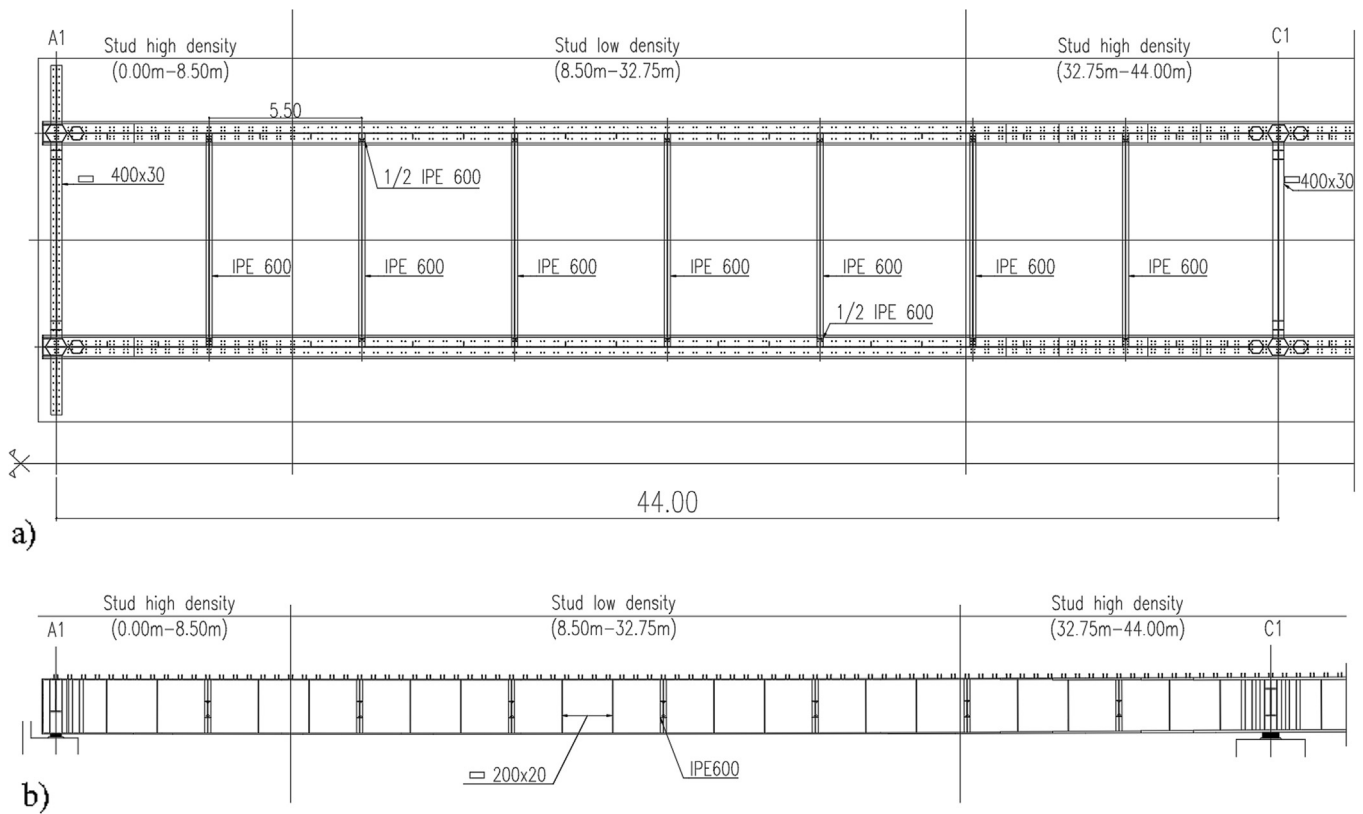


Fig. 2. Metallic girders [28]: (a) horizontal plan (m); (b) side view (m).

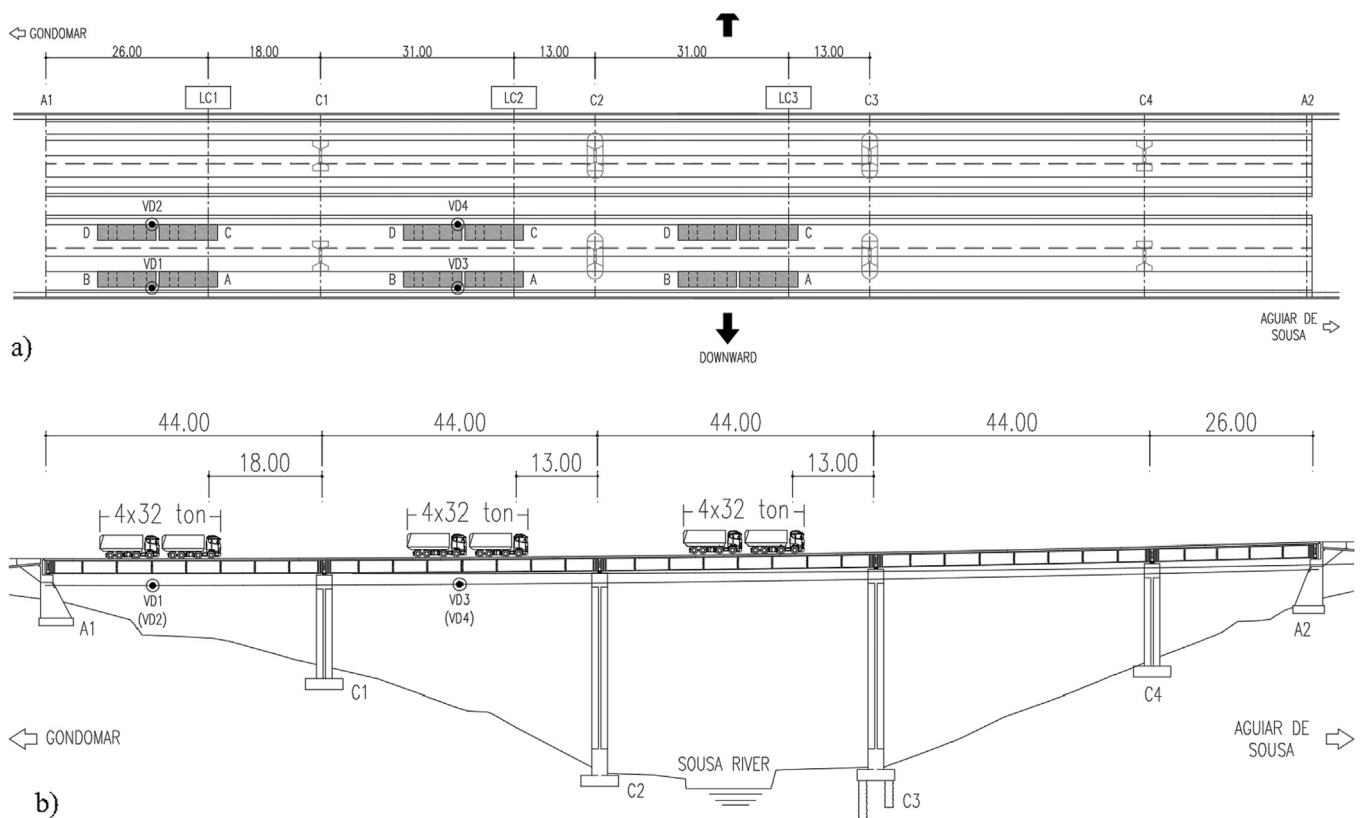


Fig. 3. Instrumentation and vehicle position in considered LCs: (a) Plan view; (b) Side view [22].

Table 1
Registered vertical displacements^{*,†} [22].

LC	VD1 [mm]	VD2 [mm]	VD3 [mm]	VD4 [mm]
LC1	16.01 (0.25)	14.48 (0.50)	−4.11 (−) [†]	−3.51 (−) [†]
LC2	−4.10 (−) [†]	−3.84 (−) [†]	14.00 (0.20)	13.40 (0.12)
LC3	1.86 (−) [†]	1.84 (−) [†]	−3.47 (−) [†]	−2.92 (−) [†]

* Negative value corresponds to a displacement in upward direction. The CV of displacements, in percentage [%], is provided between brackets.

† Non-available data on the load-test report [22].

geometry becomes more accurate, but also more complex. For the purpose of this paper, two rectangular layers are used. The reinforcing steel is considered to be embedded in precast concrete slab [12].

Concrete material was described by a SBETA material model, which is defined by the elasticity modulus, E_c , the compressive strain at compressive strength, ϵ_c , the compressive strength, f_c , the tensile strength, f_t , the critical displacement, w_d , and the fracture energy, G_f [27]. Steel was modeled by a bilinear with hardening Von Mises material model, being described by the elasticity modulus, E_s , the yield

strength, σ_y , the limit strain, ϵ_{lim} , and the ultimate strength, σ_u [27]. Both these constitutive material laws are detailed at ATENA® library [27].

There are two distributions of headed studs along the bridge: low (groups of 6 studs) and high (groups of 10 studs). The space between each group of studs, 0.50 m, is the same for both low and high stud densities [28] (Fig. 2). From the models available in ATENA [27] for interface elements, the Mohr-Coulomb [27] was selected, as it allows the definition of a very rigid interface until the strength of the connection, corresponding to the cohesion (c) in the Mohr-Coulomb model, is reached. After this, the tangential stiffness (K_{TT}) becomes very low. The small impact of the normal force on the interface is modelled by using a small friction angle (ϕ). It is assumed that the connection between steel and concrete is very rigid until plastification of the head studs, given by the tensile strength ($f_{t,stud}$). After this, the normal stiffness (K_{NN}) drops significantly. Accordingly, both the compression stiffness and the tensile strength parameters are assumed to present high values in order to guarantee the full composite behavior. The cohesion is computed based on the stud maximum load capacity and on expressions from EN 1994-1-1 [29], being obtained the values of 3.24

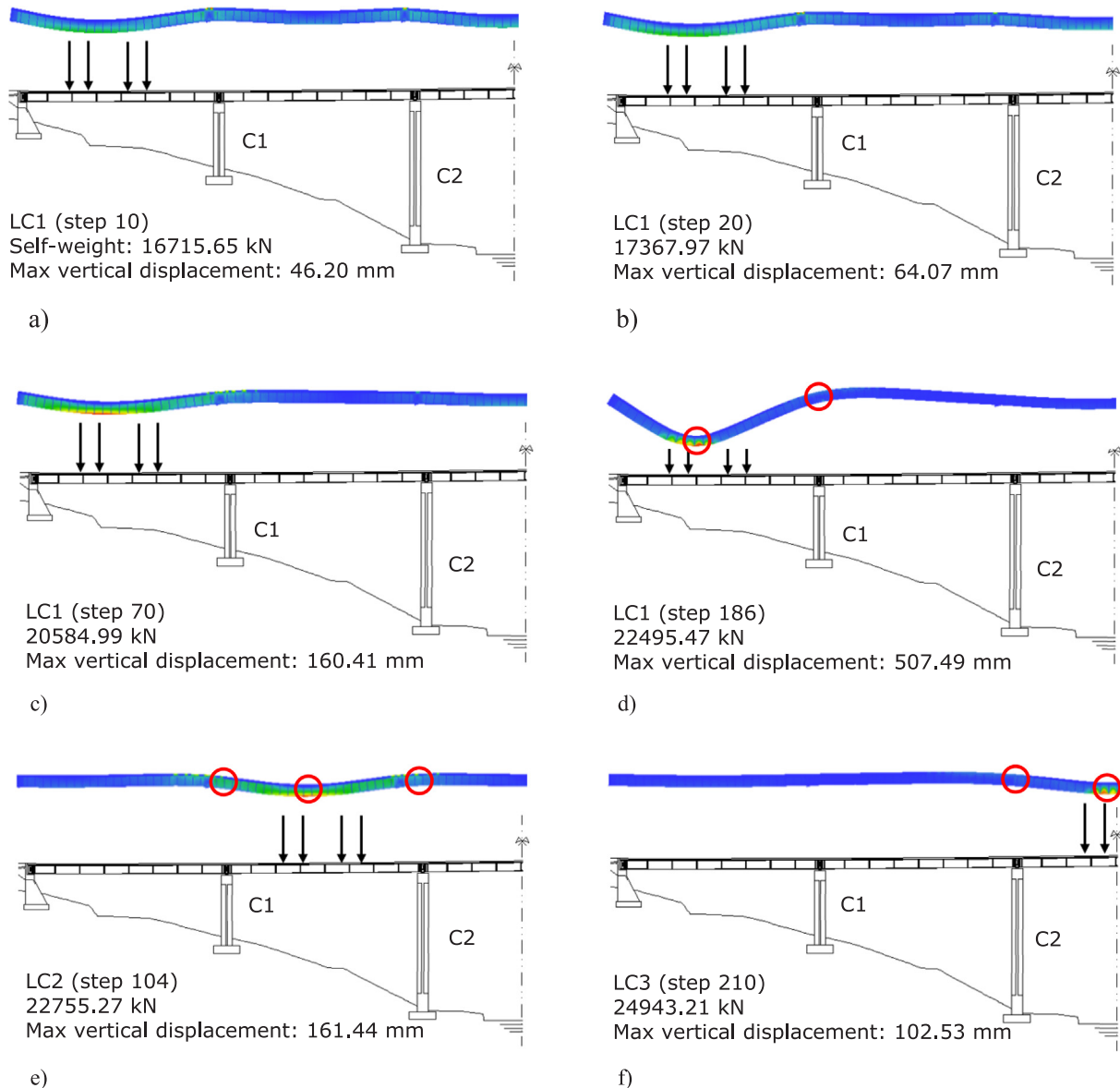


Fig. 4. Bridge vertical deformation (VD1) [12]: (a) Self-weight (step 10); (b) LC1 (step 20); (c) LC1 (step 70); (d) LC1 (step 186); (e) LC2 (step 104); (f) LC3 (step 210).

and 1.94 MPa for the situations of high and low density of studs, respectively (see Fig. 2). According to EN 1994-1-1 [29], the characteristic stud maximum load capacity is 102.07 kN (P_{Rk}), and the mean value ($P_{Rm} = 113.41$ kN) is obtained by dividing the previous value per 0.90 [29]. By considering this value for one stud, it is then possible to determine the cohesion value based on the number of studs and their spacing [29], i.e., by multiplying the mean stud load capacity by the number of studs per unit area of interface. The shear stiffness is computed based on the stud stiffness value. The stud stiffness value is very difficult to quantify as it depends from several factors [30], such as the type of used concrete and its modulus of elasticity, as well as on the studs dimensions. Therefore, results obtained from experimental tests (as the push-out tests described in EN1994-1-1 [29]) with the same type of concrete and stud geometry might be used to quantify this parameter. In this case, the value of 325 kN/mm was defined based in expert knowledge, gathered from tests previously developed by the authors [30], and in existing literature [31,32]. By taking this value into consideration, it is then possible to determine the value of the shear stiffness, 9.29×10^3 and 5.57×10^3 MPa/mm, respectively, for high and low density of studs.

The finite element mesh is mainly composed of quadrilateral elements. Additionally, interface elements are used to simulate the steel to concrete interface and spring elements try to simulate the horizontal support conditions. Reinforcement bars are modelled using nonlinear truss elements embedded in the concrete slab, in order to simulate the web reinforcements and both top and bottom flanges of the steel profile, resulting in a simpler and lighter numerical model.

The trucks are modelled as a load per axle. The load position varies with the LC. These vehicles are loading half of the bridge cross section, considering the respective symmetry. The dead load is firstly applied in 10 steps, with a factor of 0.1, and then the vehicle load is added in 10 steps. The differences in vertical displacements between the loaded and unloaded structure are compared to the experimental values in Table 1. The structure is then loaded up to failure by progressively increasing the vehicle load.

3.2.2. Numerical results

After the bridge is modelled, a calibration procedure is performed by comparing numerical results with those obtained on field test, allowing to validate the developed model and considered assumptions. In order to do that, the obtained numerical results given by Figs. 4 and 5 are analysed in detail.

Fig. 4a presents the bridge vertical deformation for the dead load only (step 10). The most critical sections are located at the interior support and at 40% of the span length, respectively, for negative and positive bending moment.

Fig. 4b shows the bridge deformation for dead load plus live load for LC1, step 20 (vehicles are located at the first span). Fig. 4c represents the beam deformation for load step 70 close to collapse. By comparing on Fig. 4b it is possible to verify an increase on the first span deformation. Fig. 4d presents the bridge deformation for step 186 (bridge collapse). By comparing this figure with Fig. 4c, it is possible to verify a higher deformation at first span while all the others are being progressively relieved. The collapse mechanism is characterized by two plastic hinges, respectively, at column C1 (step 70) and at 40% of the span length (step 186). Applied loads are redistributed from the first to the second hinge.

Fig. 4e shows the bridge deformation obtained for LC2, in which the vehicles are positioned in the second span. In this situation the collapse mechanism is defined by three hinges, respectively, at column C1 and C2 (step 70) and at middle span (step 104).

Fig. 4f shows the obtained bridge deformation with LC3, in which the vehicles are positioned in the third span. In this case, the collapse mechanism is defined by three hinges, respectively, at column C2 and C3 (step 70) and at middle span (step 210).

Strain values on the first span are shown in Fig. 5a. Localized

cracking is detected close to supports, where the concrete slab and part of the steel profile are in tension. Fig. 5b shows the stresses in the interface. Under sagging moment, the interface stress value is 0.66 MPa (low density) while for hogging bending moment region this value is 1.44 MPa (high density). Such results are far from the interface cohesion values computed in Section 3.2.1.

Fig. 5c shows the strains values at the critical span. An increase in cracking at hogging bending moment region, above the support, is observed. For the sagging bending moment region, part of the concrete slab is in compression and part is in tension, which means that the neutral axis moved in the upward direction. As shown in Fig. 5d the maximum interface stresses is 0.93 MPa (low density) under sagging moment and 1.47 MPa (high density) in the hogging moment region, which are lower than the interface cohesion values.

Fig. 5e shows the strain for the critical span, in the support region. The steel profile is partly in tension and partly in compression. The maximum tensile strain is verified at sagging bending moment region, at the bottom fibers of the steel profile. The steel profile is, in this region, in tension and the concrete slab is partly in compression and partly in tension. In this situation, localized cracking, due to concrete crushing, is detected at sagging bending moment region. Fig. 5f presents the interface tangential stresses. In this situation, a value of 1.37 MPa (lowest density) is obtained for sagging moment and a value of 2.20 MPa (highest density) for hogging bending moment, which are closer to the interface cohesion values.

The strain values presented in Fig. 5g shows that cracking in the concrete slab occurs in both hogging and sagging bending moment regions. Over the supports, the concrete slab is completely in tension, whereas the steel profile is partly in tension and partly in compression. The steel profile and a portion of the concrete slab are in tension, which indicates that the neutral axis is positioned in the top fibers. Fig. 5h presents interface stresses for the same load step. A maximum value of 1.62 MPa (low density) is verified for positive bending moment region and a maximum value of 3.24 MPa (high density) is measured for negative bending moment region. This means that the cohesion value for high density region is attained and a redistribution of tangential stresses is produced.

The analysis stops, for the three LCs, when the reinforcement limit strain at hogging bending moment region is reached. This corresponds to a bending failure mode with concrete crushing, and yielding of both reinforcement bars and steel profile. Moreover, it is verified that the ultimate moment depends on the LC considered. It also varies with the parameter values defined. In this situation, the developed model will be applied in a probabilistic analysis, considering different LCs, for which the parameter values are randomly generated. Therefore, a maximum number of 300 load steps is established, in order to take into account all possibilities.

Table 2 presents the computed displacements at VD1 and VD2 for the three considered LCs. In this situation, there are four comparison points (VD1 and VD2 correspond to VD1*; VD3 and VD4 correspond to VD2*) and three LC, which results in twelve components. The error between numerical and experimental data, as presented in Table 1, is computed for each case. It is important to note that the developed numerical model is less stiff than the real structure.

Fig. 6 presents the load-test vertical displacements and temperature. Based on these experimental results, and in the numerical results presented in Table 2, it is possible to confirm the good correlation between both, with the numerical vertical displacements being, in average, 17.44% higher than the experimental ones. Sousa et al. [23] described this difference and justified it as a result of considering the concrete elasticity modulus (E_c) based on EN 1992-1 [20], which is an under-estimation of the real value. Also, neglecting the reinforcements at support sections and at bridge span, as well as all the other non-structural elements (e.g. safety guards, cornices, etc.), lead to a less stiff structure. These modelling assumptions result in a conservative assessment, associated with a lower reliability index and, therefore, a

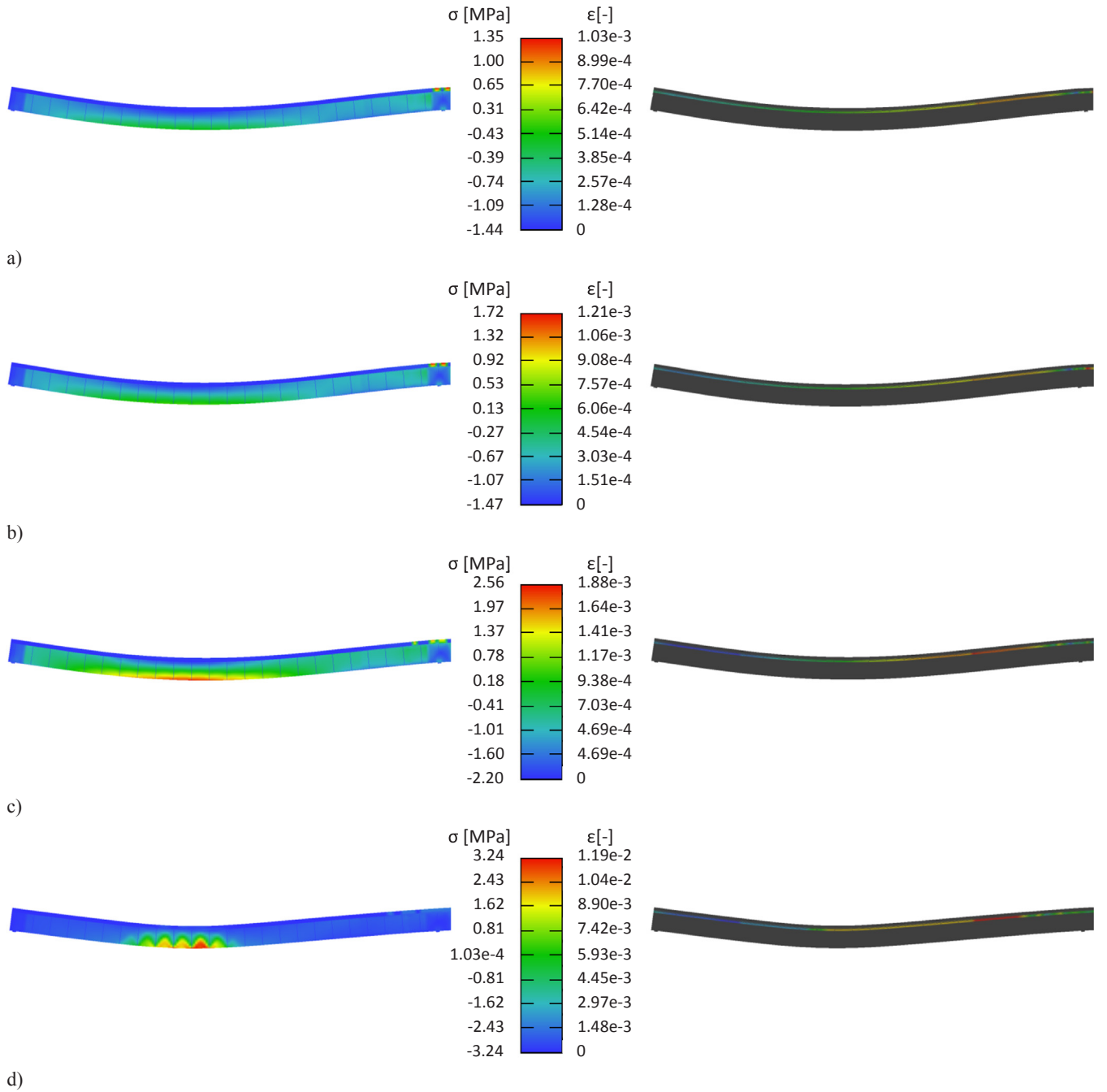


Fig. 5. Obtained results for strain and interface stress for LC1 [12]: (a) Self-weight (step 10); (b) step 20; (c) step 70; (d) step 186.

Table 2
Obtained displacement values for calibrated model[†] [12].

LC	VD1 [†] [mm]	Error [%]	VD2 [†] [mm]	Error [%]
LC1	17.77	16.86	−5.09	34.43
LC2	−4.90	23.56	14.32	4.58
LC3	1.40	24.32	−4.82	51.99

[†] Negative value corresponds to a displacement in upward direction.

higher failure probability. Despite that, a good compromise between cost and accuracy is achieved.

3.2.3. Sensitivity analysis

Sensitivity analysis is performed to identify the critical parameters

in the structural performance of the bridge, considering the three LCs and both service and failure loadings. Studied parameters are related to material, geometry and mechanical properties. If importance measure (b_k) defined in Eq. (1) is equal or higher than 10% (b_{lim}), the corresponding parameter will be considered as critical.

A total of 20 parameters are considered as follow: (a) concrete modulus of elasticity (E_c), tensile strength ($f_{t,c}$), compressive strength (f_c), fracture energy (G_f) and concrete specific weight (γ_{conc}); (b) reinforcement steel yield strength ($\sigma_{y,l}$), ultimate limit strength ($\sigma_{u,l}$) and strain ($\epsilon_{lim,l}$); (c) laminated steel profile yield strength ($\sigma_{y,p}$) and hardening modulus (H_p); (d) steel-concrete interface – shear stiffness (K_{TT}) and cohesion (c); (e) concrete slab width (b_{slab}) and height (h_{slab}); (f) laminated steel profile web thickness (b_{web}), and both top ($A_{fl,sup}$) and bottom ($A_{fl,inf}$) flanges area; (g) reinforcing steel area ($A_{s,l}$); (h) top concrete cover (c_{sup}); (i); and (j) pavement weight (p_{pav}).

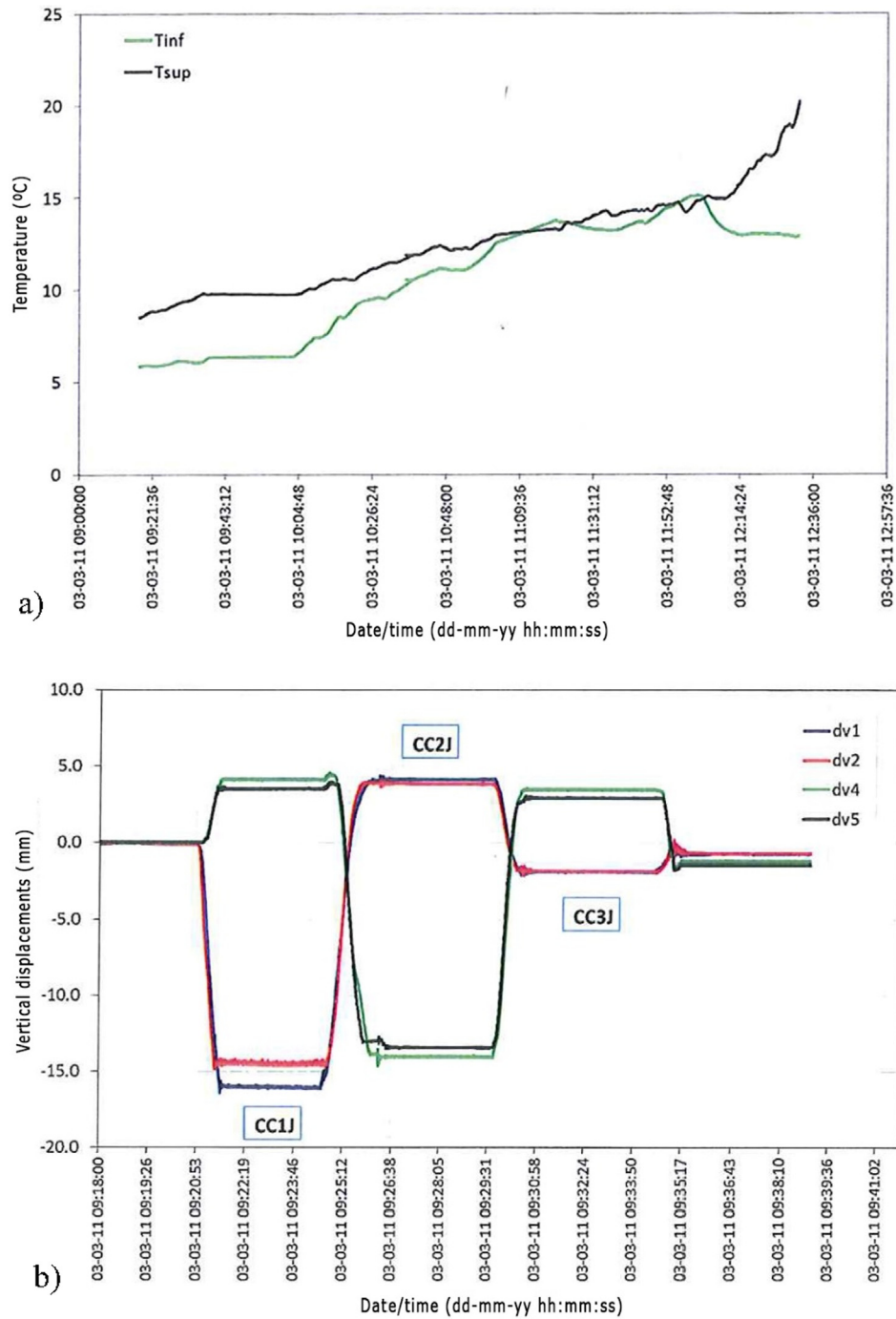


Fig. 6. (NewMensus 2011): Obtained field testing results: (a) Temperature evolution over time; (b) Vertical displacements.

The evaluated parameters and corresponding CVs and standard deviations (σ), used to compute the importance measures are given in Table 3. For some of these parameters, such values are provided in bibliography [14,33]. However, for others parameters, it is possible to sampling the input parameters, to compute the value of interest parameter through provided analytical expressions by bibliography [21,29], and perform a fitting curve procedure to obtain the CV and σ . Thus, and following the previous procedure, the CV and σ are obtained for the following parameters: (1) for the steel profile hardening modulus (H_p), they are computed through the CV of yield strength, limit strength and limit strain; (2) for the interface parameters (K_{TT} and c), they are computed through the CV of concrete [20] and headed stud material and geometry [19] parameters; and (3) for the pavement self-weight

(p_{pav}), a combination of the CV of the pavement thickness and of bituminous specific weight is considered.

The results obtained from the sensitivity analysis under service loads are shown in Fig. 7. The importance measures are normalized relative to the concrete tensile strength ($f_{t,c}$). For low intensity loadings, concrete is stressed in the elastic region and its elastic properties are critical. The influence of both reinforcing steel ($\sigma_{y,l}$, $\sigma_{u,l}$ and $\epsilon_{lim,l}$) and laminated steel profile ($\sigma_{y,p}$ and H_p) material properties is very low. In this situation, the critical parameters are: (1) concrete elasticity modulus (E_c); (2) concrete tensile strength ($f_{t,c}$); (3) reinforced concrete slab height (h_{slab}); (4) concrete density (γ_{conc}); and (5) pavement weight (p_{pav}). Accordingly, from 20 parameters, only 5 are considered to be critical.

Table 3
Parameter variation in sensitivity analysis [14,19,20,33].

Parameter	PDF	CV [%]	Parameter	PDF	CV [%]	Parameter	PDF	CV [%]	Parameter	PDF	CV [%]	Parameter	PDF	σ [mm]
Concrete elasticity modulus (E_c)	Normal	10.00	Reinforcing steel yield strength ($\sigma_{y,l}$)	Normal	5.00	Steel profile hardening modulus (H_p)	Normal	20.00	Laminated steel profile dimensions – bottom flanges area ($A_{fl,inf}$)	Normal	2.00	Reinforced concrete slab width (b_{slab})	Normal	5.00
Concrete tensile strength ($f_{t,c}$)	Normal	20.00	Reinforcing steel limit strength ($\sigma_{u,l}$)	Normal	5.00	Steel to concrete interface – shear stiffness (K_{T77})	Normal	10.00	Reinforcing steel area ($A_{s,l}$)	Normal	2.00	Reinforced concrete slab height (h_{slab})	Normal	10.00
Concrete compressive strength (f_c)	Normal	10.00	Reinforcing steel limit strain ($\epsilon_{lim,l}$)	Normal	15.00	Steel to concrete interface – cohesion (c)	Normal	12.50	Concrete specific weight (γ_{conc})	Normal	3.00	Laminated steel profile web thickness (b_{web})	Normal	1.00
Fracture energy (G_f)	Normal	10.00	Steel profile yield strength ($\sigma_{y,p}$)	Normal	5.00	Laminated steel profile dimensions – bottom flanges area ($A_{fl,sup}$)	Normal	2.00	Pavement weight (p_{pav})	Normal	10.00	Superior reinforcement concrete cover (c_{sup})	Normal	1.50

Obtained results, from sensitivity analysis under failure loads, are shown in Fig. 8a, except for the results for the steel profile yield strength ($\sigma_{y,p}$), which are given in Fig. 8b. The computed importance measures are normalized in relation to the steel profile yield strength of plate 2 ($\sigma_{y,p2}$). In this case, a large variability in importance measure values is obtained for the six assessed steel plates, being each yield strength importance measure considered independently.

According to Fig. 8b, the laminated steel profile yield strength ($\sigma_{y,p}$) presents a high importance on the structure behavior. Such influence is stronger in plate 1 ($\sigma_{y,p1}$) and plate 2 ($\sigma_{y,p2}$) located in the first and second span, for the considered LCs. Obtained results indicate as critical parameters: (1) concrete elasticity modulus (E_c); (2) concrete tensile strength ($f_{t,c}$); (3) concrete compressive strength (f_c); (4) reinforcing steel yield strength ($\sigma_{y,l}$); (5) yield strength for plate 1 ($\sigma_{y,p1}$) and for plate 2 ($\sigma_{y,p2}$). Therefore, from 20 evaluated parameters, 5 of them are considered as critical.

3.3. Model identification

In this stage, the most likely values for the parameters identified in the previous sections through a model identification process using vertical displacements under service loads. Two additional parameters for which there is limited information (horizontal spring stiffness at supports, k_1 and k_2) are also included.

An evolutionary strategies algorithm in its plus version is used to find the optimal parameter values [13]. A parent population, μ , and a parent for recombination, ρ , of 10 individuals, and an offspring population, λ , of 50 individuals were defined. The algorithm will run until the fitness function criteria is reached. The generation gap, n , used for the fitness function tolerance criterion was established as 2% of the maximum generation's number (1000). Therefore, the improvement on minimum fitness value is evaluated from a gap of 20 generations.

The fitness function relates numerical and experimental vertical displacements, at 17 m and 66 m of the bridge length, for the three LCs considered. In order to perform the model identification, it is necessary to determine the threshold value, ϵ , that defines the fitness function convergence criteria. Thus, it is first necessary to identify and quantify the different sources of error [12,23–25,34–36], see Table 4.

The fitness value criterion establishes that its improvement (Δf) should be less than or equal to a threshold value (ϵ), which can be understood as the model identification procedure precision [12,37]. By applying the law of propagation of uncertainty [9], a threshold value (ϵ) of 25.84% is obtained.

The model identification procedure is executed five times, considering different randomly generated starting points, as to limit the probability of underperforming results. Each analysis provides a final population of 10 models, resulting in a total of 50 models. Based on the principle that the most suitable model is that with smaller deviation from the initial mean values (see Table 5), unless some accidental situation is detected, the best model is that which presents the highest likelihood value [12,37]. Fig. 9 presents the obtained normalized values for the maximum likelihood for all the selected models. In this situation, model 20, from the second analysis, presents the highest value, being thus the selected model.

Table 5 indicates initial and identified values for the critical parameters considered in the model identification procedure, showing that the used concrete presents a higher quality than initially expected. With respect to horizontal spring stiffness results indicate that the identified k_1 and k_2 values are respectively lower and higher, respectively, than the initial prediction. The slab height (h_{slab}) is slightly higher, around 3%, than the design value. The concrete self-weight (γ_{conc}) is practically unchanged. However, the obtained pavement load (p_{pav}) is 15% higher than the design value. This might be due to the irregularity in bituminous thickness.

The comparison between the fitness function, considering initial and identified critical parameters value shows a reduction in error from

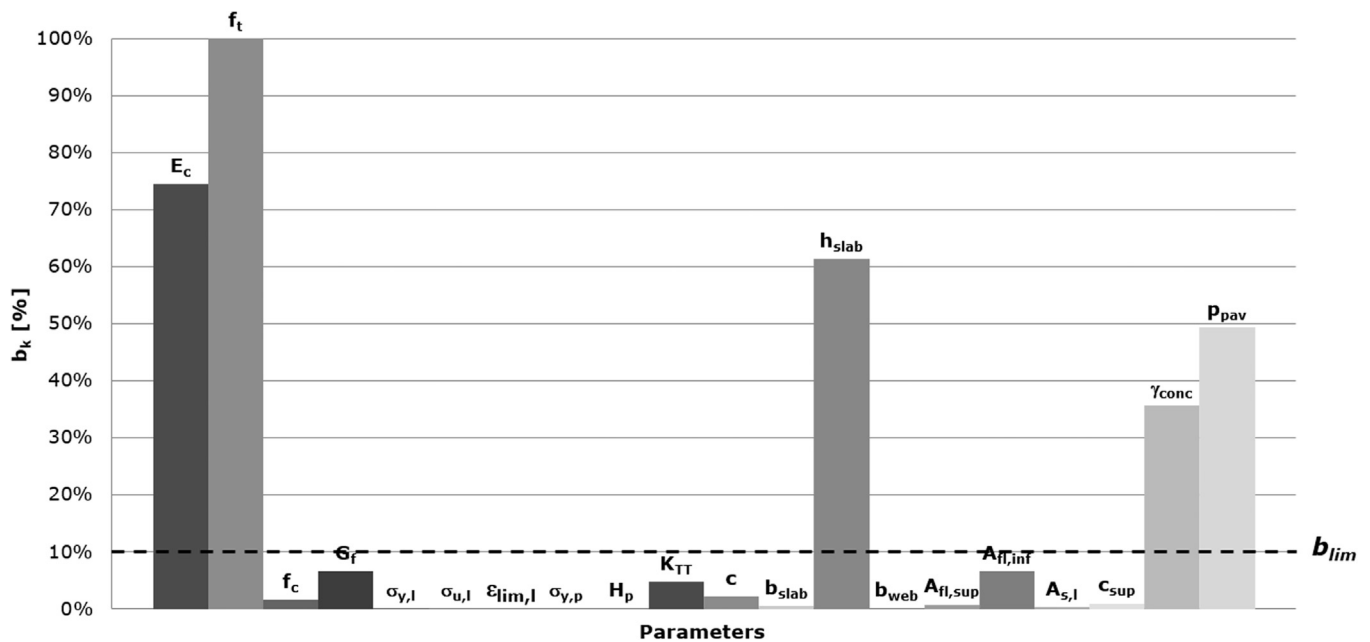


Fig. 7. Sensitivity analysis under service loads [12].

67.33% to 53.74%, being an improvement of more than 20%. Table 6 presents VD1* and VD2* displacement values before and after model identification for model 20. The results show that very small errors are obtained for all sensors and load, with the exception of VD1* under LC3.

3.4. Probabilistic analysis

The numerical model previously developed is now enhanced by defining the critical parameters as random variables. Non-critical parameters are considered to be deterministic. The assigned PDF and CV for each critical parameter are given in Table 3. After generating the random values for each critical parameter, a set of failure load factors is obtained for each LC. A curve fitting procedure is then developed in order to determine the most suitable PDF as described in Section 2.2. According to this process, the Normal distribution is considered to be that which better represents the obtained results.

3.4.1. Complementary tests

During construction, complementary tests were developed in order to control the quality of the concrete used in the precast slab and to classify the structural materials used (concrete, reinforcing steel and steel used in laminated steel profiles). In order to assess the concrete material quality, uniaxial compressive tests were performed in cubic specimens according to NP EN 13747 [38] for precast concrete slab, and according to NP 206-1 [39] for cast in-situ concrete. The reinforcing steel quality was controlled through uniaxial tensile tests, according to LNEC E 456 specification [40]. The steel profile quality was assessed through uniaxial tensile tests, according to EN 10002-1 [41].

The results obtained are shown in Table 7. Regarding concrete, obtained results indicate that the quality is slightly superior than the predicted, confirming the model identification results. With respect to reinforcing steel, results confirm the steel quality considered in the design phase. The steel profile material quality is slightly superior to that considered in design.

3.5. Bayesian inference

The results obtained from complementary tests are then used to update the critical parameters, through a Bayesian inference algorithm

[37,42,43]. The main objective of Bayesian inference algorithm is the consideration of new collected data into analysis procedure, in order to reduce the statistical uncertainty of each assessed parameter [12,37,42,44]. This is achieved by the Bayes theorem, which weights the prior information and new collected data (likelihood), obtaining a posterior distribution. The prior distributions, which are those that have as a mean value the initial parameter value or the ones obtained from model identification, may be updated. An important aspect of these techniques is the choice of the adopted prior distribution. A non-informative prior is useful when no prior information is available, being, however, necessary to verify if the computed posterior distribution is proper [42]. The Jeffrey's non-informative prior is a good choice for the non-informative prior distribution, once returns a proper posterior distribution. On the contrary, if some data is available, then the informative prior may be employed instead. In this situation, conjugate families are advantageous, from a mathematical standpoint, once the posterior distribution follows a known parametric form. A more detailed explanation is given at [12,37]. Accordingly, four different analyses are respectively developed: initial values (Analysis 1); model identification values (Analysis 2); initial values + Bayesian inference (Analysis 3); and model identification values + Bayesian inference (Analysis 4). The mean values (μ) from the initial model are those considered in the design phase, while the CVs are those presented in Table 3. The updated model is respectively based on the initial one, but considering the mean values (μ) obtained from model identification (Table 5). In this case, the CVs are obtained in a similar way by using the CVs from Table 3.

Bayesian inference procedure was developed by considering an informative and a non-informative (Jeffrey's) prior, being the adopted posterior PDF that with the lowest standard deviation [12,37]. Table 8 gives the probabilistic models for the critical parameters resulting from each of the analysis performed.

The analysis of these results confirms the complementary tests, once the obtained mean is higher than the initial prediction. The uncertainty is lower than the initial one, once the CV has been reduced.

3.6. Loading curve

In order to assess the bridge safety, the resistance and loading PDF must be compared. In this analysis, the loading PDF is defined based on

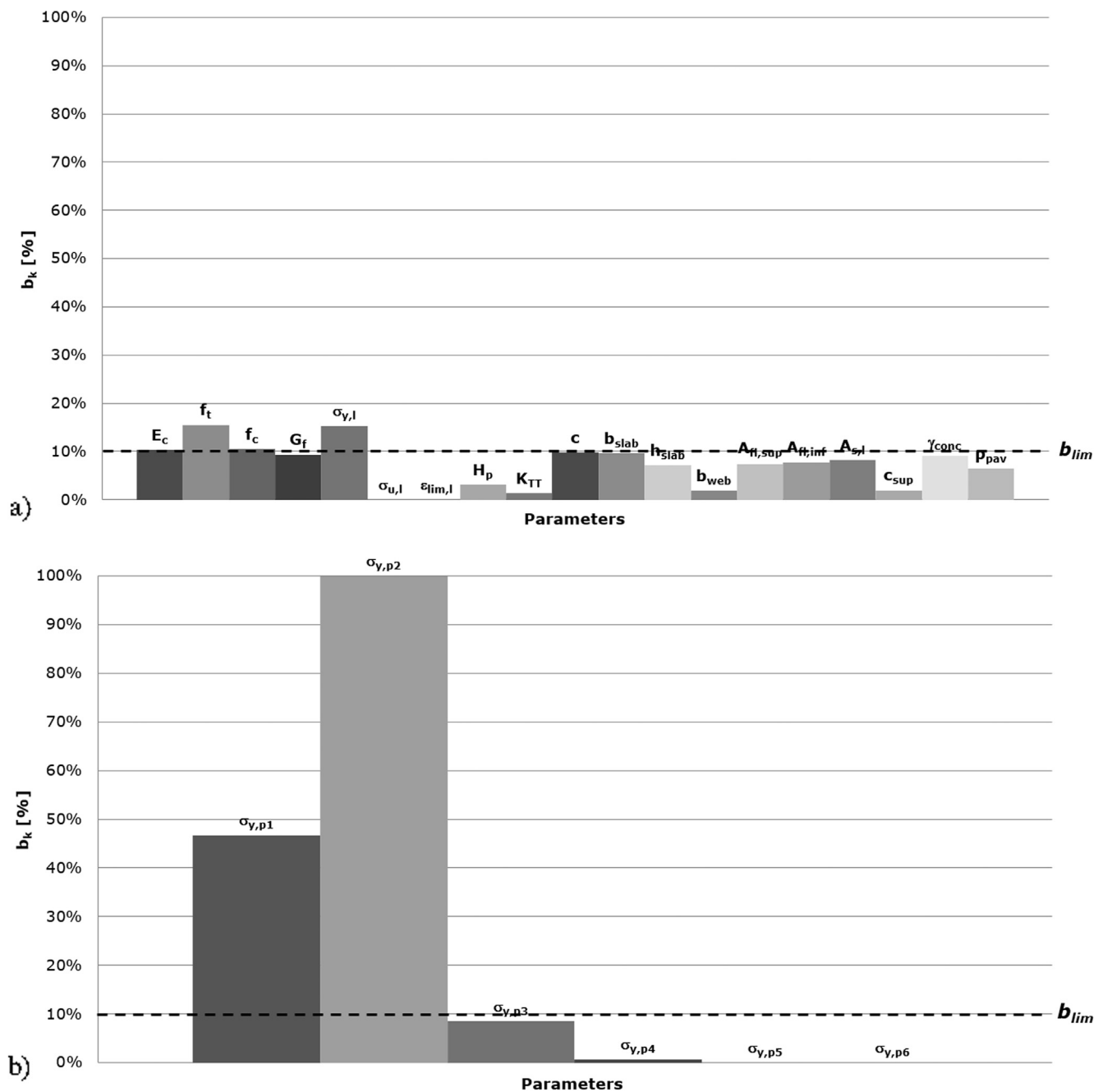


Fig. 8. Sensitivity analysis under failure loads: (a) General parameters; (b) Steel profile yield strength [12].

load model LM71, which is the standard load model for normal roadway traffic presented by the European code [45]. The LM71 is a road bridge static vertical load model intended for the determination of road traffic effects, being composed by double-axle concentrated loads and uniformly distributed loads. This model can be used on both local and global verification of bridge elements.

The considered LCs will correspond to those established at the load tests [22]. The load model LM71 is modelled as a Gumbel distribution, considering a 95th percentile and a return period of 50 years [33]. Additionally, a CV of 15% is adopted [33], corresponding to a mean value of the total applied load 4939.40 kN and a standard deviation of 740.91 kN. The loading values are then randomly generated through a LHS algorithm.

3.7. Safety assessment

The safety assessment consists of comparing resistance (R) and loading (S) PDF for the bridge in analysis, according to the limit state function ($Z = R - S$). The load model is introduced in the previous developed numerical models [27] and then, the bridge is loaded up to failure. This analysis is developed for each LC and for several randomly generated models. Then, a curve fitting procedure is developed to compute the resistance PDF parameters. Obtained mean (μ) and standard deviation (σ) values are given in Table 9, being then computed the failure probability, p_f , and the corresponding reliability index, β , as a comparison between the resistance and the effect of loads curves.

An overall analysis of those results allows to conclude that, for the considered LCs, and for the developed numerical model, the overall bridge resistance is substantially higher than the applied load model, by comparing the resistance PDF mean of each analysis, from Table 9, with

Table 4
Errors: sources and quantification.

Error sources	Quantification method		Error [%]
Experimental uncertainties	Sensor accuracy	Manufacturer (includes cable and acquisition equipment losses)	$1.71 * 10^{-1}$ (VD1 and VD2); $2.98 * 10^{-1}$ (VD3 and VD4)
	Stability	Static load test (null fatigue problems)	→0.00
	Robustness	Short term test (null environmental effects)	→0.00
	Load positioning	Test assembly perfectly controlled	→0.00
	Load intensity	Precisely measured	→0.00
Numerical uncertainties	Finite element method	Based on preliminary study (by comparing to a refined mesh model)	1.80% (VD1 [†]); 9.77% (VD2 [†]) [*]
	Inaccurate assumptions	Based on preliminary study (by comparing to a short load step model)	$3.53 * 10^{-1}\%$ (VD1 [†]); 2.81% (VD2 [†]) [*]
	Model exactitude	Model “as built”	→0.00
	Considered hypothesis	Introduction of five reinforced concrete slab layers	3.64% (VD1 [†] and VD2 [†])
		Introduction of a medium density region at interface	5.75% (VD1 [†] and VD2 [†])
		Introduction of a pavement macro element	1.82% (VD1 [†] and VD2 [†])
		Removing the web reinforcements	1.07% (VD1 [†] and VD2 [†])

* Values calculated for service phase [12].

Table 5
Obtained initial and model identification parameter values for service region [12].

Numerical model			Initial value	Model identification
Parameter	Concrete elasticity modulus (E_c)	[GPa]	35.00	35.98
	Concrete tensile strength ($f_{t,c}$)	[MPa]	3.50	4.03
	Horizontal spring stiffness at support (k_1 – C1 axis)	[kN/m]	56.69	36.98
	Horizontal spring stiffness at support (k_2 – C2 axis)	[kN/m]	9.93	12.90
	Reinforced concrete slab height (h_{slab})	[m]	0.15	0.16
			0.25	0.25
	Concrete specific weight (γ_{conc})	[kN/m ³]	24.00	24.34
	Pavement weight (p_{pav})	[kN/m]	6.50	7.38
			6.81	7.73

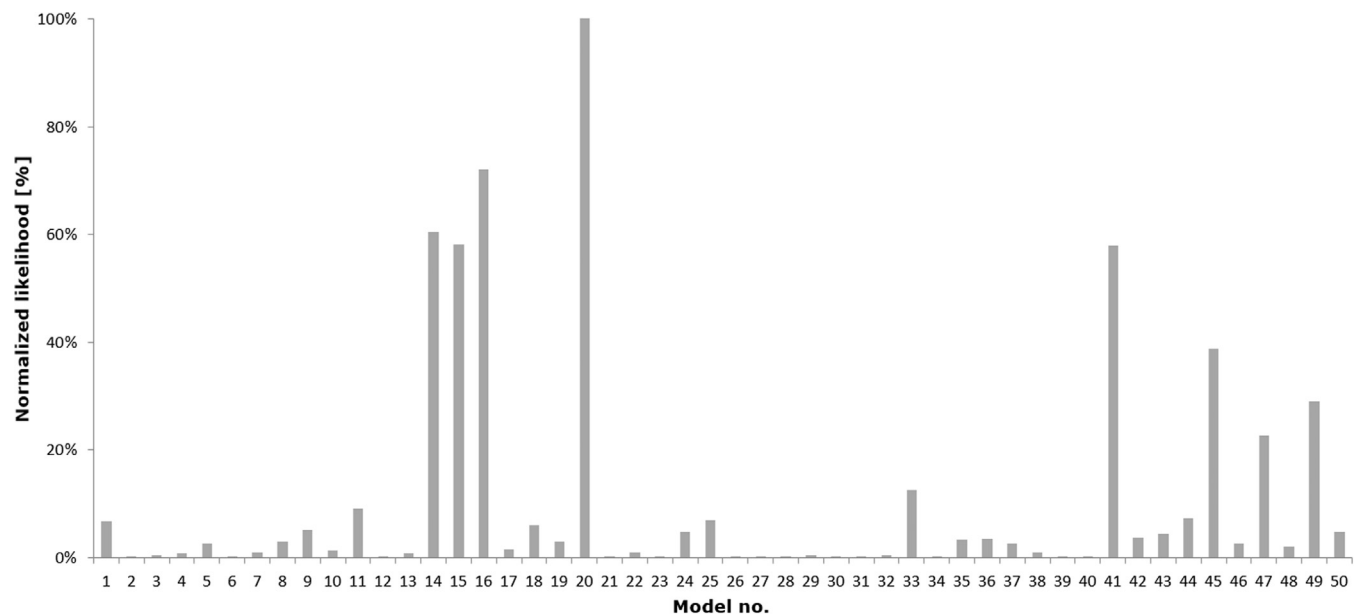


Fig. 9. Model identification [12]: engineering judgment evaluation.

Table 6
Obtained displacement values for calibrated model considering model identification[†] [12].

LC	VD1 [†] [mm]		Error [%]	VD2 [†] [mm]		Error [%]
	Before model identification	After model identification		Before model identification	After model identification	
LC1	17.77	15.43	5.02	−5.09	−3.57	7.87
LC2	−4.90	−3.64	8.31	14.32	12.06	11.97
LC3	1.40	1.04	43.78	−4.82	−3.48	8.92

[†] Negative value corresponds to a displacement in upward direction.

Table 7
Obtained material properties from complementary tests [12].

Parameter		Initial value	Mean value (μ)	Standard deviation (σ)
<i>Concrete (no. samples = 10)</i>				
Elasticity modulus (E_c) [*]	[GPa]	35.00	37.04	0.63
Tensile strength ($f_{t,c}$) [*]	[MPa]	3.50	3.98	0.14
Compressive strength (f_c) [*]	[MPa]	48.00	56.86	3.21
<i>Reinforcing steel material (no. samples = 10)</i>				
Yield strength ($\sigma_{y,l}$) [*]	[MPa]	560.00	562.94	21.42
Limit strength ($\sigma_{u,l}$)	[MPa]	644.00	645.49	20.36
Limit strain ($\epsilon_{lim,l}$)	[%]	80.00	96.39	35.78

No. of steel plate	Thickness [mm]	Yield strength ($\sigma_{y,p}$) [MPa]			Tensile strength ($\sigma_{u,p}$) [MPa]			Tensile strain ($\epsilon_{lim,p}$) [%]		
		Initial Value	Mean value (μ)	Standard deviation (σ)	Initial Value	Mean value (μ)	Standard deviation (σ)	Initial Value	Mean value (μ)	Standard deviation (σ)
<i>Steel profile material (no. samples = 10)</i>										
1 [*]	≤ 16	355	388.32	17.52	470–530	540.39	18.18	20–22	28.71	2.33
2 [*]	≤ 40	345	377.38	17.02	470–530	540.39	18.18	20–22	28.71	2.33
3	≤ 60	335	366.44	16.53	470–530	540.39	18.18	19–21	27.35	2.22
4	≤ 80	325	355.51	16.04	470–530	540.39	18.18	18–20	25.98	2.11
5	≤ 100	315	344.57	15.54	470–530	540.39	18.18	18–20	25.98	2.11
6	≤ 110	295	322.69	14.56	450–600	567.41	19.09	18–18	24.61	2.00

* Data considered as likelihood in Bayesian inference.

Table 8
Input parameter values for reliability analysis [12].

Parameters	PDF		Analysis 1		Analysis 2		Analysis 3 [*]		Analysis 4 [*]	
			μ	σ	μ	σ	μ	σ	μ	σ
Concrete elasticity modulus (E_c)	[GPa]	Normal	35.00	3.50	35.98	3.60	37.04	0.63	36.51	0.52
Concrete tensile strength ($f_{t,c}$)	[MPa]	Normal	3.50	0.70	4.03	0.81	3.99	0.15	3.99	0.15
Concrete compressive strength (f_c)	[MPa]	Normal	48.00	4.80	48.00	4.80	56.86	3.24	56.86	3.24
Reinforcing steel yield strength ($\sigma_{y,l}$)	[MPa]	Normal	560.00	28.00	560.00	28.00	562.92	21.61	562.92	21.61
Laminated steel profile yield strength ($\sigma_{y,p}$)	[MPa]	Normal	355.00	17.75	355.00	17.75	387.93	18.35	387.93	18.35
Steel plate 1 yield strength ($\sigma_{y,p1}$)	[MPa]	Normal	355.00	17.75	355.00	17.75	387.93	18.35	387.93	18.35
Steel plate 2 yield strength ($\sigma_{y,p2}$)	[MPa]	Normal	345.00	17.25	345.00	17.25	387.93	18.35	387.93	18.35

* Posterior data, obtained from Bayesian inference.

Table 9
Resistance PDF (R) [12].

Numerical model	PDF	LC1		LC2		LC3		p_f [*]	β [*]
		μ [kN]	σ [kN]	μ [kN]	σ [kN]	μ [kN]	σ [kN]		
Analysis 1	Normal	24796.00	902.40	39294.00	700.82	35991.00	659.80	3.59×10^{-16}	8.32
Analysis 2	Normal	24749.00	936.94	39550.00	780.70	35990.00	665.32	4.26×10^{-16}	8.30
Analysis 3	Normal	26770.00	904.49	41210.00	751.58	37148.00	648.64	1.17×10^{-17}	8.73
Analysis 4	Normal	26769.00	911.05	41188.00	742.84	37270.00	649.74	1.19×10^{-17}	8.72

* Considered the most critical value from all LCs.

the loading PDF mean (4939.40 kN). By comparing the obtained resistance PDF for the four probabilistic models, it is possible to conclude that model identification practically did not change the obtained results. This is due to the fact that the majority of assessed parameters in model identification, in service phase, do not influence the bridge behavior up to failure. The application of a Bayesian inference procedure leads to an increase in the failure load, confirming an additional structural resistance capacity which was not initially identified. When evaluating the CV, it is possible to conclude that both initial and model identification models provide similar results. A slight decrease on this value is verified with the Bayesian inference procedure. This is due to a decrease on the standard deviation value of some of the updated parameters (Table 8).

The values obtained with this safety assessment procedure, respectively, the probability of failure, p_f , and the reliability index, β , are indicated at Table 9. By analyzing these values, it is confirmed what

was previously specified, namely: (1) obtained reliability index (β) values are high according to fib target reliability values [46]; (2) obtained results from the probabilistic numerical model, considering the initial and the identified parameter values, are close; and (3) the application of a Bayesian inference procedure increases the reliability index (β).

According to fib Task Group 5.1 [46], and considering that an overall analysis of the structure is developed, it is possible to conclude that the assessed bridge is in very good situation ($8 < \beta \leq 9$). This is in agreement with Tabsh and Nowak [47] guidelines, which indicate that a β -value higher than 5–6 corresponds to a structure with a very good performance.

4. Conclusions

This paper presents a framework for the probabilistic-based

assessment of existing structures. This framework accurately evaluates the structural safety and condition, contemplating all sources of uncertainty. It is composed of two main steps. In the first step the numerical model is updated through a model identification procedure. In the second step, the updated deterministic model is converted into a probabilistic model and a probabilistic analysis is developed. Finally, each parameter distribution may be updated, as complementary data is obtained through a Bayesian inference algorithm. The developed algorithm presents a high computational cost. In order to minimize it, a sensitivity analysis, in which the most important parameters are selected, should be previously applied.

The developed probabilistic assessment framework is applied to a composite steel-concrete bridge (Sousa River Bridge). The developed numerical model and a sensitivity analysis, executed both under service and ultimate loading conditions, are also presented. Then, the model identification algorithm is applied with the results obtained during the load test in the service phase. A probabilistic analysis is further developed by introducing randomness in each critical parameter. A Bayesian inference procedure is also applied to update some parameters distributions with results from complementary tests. The obtained results are used to evaluate the reliability of the bridge.

The main conclusions taken from developed framework and its application are: (1) model identification in service phase improves the numerical model results, by predicting more accurately the load-deflection behavior in around 20%. In fact, as the load test aims at not damaging the structure, information gathered can only inform on parameters relevant to in-service condition rather than ultimate states; (2) the model identification influence is small when comparing all probabilistic models, due to the fact that the majority of the assessed parameters in service phase do not influence the bridge behavior in failure phase. In this sense, an additional model identification process could be used, but one that considers complementary tests results for critical parameters describing failure region; (3) complementary tests, as non-destructive or material characterization tests, are recommended when model identification is only performed in service phase; (4) obtained values from model identification confirmed that used materials quality is close, or slightly higher, than the initial estimates; (5) the Bayesian inference increases the accuracy of probabilistic models by reducing the statistical uncertainty, once all posterior computed CVs are lower than the initial ones.; and (6) the bridge failure load was higher than the expected, considering the mean and the nominal values from design. In line with these conclusions, the present work allowed the prediction of the structural behaviour of Sousa River bridge with higher accuracy, based on collected data from field tests and by applying the developed framework. Furthermore, the fitness function allows to contemplate various measurement sources at the same time, making the model identification more robust and precise, particularly when studying the interface, for which large uncertainty exists. Additionally, Bayesian Inference allows the continuous updating of the reliability index, based on new information from monitoring devices. Accordingly, with this framework it will be possible to assess the structural behaviour through a more robust, accurate and continuous process. Therefore, the obtained results pointed out a relevant improvement in reliability assessment, allowing a more fundamental decision regarding the repair and strengthening of existing structures.

Although the presented framework was applied to a composite steel-concrete bridge, it is possible to employ it to any type of structures, such as reinforced concrete [37] or masonry bridges, providing basis for more robust and accurate decision-making analysis. Also, the application of the presented probabilistic-based framework to such a massive structure allows the identification and consideration of additional uncertainties and errors, which cannot be considered in controlled environments (e.g. laboratory tests), enhancing the advantages of the developed framework.

Additionally, to this work, it is pointed out the connection between service and failure regions as a topic of future developments, since most

of the parameters obtained in service cannot be used for failure. Thus some dynamic tests or non-destructive tests would be useful to characterize some structural parameters in service region, which can be correlated to others on failure regions. Another relevant drawback is the computational cost, especially when applied to more complex structures, such as the Sousa River bridge. Regarding the field tests, this analysis was performed for a particular load configuration, i.e., with a well-known and particular load magnitude and position. For the operation stage, the load model will also change, and real time vehicle measurement (counting and weighting) would be relevant for performing the structural assessment on operation stage.

References

- [1] Enevoldsen I. Experience with probabilistic-based assessment of bridges. *Struct Eng Int* 2001;11:251–60. <https://doi.org/10.2749/101686601780346814>.
- [2] Wisniewski D, Casas JR, Ghosn M. Simplified probabilistic non-linear assessment of existing railway bridges. *Struct Infrastruct Eng* 2009;5:439–53. <https://doi.org/10.1080/15732470701639906>.
- [3] Enright MP, Frangopol DM. Reliability-based condition assessment of deteriorating concrete bridges considering load redistribution. *Struct Saf* 1999;21:159–95. [https://doi.org/10.1016/S0167-4730\(99\)00015-6](https://doi.org/10.1016/S0167-4730(99)00015-6).
- [4] Faber MH, Val DV, Stewart MG. Proof load testing for bridge assessment and upgrading. *Eng Struct* 2000;22:1677–89. [https://doi.org/10.1016/S0141-0296\(99\)00111-X](https://doi.org/10.1016/S0141-0296(99)00111-X).
- [5] Casas JR, Wisniewski D. Safety requirements and probabilistic models of resistance in the assessment of existing railway bridges. *Struct Infrastruct Eng* 2011;9:529–45. <https://doi.org/10.1080/15732479.2011.581673>.
- [6] Caspeele R, Taerwe L. Influence of concrete strength estimation on the structural safety assessment of existing structures. *Constr Build Mater* 2014;62:77–84. <https://doi.org/10.1016/j.conbuildmat.2014.03.033>.
- [7] Bergmeister K, Novák D, Pukl R, Cervenka V. Structural assessment and reliability analysis for existing engineering structures, theoretical background. *Struct Infrastruct Eng* 2009;5:267–75. <https://doi.org/10.1080/15732470601185612>.
- [8] Jacinto L, Neves LC, Santos LO. Bayesian assessment of an existing bridge: a case study. *Struct Infrastruct Eng* 2016;12:61–77. <https://doi.org/10.1080/15732479.2014.995105>.
- [9] JCGM. Evaluation of measurement data – guide to the expression of uncertainty in measurement. JCGM 2008;100:2008.
- [10] Henriques AAR. Application of new safety concepts in the design of structural concrete (Aplicação de novos conceitos de segurança no dimensionamento do betão estrutural) [Ph.D Dissertation]. Porto, Portugal: Universidade do Porto; 1998. [in Portuguese].
- [11] Moreira VN, Fernandes J, Matos JC, Oliveira DV. Reliability-based assessment of existing masonry arch railway bridges. *Constr Build Mater* 2016;115:544–54. <https://doi.org/10.1016/j.conbuildmat.2016.04.030>.
- [12] Matos JC. Uncertainty evaluation of reinforced concrete and composite structures behavior [Ph.D. Dissertation]. Guimarães, Portugal: University of Minho; 2013.
- [13] Beyer H-G, Schwefel H-P. Evolution strategies – a comprehensive introduction. *Nat Comput* 2002;1:3–52. <https://doi.org/10.1023/A:1015059928466>.
- [14] Joint Committee on Structural Safety (JCSS). Probabilistic Model Code, 12th Draft. JCSS – Joint Committee on Structural Safety; 2001.
- [15] Olsson A, Sandberg G, Dahlblom O. On Latin hypercube sampling for structural reliability analysis. *Struct Saf* 2003;25:47–68. [https://doi.org/10.1016/S0167-4730\(02\)00039-5](https://doi.org/10.1016/S0167-4730(02)00039-5).
- [16] Iman RL, Conover WJ. A distribution-free approach to inducing rank correlation among input variables. *Commun Stat – Simul Comput* 1982;11:311–34. <https://doi.org/10.1080/03610918208812265>.
- [17] Nowak AS, Collins KR. Reliability of structures. Thomas Casson: McGraw-Hill; 2000.
- [18] Melchers RE. Structural reliability analysis and prediction. John Wiley & Sons; 1999.
- [19] Nelson Bolzenschweiß-Technik. European Technical Approval for NELSON-headed studs. ETA 03/0041 and ETA 03/0042 13. Deutsches Institut für Bautechnik; 2003.
- [20] CEN. EN 1992-1-1, Eurocode 2: design of concrete structures – Part 1-1: general rules and rules for buildings. Brussels, Belgium: European Committee for Standardization; 2004.
- [21] CEN. EN 1993-1-1, Eurocode 3: design of steel structures – Part 1-1: general rules and rules for buildings. Brussels, Belgium: European Committee for Standardization; 2010.
- [22] NewMensur LF-. Instrumentação e Observação do Comportamento da Ponte sobre Rio Sousa II durante o Ensaio Carga; 2011.
- [23] Sousa H, Bento J, Figueiras J. Assessment and management of concrete bridges supported by monitoring data-based finite-element modeling. *J Bridge Eng* 2014;19. [https://doi.org/10.1061/\(ASCE\)BE.1943-5592.0000604](https://doi.org/10.1061/(ASCE)BE.1943-5592.0000604).
- [24] Sousa H, Bento J, Figueiras J. Construction assessment and long-term prediction of prestressed concrete bridges based on monitoring data. *Eng Struct* 2013;52:26–37. <https://doi.org/10.1016/j.engstruct.2013.02.003>.
- [25] Sousa H, Cavadas F, Abel Henriques A, Bento J, Figueiras J. Bridge deflection evaluation using strain and rotation measurements. *Smart Struct Syst* 2013;11:365–86. <https://doi.org/10.12989/ss.2013.11.4.365>.

- [26] Fonseca AAD, Bastos R, Mato FM, Matute L, Infante D. Henrique Bridge: construction and monitoring (Ponte Infante D. Henrique: construção e monitorização). Porto, Portugal: AFAssociados – Projectos de Engenharia, SA; 2002. p. 10.
- [27] Cervenka V, Jendele L, Cervenka J. ATENA* Program documentation, Part 1: theory. Prague, Czech Republic; 2009.
- [28] LisConcebe. A43 – Gondomar/Aguiar de Sousa (IC24), Projeto de Execução, Obras de Arte Especiais, Ponte sobre Rio Sousa II (Alteração da Metodologia Construtiva); 2009.
- [29] CEN. EN 1994-1-1, Eurocode 4: design of composite steel and concrete structures – Part 1-1: general rules and rules for buildings. Brussels, Belgium: European Committee for Standardization; 2004.
- [30] Valente IB. Experimental studies on shear connection systems in steel and light-weight concrete composite bridges [PhD. Dissertation]. Guimarães, Portugal: University of Minho; 2007.
- [31] Zum P. Zusammenwirken hochfester Baustoffe in Verbundkonstruktionen [PhD. Dissertation]. Aachen, Germany: RWTH AACHEN University; 2001.
- [32] Hegger J, Sedlacek G, Döinghaus P, Trumpf H. Studies on the ductility of shear connectors when using high-strength concrete. International symposium on connections between steel and concrete. Stuttgart, Germany. 2001. p. 1025–45.
- [33] Safety Wisniewski D. Formats for the Assessment of Concrete Bridges with special focus on precast concrete [PhD. Dissertation]. Guimarães, Portugal: University of Minho; 2007.
- [34] Goulet J-A, Kripakaran P, Smith IFC. Langesand bridge in Lucerne, results from phase-I static-load tests. Lausanne, Switzerland: EPFL – École Polytechnique et Fédérale de Lausanne; 2009.
- [35] Goulet J-A, Kripakaran P, Smith IFC. Structural identification to improve bridge management. 33rd IABSE Symposium. Bangkok, Thailand. 2009.
- [36] Goulet J-A, Smith IFC. CMS4SI structural identification approach for interpreting measurements. IABSE Symposium Report, vol. 97. 2010. p. 55–62. <https://doi.org/10.2749/222137810796024330>.
- [37] Matos JC, Cruz PJS, Valente IB, Neves LC, Moreira VN. An innovative framework for probabilistic-based structural assessment with an application to existing reinforced concrete structures. Eng Struct 2016;111:552–64. <https://doi.org/10.1016/j.engstruct.2015.12.040>.
- [38] CEN. EN 13747: Precast concrete products — floor plates for floor systems. Brussels, Belgium: European Committee for Standardization; 2005. p. 90.
- [39] CEN. EN 206: concrete – specification, performance, production and conformity. Brussels, Belgium: European Committee for Standardization; 2007. p. 98.
- [40] LNEC. LNEC E 456: Varões de aço A500 ER para armaduras de betão armado. Características, ensaios e marcação. Lisbon, Portugal: Laboratório Nacional de Engenharia Civil; 2007.
- [41] CEN. EN 10002-1, Metallic materials – tensile testing, Part 1: method of test at ambient temperature. Brussels, Belgium: European Committee for Standardization; 2001.
- [42] Bernardo JM, Smith AFM. Bayesian theory. Chichester, England: John Wiley & Sons, Ltd; 2004.
- [43] Moreira VN, Matos JC, Oliveira DV. Probabilistic-based assessment of a masonry arch bridge considering inferential procedures. Eng Struct 2017;134:61–73. <https://doi.org/10.1016/j.engstruct.2016.11.067>.
- [44] Safety Jacinto LA. Assessment of existing bridges – bayesian probabilistic approach (Avaliação da Segurança de Pontes Existentes – Abordagem Probabilística Bayesiana) [Ph.D. Dissertation]. Lisboa, Portugal: Universidade Nova de Lisboa; 2011. [in Portuguese].
- [45] CEN. EN 1991-2, Eurocode 1: actions on structures – Part 2: traffic loads on bridges. Brussels, Belgium: European Committee for Standardization; 2003.
- [46] fib Task Group 5.1. Bulletin No. 22: Monitoring and Safety Evaluation of Existing Concrete Structures: State-of-art Report. 2883940622, 9782883940628. Lausanne, Switzerland: International Federation for Structural Concrete (fib); 2003.
- [47] Tabsh SW, Nowak AS. Reliability of highway girder bridges. J Struct Eng 1991;117:2372–88. [https://doi.org/10.1061/\(asce\)0733-9445\(1991\)117:8\(2372\)](https://doi.org/10.1061/(asce)0733-9445(1991)117:8(2372)).

Round-Robin Modelling of the Load-bearing Capacity of Slender Columns by Using Classical and Advanced Non-linear Numerical and Analytical Prediction Tools

Alfred Strauss , Prof., Senior Scientist, Department of Civil Engineering and Natural Hazards, University of Natural Resources and Life Sciences, Vienna, Austria; **Ana Mandić Ivanković**, Prof., Senior Scientist, Department for Structural Engineering, University of Zagreb Faculty of Civil Engineering, Zagreb, Croatia; **Vladimir Benko**, Prof., Senior Scientist, Department of Concrete Structures and Bridges, Slovak University of Technology in Bratislava, Bratislava, Slovakia; **José Matos** , Prof., Senior Scientist, Institute for Sustainability and Innovation in Structural Engineering (ISISE), University of Minho, Braga, Portugal; **Pierre Marchand**, Dr, Scientist, MAST-EMGCU, Univ Gustave Eiffel, IFSTTAR, Marne-la-Vallée, France; **Roman Wan-Wendner** , Prof., Senior Scientist, University of Natural Resources and Life Sciences, Vienna, Austria; Ghent University, Ghent, Belgium; **Neryvaldo Galvão**, PhD, Institute for Sustainability and Innovation in Structural Engineering (ISISE), University of Minho, Braga, Portugal; **André Orcesi**, Dr, Senior Scientist, MAST-EMGCU, Univ Gustave Eiffel, IFSTTAR, Marne-la-Vallée, France; **Jakub Dobrý**, PhD, Department of Concrete Structures and Bridges, Slovak University of Technology in Bratislava, Bratislava, Slovakia; **Mohammad El Hajj Diab**, Dr, Scientist, MAST-EMGCU, Univ Gustave Eiffel, IFSTTAR, Marne-la-Vallée, France; **Krešimir Ninčević**, PhD; **Michael Hauser**, PhD, Department of Civil Engineering and Natural Hazards, University of Natural Resources and Life Sciences, Vienna, Austria; **Mladen Srbić**, PhD; **Dominik Skokandić**, Dr, Scientist, Department for Structural Engineering, University of Zagreb Faculty of Civil Engineering, Zagreb, Croatia. Contact: alfred.strauss@boku.ac.at
DOI: 10.1080/10168664.2020.1740069

Abstract

Non-linear finite element analyses have intrinsic model and user factors that influence the results of the analyses. However, non-linear finite element analysis can provide a tool to assess safety using realistic descriptions of material behaviour with actual material properties. A realistic estimation of the existing safety and capacity of slender column elements can be achieved by means of “true” material properties. Nevertheless, it seems that for some structural components, such as slender columns, non-linear finite element analyses can, due to its complexity and its various setting parameters, cause the risk of overestimating the real performance of analysed components or systems. Hence, an invited expert group has carried out an investigation into the experimental testing and the prediction of the bearing capacity of slender columns by performing independent non-linear finite element analyses in order to determine the practical applicability, and its inconsistencies, with respect to the stability failure of slender columns. This work aims the characterization of modelling uncertainties, concerning the prediction of slender columns stability when forecasted by non-linear finite element analysis.

Keywords: non-linear finite element analyses; slender column elements; model and modelling uncertain tests; round-robin modelling tests

Introduction

Non-linear calculation methods allow realistic prediction of the load-deformation curve of a reinforced concrete structure given the non-linear stress-strain relationship of the concrete and steel reinforcement¹⁻³ and enable an accurate design in the ultimate and serviceability limit states when compared to other proven approximations methods such as the moment magnification procedure according to ACI 318-14. However, geometrical and mathematical non-linear design of slender members, such as columns in the ultimate limit

state, is still a matter of controversy because of the known inconsistencies in the design concept. Therefore, despite the explicit possibilities in EN 1992-1-1 of using non-linear methods, there is still a need for research. This investigation focuses on an a priori collaborative round-robin test of numerical simulations to predict the load capacity of slender single columns with respect to a posteriori experimental series.⁴ The results show, on the one hand, that the non-linear numerical calculations clearly overestimate the load-bearing capacity of the slender columns in some cases, and on the other hand,

that the current design code proposed approximation methods, e.g. the nominal curvature-based method, provide results which are too conservative. In the future, the development of generally applicable and consistent proof formats for non-linear calculations⁵ will be necessary, along with providing the users of the available software packages with “best practice” guidelines for safe use. Nonlinear calculations were compared with a series of experimentally verified slender columns.^{4,6-9}

State of the Art “Design of Slender Columns”

EN 1992-1-1¹⁰ includes the general method (§5.8.6), the procedure with nominal stiffness (§5.8.7) and the method with nominal curvatures (§5.8.8) hence basically providing three verification methods for the design of slender compressive elements. We believe the results with these three methods should be compared with those proposed in this paper. The general procedure is based on a non-linear system theory. The simplified nominal curvature method and the simplified nominal stiffness method account for the theory and for the non-linear effects, either by a computational reduction in system bending-stiffness rating or by a computational increase of the moment based on an estimated bending maximum-

curvature in the relevant cross-section. These proximity techniques are well accepted, allow safe use, and provide satisfying results within the intended range of applications. However, with very slender columns, the nominal curvature method sometimes results in a very conservative design due to the simplicity of the application, in particular for large eccentricity.¹¹ Generally, scientists resort to the so-called general procedure for slender aesthetic structural pillars and bridge piers, despite the widespread availability of powerful calculation programmes. For a description of the realistic relationship between compressive stress and strain of the concrete, a rational function calibrated on pressure tests and based on mean values is given in EN 1992-1-1, point 3.1.5, which is applicable to non-linear methods both for ultimate and serviceability limit states. In particular, the mean value of the concrete compressive strength is reduced to the design value and the mean value of the modulus of elasticity, defined as a secant modulus, is reduced by the factor $\gamma_{cE} = 1.2$. It should take into account the direct determination of additional moments from second-order theory and the beneficial effects of concrete tension stiffening or the appropriate procedures for the adverse effects of creep under long-term loading. The determination of the ultimate limit state and practically applicable methods for the consideration of the tensile stiffening in EN 1992-1-1 will not be discussed in detail here, more insight can be found in the relevant literature.^{12,13} In this context, it should be noted that DIN EN 1992-1-1¹⁰ is based on so-called calculation values of the material properties which should provide more consistent results in non-linear system calculations as well as with regard to the probabilistic calculations. It is more consistent and respects the terms of the Eurocode underlying safety concept.^{4,14} The aforementioned modifications of the modulus of elasticity in case of very slender columns leads to large additional moments due to second-order effects and to a significant reduction in the bearing capacity. The method proposed by Quast,¹³ and reintroduced in DIN EN 1992-1-1,¹⁰ for the determination of internal forces by means of reduced mean values is recommended as an alternative with respect to the general procedure. However, the actual design takes place in a second step at the

cross-sectional level. This method gives good results, but only partially pursues the principles of the generally valid semi-probabilistic safety concept. Principles and different approaches in non-linear calculations found in Austrian annex, German code and Eurocode were analysed and can be found in Ref. [15].

Modelling and Test Series of Columns

Objectives

Non-linear finite element analyses are becoming increasingly interesting for the structural assessment and life cycle assessment of existing reinforced concrete structures.^{16,17} This fact has recently been discussed in relevant technical committees and experts have developed application rules and recommendations for non-linear analyses as well as for the related safety formats.^{18,19} Many of the non-linear FEM software products are based on sophisticated models of fracture mechanics, such as combined fracture plasticity models, orthotropic smeared crack formulations, rip band models, hardening / -softening plasticity models, and complex solution algorithms, such as the integration of complex constitutive equations. A meaningful non-linear FEM analysis, therefore, requires the user to have a basic knowledge of material models, solution algorithms, choosing the appropriate boundary conditions (bearing and supporting conditions, idealization of load cases - its properties and its combination, incremental loading procedure) and selecting the appropriate finite element type and meshing associated with the considered structural system or detail.⁶ For realistic modelling and proper fulfillment of the above requirements, it is common practice that calibrations of the non-linear finite element models are performed on already tested systems before they are applied to real structures in an adapted manner.

The IABSE Task group 1.4 under auspices of the IABSE Commission 1 (Performance and Requirements) carried out a study to predict the safety level and the capacity of slender compressive elements in relation to the non-linear FEM analyses. In particular, the questions addressed were to what extent the non-linear FEM analyses allow (a) a

reliable prediction of the N - M interaction pathways, (b) an assessment of the actual safety level and (c) the assessment of the modelling uncertainties. In the run-up to a test campaign of slender columns in the laboratories of the University of Bratislava, ten institutions from the University and industrial sectors with experience in non-linear finite element modelling were invited to predict the performance of the columns by using non-linear modelling techniques. In the first phase, the experts were informed about the classical reinforcement plans and formwork plans as well as the standard material specifications of the concrete and reinforcing steel. For modelling, the initial eccentricity e_1 , which was predefined for the experimental setup, as well as the storage conditions of the columns, were announced. The load-deformation curves and N - M paths obtained from the modelling were collected and evaluated in a common diagram. In the second phase, the experts were provided with more detailed information on the material properties of the materials obtained during the test procedure and information on the test setup. In the third phase, the records of the monitoring systems were made available during the test procedure. This step-by-step provision of information is instrumental in model uncertainty and subsequent results, and shows some correlation to the information available in practice during design, execution- and monitoring.

Initial Design

The first task in planning the test campaign was to properly design the cross-sectional geometry and the reinforcement layout of the columns, and to determine the initial eccentricity of the axial force to achieve the desired column system stability failure. The major objective of this task was to design the slender column according to the Eurocode standard, while the design has to show a stability failure before reaching the pre-defined N - M interaction diagram. The N - M load path has to end in front of the interaction diagram and the cross-section compressive strain has to be far away from its ultimate strain capacity. The final layout, as presented in Fig. 2, shows a system stability failure with a cross-section compressive strain of $\varepsilon_{c1} = 1.5\text{‰}$, see also,¹³ which is far away from threshold of $\varepsilon_{cu} = 3.5\text{‰}$ (Fig. 1).

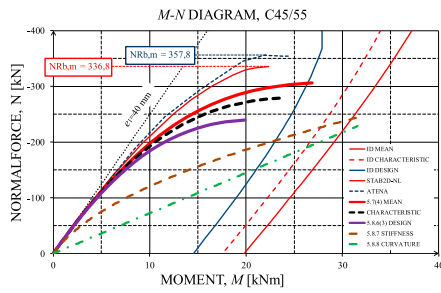
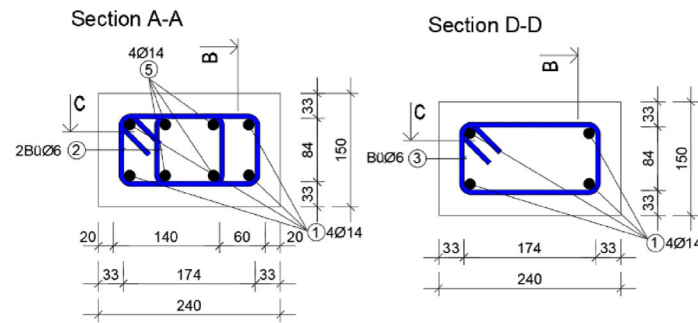


Fig. 1: Non-linear finite element optimization procedures for the C45/55 column

The University of Bratislava used non-linear finite element calculations¹³ for this column design, in particular for the determination of the maximum normal force N_{\max} and the initial eccentricity e_1 causing the stability failure. For these non-linear finite element calculations, the University of Bratislava used the standard properties of the concrete C45/55 and the reinforcement B500B. Further information can be found in Ref. [4].

The columns have a rectangular cross-section with a width $b = 240$ mm, a depth $t = 150$ mm and a length $l = 3840$ mm inclusive of the load introduction plates ($t = 20$ mm) at the top and bottom of the columns. The columns are reinforced with four bars, $\varnothing 14$ mm in diameter. These four bars are supplemented with another four bars with diameter of $\varnothing 14$ mm and length of 600 mm on both ends of the columns. The supplementary bars are



REINFORCEMENT STEEL B 500B

BAR NUMBER	DIAMETER OF BAR \varnothing [mm]	LENGTH OF BAR [m]	AMOUNT OF BAR [m]	OVERALL LENGTH [m]		
				$\varnothing 6$	$\varnothing 10$	$\varnothing 14$
1	14	3,80	4			15,20
2	6	0,64	56	35,84		
3	6	0,76	18	13,68		
4	10	0,84	2		1,68	
5	14	0,60	8			4,80
SUMMARIZED				LENGTH [m]	49,52	1,68
				WEIGHT [kg/m]	0,222	0,617
				WEIGHT [kg]	10,99	1,04
				WEIGHT [kg]	36,19	

CONCRETE: 0,137 m³

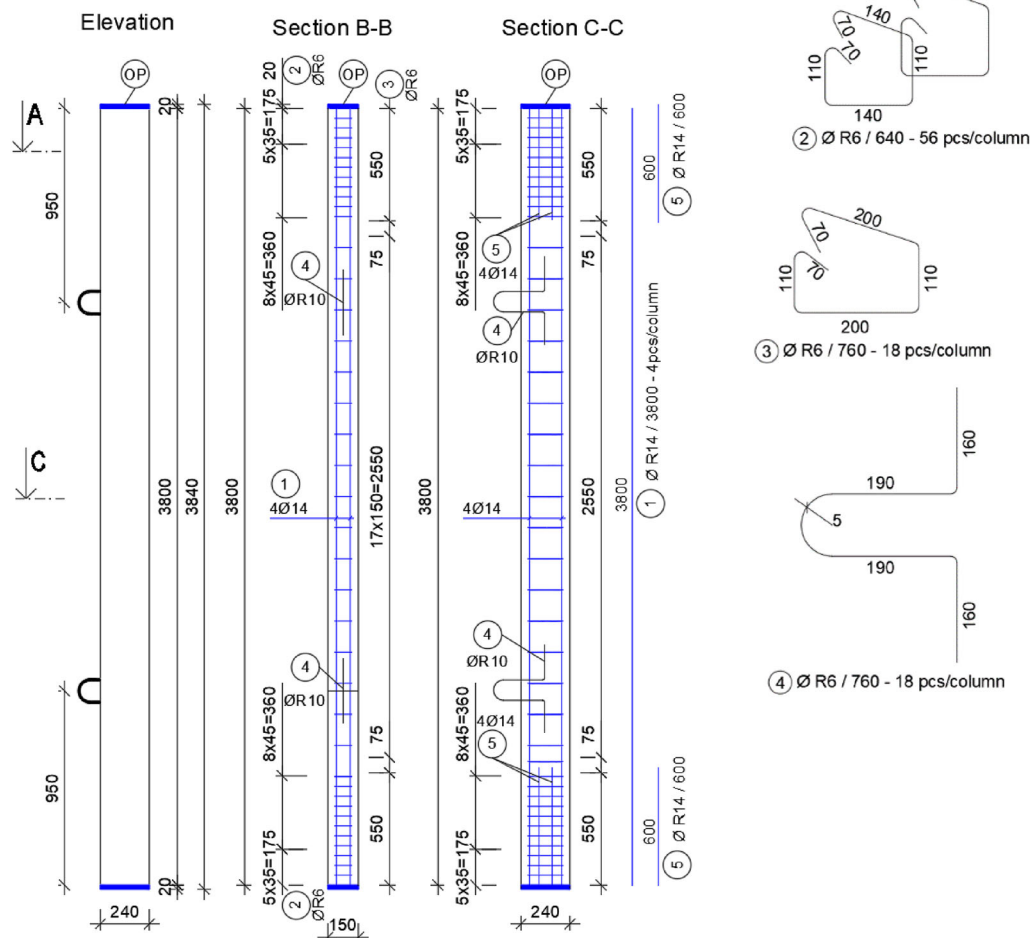


Fig. 2: Reinforcement and formwork plans of the investigated slender columns

welded to 20 mm thick steel plates. The transverse reinforcement consists of two leg stirrups with diameter of \varnothing 6 mm. As the local failure in the ending parts can precede the stability collapse of the columns, the resistance is increased by doubling the transverse reinforcement along the length of the additional bars. The geometry and the reinforcement of columns are presented in Fig. 2. The reinforced concrete columns are prefabricated elements with predefined production tolerances and a concrete cover of $c_{nom} = 20$ mm. The concrete cover was guaranteed by spacers to be mounted on the reinforcement cage.

Initial Capacity Prediction

In a first round, before the invitation of the IABSE expert group, Bratislava University invited service providers in the field of non-linear finite element modelling to make a prognosis of the expected test results of the slender columns described above. The detailed information about the invited institutions and the software products used can be found in Ref. [7]. In addition to the characteristic values of the column stability failures, the invited institutions provided the N - M interaction and the N - e_2 curves which allowed a deeper insight into the system responses during the loading process and thus into the initiation or change of fracture processes, where e_2 = displacement normal to the longitudinal axis in midspan of the column. The associated N - e_2 graphs in Ref. [4] showed the linear elastic regions, the first-crack formations, the fracture-dominated regions and the softening-specific regions. These analyses allowed a first characterization of the model or modelling uncertainties in

the respective stress areas. Consequently, these initial studies provided the basis for the requests sent to the IABSE members in the follow-up.

Test Series of Columns

The experimental procedure on the test specimens denoted S1-1 to S1-6 was divided into two groups: (a) group I comprised the columns S1-1 to S1-3 which were loaded at $e_1 = +40$ mm closer to those column surfaces that were closer to the floor during casting, see Fig. 3; and (b) group II comprised the columns S1-4 to S1-6 which were loaded at $e_1 = -40$ mm closer to those column surfaces that were closer to the filling opening during casting.

The monitoring set-up considered for this experimental campaign is shown in Fig. 4. This figure presents the arrangement of the LVDT sensors at the surfaces at half the height of the slender columns with a measuring distance $l_0 = 300$ mm. The values measured on the compressed side were as follows: e_2 – second-order eccentricity, TP1 and TP2 – compressive strain in the concrete and D1 – distance from the chosen base. On the side in tension these values were measured: E2 – second-order eccentricity, TP3 and TP4 – strain of concrete and D2 – distance from the chosen base.

The results from the six tested columns, which comprised the maximum load capacity N_{max} , the displacement e_2 normal to the column longitudinal axis at the N_{max} load level and the associated bending moment M_{max} are presented in Table 1. It is observed that the maximum load capacity N_{max} of group I shows significant higher

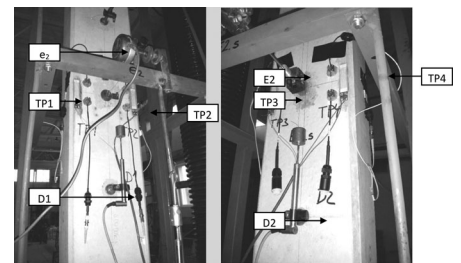


Fig. 4: Monitoring set up and sensor positions of the investigated slender columns

values and a different N - M interaction performance compared to group II. The points shown in Fig. 5 represent the tested maximum normal force load capacity N_{max} of each single column. Some of these points show the system stability failure before the N - M interaction threshold as defined in EN 1992-1-1.¹⁰ The right-hand graphic of Fig. 5 shows the load-vs-strain graphs in the fracture-prone cross-section at half the height of the columns. The concrete compressive strains in the inner fibre of the cross-section were recorded for the column stability loss between 1.4 and 1.8‰, and were far away from the permissible concrete compressive strains of 3.5‰. The associated concrete/reinforcement tension strains in the outer fibre of the cross-section were recorded between 1.4 and 3.1‰, see Fig. 5.

A more detailed analysis of the recorded data of the monitoring system and the test machine disclosed that the differences between group I and group II columns as presented in Table 2 did not result from the monitoring set-up nor from the machine-specific properties but rather from the manufacturing processes of the columns. The analyses of the concrete homogeneity and the fracture properties in the column cross-sections at half of the column heights (in the area of the Monitoring Set Up) finally allowed the conclusion that the concreting direction, despite a good concrete vibration, causes an inhomogeneity in the cross-section of the material properties such that, in consequence, the loading location $e_1 = +40$ mm or $e_1 = -40$ mm causes a significant difference in the associated load capacity N_{max} . Finally, the model uncertainties of the experimental test results could be derived according to the EN 1992-1¹⁰ methods with $\theta_{Nmax} = N_{max,mean}(Serie\ I)/N_{max,mean} = 1.06$ for the load capacity, with $\theta_{e2,Nmax} = e_{2,Nmax,mean}(Serie\ I)/e_{2,Nmax,mean} = 1.02$ for the horizontal deformation and

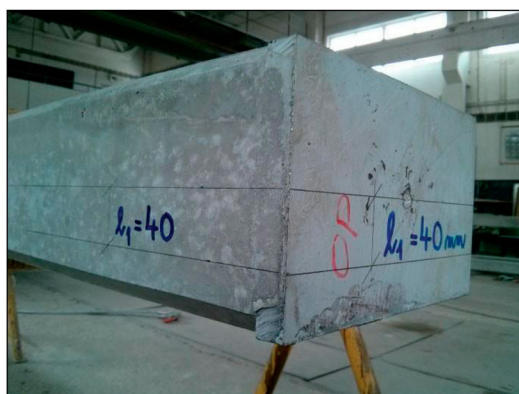
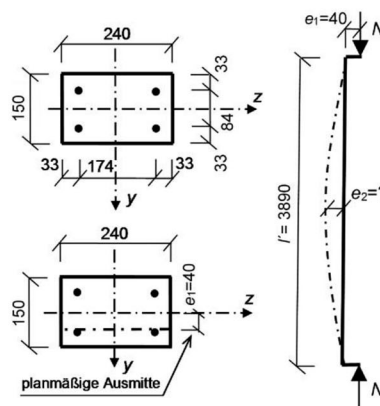


Fig. 3: Column test specimen from C45/55 and a load eccentricity $e_1 = +40$ mm, optimised for stability failure



Group	Test	N_{max} [kN]	e_2 [mm]	M_{max} [kNm]
I	S1-1	324.4	57.6	31.7
I	S1-2	323.4	42.7	26.8
I	S1-3	332.6	38.3	26.0
II	S1-4	271.2	58.4	26.7
II	S1-5	296.0	59.4	29.4
II	S1-6	311.4	55.0	29.6
	S1-1 to S1-3	326.8 (0.02)	46.2 (0.22)	28.2 (0.11)
	S1-4 to S1-6	292.9 (0.07)	57.6 (0.04)	28.6 (0.06)
	S1-1 to S1-6	309.8 (0.07)	51.9 (0.17)	28.4 (0.08)

Note: Values in brackets represent the Coefficients of Variation.

Table 1: Descriptive statistical parameters of the experimental results of the considered test series C45/55 without considering sample size aspects

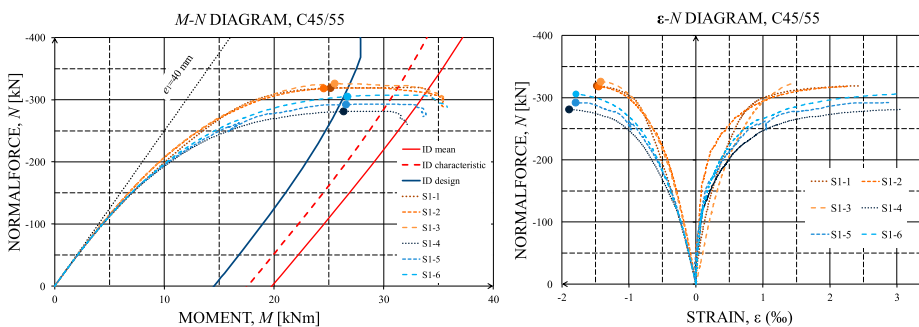


Fig. 5: By testing determined interaction between normal force – bending moment and normal force - strain of the specimens S1-1 to S1-6 vs. the N-M section interaction diagram (blue graph = design values, red dashed graph = characteristic values, red graph = mean values)⁶

with $\theta_{M,Nmax} = \theta_{M,Nmax,mean}(\text{Serie I}) / \theta_{M,Nmax,mean} = 1.01$ for the moments at the load level of the load capacity N_{max} .

Small Specimens Conformity Tests

Tests-Information for NL-FEM Modelling

In addition to the column tests, concrete conformity tests were also carried out. Associated results were subsequently provided after the first NLFEM prediction round as additional information for the non-linear modelling (see the section Round-Robin Modelling Posed Data and Questions for further details on the NLFEM information provision procedure). In general, the properties of concrete are characterized via the compressive strength according to EN 206-1,²⁰ the exposure classes and the slump value. Nevertheless, any realistic modelling of structures requires the

consideration of (a) geometrical non-linear effects (when relevant) and non-linear behaviour of concrete (usually referred to as fracture-mechanical parameters) which can be captured by e.g. a varying modulus of elasticity E_c (according to the stress levels), tensile strength f_t and specific fracture energy G_f ,²¹ and (b) of random uncertainties in material and geometrical properties caused by (among other things) natural effects, manufacturing processes and curing.²² These requirements together with the newly characterized concrete classes in the Eurocode concept gave rise to the experimental investigations with the concrete C45/55 and C100/115, as used for the discussed columns, according to EN 206-1 or ÖNORM B 4710-1.²³ In particular, the standardized compression test (EN 12390-3),²⁴ the standardized three-point bending test of notched specimens (EN 14651)²⁵ and the wedge-splitting test (ÖNORM B 3592)²⁶ were applied in

the course of the investigations. The experiments enabled a partially redundant identification of the material properties mentioned above beyond the code information.

Table 2 shows the detailed results of the cube compression tests, cylinder compression tests and three-point bending tests according to EN206-1²⁰ for the small scale specimens of column C45/55 which were considered from the partners in the 2nd modelling round. Table 5 shows the detailed results of the Cube compression tests, cylinder compression tests and three-point bending tests according to EN206-1²⁰ for the small scale specimens of column C100/115.

Compression Test

In order to determine the compressive strength according to EN 12390-3, test cubes of the investigated concrete type C45/55 and C100/115 (see Tables 2 and 3) with the dimensions 150/150/150 mm were loaded with a gradual increase of the stress level starting with 0.5 up to 0.8 MPa/s until the maximum load was reached. The maximum load was defined as that test load at which an increase within a period of 4 s was no longer possible.

The first set of cubes of series C45/55 and of series C100/115 were tested after 7 days of immersion in water and 21 days of exposure to air at an average air humidity of 60% and an air temperature of 21°C, see Table 3.

The second set of cubes of series C45/55 and of series C100/115 were tested after 103 days. The examinations of the Series 2 test cubes were conducted under similar storage and exposure conditions as Series 1, see Table 3. A similar testing campaign as on cubes 150 mm/150 mm/150 mm had also been performed on cylinders with a diameter of 150 mm and a height of 300 mm, see Tables 2 and 3. The results of these comprehensive compression testing campaigns are presented in Tables 2 and 3 and were provided to the modelling expert group after their first simulation results, see the section Three-Point Bending Fracture Test.

Three-Point Bending Fracture Test

One of the typical tests to obtain material parameters, and fracture parameters, in particular, is the fracture test of specimens with a central edge

Cube 150 × 150 × 150 mm number	Age [day]	Density [kg/m³]	Failure load F_{max} [N]	Compressive strength [MPa]	
1	28	2410 ± 10	1455.3	64.0	64.0 ± 0.8
2	28	2410 ± 10	1467.6	64.7	64.7 ± 0.8
3	28	2410 ± 10	1514.5	66.6	66.6 ± 0.8
4	28	2410 ± 10	1434.3	62.9	62.9 ± 0.8
5	28	2410 ± 10	1456.2	64.1	64.1 ± 0.8
6	28	2410 ± 10	1545.4	68.5	68.5 ± 0.8
7	103	2380 ± 10	1690.7	74.7	74.7 ± 0.9
8	103	2370 ± 10	1632.0	72.1	72.1 ± 0.9
9	103	2370 ± 10	1665.8	73.9	73.9 ± 0.9
10	103	2380 ± 10	1693.4	74.7	74.7 ± 0.9
11	103	2380 ± 10	1625.2	72.2	72.2 ± 0.9
12	103	2380 ± 10	1704.6	75.4	75.4 ± 0.9
				Rounded to 0.1MPa + U	
Cylinder $\phi 150 \times 300$ mm number	Age [day]	Density [kg/m³]	Failure load F_{max} [N]	Compressive strength [MPa]	
1	28	2420 ± 20	980.7	54.6	54.6 ± 0.8
2	28	2400 ± 20	946.7	52.4	52.4 ± 0.8
3	28	2400 ± 20	902.1	49.6	49.6 ± 0.7
4	28	2390 ± 30	902.8	49.5	49.5 ± 0.8
5	28	2400 ± 10	945.3	52.2	52.2 ± 0.8
6	28	2390 ± 10	893.8	49.2	49.2 ± 0.6
7	104	2390 ± 10	1015.9	56.6	56.6 ± 0.8
8	104	2400 ± 20	921.1	51.7	51.7 ± 0.7
9	104	2350 ± 20	952.9	52.7	52.7 ± 0.7
10	104	2360 ± 30	1046	57.9	57.9 ± 0.8
11	104	2370 ± 10	820.5	45.7	45.7 ± 0.6
12	104	2390 ± 10	1055.8	58.7	58.7 ± 0.6
				Rounded to 0.1MPa + U	
Beam 100 × 100 × 400 mm number	Age [day]	Density [kg/m³]	Failure load F_{max} [N]	Compressive strength [MPa]	Modulus of elasticity [MPa]
1	28	2410.2	496 062	49.61	35 834
2	28	2429.3	442 777	44.28	37 917
3	28	2416.6	480 298	48.03	38 064
4	104	2367.7	463 782	46.38	35 248
5	104	2355.3	407 064	40.71	35 437
6	104	2349.5	473 738	47.37	32 796

Table 2: Cube compression tests, cylinder compression tests and three-point bending tests according to EN206 -I²⁰ for the small scale specimens of column C45/55

notch in a three-point bending configuration. Outcomes of such tests are not only basic mechanical parameters such as the modulus of elasticity, but also fracture parameters describing

the behaviour of material during the fracture process and its crack propagation resistivity. Those parameters include effective crack elongation, effective fracture toughness, effective

toughness and specific fracture energy. The volume density of the tested material can be also evaluated. In addition, compressive strength values can be obtained via

Cube 150 × 150 × 150 mm number	Age [day]	Density [kg/m ³]	Failure load F_{max} [N]	Compressive strength [MPa]	
1	28	2420 ± 10	2238.0	97.9	97.9 ± 1.2
2	28	2410 ± 10	2233.0	98.3	98.3 ± 1.2
3	28	2420 ± 10	2229.1	98.6	98.6 ± 1.2
4	28	2420 ± 10	2136.0	94.5	94.5 ± 1.1
5	28	2410 ± 10	2085.8	92.1	92.1 ± 1.1
6	28	2410 ± 10	2139.3	93.9	93.9 ± 1.1
7	116	2400 ± 10	2366.0	104.4	104.4 ± 1.2
8	116	2410 ± 10	2379.4	104.6	104.6 ± 1.2
9	116	2410 ± 10	2431.2	107.1	107.1 ± 1.3
10	116	2420 ± 10	2391.8	105.8	105.8 ± 1.3
11	116	2400 ± 10	2442.0	108.1	108.1 ± 1.3
12	116	2410 ± 10	2461.0	108.1	108.1 ± 1.3
Rounded to 0.1MPa + U					
Cylinder $\phi 150 \times 300$ mm number	Age [day]	Density [kg/m ³]	Failure load F_{max} [N]	Compressive strength [MPa]	
1	28	2410 ± 20	1625.1	89.3	89.3 ± 1.3
2	28	2420 ± 20	1367.9	75.3	75.3 ± 1.1
3	28	2400 ± 20	1512.2	82.8	82.8 ± 1.0
4	28	2390 ± 30	1692.2	93.2	93.2 ± 1.1
5	28	2400 ± 10	1307.8	72.2	72.2 ± 0.9
6	28	2390 ± 10	1647.5	91.5	91.5 ± 1.8
7	117	2430 ± 10	1790.8	99.4	99.4 ± 1.2
8	117	2460 ± 30	1251.5	70.4	70.4 ± 1.2
9	117	2430 ± 10	1567.6	86.9	86.9 ± 1.1
10	117	2450 ± 10	1639.3	85.9	85.9 ± 1.1
11	117	2430 ± 10	1579.1	87.7	87.7 ± 1.1
12	117	2450 ± 20	1591.5	89.0	89.0 ± 1.3
Rounded to 0.1MPa + U					
Beam 100 × 100 × 400 mm number	Age [day]	Density [kg/m ³]	Failure load F_{max} [N]	Compressive strength [MPa]	Modulus of elasticity [MPa]
1	28	2420.8	729 775	72.98	42 009
2	28	2408.8	729 542	72.95	42 309
3	28	2425.3	707 412	70.74	41 148
4	104	2392.1	491 390	49.14	37 185
5	104	2385.2	526 881	52.69	36 396
6	104	2392.7	501 324	50.13	37 714

Table 3: Cube compression tests, cylinder compression tests and three-point bending tests according to EN206-1²⁰ for the small scale specimens of column C100/115

compression tests of broken parts of the specimens tested in bending. In particular, such tests enable the comparison between the compressive strength of the code specified cubes and prisms with a rectangular cross-section. Beam specimens prepared for the three-point bending tests had original dimensions 100 mm/100 mm/

400 mm and were casted, cured and stored under conditions identical to those used for the compression tests. The loading span of each beam was 380 mm. The specimen had a central edge notch with a depth of about 35 mm (1/3 of the height of the specimen). The loading of specimens was applied continuously with a constant increment of displacement (about 0.1 mm/min) in the centre of the span. The result of the measurement is a load vs. mid-span deflection diagram (l–d diagram). It includes both pre-peak and post-peak branches. The results of these comprehensive compression testing campaigns are presented in Tables 2 and 3 and were provided to the modelling expert group after their first simulation results, see the section Three-Point Bending Fracture Test.

Round-Robin NL-FEM Modelling

IABSE Commission 1; Task Group TG 1.4

As mentioned previously, the IABSE WC1 group was invited to join the Round-Robin Tests after Bratislava University had already invited service providers in the field of non-linear finite element modelling to make a prediction of column stability failure. The tasks and questions for the IABSE WC1 group were formulated more comprehensively and it was also of high interest to put a special focus on the comparison of results from different approaches, not only Finite Element Methods but also analytical approaches, in order to reveal any discrepancies between modelling techniques.

The non-linear modelling comprises the scattering of material parameters, the variable deformation and deflection effects during the loading process and the non-linear material laws. Time-dependent changes in material properties and its spatial distribution were not objectives of these studies and were eliminated mainly by specific production and testing procedures of the columns. These aspects are of interest in one of the next research steps.

The IABSE WC1 group motivation for participating in the Round-Robin Tests included the following:

- Non-linear numerical modelling is increasingly attracting interest in

everyday engineering. In fact, the method is very powerful for the replication of the real structural behaviour and also for using material efficiently in the structure.

- Non-linear numerical modelling is more demanding for the users due to the requirements in: (a) a much more extensive characterization of the input quantities of the material constitutive laws, (b) a more complex structure discretization (to divide the structure in more parts in order to better describe the mechanical performance of the structure) with respect to classical methods, (c) the appropriate selection of the finite element types, (d) choosing the appropriate solution procedure, (e) a more complex interpretation of the simulation results and (f) the possible iterative adaptation for an optimized finite element model and results.
- Traditional deterministic methods are not sufficient to properly design and assess new and existing general or advanced engineering structures and their components which are subjected to a variety of complex loading conditions from natural and artificial environments. Due to uncertainties in loading conditions, material behaviour, geometric configurations and boundary conditions, the stochastic analyses techniques (which account for all of these uncertain aspects) must be applied to provide rational reliability analyses and to describe realistically the existing behaviour of engineering structures. Therefore, stochastic analyses techniques and their proper application for engineering structures requires a training programme that is portable, provides global acknowledgment, improves structural performance and sets benchmarks within the industry.
- The necessity for code-based and general safety formats for non-linear finite element analyses techniques as well as the handling of the model and modelling uncertainties.

Round-Robin Modelling Process Steps

In the IABSE Commission 1 Task Group (TG1.4) meetings, the following analyses and modelling process steps exclusively relating to non-linear modelling and based on the experimental

designs of the Slovak University of Technology in Bratislava were discussed and mutually agreed upon. However, with respect to the amount of accessible information for non-linear modelling, the preliminary interests were (a) to elaborate on the scatter in the non-linear finite element predictions of the column stability failures that had been conducted by a smaller group from the Slovak University of Technology in Bratislava (STUBA) prior to the IABSE TG1.4 group participation in the round-robin simulations, and (b) to investigate and predict the column test results for concrete C45/55 and C100/115 as presented in Table 1 for C45/55. For the Round-Robin modelling procedure, there was an agreement on the following process steps in the context of the amount of accessible information for non-linear modelling.

- **1st** Round-Robin modelling process step: *Deterministic analyses based on the drawings without conformity test results* – only drawings of the column with embedded reinforcement and point of axial load input (static sketch) were available. Participants were asked to analyse two piers – one made of concrete C45/55 and the other of concrete C100/115 in accordance with available codes and standards.
- **2nd** Round-Robin modelling process step: *Deterministic analyses based on the drawings with conformity test results* – results of concrete samples were provided both for concrete C45/55 and C100/115. Results were based on the testing of 3 blocks 100/100/400 mm (104 days), 6 cubes 150/150/150 mm (103 days) and 6 cylinders $\phi 150/300$ mm (104 days). The results comprised of age, density, failure load and compressive strength of specimens, as well as modulus of elasticity for block specimens.
- **3rd** Round-Robin modelling process step: *Analyses based on the drawings with defined input parameters* – the partners received input data (already prepared for the probabilistic analyses) in the form of probabilistic resistance models for concrete grades C45/55 and C100/115 in order to have the possibility to characterize the modelling uncertainties. Some of the partners included in this 3rd Round-Robin not the information about the conformity test results.

- **4th** Round-Robin modelling process step: *Deterministic analyses based on the drawings with conformity test results and the test results of the column* –partners were provided with experimental test results of the column specimen to update their models or to comment on their compliance with the experimental results.
- **5th** Round-Robin modelling process step: *Probabilistic analyses based on the drawings with conformity test results and the test results of the column* - no additional input was provided. The goal of this round was to focus on correlation effects and spatial variability. The goal of this round was to focus on correlation effects and spatial variability. A comprehensive probabilistic analysis is not the subject of this article due to the page limitation, which is dealt with in a subsequent article.
- **U-MINHO:** José Matos, Neryvaldo Galvão; University of Minho, Institute for Sustainability and Innovation in Structural Engineering (ISISE).
- **IFSTTAR:** Pierre Marchand, André Orcesi, Mohammad El Hajj Diab, IFSTTAR – The French institute of science and technology for transport development and networks.
- **CDL:** Roman Wan-Wendner; Ghent University, Belgium and Krešimir Ninčević; Christian Doppler Laboratory, University of Natural Resources and Life Sciences Vienna, Austria.

Round-Robin Modelling Posed Data and Questions

For each of the expert groups, the different levels of information as described in the section Round-Robin Modelling Process Steps (1st to 5th round-robin modelling) were prepared and made available in chronological order after each completed round. The information of Figs. 2 and 3 were available as basic data. The expert groups were asked to generate and provide the data for the preparation of the following diagrams (see Figs. 10–16) of the columns made of C45/55 and C100/115 on the basis of the prior knowledge of the original modelling group, see the section Initial Capacity Prediction

- diagram presenting the normal force N vs. Moment M curves
- diagram presenting the normal force N vs. strain ε_c curves
- diagram presenting the normal force N vs. displacement e_2 curves.

The data were merged into the diagrams shown in the section Task group TG 1.4 Experts predictions: 1st round - Deterministic analyses based on drawing information and thus provided a very good insight into the differently modelled system responses during the entire load cycle up to the stability failure and during the post-peak. The provided N - M interaction and the N - e_2 curves allowed a deeper insight into the system responses during the loading process and thus into the initiation or change of fracture processes, hence, the experts were also asked to characterize the maximum load capacity N_{\max} , the displacement e_2 at the N_{\max} load level and the associated bending moment M_{\max} from their

non-linear analyses. These values allow unambiguous comparability of the predictions with the experimentally obtained data shown in Table 1.

In order to gain a deeper insight into the causes of the deviations in the non-linear modelled column responses, each expert group was asked to produce a report on the modelling in accordance with the Guidelines for non-linear finite element analysis of concrete structures²⁷ which summarized the input values, the constitutive laws used, the discretization strategy, the modelled constraints and the solution algorithms as well as other parameters.

This chosen procedure should make it possible to reconstruct the gradual adaptation of the non-linear model formations and the improvement in the predictions of the stability failure of the columns after each new round-robin information level, see the section Round-Robin Modelling Process Steps, and to exclude human errors if possible. Furthermore, this procedure provides an insight into the advanced NLFEM settings, constitutive laws, solution algorithms, etc. as chosen by the experts.

Modelling Strategy

A thorough planning of a finite element analysis reduces the risks of errors and the required time and thus cuts costs.²⁷ Furthermore, the results of a finite element analysis should be reported in a standard fashion in order to reduce the time and costs associated with reviewing and archiving the analysis. More information on performing and reporting the results of a finite element analysis can be found in Ref. [27]. According to Hendriks,²⁷ the analysis report should contain at least: 1. Specifications; 2. Model Preparation and Checking; 3. Analysis; 4. Validation and 5. Post Analysis Checks, see Ref. [27] for more details. From the above-mentioned submitted reports, it could be seen that most of the partners implemented these recording steps in their analyses. In the following, one briefly summarizes the overall modelling strategies considered by the experts. In particular, all the partners agreed that non-linear finite element modelling was a suitable analysis type. Some expert groups processed the tasks by using finite element bar elements, some using finite element

Round-Robin Modelling Experts

The experts in this study are well-regarded professionals in the fields of deterministic and probabilistic Non-linear Finite Element and Discrete Element modelling techniques for structural concrete systems. Correspondingly, the performance predictions involved at least one substantive and one normative expert. The use of different expert characteristics aimed to reduce bias in the estimation outcomes. The experts in the specific study were drawn from the IABSE WC1 group and they include researchers, engineers and senior scientists. As a minimum, they have 3 years of professional experience in Non-linear Finite Element modelling and probabilistic modelling and they have completed the training programmes for non-linear simulation techniques. The following expert groups participated in the Round-Robin modelling process:

- **STUBA:** Vladimir Benko, Slovak University of Technology in Bratislava, Department of Concrete Structures and Bridges.
- **BOKU:** Alfred Strauss; University of Natural Resources and Life Sciences Vienna, Institute of Structural Engineering.
- **UNIZG-FCE:** Ana Mandić Ivančević, Mladen Srbić and Dominik Skokandić; University of Zagreb Faculty of Civil Engineering, Department of Structural Engineering.

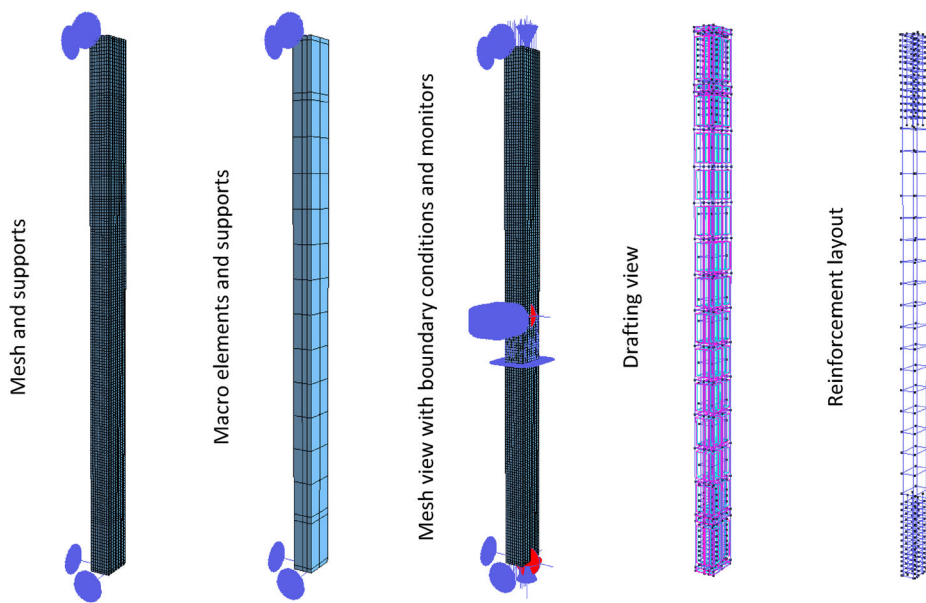


Fig. 6: Characteristics of the ATENA Scientific 3D Finite Element Model for the slender column C45/55 & C100/115

beam elements and some using finite element solids. An analytical model was also considered as an alternative modelling strategy by one partner. The software packages used include ATENA 2D Release 2016, ATENA 3D Engineering Release 2018, ATENA 3D Science Release 2019, DIANA Release 2019, Sofistik, Fedea-slab as well as others.

BOKU provided e.g. the type, the number, and the integration scheme of elements, as well as the associated boundary conditions as presented in Fig. 6. In particular, Fig. 6 presents the elementation, macro zoning, boundary conditions and supports, as well as the reinforcement layout.

FCE-UNIZG provided the following details for modelling and, subsequently, for the examination of modelling:

- the beam type FE model with cross-sections and embedded reinforcement was made according to the drawing provided at the beginning of the round-robin activity,
- Axial force acting in the point constraint (KF fix kinematic condition) with default eccentricity was set up as loading. Force is acting at the top support allowing vertical translation, while support at the bottom as for all translations is constrained,
- Beam type model of the pier $L = 380$ cm long (L) with different cross-sections comprising constant outer dimension $h \cdot b = 150 \cdot 240$ cm, but following changes in

reinforcement are developed. Length of beam elements 1 cm,

- Longitudinal reinforcement is modelled as single reinforcement in cm^2 (A_s) and shear reinforcement is modelled in shear cuts in cm^2/m (A_{ss}) of the column length,
- Axis distances of reinforcement were set up as determined with drawings with $d_1 = 33$ cm,
- The same simple finite element model of the system was kept through all of the assignment rounds.

Concrete was modelled using set up stress-strain relation for non-linear structural analysis according to 3.1.5 in EN 1992-1-1:2004, with f_{cm} e.g. from FEM database, as shown in Fig. 7. FCE-UNIZG used the concrete stress-strain relation for non-linear analysis according to EN 1992-1-1: 2004, as shown in Fig. 7. It is worth mentioning that the descending part of the stress-strain curve cannot be approached in this way with

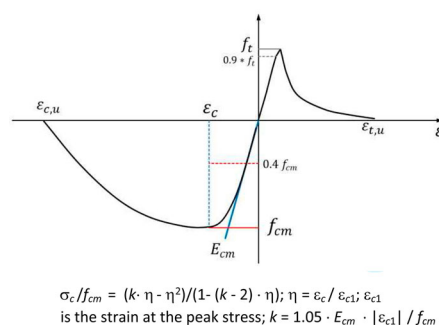


Fig. 7: Schematic representation of the concrete stress-strain relation for non-linear analysis according to EN 1992-1-1:2004

all of the available software (i.e. Sofistik). Namely, until the top point of the stress-strain curve, the Elastic Modulus is positive and monotone, but after the top point the stiffness would be negative, and therefore cannot be handled. The same approach with a controlled deformation analysis gave the same results. For the purpose of this assignment, in order to reveal the maximum axial force N_{max} load level and adequate bending moment M_{Nmax} , the ascending part of the curve should be sufficient.

CDL group introduced a discrete constitutive concrete model developed in Refs. [28,29] and used it to perform the non-linear analyses (Fig. 8). The well-established Lattice-Discrete Particle Model (LDPM) simulates the behaviour of concrete at the meso-scale and reproduces largely its inherent material heterogeneity. The behaviour of the material is simulated by the mechanical interaction of coarse aggregate pieces embedded in a cementitious matrix. The assumed spherical aggregates were randomly placed in a predefined geometrical domain, following a Fuller sieve curve. After the aggregate placement, polyhedral cells were created by a three-dimensional tessellation following a Delaunay tetrahedralisation. Nodes with zero radius were generated on the external surfaces to define the concrete domain and to facilitate the load application and the boundary conditions. Finally, the material behaviour was described by a set of vectorial constitutive equations imposed on the facets of each neighbouring polyhedral cell. They directly captured the governing lower scale phenomena that are cohesive softening in tension, frictional shear under low confinement and hardening with pore collapse under high confinement. A more detailed description and model formulations can be found in Refs. [28,29].

The main relevant mechanical parameters of the damage model for this problem are normal modulus, tensile strength, tensile characteristic length and shear strength ratio. As these parameters represent the local meso-scale properties of cement paste attached to coarse aggregate pieces, they have to be inversely calibrated based on simulated standard tests. In this case, three different numerical models were used to calibrate the above-mentioned parameters. A unique set of parameters was chosen in order to capture all concrete short-

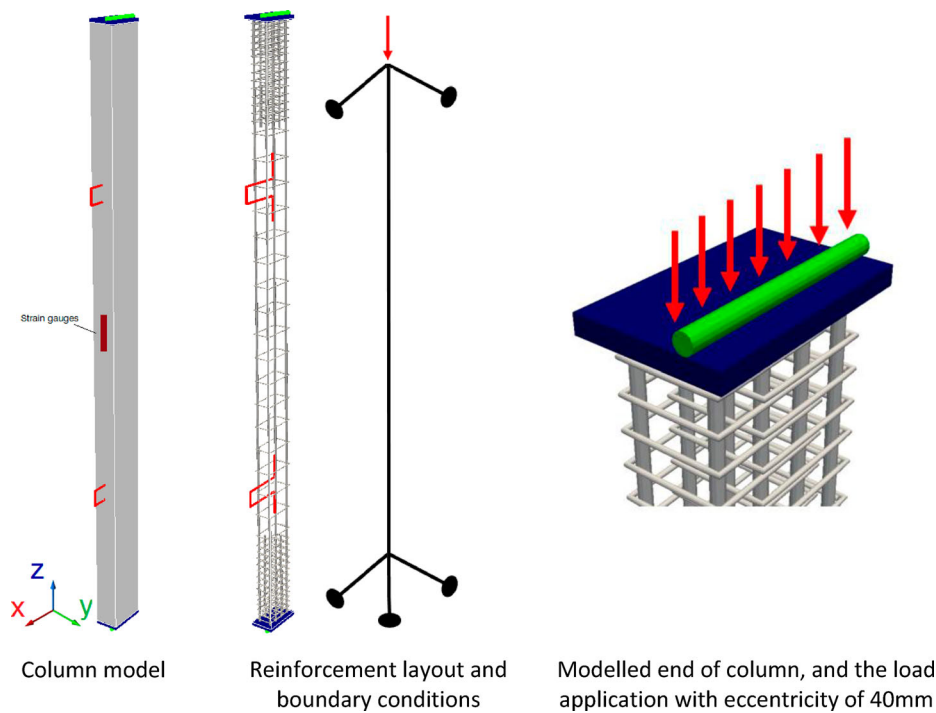


Fig. 8. Column model used in the LDPM analysis with some relevant details

term properties in order to simulate the concrete cube and cylinder compression tests and four-point bending tests (firstly for code suggested properties = 1st round-robin modelling and secondly for experimentally obtained ones = 2nd round-robin modelling).

The LDPM meso-scale concrete parameters were calibrated in order to represent concrete properties suggested by the codes for the C45/55 and C100/115 concrete strength classes. Based on the suggested code equations, calibrations were performed to obtain the concrete properties detailed in Table 4.

IFSTTAR considered two models. First, a finite element method,

denoted IFSTTAR1, with nonlinear static analysis was applied using the MATLAB toolbox FEDEASLab,³⁰ where the multilayer approach was used to model the column with corotational formulations to take into account the geometrical non-linearities. Second, an analytical model (denoted IFSTTAR2) was used as an alternative to a finite element modelling. In this model, one determines a $M-\chi$ (bending moment – curvature) relationship for different values of N (axial load). To do so, different values of couple $(\epsilon_{inf}, \epsilon_{sup})$ are considered, corresponding to the strain at lower and upper chord of the cross-section. For each couple the axial force N and bending moment M are determined

by integrating the concrete stress and force in the rebars. For each values of axial force N_i considered, one determines the couples $(\epsilon_{inf}, \epsilon_{sup})$ for which $N = N_i$ and the corresponding bending moments values. One can then deduce the corresponding curvature values χ to obtain a graph $M-\chi$ at $N = N_i$. Then, one integrates the curvature along the half height of the column (resolving an ordinary differential equation) with different eccentricity values at mid-height, and one chooses the eccentricity at mid-height of the column leading to the adequate value of eccentricity at the top of the column. Gathering all the couples $N - e_2$ obtained according to the process described above, one obtains the global law N function of e_2 . This procedure takes into account the two cross-sections that co-exist in this column with cross-section 1 (4 longitudinal 14 mm diameter rebars at the middle of the column) and cross-section 2 (8 longitudinal 14 mm diameter rebars at the top and the bottom of the column). Besides, the model relies on the bilinear law described in clause 3.2.7 (2a) of EN1992-1-1 for steel rebars, the law for C45/55 as stipulated by EN 1992-1-1 and the fib Model Code³¹ law for C100/115, as 100 MPa is out of scope of EN 1992-1-1 (see Table 5).

Task group TG 1.4 Experts predictions: 1st round - Deterministic analyses based on drawing information

As already outlined in the section Round-Robin Modelling Process Steps, the code information and the details of the design drawings were used as the basis for the modelling of the slender column elements by the 8 partners. Figures 9 and 10 present the NL-FEM system/column responses obtained from each partner in the “Normal-force-Moment $N-M$ ”, the “Normal-force-Concrete Strain $N-\epsilon_c$ ” and the “Normal-force-Horizontal Displacement $N-e_2$ ”. The following features can be read from these diagrams: (A) The “Normal-force-Moment $N-M$ ” diagram in the top/left of Fig. 9 shows a minimum value of $N_{min,NLFEM,C45/55} = 300\text{kN}$ and a maximum value $N_{max,NLFEM,C45/55} = 400\text{kN}$ of the NL-FEM calculations for the column designed for concrete type C45/55. For the column designed for concrete type C100/115, the minimum value of $N_{min,NLFEM,C100/115} = 380\text{kN}$ and the maximum value

X	Variable	Unit	X _k
Concrete C45/55			
f_{cm}	Concrete compressive strength - mean	MPa	53.0
$f_{cm,cube}$	Concrete compressive strength cube - mean	MPa	63.0
$f_{ctm,fl}$	Concrete tensile strength	MPa	6.3
E_{cm}	Initial tangent concrete modulus of elasticity	MPa	36280
Concrete C100/115			
f_{cm}	Concrete compressive strength - mean	MPa	108.0
$f_{cm,cube}$	Concrete compressive strength cube - mean	MPa	123.0
$f_{ctm,fl}$	Concrete tensile strength	MPa	8.7
E_{cm}	Initial tangent concrete modulus of elasticity	MPa	42880

Table 4: Concrete resistance model derived for 1st round of modelling

X	Variable	Unit	X _k
Concrete C45/55			
f_{cm}	Concrete compressive strength - mean	MPa	53
E_{cm}	Initial tangent concrete modulus of elasticity	MPa	36 300
Concrete C100/115 (according to fib Model Code)			
f_{cm}	Concrete compressive strength - mean	MPa	108
E_{ci}	Tangent modulus of elasticity of concrete at a stress		47 500
E_{cI}	Secant modulus from the origin to the peak compressive stress	MPa	36 000
$\varepsilon_{c,I}$	Concrete strain at maximum compressive stress		-3 ‰
$\varepsilon_{c,lim}$	Ultimate strain of concrete in compression		-3 ‰

Table 5: Concrete resistance model derived for 1st round of modelling

$N_{max,NLFEM,C100/115} = 520$ kN were obtained, see Fig. 10. The moments attributed to the above indicated normal forces are $M_{Nmin/C45/55} = 28$ kNm and $M_{Nmax/C45/55} = 32$ kNm for slender column elements designed for concrete C45/55 (see Fig. 9) and $M_{Nmin/C100/115} = 34$ kNm and $M_{Nmax/C100/115} = 40$ kNm for slender column elements designed for concrete C100/115 (see Fig. 10). These scatters in values include the blurring of the software specific algorithms as well as the blurring or errors generated in the

model input parameters by the users. (B) The “Normal-force-Concrete Strain $N-\varepsilon_c$ ” diagram in the top/right of Fig. 9 shows a clear transition from linear to non-linear performance and consequently to failure due to concrete crash in the compression zone. In all of the partner’s graphs, the non-linear behaviour of the slender columns was evident after a normal force of approximately $N \cong 180$ kN for C45/55 and C100/115 (see Fig. 10). The concrete compression strain ε_c for C45/55 (Fig. 9) and C100/115 (Fig. 10) was calculated at the bearing capacity by most

of the partners with $\varepsilon_c = 2$ ‰ and the associated reinforcement tension strains in the tension zone of the column between $\varepsilon_s = 2.8$ ‰ to 3.6‰ (C) The “Normal-force-Horizontal Displacement $N-e_2$ ” diagram in the bottom-left of Fig. 9 shows a jump in the horizontal displacement e_2 for some of the partners calculations at approx. $N \cong 180$ kN for C45/55 and C100/115 (see also Fig. 10). The horizontal displacements attributed to the above indicated normal forces are $e_{2,Nmin/C45/55} = 45$ mm and $e_{2,Nmax/C45/55} = 40$ mm for concrete C45/55 (see Fig. 9) and $e_{2,Nmin/C100/115} = 55$ mm and $e_{2,Nmax/C100/115} = 40$ mm for concrete C100/115 (see Fig. 10). (D) From these investigations the following statistical parameters can be determined: $N_{C45/55} = LN(m=352 \text{ kN}; \nu = 0.2)$; $M_{C45/55} = LN(m=37 \text{ kNm}; \nu = 0.25)$; $e_{2,C45/55} = N(m=42 \text{ mm}; \nu = 0.18)$; respectively $N_{C100/115} = LN(m=480 \text{ kN}; \nu = 0.18)$; $M_{C100/115} = LN(m=36 \text{ kNm}; \nu = 0.23)$; $e_{2,C100/115} = N(m=48 \text{ mm}; \nu = 0.20)$.

The 1st Round-Robin modelling process step which includes the Deterministic analyses of the invited expert groups using the information from design drawings, code information but not the information from conformity test results shows a scattering in the normal force for the C45/55 between $N_{min,NLFEM,C45/55} = 300$ kN and $N_{max,NLFEM,C45/55} = 400$ kN, which is associated with a model uncertainty of $\phi_{NLFEM,C45/55} = 1 + 50/350 = 1.14$ and with respect to the experimental data $\phi_{EXPC45/55} = 1 + 35/315 = 1.11$. For the C100/115 the scattering was between $N_{min,NLFEM,C100/115} = 380$ kN and $N_{max,NLFEM,C100/115} = 580$ kN, which is associated with a model uncertainty of $\phi_{NLFEM,C100/115} = 1 + 100/480 = 1.20$ and with respect to the experimental data $\phi_{EXPC100/115} = 1 + 100/430 = 1.23$.

Task group TG 1.4 Experts

predictions: 2nd round-

Deterministic analyses based on 1st round and specimen experiments (Tables 2 and 3)

In the second round, the test results of the small specimens experiments (Cube pressure tests, cylinder compression tests and three-point bending tests according to EN206-1) were made available to the partners. The partners adjusted their modelling input parameters using these tests information and standardized as well as

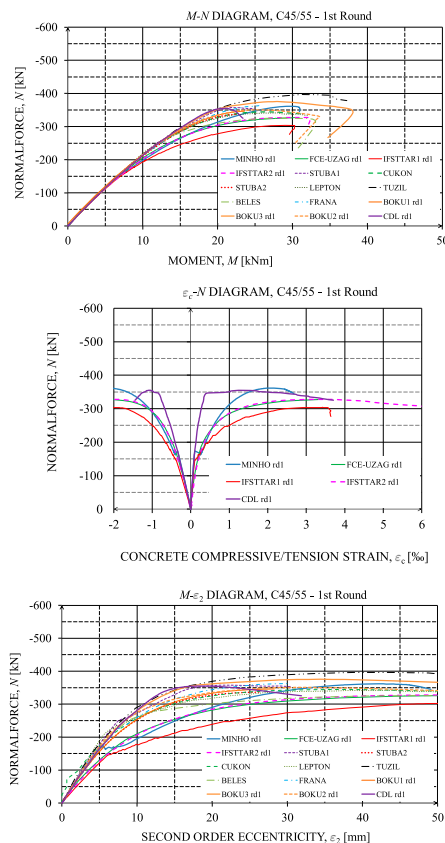


Fig. 9: Performance graphs of the slender column made of concrete C45/55 based on the code-based characteristics

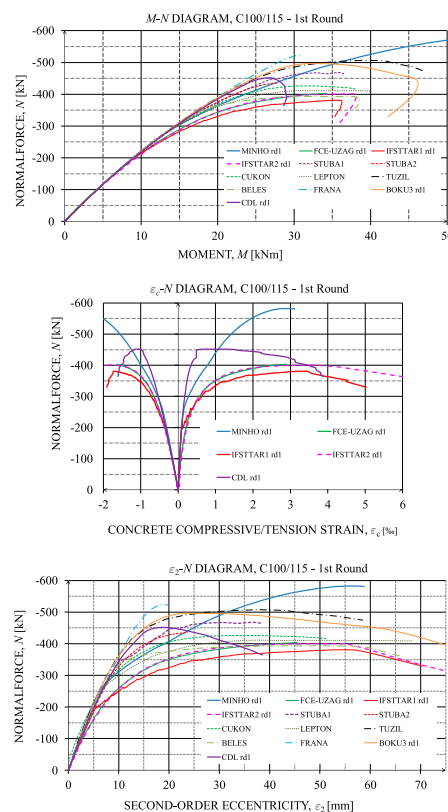


Fig. 10: Performance graphs of the slender column made of concrete C100/115 based on the code-based characteristics

X	Variable	Unit	X _k
Concrete C45/55			
$f_{ck,cube}$	Concrete compressive strength - cubes	MPa	73.83
$f_{ck,cyl}$	Concrete compressive strength - cylinders	MPa	53.88
f_{cm}	Concrete compressive strength - mean	MPa	61.88
ϵ_{c1}	Strain at max. compressive stress	‰	2.49
ϵ_{cu1}	Ultimate strain	‰	3.50
E_{cm}	Initial tangent concrete modulus of elasticity	MPa	34494
Concrete C100/115			
$f_{ck,cube}$	Concrete compressive strength - cubes	MPa	106.35
$f_{ck,cyl}$	Concrete compressive strength - cylinders	MPa	86.55
f_{cm}	Concrete compressive strength - mean	MPa	94.55
ϵ_{c1}	Strain at max. compressive stress	‰	2.80
ϵ_{cu1}	Ultimate strain	‰	2.80
E_{cm}	Initial tangent concrete modulus of elasticity	MPa	37098

Table 6: Concrete resistance model derived by FCE-UNIZG for the 2nd round of modelling

advanced updating procedures. This type of information also assisted in characterizing the time-dependence of the input parameters of the modelling, with the input parameters of the modelling established by most of the partners for the time of 108 days at the time of the support tests. As illustration, FCE-UNIZG updated the concrete models of the 1st round with the material tested data as shown in Table 6.

Although data for 28 and 103/116/117 days old concrete was provided, data for older concrete was used as suggested by the initiator of the round-robin activity. Concerning the LPDM analysis, in contrast to the 1st round where the concrete calibration was based on code suggestions, in the 2nd round the experimentally obtained values for concrete properties were considered. The LPDM meso-scale concrete parameters were calibrated based on the experimentally obtained values, as shown in Table 6. Figures 11 and 12 present the NL-FEM system/column responses obtained from each partner in the “Normal-force-Moment- $N-M$ ”, the “Normal-force-Concrete Strain $N-\epsilon_c$ ” and the “Normal-force-Horizontal Displacement $N-e_2$ ”.

2nd round – Discussions with respect to 1st round:

The following conclusions can be drawn from these investigations: the

variations in the normal forces as well as the moments were reduced in relation to the first round and the results approximate the experimental values. This applies to the columns of both concrete C45/55 and C100/C115.

The 2nd Round-Robin modelling process step which includes the deterministic analyses of the invited expert groups using the information from design drawings, code information and the information from small-scale conformity test results shows a scattering in the normal force for the C45/55 between $N_{min,NLFE,C45/55} = 330\text{ kN}$ and $N_{max,NLFE,C45/55} = 400\text{ kN}$, which is associated with a model uncertainty of $\phi_{NLFE,C45/55} = 1 + 35/365 = 1.10$ and with respect to the experimental data $\phi_{EXP,C45/55} = 1 + 50/315 = 1.15$. For the C100/115 the scattering was between $N_{min,NLFE,C100/115} = 370\text{ kN}$ and $N_{max,NLFE,C100/115} = 520\text{ kN}$, which is associated with a model uncertainty of $\phi_{NLFE,C100/115} = 1 + 75/445 = 1.16$ and with respect to the experimental data $\phi_{EXP,C100/115} = 1 + 15/430 = 1.03$.

Task group TG 1.4 Experts predictions: 3rd round - Deterministic analyses for characterizing the modelling uncertainties

In this process step, the modelling uncertainty was of primary interest. The material laws implemented in the finite element software codes and the

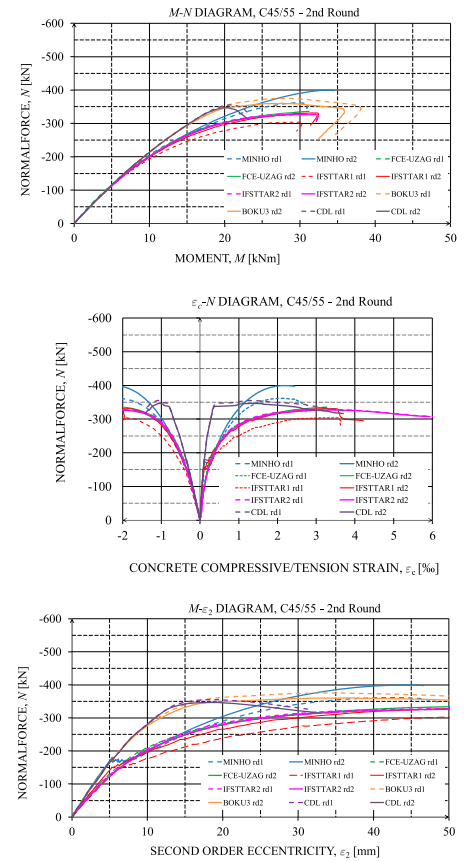


Fig. 11: Performance graphs of the slender column made of concrete C45/55 based on the small-scale specimen results (2nd round)

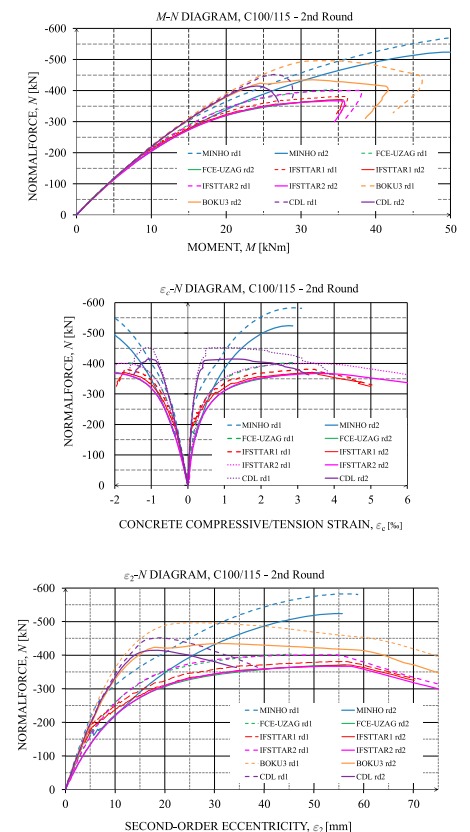


Fig. 12: Performance graphs of the slender column made of concrete C100/115 based on the small-scale specimen results (2nd round)

solution algorithms were blurred, resulting in modelling uncertainties that were part of the model uncertainties. To determine this type of modelling uncertainty, the model input parameters for the partners participating in the Round-Robin Test were processed as shown in Table 7. By means of this preparation and the 2nd round adaptation process, it was ensured that the scattering of the results only originates from the uncertainties in the material laws and software

algorithm resolution. In general, a comprehensive processing of the model input parameters into nominal values, characteristic values, mean values and distribution types had been performed for the non-linear deterministic analyses.

Figures 13 and 14 present the NL-FEM system/column responses obtained from each partner in the “Normal-force-Moment $N-M$ ”, the “Normal-force-Concrete Strain $N-\epsilon_c$ ” and the

“Normal-force-Horizontal Displacement $N-e_2$ ”.

3rd round – Findings regarding modelling uncertainties:

The 3rd Round-Robin modelling process step which included the *Deterministic analyses of the invited expert groups using the information from design drawings, code information and the information from the pre-defined input parameters for a probabilistic*

X	Variable	Dist.		Unit	X_k	μ	σ
C45/55							
X_1	f_c	Concrete compressive strength	LN	MPa	45.0	53.0	5.13
X_2	f_{ct}	Concrete tensile strength	LN	MPa	2.7	3.8	0.78
X_3	G_F	Concrete fracture energy	LN	MPa	104	149	30.8
X_4	E_{ci}	Initial tangent concrete modulus of elasticity	LN	GPa	37.5	37.5	4.91
X_5	$\epsilon_{c,1}$	strain at max. compressive stress	LN	‰	−2.50	−2.50	tbd.
X_6	$\epsilon_{c,lim}$	Ultimate strain	LN	‰	−3.50	−3.50	tbd.
X_7	$\epsilon_{ct,max}$	Maximum tensile strain	LN	‰	0.15	0.15	tbd.
X_8	k_1	Tension stiffening factor (f_{ct})	LN		0.6	0.6	tbd.
X_9	k_2	Tension stiffening factor ($\epsilon_{ct,max}$)	LN		5.0	5.0	tbd.
X_{10}	f_y	Reinforcing steel yield strength	LN	MPa	500	548	40.0
X_{11}	E_s	Reinforcing steel modulus of elasticity	Det.	GPa	200	200	-
X_{12}	k	Ratio $(f_t/f_y)_k$ for ductility class B	Det.	‰	1.08	1.08	-
X_{13}	ϵ_u	Strain at max. tensile stress	Det.	‰	50	50	-
X_{14}	b	Width	N	cm	24.0	24.0	0.90
X_{15}	h	Height	N	cm	15.0	15.0	0.30
X_{16}	A_{s1}	Reinforcement area	N	cm ²	3.08	3.08	0.062
X_{17}	A_{s2}	Reinforcement area	N	cm ²	3.08	3.08	0.062
X_{18}	d_1	Axis distance of reinforcement	B	cm	3.30	3.30	0.66*
X_{19}	d_2	Axis distance of reinforcement	B	cm	3.30	3.30	0.66*
X_{20}	L	Length	Det.	m	1.92	-	-
X_{21}	e_0	Eccentricity	N	cm	4.00	4.00	tbd.
X_{22}	θ_R	Resistance model uncertainty	LN	-	1.00	1.00	tbd.
C100/115							
X_1	f_c	Concrete compressive strength	LN	MPa	100.0	108.0	4.99
X_2	f_{ct}	Concrete tensile strength	LN	MPa	3.7	5.2	1.08
X_3	G_F	Concrete fracture energy	LN	MPa	119	170	35.0
X_4	E_{ci}	Initial tangent concrete modulus of elasticity	LN	GPa	48.9	48.9	6.23
X_5	$\epsilon_{c,1}$	Strain at max. compressive stress	LN	‰	−3.0	−3.0	tbd.
X_6	$\epsilon_{c,lim}$	Ultimate strain	LN	‰	−3.0	−3.0	tbd.

Notes: a, b = $\mu \pm 3\sigma$.

Table 7: Model input parameters used for characterizing modelling uncertainties

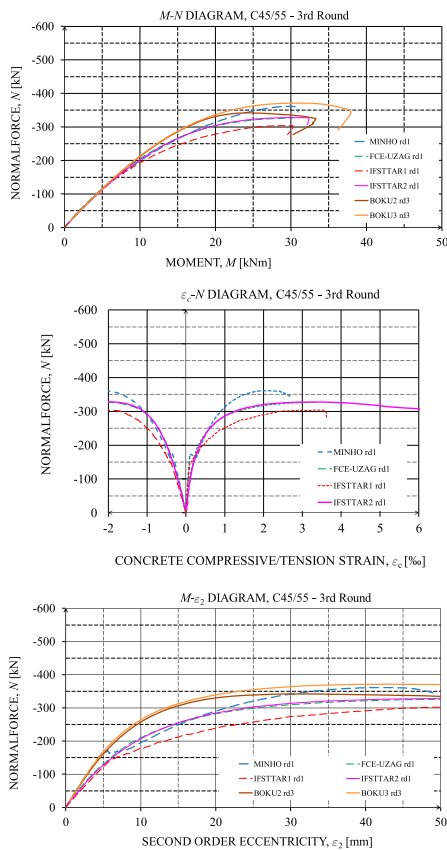


Fig. 13: Performance graphs of the slender column made of concrete C45/55 based on parameters for the determination of the modelling uncertainties (3rd round)

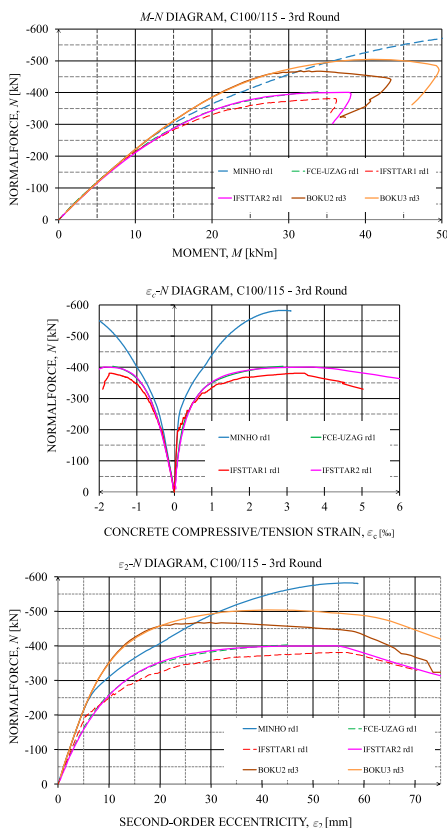


Fig. 14: Performance graphs of the slender column made of concrete C100/115 based on parameters for the determination of the modelling uncertainties (3rd round)

analysis showed a scattering in the normal force for the C45/55 between $N_{min,NLFE,C45/55} = 300$ kN and $N_{max,NLFE,C45/55} = 365$ kN, which is associated with a model uncertainty of $\phi_{NLFE,C45/55} = 1 + 32.5/332.5 = 1.10$ and with respect to the experimental data $\phi_{EXP,C45/55} = 1 + 17.5/315 = 1.06$. For the C100/115 the scattering was between $N_{min,NLFE,C100/115} = 380$ kN and $N_{max,NLFE,C100/115} = 505$ kN, which is associated with a model uncertainty of $\phi_{NLFE,C100/115} = 62.5/443 = 1.14$ and with respect to the experimental data $\phi_{EXP,C100/115} = 13/430 = 1.03$.

Task group TG 1.4 Experts

predictions: 4th round -

Deterministic analyses based on 1st & 2nd rounds and column tests

After the production of experimental samples and preparation of laboratory conditions, the concrete columns were tested in The Central laboratory of the Civil Engineering faculty SUT Bratislava. During the experiment, measurements were taken on both sides of the concrete cross-section. Despite the fact that columns were fabricated using the same materials and great care was taken for accuracy, the differences in results are notable. The major difference in buckling force reaches 15.9%, whereas in deformations of columns in the middle (ϵ_2) it goes up to 44.9%. The measurements were taken on 6 testing samples of slender concrete columns.

In this 4th round (Figs. 15 and 16), model results from the 2nd round and experimental results of the column tests were to be compared and reasons for deviations were to be investigated and elaborated upon. As illustration, the main idea of FCE-UZAG regarding the updating process was to adjust the assumed loading points of the out-of-centre forces and to adjust the geometrical sizes including the initial deformations in the testing device of the columns on the basis of the mean values obtained from previously calculated column test results. This procedure was to be applied for columns C45/55 and C100/115. However, the group compared results and concluded that their results were in good compliance with the experimental tests. Hence, the group did not go further with updating the model. Finally, the features of diagrams for the four rounds are summarized in Table 8.

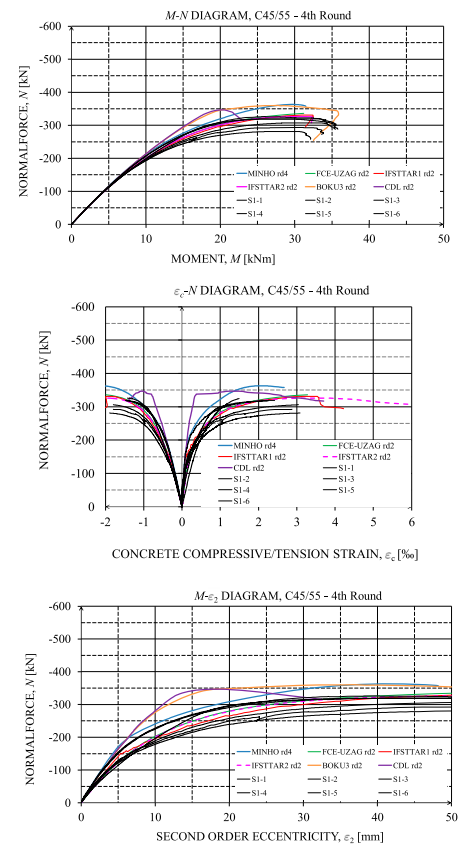


Fig. 15: Performance graphs of the slender column made of concrete C45/55 based on the information about the column experiments (4th round)

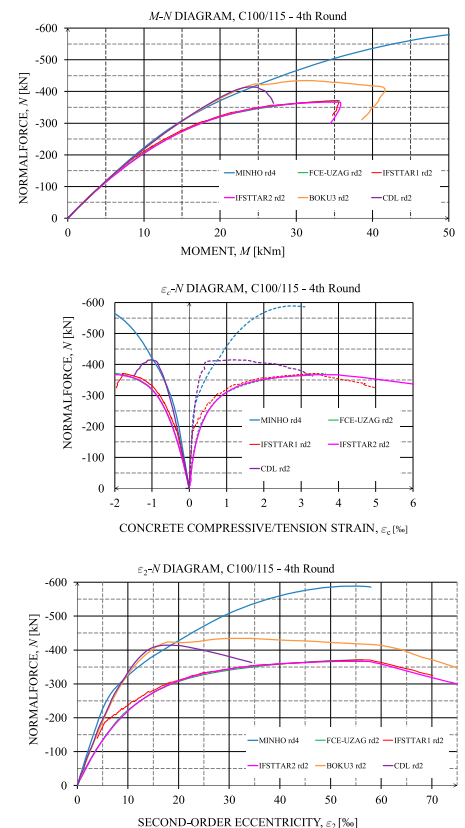


Fig. 16: Performance graphs of the slender column made of concrete C100/115 based on the information about the column experiments (4th round)

Variable	Unit	1 st Round	2 nd Round	3 rd Round*	4 th Round	Experiment
C45/55						
$N_{min,NLFEM,C45/55}$	kN	300	330	300	330	270
$N_{max,NLFEM,C45/55}$	kN	400	400	365	355	360
$N_{NLFEM,C45/55}$	kN	100	70	65	25	90
$M_{Nmin/C45/55}$	kNm	28	32	30	32	29
$M_{Nmax/C45/55}$	kNm	32	34	31	30	27
$M_{N/C45/55}$	kNm	4	2	1	2	2
e_c	‰	2	1–2	2	1–2	1.5–1.9
e_t	‰	2.8–3.6	2.5–3.7	2.8–3.6	2.5–3.7	1.5–3.2
$e_{2,Nmin/C45/55}$	mm	45	50	50	50	45
$e_{2,Nmax/C45/55}$	mm	40	47	40	42.5	35
$e_{2,N/C45/55}$	mm	5	3	10	7.5	10
C100/115						
$N_{min,NLFEM,C100/115}$	kN	380	370	380	370	
$N_{max,NLFEM,C100/115}$	kN	580	520	505	440	
$N_{NLFEM,C100/115}$	kN	200	150	125	70	
$M_{Nmin/C100/115}$	kNm	36	36	35	36	
$M_{Nmax/C100/115}$	kNm	52	49	42	32	
$M_{N/C100/115}$	kNm	16	13	7	4	
e_c	‰	2	1.7–2	1.7–2	1.2–1.8	
e_t	‰	2.8–3.6	2.8–3.6	2.8–3.5	2.0–3.5	
$e_{2,Nmin/C100/115}$	mm	56	57	56	56	
$e_{2,Nmax/C100/115}$	mm	55	55	43	35	
$e_{2,N/C100/115}$	mm	1	2	13	21	

*Results of the deterministic analyses for characterizing the modelling uncertainties.

Table 8: Summary rounds 1–4

The 4th Round-Robin modelling process step which included the Deterministic analyses of the invited expert groups using the information from design drawings, code information, the information from small-scale conformity test results and the information from the tested columns showed a scattering in the normal force for the C45/55 between $N_{min,NLFEM,C45/55} = 330$ kN and $N_{max,NLFEM,C45/55} = 355$ kN, which is associated with a model uncertainty of $\phi_{NLFEM,C45/55} = 1 + 13/343 = 1.04$ and with respect to the experimental data $\phi_{EXP,C45/55} = 1 + 28/315 = 1.09$. For the C100/115 the scattering was between $N_{min,NLFEM,C100/115} = 370$ kN and $N_{max,NLFEM,C100/115} = 440$ kN, which is associated with a model uncertainty of

$\phi_{NLFEM,C100/115} = 1 + 35/405 = 1.09$ and with respect to the experimental data $\phi_{EXP,C100/115} = 1 + 25/430 = 1.06$.

Conclusions

In this paper, the bearing capacity of two slender concrete column elements, experimentally investigated through failure testing, were assessed by a number of experts in a round-robin NL-FEM analyses, using successively improved analyses. At the early stage of this structural NL-FEM based assessment using standard input information from codes and standardized methods, significant uncertainties in the output results were identified when

benchmarking the expert numerical analysis results with the experimental results. Consequently, enhanced non-linear FE analyses were carried out using small and large scale test results and the information from the partners. The main conclusions were:

- The initial structural NL-FEM of the columns (1st Round-Robin modelling process based on code information) indicated a higher normal force capacity than the tested columns and a high scattering of the results of the experts. It was shown that the modelled capacity had a significantly higher load-carrying capacity than the experiments.
- The enhanced structural NL-FEM of the columns (2nd Round-Robin modelling process), which was based on test information from laboratory small scale tests, revealed a remarkable improvement in the prediction of the load-carrying capacity with respect to the experimental results. The experts were not informed about the results of the experimentally tested columns. In addition, most of the NL-FEM analyses at this stage also revealed a failure mechanism where the column stability loss occurs far away from the Code defined N-M Interaction limit and the concrete compression strain in the high loaded cross-section at stability failure shows 2‰ at maximum, which is significantly lower than the 3.5‰ acceptable limit.
- A further enhanced structural NL-FEM of the columns (4th Round-Robin modelling process) based on test information from the full-scale column tests, where the experts were informed about the results of the experimental tested columns, were no longer needed by most of the experts for the improvements of the predictions.
- the 1st Round-Robin modelling process (based on code information) and due to the scattering (model uncertainties) show from most of the partners an overestimation of the NL-FEM simulations with respect to the test results. Hence, it can be expected that there will be cases where the PSF method combined with NL-FEM leads to inaccurate un-safe prediction of the structural behaviour of slender column systems. Hence it is recommended that an additional system safety factor, which is not

yet included in Eurocode, is included, in particular for NL-FEM analyses methods.

- Nonetheless, the bearing capacity of slender concrete column elements, such as computed by NL-FEM, is several times higher than the simplified code procedures, such as the nominal stiffness or nominal curvature method. Before such disparity, special training should be advised, and recommendations should be provided in the codes for NL-FEM analysis of slender columns in order to take full advantage of such methods for a more efficient, less conservative and accurate design procedure.
- In addition, it has been shown that the model uncertainty has an important influence on the safety verification and, thus, the prediction of the bearing capacity. Consequently, model uncertainty has to be taken into account properly, otherwise it can lead to an inaccurate structural assessment. Among the proposed safety concepts, it is only the improved ECOV²⁷ and the full probabilistic method that account for the model uncertainty rationally.
- There is a lack of studies on the model uncertainty factor and its coefficient of variation for enhanced structural assessment using non-linear FE analysis. Therefore, further studies are needed. A large number of decisions are required from the experts when dealing with non-linear FE analysis. As such, in order to reduce the analyst-dependent variability (modelling uncertainties) in the results and also the model uncertainties, guidelines for such analyses should be developed, examined and used.

This paper demonstrated that it is feasible to use NL-FEM analysis for the structural prediction of the bearing capacity of slender concrete columns. Such analyses are computationally more demanding than standard methods (nominal stiffness or nominal curvature method) and cognitively more demanding to the analysts, when it comes to the modelling and solution techniques, the use of information and the interpretation of NL-FEM results. In order to reduce the risk of errors in capacity predictions, it is recommended that specific training and experience for formulation in codes are associated requirements for NL-FEM analysts. In addition, a

discussion about a safety factor associated with NL-FEM applications should be initiated. Nevertheless, the studies of this paper demonstrate that NL-FEM analysis can provide a tool to assess safety using realistic descriptions of material behaviour with actual material properties. In this way, a realistic estimation of the existing safety levels can be obtained utilizing “hidden” capacities by using “true” material properties.

Acknowledgements

The authors would like to acknowledge IABSE COM1 and the IABSE TG1.4 members for supporting this project.

Funding

This paper was partly carried out during research exchanges at TU Brno (BUT), Lehigh University (LU). The authors acknowledge also the financial support provided by the SAFEBRIDGE ATCZ190 EU Interreg project, the Scientific Grant Agency of the Ministry of Education of Slovak Republic, the Slovak Academy of Sciences VEGA No. 1/0696/14, and Slovak Research and Development Agency under the contract No. APVV-15-0658. The computational results presented have been achieved [in part] using the Vienna Scientific Cluster (VSC).

ORCID

Alfred Strauss  <http://orcid.org/0000-0002-1674-7083>

José Matos  <http://orcid.org/0000-0002-1536-2149>

Roman Wan-Wendner  <http://orcid.org/0000-0003-3616-5694>

References

- [1] Suda J, Strauss A, Rudolf-Miklau F, Hubl J. Safety assessment of barrier structures. *Struct. Infrastruct. Eng.* 2009;5(4):311–324.
- [2] Červenka V. Global safety format for non linear calculation of reinforced concrete. *Beton und Stahlbetonbau* 2008;103:37–42.
- [3] Strauss A, Wendner R, Bergmeister K, Reiterer M, Horvatits J. Monitoring and influence lines based performance indicators [Modellkorrekturfaktoren als “performance Indikatoren” für die Langzeitbewertung der integralen Marktwasserbrücke S33.24]. *Beton- und Stahlbetonbau*. 2007;106(4):231–240.
- [4] Benko V, et al. Failure of slender columns of loss of stability. In: *Key Engineering Materials*. Vol. 691, 2016; s. 185–194. ISSN 1013-9826.
- [5] Strauss A, Vidovic A, Zambon I, Dengg F, Matos JC. Performance indicators for roadway bridges. *Maintenance, Monitoring, Safety, Risk and Resilience of Bridges and Bridge Networks*

- *Proceedings of the 8th International Conference on Bridge Maintenance, Safety and Management (IABMAS)*; 2016; 965–970.

[6] Benko V, et al. The reliability of slender concrete columns subjected to a loss of stability. In: *Advances and Trends in Engineering Sciences and Technologies II: proceedings of the 2nd International Conference on Engineering Sciences and Technologies*, High Tatras Mountains, Tatranské Matliare, Slovak Republic, 29 June–1 July 2016, London: Taylor & Francis Group; 2017, S. 45–50. ISBN 978-1-138-03224-8.

[7] Benko V, et al. Prediction of slender concrete columns resistance in case of stability failure. *Beton TKS*. Vol. 1; 2014.

[8] Strauss A, Benko V, Täubling B, Valašík A, Čuhák M. Zuverlässigkeit schlanker Betonstützen. *Beton- und Stahlbetonbau*. 2017;112(7):392–401.

[9] Benko V, Dobrý J, Čuhák M. Failure of slender concrete columns due to a loss of stability. *Slovak J. Civil Eng.* 2019;27:45–51.

[10] EN 1992-1-1. Eurocode 2: Design of concrete structures - Part 1-1. General rules and rules buildings; 2004.

[11] Benko V. Nichtlineare Berechnung von Stahlbetondruckglieder [Nonlinear analysis of reinforced concrete compression members]. In: *Innovationen im Betonbau 27. Fortbildungsveranstaltung, OVBB Heft 47*, 2001; s. 9–12.

[12] Moravčík M, et al. Experience with bridges of the older types of precast (Skúsenosti s mostami zo starších typov prefabrikátov). *Betonárske dni, zborník prednášok, STU v Bratislave*, 2012; s. 439–444. ISBN 978-80-8076-104-2.

[13] Pfeiffer U. Program: analysis of reinforced Concrete Structures, TUHH, Version 2.90; 2014.

[14] ÖNORM B 1992-1-1. Eurocode 2: Bemessung und Konstruktion von Stahlbeton- und Spannbetontragwerken Teil 1-1: Grundlagen und Anwendungsregeln für den Hochbau; 2011.

[15] Benko V, Dobrý J, Čuhák M. slender concrete columns at the loss of stability. In: *Better, Smarter, Stronger*. Lausanne: Fédération internationale du béton (fib); 2018. ISBN 978-1-877040-14-6.

[16] Podrúček J, Benko V, Kendický P, Strauss A. Reliability assessment of concrete columns. The international conference on bridge maintenance, safety and management, Foz do Iguaçu; Dec 5-7; 2016.

[17] Červenka V, Jendele L, Červenka J. ATENA Program Documentation – Part 1: theory. Červenka Consulting, Prague; 2007.

[18] Novák D, Vořechovský M, Teplý B. FRaE: software for the statistical and reliability analysis of engineering problems and FRaE-D: degradation module. *Adv. Eng. Softw.* 2014;7:179–192.






[19] Iman R. C.; Conover W. J. Small sample sensitivity analysis techniques for computer models, with an application to risk assessment. *Commun. Stat. Theory Methods*. 1980;A9:1749–1842.

[20] EN-206-1. Concrete – Part 1: Specification, performance, production and conformity; 2005.

- [21] Zimmermann T, Lehký D, Strauss A. Correlation among selected fracture-mechanical parameters of concrete obtained from experiments and inverse analyses. *Struct. Concrete* 2016;**17**(6):1094–1103.
- [22] Ang A-S, Tang W. *Probability Concepts in Engineering Planning*. 2nd ed. John Wiley & Sons, Inc: Hoboken, NJ; 2007.
- [23] ÖNORM-B-4710-1. Concrete – Part 1: specification, production, use and verification of conformity (rules for the implementation of ÖNORM EN 206-1); 2002.
- [24] EN-12390-3. Testing hardened concrete – Part 3: Compressive strength of test specimens; 2009.
- [25] EN-14651. Test method for metallic fibered concrete – measuring the flexural tensile strength (limit of proportionality (lop), residual); 2005.
- [26] ÖNORM-B-3592. Determination of cut-through-tensile splitting strength and specific fracture energy of building materials, combinations of building materials and composites – wedge splitting method; 2011.
- [27] Hendriks MAN, de Boer A, Belletti B. Guidelines for nonlinear finite element analysis of concrete structures. Rijkswaterstaat Centre for Infrastructure, Scope: Girder Members, Report RTD:1016:2012; 2012.
- [28] Cusatis G, Pelessone D, Mencarelli A. Lattice discrete particle model (LDPM) for failure behavior of concrete. I: theory. *Cement Concrete Composites*. 2011;**33**(9):881–890.
- [29] Cusatis G, Pelessone D, Mencarelli A. Lattice discrete particle model (LDPM) for failure behavior of concrete. II: calibration and validation. *Cement Concrete Composites*. 2011;**33**(9):891–905.
- [30] Filippou FC, Constantinides M. FEDEAS Lab getting started guide and simulation examples. Technical Report NEESgrid-TR22; 2004.
- [31] fib, Model Code 2010, 2011.

Article

Probabilistic and Semi-Probabilistic Analysis of Slender Columns Frequently Used in Structural Engineering

Alfred Strauss ^{1,*} , Michael Hauser ¹, Benjamin Täubling ¹, Ana Mandić Ivanković ², Dominik Skokandić ² , José Matos ³, Neryvaldo Galvão ³ , Vladimir Benko ⁴, Jakub Dobrý ⁴, Roman Wan-Wendner ^{1,5} , Krešimir Ninčević ¹  and André Orcesi ⁶

¹ Department of Civil Engineering and Natural Hazards, University of Natural Resources and Life Sciences, 1190 Vienna, Austria; m.hauser@boku.ac.at (M.H.); fenrelot@posteo.net (B.T.); roman.wendner@boku.ac.at or roman.wanwendner@ugent.be (R.W.-W.); kresimir.nincevic@boku.ac.at (K.N.)

² Faculty of Civil Engineering, University of Zagreb, 10000 Zagreb, Croatia; ana.mandic.ivankovic@grad.unizg.hr (A.M.I.); dskokandic@grad.hr (D.S.)

³ ISE, Department of Civil Engineering, University of Minho, 4800-058 Guimarães, Portugal; jmatos@civil.uminho.pt (J.M.); neryvaldo.galvao17@live.com (N.G.)

⁴ Faculty of Civil Engineering, Slovak University of Technology in Bratislava, 81107 Bratislava, Slovakia; vladimir.benko@stuba.sk (V.B.); jakub.dobry@stuba.sk (J.D.)

⁵ Department of Structural Engineering and Building Materials, Ghent University, 9052 Ghent, Belgium

⁶ MAST-EMGCU, IFSTTAR, University Gustave Eiffel, 77454 Marne-la-Vallée, France; andre.orcesi@ifsttar.fr

* Correspondence: alfred.strauss@boku.ac.at



Citation: Strauss, A.; Hauser, M.; Täubling, B.; Ivanković, A.M.; Skokandić, D.; Matos, J.; Galvão, N.; Benko, V.; Dobrý, J.; Wan-Wendner, R.; et al. Probabilistic and Semi-Probabilistic Analysis of Slender Columns Frequently Used in Structural Engineering. *Appl. Sci.* **2021**, *11*, 8009. <https://doi.org/10.3390/app11178009>

Academic Editor: Chiara Bedon

Received: 26 June 2021

Accepted: 11 August 2021

Published: 30 August 2021

Abstract: The stability of slender columns is a topic that has been dealt with in research and practice for many years. The importance of this topic also increases with the possibility of using non-linear modeling approaches to determine the stability and with the increasingly complex safety formats. In order to show the complexity and the variability associated with the non-linear models, two previous contributions discussed and compared (a) the results of the Round Robin Non-Linear Modeling, and (b) the existing international associated standard specifications and safety concepts with respect to experimental results. The aim herein is to determine the reliability level (safety index) on the basis of these investigations and findings and to examine the existing safety formats of classical and extended probabilistic analyses and to derive any necessary adjustments. In addition, the method of the safety format Estimation of Coefficient of Variance of resistance (ECOV) is used for the determination of the global safety resistance factors based on the non-linear analyses' findings of the Round Robin modeling partners.

Keywords: slender columns; classical and extended probabilistic analyses; verification formats; variable sensitivity analysis

Publisher's Note: MDPI stays neutral with regard to jurisdictional claims in published maps and institutional affiliations.



Copyright: © 2021 by the authors. Licensee MDPI, Basel, Switzerland. This article is an open access article distributed under the terms and conditions of the Creative Commons Attribution (CC BY) license (<https://creativecommons.org/licenses/by/4.0/>).

1. Introduction

In current structural engineering practice, structures are typically designed in order to fulfil stability and serviceability requirements. Both requirements are related to a predefined period of time (durability and service life criteria) which should be achieved at minimum cost (economical and investment criteria). These requirements are typically formulated using a so-called limit state condition which associates the input parameters reflecting the resistance and the action sides of the structural evaluation. The input, which can be physical (dimensions, material strength, loads) or of dimensionless values, is then typically associated with a given level of uncertainty [1,2]. Therefore, the input parameters are treated within a reliability framework as random variables. The limit state function (G) delineates the acceptable region of a system's performance with respect to a certain failure mode and typically represents a mathematical formulation in terms of the key input parameters. The failure is then attributed to specific combinations of the parameters and is conventionally defined by the condition $G < 0$. The failure probability of the considered

state results from the system or element reliability. These notions determine whether a structural engineering design aims to ensure stability, serviceability or other limit states. The main focus of this investigation is the structural reliability assessment of designed slender concrete columns at the ultimate state.

The general approach described above can be implemented by applying various formats of different intricacies together with their corresponding efficiencies. Recent experimental studies for slender reinforced concrete columns [3] have indicated that the classical design approaches for distinguished N - M combinations are too conservative and so cannot meet the reliability level that is required in current design standards and the desired level of structural safety required in modern societies [4–6]. Simultaneously, due to the rapidly developing computational technologies and formats, more sophisticated numerical probabilistic simulations and non-linear calculation formats are becoming more important and finding their way into engineering practice [7]. Such non-linear calculation formats require an extended understanding of a multitude of material specific properties, modeling procedures and analysis formats. Despite the explicit possibilities in EN 1992-1-1 [8] of using non-linear formats, there is still a need for the development of more consistent safety formats [9–16] for predicting the stability failure of slender columns.

A key aspect in deciding on the appropriate configuration of non-linear calculations is the consideration of possible variations in complex and interacting input parameters. To that end, Strauss et al. [4] indicated the reliability deficiencies in the above-mentioned design situation of slender columns by assessing to what extent a group of peer institutions can capture this deficiency with independent non-linear numerical analyses. Furthermore, this study allowed a quantification of the modeling and calculation uncertainties [15]. In this context, it should be mentioned that there are already several studies in which uncertainties are analyzed on the structural behavior and design of slender columns, like for example [17].

However, the uncertainties due to the variability of material properties, constitutive laws, geometries, loads and loading applications were not further investigated on the basis of a formal probabilistic analysis.

Hence, the main objective of this paper is to discuss the probabilistic verification of the stability of slender columns. The associated research questions regarding the deterministic and probabilistic non-linear calculations for slender reinforced concrete columns, see also [18–20], provided the basis for the further studies presented in this paper. The studies gave rise to the discussion and analysis of the following novel elements:

- (a) The clear definition of the steps required for the probabilistic verification of the N - M stability of slender columns with regard to scattering interaction diagrams (I - D) [see EN 1992-1] [8].
- (b) The realistic determination of the safety level (evaluation of a possible safety risk) as well as the model uncertainties [21,22] of the non-linear probabilistic support analyses compared to experimentally determined N - M graphs and in relation to the EN1992-1 specific I - D s.
- (c) The study of the sensitivities, which vary with the load level (N - M interaction load level), of the descriptive model input variables for both the column cross-sectional level and the column component level in relation to the column load-bearing capacity and the column deformation.
- (d) The determination of the global safety resistance factors according to the “Estimation of the Co-efficient of Variation” (ECOV) method using the non-linear finite element responses generated by means of Latin Hyper Cube Sampling and from responses to experiments as well as the suitability of the global safety resistance factors for reliability assessment.

2. Probabilistic Non-Linear Computation

The probabilistic elements described below were used in the following studies and are briefly explained here for clarification.

2.1. Reliability Levels

In order to assess the reliability of a structure or a structural element in general, the limit state function $g(x)$ is formulated as indicated in Equation (1),

$$g(x) = 0 \quad (1)$$

where the vector x consists of m basic variables X_i ($i = 1, \dots, m$). For the present structural reliability problem, $g(x)$ is formulated as the difference between the resistance R and the load E :

$$g(x) = K_R R - K_E E \quad (2)$$

In general, due to simplifications in the modeling, model uncertainties K_R for the resistance and K_E for the load are introduced [23], as they are meant to reduce the deviation of the numerical model from the realistic model. The limit state function is formulated in a way that negative values indicate failure and the failure probability is defined as the probability that the random combination of the input values results in an outcome in the failure domain. Mathematically the latter can be expressed through Equation (3)

$$P_f = \int_{g(x) < 0} f_x(x) dx \quad (3)$$

where $f_x(\cdot)$ is the m -dimensional joint probability density function (PDF) of the m basic variables X_i . The structural reliability is quantified through the reliability index β , which can be generally expressed and calculated—assuming a normal distribution for $g(x)$ —through Equation (4).

$$\beta = \Phi^{-1}[1 - P_f] \quad (4)$$

where $\Phi^{-1}[\cdot]$ is the inverse of the standard normal cumulative distribution function.

Several methods have been developed historically and are now available for determining these failure probabilities or the corresponding reliability, each of which has its own level of sophistication. Often in literature [24,25], as well as in modern design standards [26] the following categorization is used, starting with the level of highest complexity:

- Level III: limit state functions and distribution functions for the random variables are introduced without any approximation; calculations are usually based on Monte Carlo simulation or straightforward numerical integration;
- Level II: the amount of calculation efforts is reduced by adopting well-chosen linearization techniques, usually the so called First Order Reliability Method; the degree of accuracy may strongly depend on the details of the problem at hand;
- Level I: the variables X_i are introduced by one single value only; this value is referred to as the design value. This method does not actually calculate a failure probability but only checks whether some defined target level is attained or not. It is the basis for partial safety factor format (PSFM) which is defined in Eurocodes as the basic design format for new structures and it is the design and assessment procedure in everyday practice and is referred to as the semi-probabilistic level.

A particular challenge of many civil engineering problems lies in the fact that decisions are made based on values which are remote from the most expected (median or mean) values for a parameter. In these cases, the probability densities are very small, and the obtained results are very sensitive to the tails of the distributions. Besides, the probability of failure, although a strictly mathematical term, remains a subjective perception because it quantifies the expectation regarding structural failure. This subjective probability is not an inherent property; rather, it depends very much on the amount of information available to the calculation procedure.

For the present study two further limitations apply:

1. It is assumed that the variables in a limit state function are in a first approach independent from each other. Although correlations between variables can be taken into account in computational programs, they are difficult to determine and convolute the algorithms.
2. The analysis does not take into account human error. The failure probabilities p_f discussed herein are conditional on the assumption that there are no errors affecting the resistance and loading condition of the case study. To reduce errors, special strategies and quality control measures are required.

2.2. Limit State Design

As requested by the current codes [8,27] *Serviceability Limit State (SLS)* verifications must be performed as post-analysis checks. For the load level corresponding to the SLS, derived from the SLS combinations imposed by the current codes, the stress state, crack opening and deflections controls must be performed. Regarding the *Ultimate Limit State (ULS)*, verifications must be performed in order to obtain an adequate level of resistance against the loads imposed on the structures. The MC2010 proposes (a) the probabilistic method, (b) global resistance factor format (GRF) and (c) the partial safety factor format (PF). The Estimate of Coefficient of Variation of Resistance (ECOV) method is a particular method within the global resistance format. The forthcoming fib Model Code 2020, although its content and formats are still under discussion, should also encompass this concept.

Global Resistance Factor format (GRF): According to this format, the global resistance of the structure is a random variable. The effects of various uncertainties are integrated in the global design resistance and can be expressed by a global safety factor. The global safety coefficient is equal to the product of the safety and the model coefficients.

Partial Safety Factor format (PF): According to the Partial Safety Factor format, the basis variables are deterministic quantities representing values related to a level of confidence for each parameter. In that sense, the treatment of uncertainties and variabilities originating from various causes is distributed to the individual input parameters by means of design values assigned to variables. The variable design values are obtained by calibrating their characteristic values with corresponding partial factor. Design material properties, derived from the characteristic ones, are then used in the analysis. Understandably, the non-linear analysis is carried out for extremely low strength input parameters which can lead to a non-realistic structural response or global failure mechanism. For this reason, it is not advised to rely solely on the PF format for the design.

Estimation of Coefficient of Variation of Resistance method (ECOV): In this case, one estimation of the mean and one of the characteristic resistances are calculated using the respective set of values of the material parameters. The random distribution of resistance of reinforced concrete members can be described in a first approximation by a two-parameter lognormal distribution (the use of other distributions is possible but needs an adjustment of the following equations) while these two parameters are the mean resistance and the coefficient of variation of the material property, V_R . V_R is calculated according to [27] by:

$$V_R = \frac{1}{1.65} \cdot \ln\left(\frac{R_m}{R_k}\right) \quad (5)$$

where R_m is the mean resistance value and R_k is the characteristic value of resistance corresponding to 5% exceedance probability. The respective global safety factor γ_R is calculated as:

$$\gamma_R = e^{\alpha_R \cdot \beta \cdot V_R} \quad (6)$$

where α_R is a constant value and is assumed to be 0.8. The safety index β is to be taken in accordance with the target reliability index and applicable standards.

In this approach, the sensitivity factor of the resistance side α_R , the coefficient of variation V_R of the resistance side and the reliability index β are considered. The descriptive

elements of the action side (e.g., partial safety factor γ_E) influences the consideration only indirectly via the interrelation between α_E , α_R and β .

2.3. Sampling Methods

The Monte-Carlo (MC) method provides a powerful, adaptable, and accurate method which has been increasingly used. MC replaces an exact or approximate calculation of the probability density of the limit state function by generating a large number of individual evaluations of the function or the input parameters using random realizations x_{ik} of the underlying distributions for the random variables X_i where the index “ k ” stands for the “ k ”-th simulation ($k = 1, 2, \dots, N_{real}$), see Figure 1. When combined with a finite element model, the resistance of the analyzed component or the limit state function has to be calculated for a large number of repetitions, yielding an output distribution function. Each set of the k realizations introduced into the analyzed model leads to a solution.

$$G_k = G(a_0, x_{1k}, x_{2k}, \dots, x_{ik}, \dots, x_{nk}) \quad (7)$$

The resulting z numbers g_k are evaluated statistically according to the basic statistics and lead to the $p_f = z_0/z$, where z_0 is the number of results violating the design threshold.

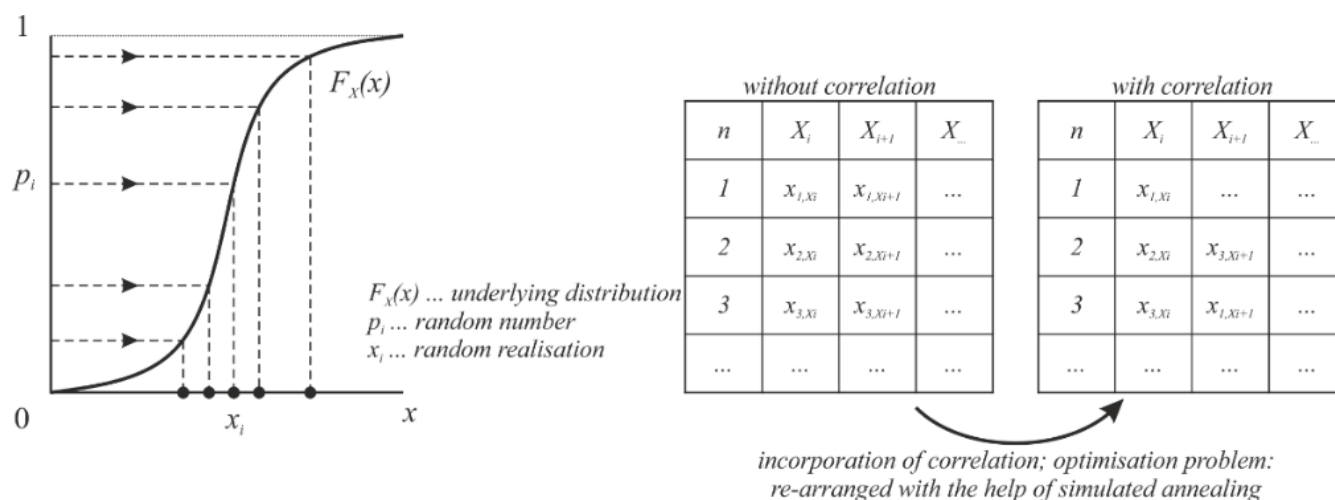


Figure 1. Monte-Carlo method simulation procedure including and not including correlation between basic variables.

The correlation between the basic variables, see Figure 1 (right), is set up by a controlled rearrangement of the sample field using simulating annealing. Simulated annealing (simulated cooling/annealing) is a heuristic approximation method.

In summary, the MC method provides an approximate solution by performing statistical sampling. It relies on repeated random sampling whereby the error decreases with the square root of $1/N_{sim}$, where N_{sim} = amount of simulations; p_i is generated randomly with uniform distribution on the interval $[0 - 1]$. However, sample points are generated without considering the previously generated sample points.

The Latin Hyper Cube Simulation (LHS) method [28] is an extended procedure and is based on the basic idea of the Monte Carlo method. In particular, in the context of statistical sampling, a square grid containing sample positions “Latin square” is used for the LHS method. During sampling there is only one sample in each row and each column accepted, see Figure 2. While p_i is chosen randomly when using the MC method, see Figure 1 left, one p_i is chosen from each of the N_{sim} -intervals, see Figure 2 left, when using the LHS method. Random samples can be taken one at a time, remembering which samples were taken so far by dividing the cumulative density function (CDF) into N_{sim} equally probable k intervals, see Figure 2. It ensures an acceptable accuracy at a low N_{sim} .

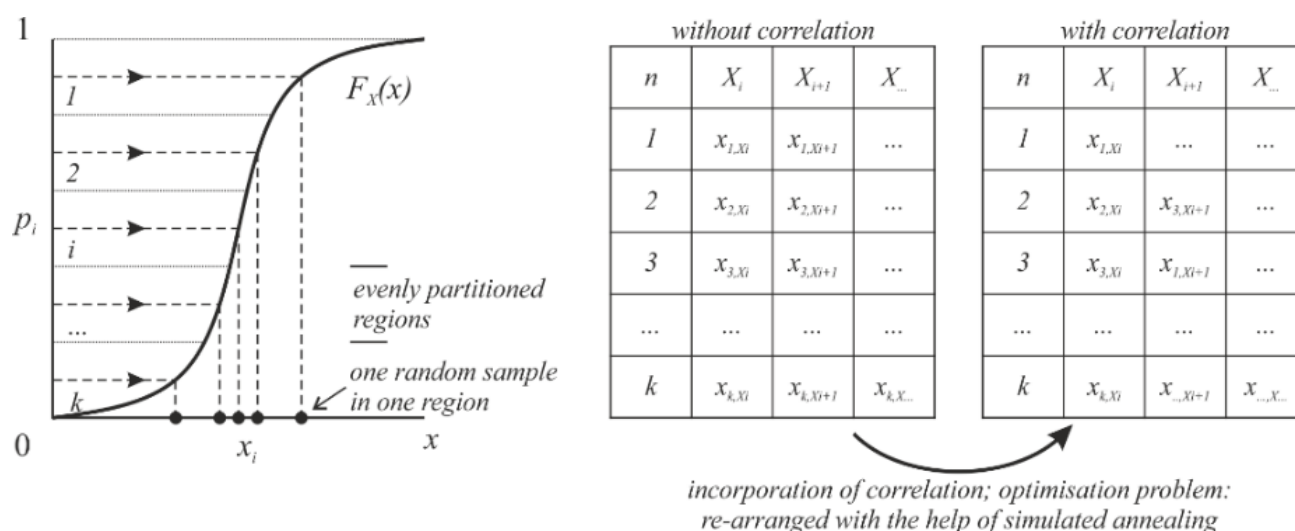


Figure 2. Latin Hyper Cube Simulation (LHS) method including and not including correlation between basic variables.

The Fractile Based Simulation (FBS) method is processed as the LHS method with a number of N_{sim} -intervals but taking only a reduced number of p_i s from this sample field for the evaluation procedures into account. The selection of the reduced p_i s is based on predefined fractile values of the CDF, for instance as shown in Figure 3. Hence, the effort of simulations can be reduced while fully including the properties of the LHS sampling field—encompassing the N_{sim} -intervals.

Since several basic variables are generally involved in a problem and the assignment of the p_i s to predefined fractile values is only possible for one basic variable, it is necessary to define a leading basic variable in advance and to formulate the dependencies of the other basic variables on this via the LHS simulation field.

The process steps of the FBS procedure are as follows, see Figure 3: (a) generate the LHS-field; (b) perform simulated annealing for correlation; (c) define the leading basic variable (on subset of fractiles) on the sample field with correlation the leading parameter X_L ; (d) determine those realizations which are closest to the pre-defined fractiles (e.g., 5%, 15%, ..., 95%); (e) select the sample sets associated with the pre-defined fractiles of the leading parameter X_L ; (f) perform the deterministic simulation of each subset; (g) collect the results of the system response X_R and order it according to the pre-defined fractiles; (h) perform a PDF-fitting; (i) perform sensitivity analysis to (I) the original LHS-field $\rho_{\alpha_{LHS}}$ and (II) the reduced FBS-field $\rho_{\alpha_{FBS}}$; (f) check leading parameter $|\rho_{\alpha_{LHS}} - \rho_{\alpha_{FBS}}| \leq error$.

More details regarding the appropriate selection of the leading basic variable are provided in [29].

The Estimation of Coefficient of Variation of Resistance method (ECOV) seems to be a further reduction to two p_i s as it is proposed in the FBS, but it is a simplified probabilistic procedure in which the random variation of resistance is estimated using only two samples. It is based on the idea that the random distribution of resistance, which is described by the COV, can be estimated from the mean and characteristic values e.g., 5%-fractile of resistance, see Figure 4. The method is not based on an LHS sampling field and hence does not take into account the correlation between basic variables but takes from all basic variables the, e.g., 5%-fractile or 50%-fractile.

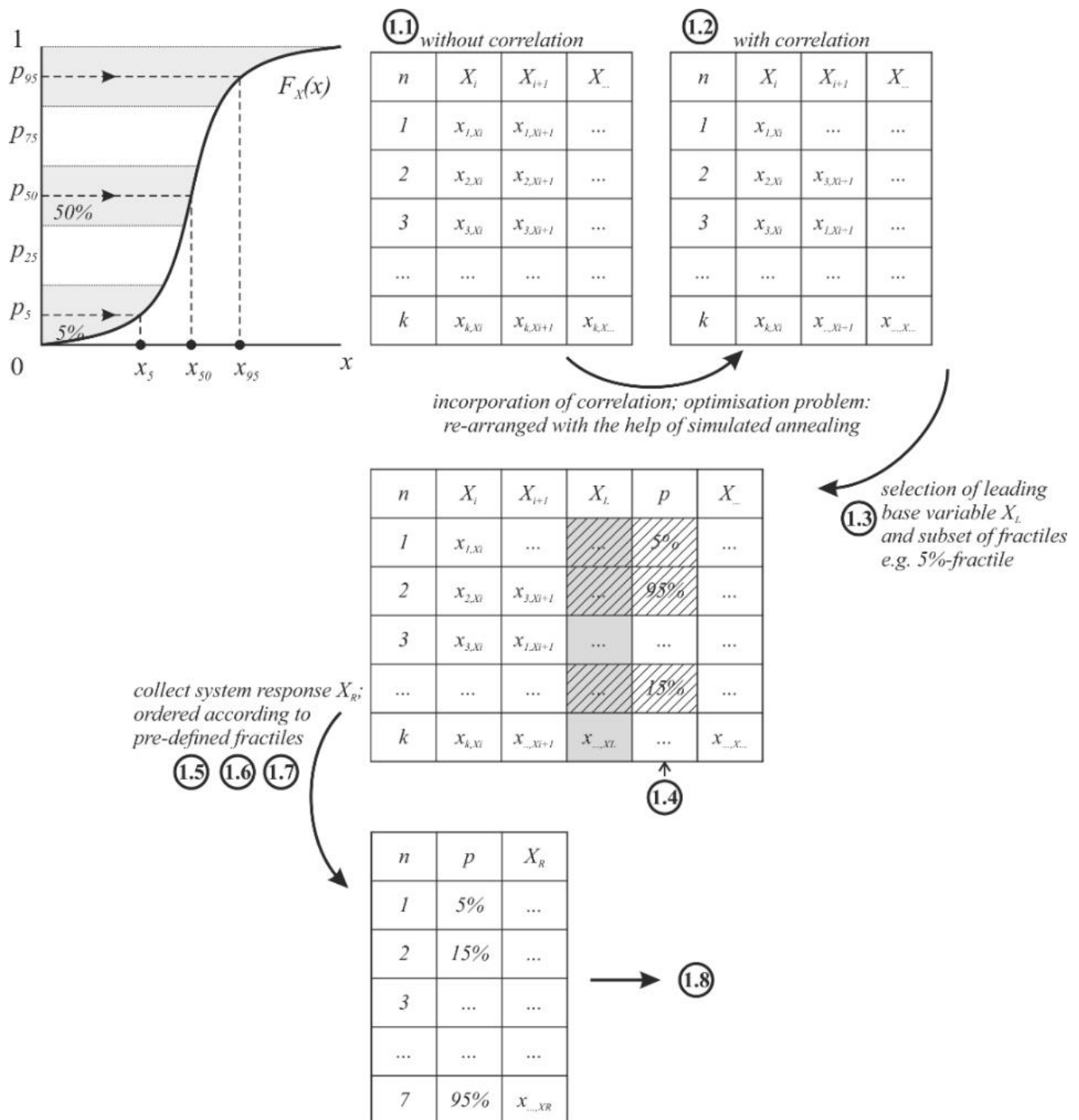


Figure 3. Fractile Based Simulation (FBS) method procedure including and not including correlation between basic variables—including the process steps.

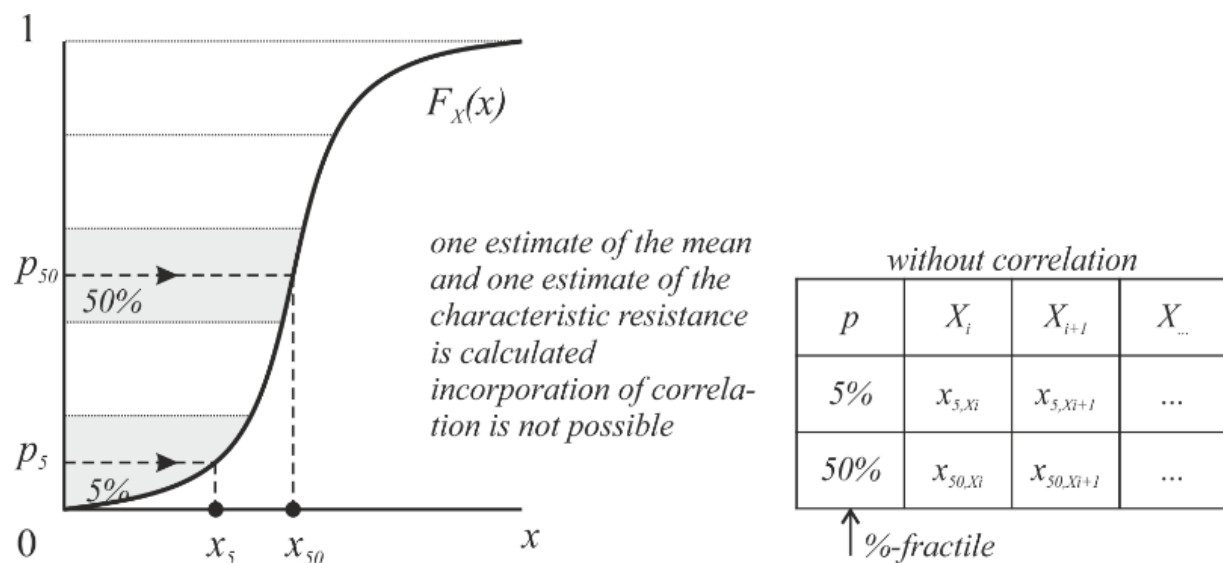


Figure 4. ECOV simulation procedure not including correlation between basic variables.

3. Investigated Columns

The geometric layout of the following columns, which were tested experimentally and numerically analyzed in a non-linear way, was chosen because it was found that the stability failure of compressed slender concrete columns occurred before reaching the material capacity in the critical cross-section when calculated using a non-linear numerical format. The procedures outlined in Section 2 were used for an initial assessment.

3.1. Layout and Test Results

The studies and analyses are based on the following experimental research for validating non-linear calculations for slender column elements. Several series of tests on slender columns were carried out and the failure loads were compared to the results of non-linear analyses and simplified formats.

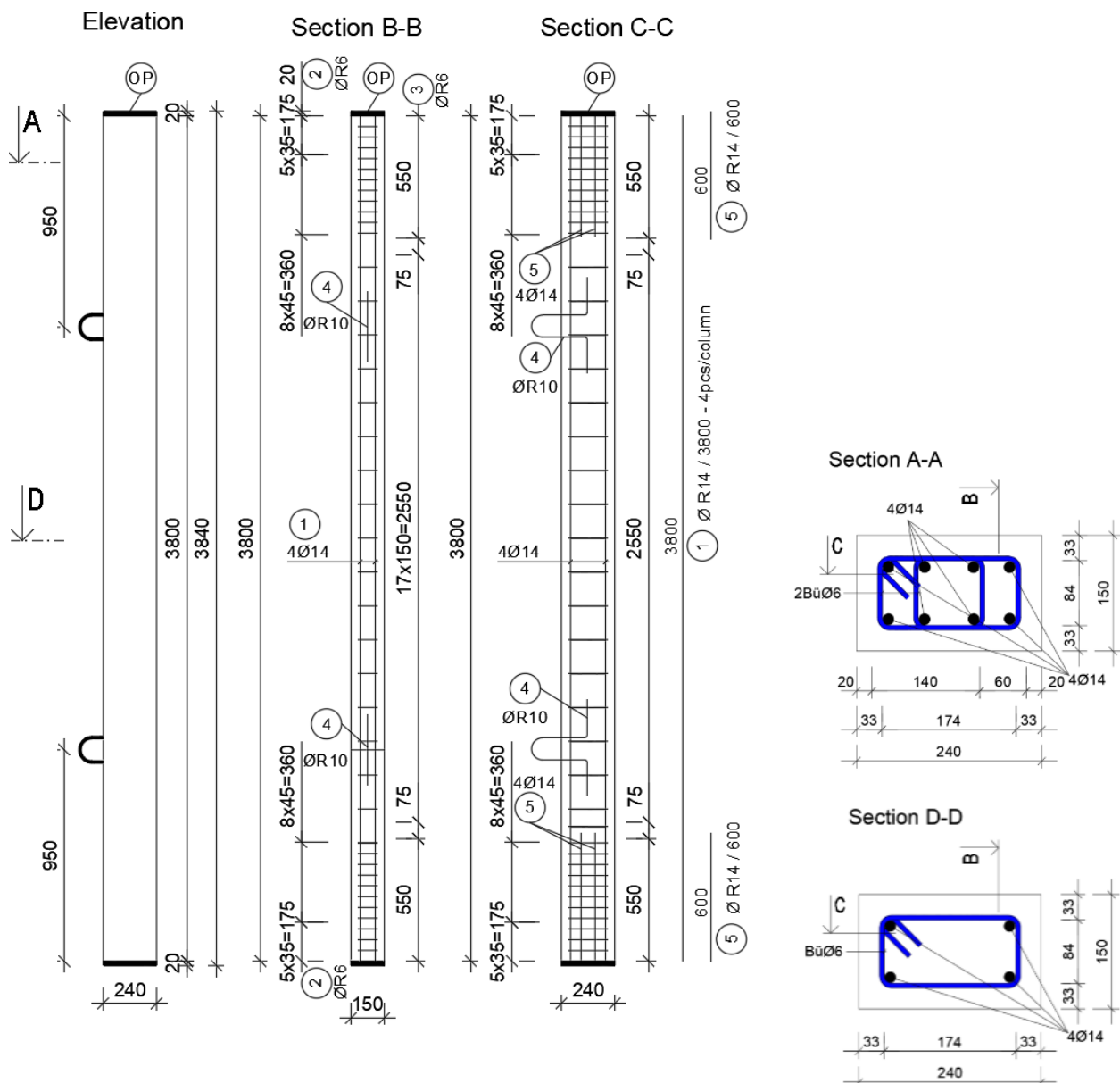
The concrete material used to construct the first series of slender columns is C45/55 while the steel used is BST 500B. In the first series, 6 columns (see also [4]) were tested. Figure 5 shows the cross-sectional dimensions and layout of the tested columns while Table 1 lists the parameters used in the calculation according to different codes. Figure 6 presents the results of the experiments while Table 2 lists the descriptive parameters used for the slender columns.

Table 1. List of parameters used in the calculation.

Description	Symbol	Unit	Value
Width of column cross-section	b	mm	240
Height of column cross-section	h	mm	150
Distance from topmost compression face to the centroid of compression reinforcement	d'	mm	33
Distance from topmost compression face to the centroid of tensile reinforcement	d	mm	117
Cross-sectional area of RC column	A_c	mm ²	36,000
Cross-sectional area of tensile reinforcement	A_s	mm ²	307.88
Cross-sectional area of compression reinforcement	A'_s	mm ²	307.88
Characteristic compressive strength of concrete (for assoc. parameters see table in Section 4.5)	f'_{ck}	N/mm ²	55
Yield strength of reinforcing reinforcement	f_{sy}	N/mm ²	500
Young modulus of reinforcing reinforcement	E_s	N/mm ²	200,000
Ultimate strain of concrete in compression	ϵ_{cu}	-	Varied
Ratio of the depth of equivalent compression block to that of actual compression	β	-	Varied
Eccentricity	e	mm	40

Table 2. Descriptive statistical parameters of the experimental results of the considered test series C45/55 without considering sample size aspects.

Test	N_{max} (kN)	e_2 (mm)	M_{max} (kNm)
S1-1	324.4	57.6	31.7
S1-2	323.4	42.7	26.8
S1-3	332.6	38.3	26.0
S1-4	271.2	58.4	26.7
S1-5	296.0	59.4	29.4
S1-6	311.4	55.0	29.6

**Figure 5.** Reinforcement and formwork drawings of the investigated slender columns.

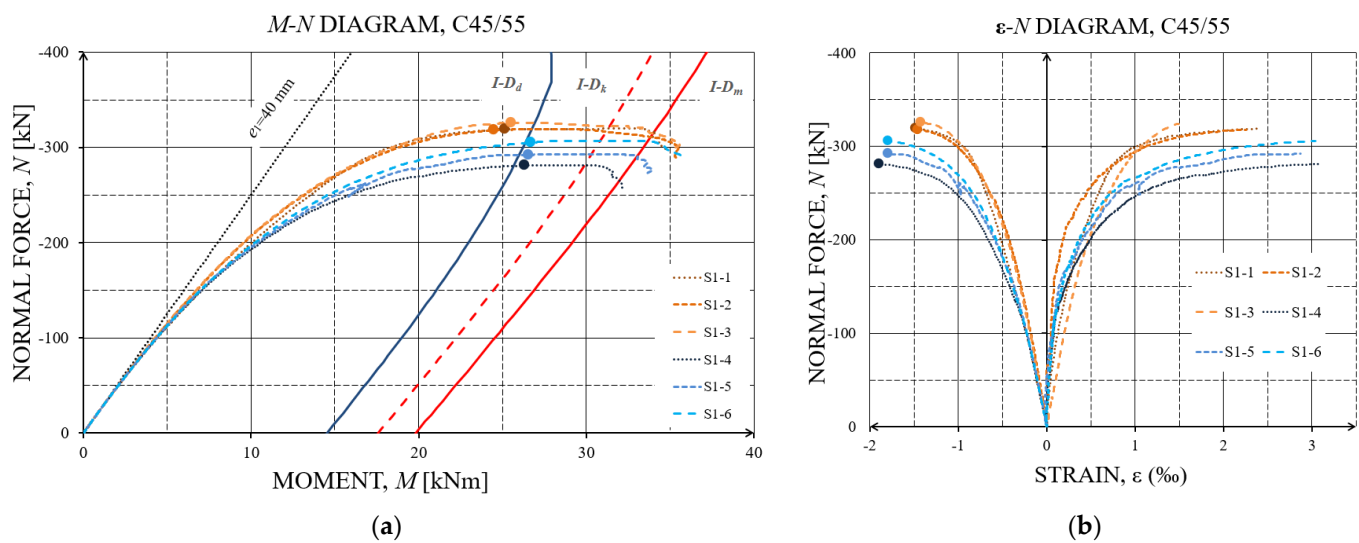


Figure 6. Experimentally determined N-M gradients vs. the Eurocode I-D (blue graph = design values, red dashed graph = characteristic values, red graph = mean values) (a) and normal force—strain (b) of the specimens S1-1 to S1-6.

The points shown in Figure 6 represent the tested maximum axial force capacity N_{max} of each single column. All of the maximum $N-M$ gradient points show the system stability failure before the mean $I-D$ (left from the $I-D_m$) as defined in EN 1992-1-1 [8]. The right-hand graphic of Figure 6 shows the load-vs.-strain graphs in the fracture-prone cross-section at half the height of the columns. The concrete compressive strains in the compressed fiber of the cross-section were recorded for the column stability loss at between 1.4 and 1.8‰ and were far away from the permissible concrete compressive strains of 3.5‰. The associated concrete/reinforcement tension strains in the pulled fiber of the cross-section were recorded at between 1.4 and 3.1‰, see Figure 6. The model uncertainties of the experimental test results were derived following [30] and EN1990 Annex D (Edition: 2013-03-15) with $\theta_Y = Y_{mean}/Y_k$. This results for N_{max} to $\theta_{N_{max}} = 1.06$, for e_2 at N_{max} to $\theta_{e2, N_{max}} = 1.02$, and for M at N_{max} to $\theta_{M, N_{max}} = 1.01$.

Based on the results from the experimental investigations, see Figure 6, and the previously discussed model uncertainty factors, the following design values of the resistance can be determined according to [4]:

$$N_d = \frac{N_m}{\gamma_{Rd}\gamma_R} = \frac{292.9}{1.06 \cdot 1.212} = 227.98 \text{ kN}$$

and

$$M_d = \frac{M_m}{\gamma_{Rd}\gamma_R} = \frac{28.6}{1.06 \cdot 1.292} = 20.89 \text{ kNm} \quad (8)$$

In addition, details of the column layout and test results of the columns made from C100/115 are also documented in [5,6]

3.2. Reliability Assessment

The current status of the standards includes a certain degree of prescribed safety, defined by partial safety factors within safety concepts, for the calculation and design of structural elements. The reliability levels and target reliability index are dependent on the consequences classes and the costs of safety measures, along with the reference period, both in EN 1992 [8] and the Model Code [27]. In general cases, an annual safety index of $\beta = 4.7$ or a failure probability of $p_f = 10^{-6}$ is defined as the minimum requirement for the bearing capacity of structures.

In the subsequent studies on the presented laboratory tested columns, the EN 1992 [9] and the Model Code [27] design-safety formats serve as a reference. These standards and design formats characterize interaction diagrams ($I-D$) which allow the determination of the permissible axial load and its corresponding moment for a pre-defined column

geometry and specific material properties. In particular in this contribution, the analytical formulations according to EN 1992 on the one side and non-linear finite element analyses approaches according to EN 1992 on the other side were used for the probabilistic computation of N - M gradients and the existing reliability/safety of the columns by using the proposed I - D s as thresholds, see also [4].

In other words, the analytical formulations of EN 1992 [8] and the Model Code [27] were converted in a first step into corresponding limit state equations [1] and probability distribution density functions were assigned to descriptive variables of these equations. The resistance thresholds in the axial forces and/or moments necessary for appropriate formulation of the limit state equations in the form of PDFs were derived from the aforementioned I - D s and the descriptive quantities of the associated basic variables from [31]. Finally, FORM and LHS methods, as presented in Section 2, were used to carry out the reliability and the sensitivity analyses.

In a further step, the reliability and the sensitivity analyses were also performed for the N - M gradients with respect to the associated I - D s by using the non-linear finite element (NLFEM) elaborations [3,32]. These probabilistic NLFEM studies, as allowed in EN 1992-1-1 [8], also primarily served to evaluate the proposed safety factors for NLFEM considerations [33].

4. Probabilistic Analyses

The following formulation was considered in general as the limit state function for probabilistic analysis and for the investigation of the safety level or reliability index:

$$g(x) = K_R \cdot R - K_E (g + q) \quad (9)$$

where K_R is the model uncertainty related to the resistance, R denotes the resistance of the respective scenario in terms of ultimate load bearing capacity, K_E is the model uncertainty related to the loads, represents the permanent loads acting on the structure while q represents the imposed service loads. In the following, the probabilistic models of the different variables in these equations are discussed.

All of the variables shown in Equation (9) on the right are basic variables which are described using PDFs. Depending on the analysis method, e.g., (a) based on the analytical formulation of the code regulations or (b) based on the NLFEM studies, the resistance side ($K_R \cdot R$) in Equation (9) corresponds to the interaction diagram (I - D) which corresponds to the function of the maximum permissible N - M values, while the action side ($K_E \cdot (g + q)$) of Equation (9) corresponds to the acting N - M load path so that the intersection of the N - M load path with the I - D characterizes the maximum permissible N - M values; further details can also be found in [33,34]. Both strategies have it in common that the model uncertainties are taken into account in determining the necessary partial safety factors.

4.1. Slenderness

The load-bearing capacity of slender columns is significantly influenced by their slenderness. The slenderness of a column is given by:

$$\lambda = \frac{l_o}{i} \quad (10)$$

where:

i is the minimum radius of gyration: $i = \sqrt{I_c/A_c}$

I_c is the moment of inertia

A_c is the concrete cross-sectional area

l_o is the effective length of the member which can be assumed to be:

$$l_o = \beta \cdot l_w \quad (11)$$

where:

l_w is the clear height of the member

β is a coefficient which depends on the support conditions.

As can be seen from above, the actual length of the overall system l_w is included in the slenderness evaluation via the equivalent length l_o . The procedures for determining the equivalent length (nomograms) have been adopted in Eurocode 2 along with the routines for determining the β value. In addition, the verification of the load-bearing capacity is carried out in the critical cross-section in the following outlines of simplified procedures.

4.2. Simplified Design Formats

In the absence of a more rigorous approach, Eurocode 2 allows the calculation of the design resistance in terms of axial force for columns in plain concrete and lightly reinforced concrete (where the reinforcement provided is less than the minimum required for reinforced concrete) as follows (Chapter 12.6—EN 1992-1-1 [8]):

$$N_{Rd} = b \times h_w \times f_{cd,pl} \times \left(1 - 2 \frac{e_{tot}}{h_w}\right) \quad (12)$$

where:

N_{Rd} is the axial resistance

b is the overall width of the cross-section

h_w is the overall depth of the cross-section

$f_{cd,pl}$ is the design compressive strength for plain concrete

$$\alpha_{cc,pl} = 0.8$$

$$f_{cd,pl} = \alpha_{cc,pl} \cdot f_{ck} / \gamma_c \quad (13)$$

where:

$$e_{tot} = e_0 + e_i \quad (14)$$

e_0 is the first order eccentricity including, where relevant, the effects of floors (e.g., possible clamping moments transmitted to the wall from a slab) and horizontal actions.

e_i is the additional eccentricity covering the effects of geometrical imperfections.

The slenderness defined in Equation (10) is explicitly included in Equation (14).

Other simplified formats may be used provided that they are not less conservative than a rigorous method. EN 1992-1-1 [8] identifies four different approaches for deriving the design capacity of slender columns: (a) the '*nominal curvature*' method where second-order moments are determined from an estimation of the column curvature. These second-order moments are added to the first-order moments to provide the total column design moment; (b) the '*moment magnification*' method where the design moments are obtained by factoring the first-order moments; (c) a *second-order analysis based on the nominal stiffness* values of the beams and columns that, again, requires computer modeling and iterative analysis; (d) a *general method* based on a non-linear analysis of the structure and allowing for second-order effects which requires the use of computer analysis. The first three methods belong to the aforementioned simplified ones. The simplified verification procedures are therefore generally divided into the following main steps: the determination of (a) the buckling length l_o , see Section 4.1, (b) the slenderness λ , (c) the load center of the action $e_o = M_{sd} / N_{sd}$, (d) the unwanted eccentricity e_a , (e) e_2 (theory II order effects), (f) $e_{tot} = e_o + e_a + e_2$ and (g) dimensioning for N_{sd} and $M_{sd} = N_{sd} \cdot e_{tot}$ using a μ - ν diagram or Equations (12)–(14).

4.3. Non-Linear Analysis Formats

EN 1992-1-1 [8] also allows non-linear formats of analysis (e.g., Non-Linear Finite Element Analyses formats) for the design and recalculation of columns for both ULS and SLS provided that equilibrium and compatibility considerations are satisfied and an

adequate non-linear behavior for materials is assumed. The analyses may be performed considering first or second order effects where: (a) at the ultimate limit state, the ability of local critical sections to withstand any inelastic deformations implied by the analysis should be checked, taking appropriate account of uncertainties; (b) for structures predominantly subjected to static loads, the effects of previous applications of loading may generally be ignored and a monotonic increase of the intensity of the actions may be assumed; and, (c) the use of material characteristics which represent the stiffness in a realistic way and where the consideration of uncertainties in material characteristics is of paramount importance.

4.4. Simplified Basic Variables X_i

For the probabilistic analyses of the slender columns according to the simple methods mentioned above, as well as according to the non-linear analysis format, it is necessary to examine and characterize the variables, which are considered decisive in the probabilistic analyses in terms of their properties, as random variables. Table 3 shows the basic variables considered in simplified verification formats and in the non-linear considerations with their distribution functions and the associated statistical descriptive parameters. All random variables are considered statistically independent, i.e., uncorrelated.

4.5. Elements of the Limit State Formulations

As a first step, the resistance of the cross-section was calculated according to standard EN1992-1-1 which enabled the drawing of the N - M gradient lines for the given cross-section for the characteristic, design and the mean values of the resistance parameters.

The resistance mechanism of the reinforced concrete cross-section must be known in order to make the load capacity assessment, as shown in Figure 7. The calculation algorithm was used to obtain the interesting cross-section moments from different normal forces. When assessing a slender column according to EN 1992-1-1 [8], creep is accordingly taken into account by a global factor. The relationship between the normal force applied to a slender column and the resulting bending moment is defined as:

$$M_{ed} = N_{ed} \cdot (e_0 + e_i + e_2) \quad (15)$$

where M_{ed} is the design bending moment, N_{ed} is the design normal force, e_0 is the initial eccentricity of the applied load, e_i is the eccentricity caused by geometric imperfection and e_2 is the eccentricity caused by second-order deformation of the system (i.e., slender column). The limits of the concrete pressure zone x_{lim} and $F_{cd,lim}$ are computed by:

$$x_{lim} = \frac{700 + d_{[m]}}{f_{yd[N/mm^2]} + 700} \quad (16)$$

Since the analyses on the component consisting of the material C100/115 are of the same interest, as the influence of the material properties on the stability problem of interest can be shown, the input parameters for the probabilistic analyses for the material C100/115 were developed in an analogous way as for the C45/55 in Table 3.

$$F_{cd,lim} = 0.8095 \cdot x_{lim} \cdot b_{Zug} \cdot f_{cd} \quad (17)$$

where b_{Zug} is the section height under tension. For the control as to whether predominantly bending failure takes place can be tracked by:

$$x = 1.202 \cdot \left(d - \sqrt{d^2 - \frac{2.055 \cdot M_{s1}}{b \cdot f_{cd}}} \right) \quad (18)$$

if

$$0 \leq x \leq x_{lim} \quad (19)$$

then the failure can be considered predominantly determined by bending.

The integrated pressure zone then results in:

$$F_{cd} = 0.8095 \cdot x \cdot b \cdot f_{cd} \quad (20)$$

and with the obtained force, it is now possible to determine the reinforcement for a cross-sectional side (with uniaxial bending).

$$A_{s1} = \frac{F_{cd} - N_{ed}}{\sigma_{s1}} \quad (21)$$

Using the equations presented, it is now possible for different M to determine the associated N for a given cross-section and reinforcement. The derivation was carried out for the design, characteristic and the mean resistance parameters. For the probabilistic calculation, 30 samples were generated from the mean values, the corresponding standard deviations and the distribution of the main random variables (see Table 3). These samples yielded 30 random values for X_1 to X_{11} . For these randomly generated values, the cross-sectional resistance was then calculated (see Table 3, bottom part) allowing the creation of a point cloud around the mean I - D as shown in figure in Section 4.7.

Table 3. Input parameters for the probabilistic analyses of the EN 1992-1-1 closed formulations provisions and the EN 1992-1 Non-Linear Finite Element provisions of the slender column made of C45/55.

X		Variable	Dis. **	Unit	X_k	μ	σ
C45/55							
X_1	$E_{ci}^{a,b,c}$	Initial tangent concrete modulus of elasticity	LN	GPa	37.5	37.5	4.91
X_2	$E_s^{a,b,c}$	Reinforcing steel modulus of elasticity	D	GPa	200	200	-
X_3^*	A_{s1}^b	Reinforcement area	N	cm ²	3.08	3.08	0.062
X_4^*	A_{s2}^b	Reinforcement area	N	cm ²	3.08	3.08	0.062
X_5^*	H^b	Height	N	cm	15.0	15.0	0.30
X_6^*	B^b	Width	N	cm	24.0	24.0	0.45
X_7^*	d^b	Axis distance of reinforcement	LN	cm	3.30	3.30	0.50
X_8^*	d_2^b	Axis distance of reinforcement	LN	cm	3.30	3.30	0.50
X_9^*	e_1^b	Eccentricity	N	cm	4.00	4.00	0.10 ***
X_{10}^*	$\varepsilon_{c,1}^b$	Strain at max. compressive stress	LN	‰	−2.40	−2.40	0.11
X_{11}	$f_c^{a,b,c}$	Concrete compressive strength	LN	MPa	45.0	53.0	5.13
X_{12}	$f_{ct}^{a,b,c}$	Concrete tensile strength	LN	MPa	2.7	3.8	0.78
X_{13}	$G_F^{a,b,c}$	Concrete fracture energy	LN	MPa	104	149	30.8
X_{14}	$\varepsilon_{c,lim}^{a,b,c}$	Ultimate strain	LN	‰	−3.50	−3.50	0.10 ***
X_{15}	$\varepsilon_{ct,max}^{a,b,c}$	Maximum tensile strain	LN	‰	0.15	0.15	0.10 ***
X_{16}	k_1^b	Tension stiffening factor (fct)	LN		0.6	0.6	0.10 ***
X_{17}	k_2^b	Tension stiffening factor ($\varepsilon_{ct,max}$)	LN		5.0	5.0	0.10 ***
X_{18}	$f_y^{a,b,c}$	Reinforcing steel yield strength	LN	MPa	500	548	40.0
X_{19}	k^b	Ratio (ft/fy)k for ductility class B	D	‰	1.08	1.08	-
X_{20}	ε_u^b	Strain at max. tensile stress	D	‰	50	50	-
X_{21}	$L^{a,b,c}$	Length	D	M	1.92	-	-
X_{22}	θ_R^b	Resistance model uncertainty	LN	-	1.00	1.00	0.10 ***
Variables for each step of the analysis at the system level—obtained from non-linear analysis in Sofistik software							
X_{23}	$\varepsilon_{c,c}^b$	Concrete compressive strain	D	‰	Software-based		
X_{24}	$\varepsilon_{c,t}^b$	Concrete tension strain	D	‰	Software-based		
X_{25}	N^b	Axial acting force	D	kN	Software-based		
X_{26}	α_v^b	Concrete force associated coefficient	D	/	Calculated		
X_{27}	k_a^b	Concrete compressive border zone associated coefficient	D	/	Calculated		
X_{28}	e_2^b	Second-order eccentricity	D	Mm	Software-based		

(*) Variables are shown graphically in Figure 7; (**) normal distribution, N; log normal distribution LN, deterministic value, D; (***) values determined by an expert appraisal; (a) values used for the standard based analyses (Section 4.7); (b) values used for the cross-section analyses (Section 4.6.1); (c) values used for the component analyses (Section 4.6.2).

4.6. Sensitivity Analyses

The aim of a sensitivity analysis is to determine the relative significance of each random variable in its effect on the stability of the slender column. The analysis was performed at two levels: at the cross-sectional level (parameters used for the verification of the cross-section load-bearing capacity) on the one hand and at the system level (parameters used for the verification of the column load-bearing capacity) on the other hand. The sensitivity analyses were performed for concrete strengths C45/55 and C100/115.

4.6.1. Cross-Sectional Level

Sensitivity analysis at the cross-section level is performed based on the FORM probabilistic method for reliability analysis. The Limit State Equation (LSE) is defined as an equilibrium equation for the cross-section simultaneously exposed to axial force and bending moment. Equilibrium of inner forces (Figure 7) is achieved when both the sums of bending moments and axial forces are equal to zero.

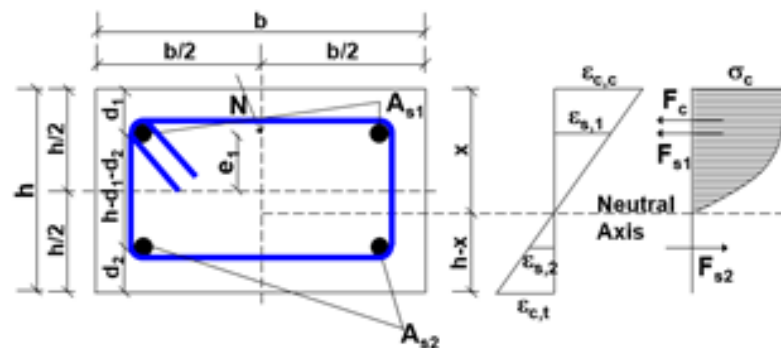


Figure 7. Column cross-section with strains, stresses and inner force diagrams.

The axial force applied to the column is equal to the sum of forces in the concrete and steel reinforcement:

$$N = F_c + F_{s1} - F_{s2} \quad (22)$$

and the LSE for cross-sectional analysis is then equal to the sum of moments:

$$\sum M = F_c \cdot k_c + F_{s1} \cdot k_{s1} + F_{s2} \cdot k_{s2} - N \cdot k_N = 0 \quad (23)$$

where:

$$k_c = x \cdot k_a; k_a \quad (24)$$

$$k_{s1} = x - d_1 \quad (25)$$

$$k_{s2} = h - x - d_2 \quad (26)$$

$$k_N = e_1 + e_2 + x - h/2 \quad (27)$$

The probabilistic analysis was conducted for multiple steps where the normal force was increased incrementally in each step in order to compute the sensitivity factor of each random variable, as detailed in Table 3, and their variations with different load sizes. The sensitivity factor values α_i are used to provide the relative importance of each individual random variable. By definition, the sum of squares of sensitivity factors for each random variable is equal to 1:

$$\sum_{i=1}^n (\alpha_i)^2 = 1 \quad (28)$$

Figure 8a shows the sensitivity analyses and sensitivity factors, calculated via the First Order Reliability Method (FORM), versus N/N_{max} with $N_{max} = 335.5$ kN while Figure 8b shows the maximum and minimum strains in the column longitudinal axis up to the maximum bearing capacity of $N = 335.5$ kN for the column made of C45/55. It

can be seen from the graphs that at the beginning of the loading procedure, the concrete modulus of elasticity $X_1(E_{ci})$ has a major impact on results but as the force increases, its impact diminishes as the concrete is entering a non-linear state of behavior. Due to small uncertainties in the statistical parameters of areas of reinforcement, their impact on the results can be neglected. The axis distance of reinforcement in compression $X_7(d_1)$ has a major impact at the beginning of the loading, but reduces as the force increases, while the impact of axis distance of reinforcement in tension $X_8(d_2)$ increases with the force and deformation of the concrete in tension. Its impact reaches its peak values as the concrete deformation in tension reaches its maximum, just before the cracking of the concrete. The impact of the concrete compressive strength $X_{11}(f_c)$ increases along with the loading and reaches its peak value at the point when the concrete deformation in compression and tension are equal (absolute values). After the peak (when the force is around 280 kN), its impact decreases as the tension area of the concrete increases.

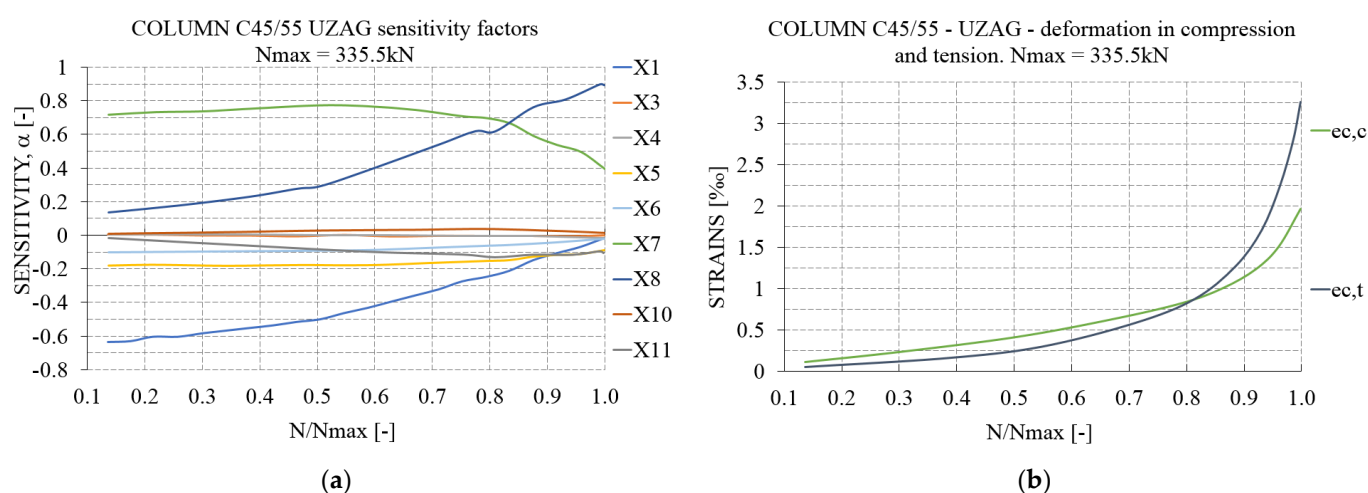


Figure 8. Sensitivity analyses at the cross-section level: (a) sensitivity of material parameters with respect to the applied normalized normal force (maximum bearing capacity of $N = 335.5$ kN); (b) strains in compression and tension with respect to the applied normal force, see also Table 3.

4.6.2. Component Level

The component sensitivity analysis was performed using the advanced Monte Carlo-based Latin Hyper Cube sampling technique with 60 generated column samples of the non-linear numerical finite element model (P-NLFEM). The P-NLFEM was developed by the University of Natural Resources and Life Sciences using ATENA Scientific software [35]. In the course of the step-by-step axial loading process, the basic variables of the model input data were determined for each loading step with a step size increment of $\Delta N = 10$ kN. The development of the sensitivity factors calculated using the Kendal Tau algorithm [36] were analyzed and are plotted as a function of the axial (normal) force N of the column in Figure 9a and the transverse deformation of the column at half the system length in Figure 9b. The Kendall rank correlation coefficient, commonly referred to as the Kendall's r coefficient, was used to measure the ordinal association between two measured quantities, e.g., model input variable i and model response k . The sensitivity analyses according to FORM were not applied here as the Kendal Tau algorithm allows a much simpler handling of the sensitivity considerations for finite element applications. Comparative studies have shown that both methods lead to almost the same results Figure 9d shows the statistical responses of the horizontal column deflections versus the gradually applied normalized axial force N . At the component level, the variables X_7 and X_8 were not taken into account in the sensitivity analyses because (a) the exact locations of the reinforcement were quarantined by an extraordinary quality control during the fabrication of the columns and (b) the influence of the material laws, solution algorithms, non-linear fracture processes and slenderness on the instability process were the focus of interest. As can be seen in

Figure 9a, the modulus of elasticity of the concrete $X_1(E_{ci})$ as well as the compressive strength $X_{11}(f_c)$ dominate in the ultimate failure load in compression. When considering the sensitivity factors with regard to the horizontal deflection in the middle height of the column, see Figure 9b, the tensile strength of the concrete $X_{12}(f_{ct})$ and the compressive strength $X_{11}(f_c)$ both play a significant role initially; however, the modulus of elasticity of the concrete $X_1(E_{ci})$ becomes more important with increasing horizontal deflection. On the basis of the 60 Latin Hyper Cube samples, Figure 9d provides an insight into the scatters in the relationship between the axial force and the horizontal displacement in the middle height of the column, computed in ATENA.

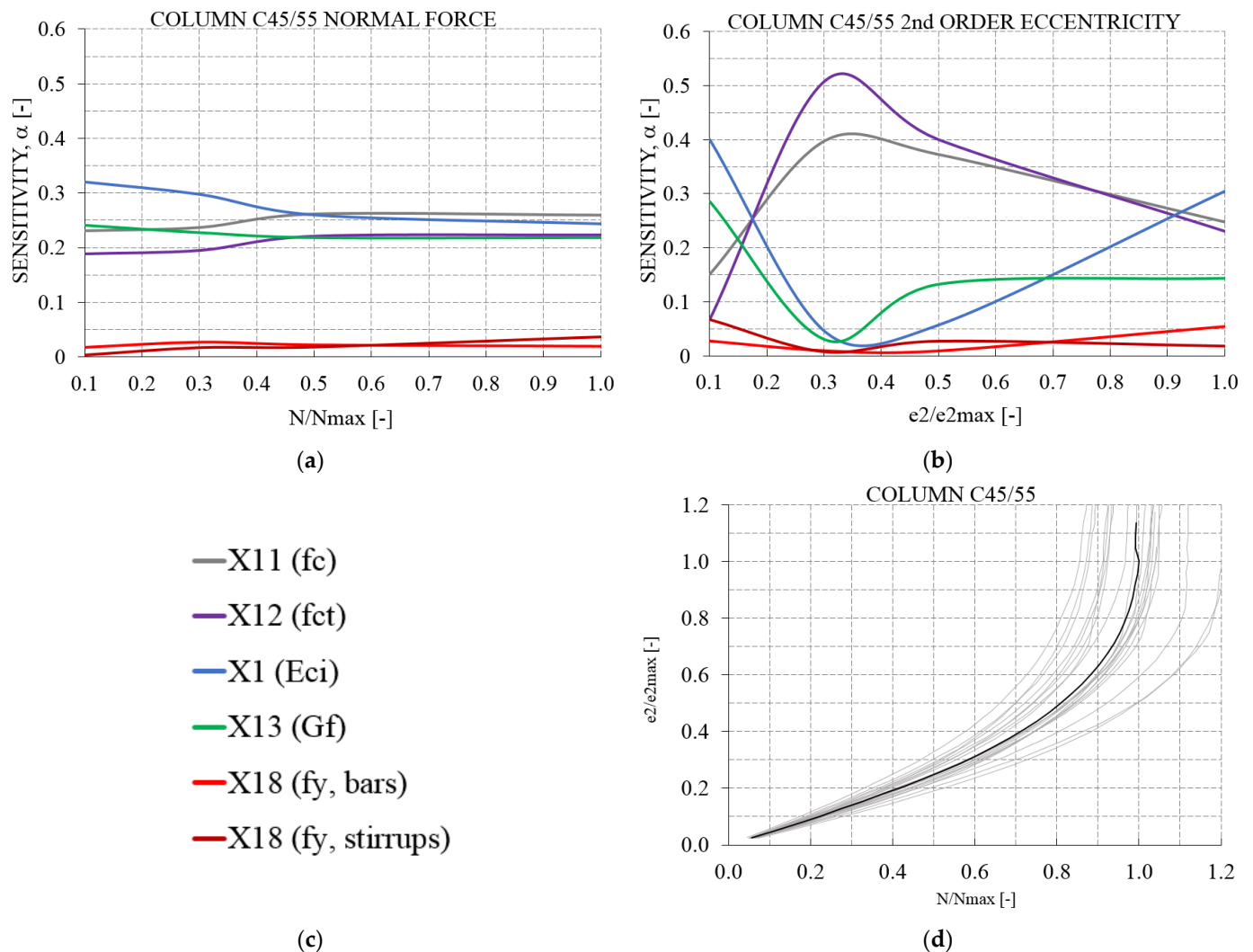


Figure 9. Sensitivity analyses at the component/column level based on the probabilistic non-linear analysis of the considered column made of C45/55, see Section 4.4: (a) sensitivity of material parameters with respect to the normalized applied axial force; (b) sensitivity of material parameters with respect to the normalized horizontal displacement at middle height of the column; (c) basic variables of considered material models; (d) normalized horizontal displacement vs. normalized axial force.

As can be seen from the graph in Figure 10a for the C100/C115 concrete column, the modulus of elasticity of the concrete $X_1(E_{ci})$, as well as the compressive strength $X_{11}(f_c)$ and fracture energy $X_{13}(G_f)$ dominate in the ultimate failure load. When considering the sensitivity factors with regard to the horizontal deflection in the column middle height, see Figure 10b, the tensile strength of the concrete $X_{12}(f_{ct})$ and the compressive strength $X_{11}(f_c)$ both play a significant role as the horizontal displacement increases, however, the modulus

of elasticity of the concrete $X_1(E_{ci})$ and the concrete fracture energy $X_{13}(G_f)$ are initially more important. Figure 10d provides an insight into the scatters in the relationship between the axial force and the horizontal displacement in the middle height of the column made of C100/115 in a similar way as was reported in the previous section for the C45/55 column.

A closer comparison between the sensitivity factor curves of the C45/55 and C100/115 columns shows clear differences. For example, $X_1(E_{ci})$ becomes more important for the normal force analysis with higher strength, see Figures 9a and 10a. For the horizontal deflection sensitivity analysis, $X_1(E_{ci})$ becomes less important and $X_{13}(G_f)$ becomes more important with increasing strength and load, see Figures 9b and 10b.

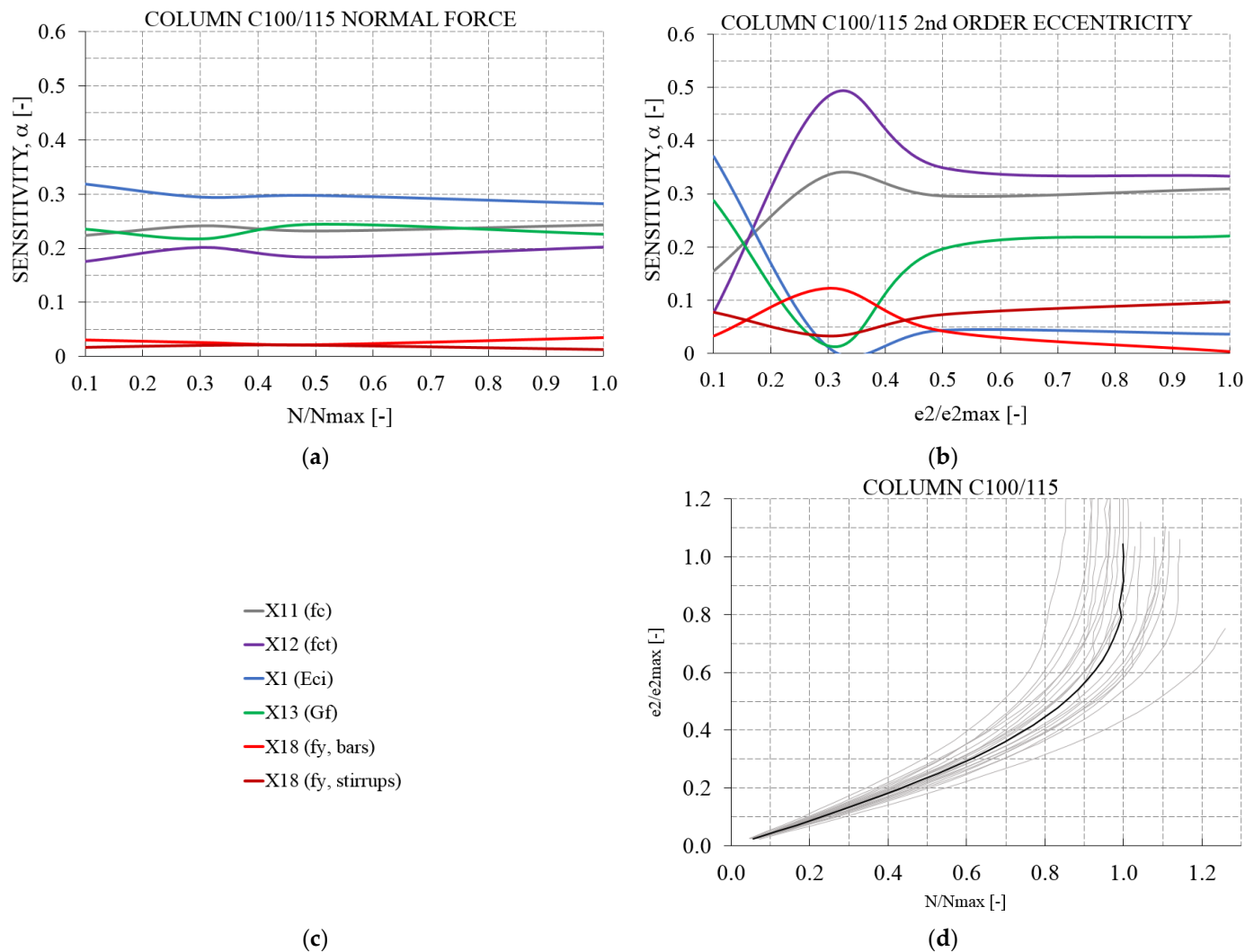


Figure 10. Sensitivity analyses at the component/column level based on the probabilistic non-linear analysis of the considered column made of C100/115, see Section 4.4: (a) sensitivity of material parameters with respect to the normalized applied axial force; (b) sensitivity of material parameters with respect to the normalized horizontal displacement at middle height of the column; (c) basic variables of considered material models; (d) normalized horizontal displacement vs. normalized axial force response.

4.7. Standard Based Analyses

In a first approach to these probabilistic investigations, the focus was on the simplified procedures defined in EN1992-1 [8]. There were recognized calculation methods for these procedures which included semi-probabilistic proof at the design level. The probabilistic analysis was therefore divided into (a) preparation of the verification procedure (nominal stiffness method) for the stochastic procedure, including the removal/correction of the

partial safety factors, and the associated factors, in order to be able to analyze the verification procedure without the safety elements, (b) structuring of the prepared verification procedure in the form of a limit state equation, see Equation (1), and (c) definition of the basic random variables X_i for the limit state equation. For the correlation between the input parameters of the EN1992-1-1 [8], provision was not explicitly discussed, since the provision formulation implements correlations implicitly. For the numerical probabilistic analysis, an explicit definition of the correlations between the input parameters was made according to [31].

Figure 11a shows the scattering failure loads obtained from the EN1992-1 nominal stiffness calculation (pink point set) and the gradients of the tested columns (dashed lines) in relation to the I - D curves constructed according to EN1992-1-1 [8] for the design, characteristic and mean levels. These sets of I - D curves show the theoretical failure of the column in terms of stability when the maxima of the N - M gradients are on the right side of the I - D curves. The analyses were processed according to LHS procedure for 30 samples in which the values in Table 3 served as input characteristics. For a realistic modeling with respect to the interaction diagram, as is the case with EN1992-1-1 [8], non-linear modeling poses a safety/reliability problem. This fact can be seen in Figure 11b where, in the histograms of the maximum normal force associated with Figure 11a, the PDF in pink obtained according to EN1992-1-1 is clearly below the one derived from the experiments (PDF in blue), see also Table 2. For the determination of the PDFs of the test results, the probabilistic results of the optimized NLFEM model [4] have also been considered.

However, when the experimentally obtained blue PDF of the secondary moments are considered, see Figure 11b on the right, they are clearly below the PDF obtained from the standard in pink which partly is on the left side of the I - D as defined according to EN1992-1-1 and hence shows a reliability shortcoming.

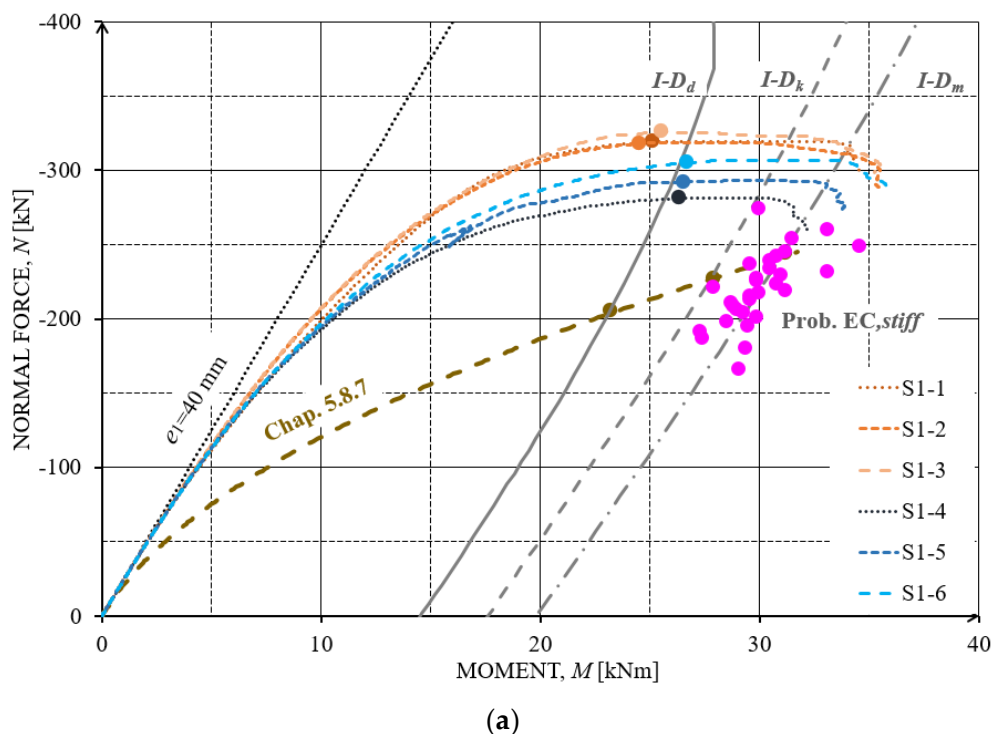


Figure 11. Cont.

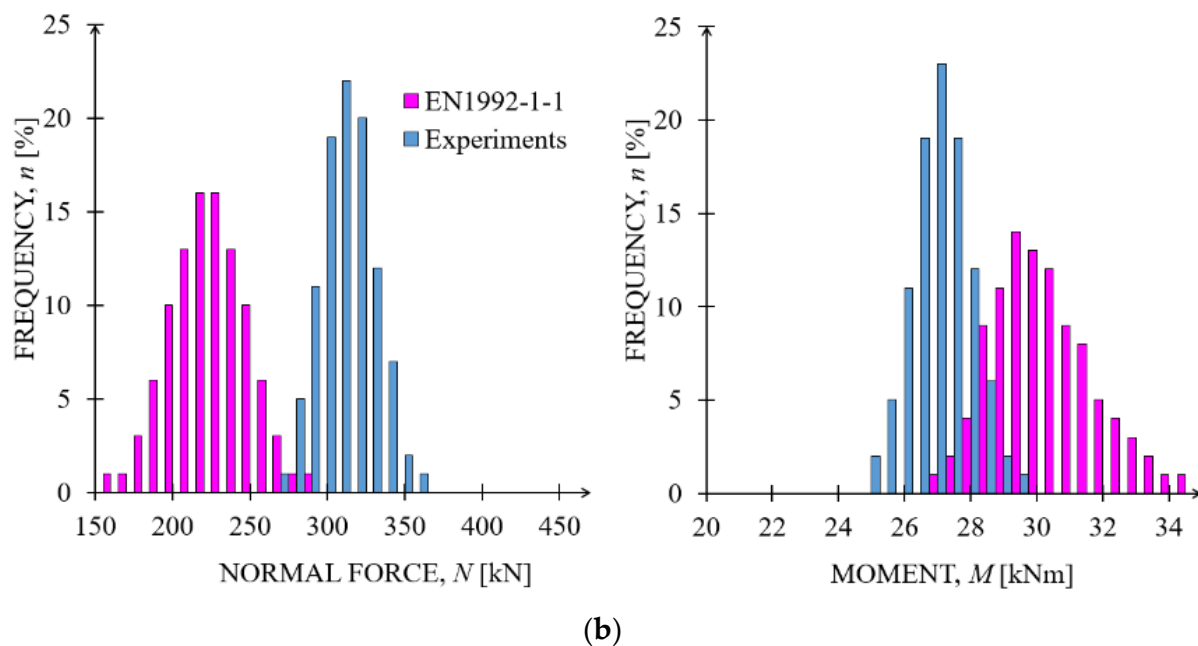


Figure 11. Statistical scattering failure loads obtained according to EN1992-1 nominal stiffness calculations (pink point set). (a) Nominal stiffness calculated and experimental N - M gradients vs. the Interaction Diagrams I - D according to EN1992-1 at the design, characteristic and mean levels, and, (b) histogram of the maximum calculated axial forces (pink) vs. those tested experimentally (blue) and histogram of the maximum calculated moments (pink) vs. those tested experimentally (blue).

4.8. Non-Linear Finite Element Analyses

4.8.1. General

The interest in probabilistic analyses was further extended to non-linear numerical methods suggested in EN1992-1-1, see Section 4.3. For these analyses, we used the non-linear numerical results already carried out in the 1st of this paper series [4] and tested in the form of a multi-stage process.

The probabilistic analysis was carried out as follows: (a) the preparation of the numerical non-linear models for the stochastic procedure including the definition of the random variables (scattering quantities) used in the non-linear numerical analysis for material laws, geometries and loading procedure, see Tables 3 and 4, (b) the formulation of the correlations between the random variables (see Table 5), (c) the implementation of the statistical structural responses of the probabilistic non-linear numerical analyses into the reliability-based verification method in the form of a limit state equation, see Equation (1), (d) the definition of the random variables X_i for the limit state equation, (e) the generation of the n -simulation sets, or sample sets using LHS technique for non-linear finite element calculations (for LHS see Section 2.3, for NLFEM see Section 4.3) based on the probabilistic parameters of the random variables displayed in Tables 4 and 5, (f) the n -fold repetition of the NLFEM computation and the structuring of the statistical system responses in response vectors of dimension n suitable for the reliability assessment and (g) the determination of the reliability and failure probabilities with regard to predefined limit values and the study of the sensitivities of the input base variables with regard to the examined limit state equations.

Table 4. Input parameters for the probabilistic analyses of the EN 1992-1 Non-Linear Finite Element provisions of the slender column made of C100/115 (details regarding C45/55 are provided in Table 3).

X		Variable	Dist.	Unit	X_k	μ	σ
C100/115							
X ₁	E_{ci}	Initial tangent concrete modulus of elasticity	LN	GPa	48.9	48.9	6.23
X ₂	E_s	Reinforcing steel modulus of elasticity	D.	GPa	200	200	-
X ₁₁	f_c	Concrete compressive strength	LN	MPa	100.0	108.0	4.99
X ₁₂	f_{ct}	Concrete tensile strength	LN	MPa	3.7	5.2	1.08
X ₁₃	G_F	Concrete fracture energy	LN	MPa	119	170	35.0
X ₁₈	f_y	Reinforcing steel yield strength	LN	MPa	500	548	40.0

The correlations according to [32] were set up for the numerical simulations as shown in Table 5.

Table 5. Correlation between basic variables for EN 1992-1 Non-Linear Finite Element provisions of the slender columns made of C45/55 and of C100/115 [32].

C45/55 and C100/115							
		E_{ci}	E_s	f_c	f_{ct}	G_F	f_y
X ₁	E_{ci}	1	0	0.7	0.6	0.8	0
X ₂	E_s		1	0	0	0	0
X ₁₁	f_c			1	0.9	0.7	0
X ₁₂	f_{ct}				1	0.5	0
X ₁₃	G_F					1	0
X ₁₈	f_y						1

4.8.2. Pre NLFEM-Modeling

The IABSE Working Commission Group 1 organized a NLFEM round-robin modeling [4] for the previously discussed columns with the following process steps in the context of the amount of accessible information for non-linear modeling: 1st Round-Robin Modeling Process Step: *Deterministic analyses based on the drawings without conformity test results*; 2nd Round-Robin Modeling Process Step: *Deterministic analyses based on the drawings with conformity test results*; 3rd Round-Robin Modeling Process Step: *Analyses based on the drawings with defined input parameters*; 4th Round-Robin Modeling Process Step: *Deterministic analyses based on the drawings with conformity test results and the test results of the column*; 5th Round-Robin Modeling Process Step: *Probabilistic analyses based on the drawings with conformity test results and the test results of the column*. For more details regarding these process steps and a list of the Round-Robin Modeling Experts see [4].

The received deterministic structural responses (4th process step) allowed an unambiguous comparability of the predictions with the experimentally obtained data as shown in Table 2.

The results from the group investigations according to the 1st paper of this paper series can be summarized as follows (see [4]): the 1st Round-Robin Modeling Process Step revealed a modeling uncertainty based on the minimum and maximum values found by the partners for the C45/55 column of $\varphi_{EXP,C45/55} = 1 + (N_{max,NLFEM,C45/55} - N_{min,NLFEM,C45/55})/N_{mean,EXP,C45/55} = 1.14$. This uncertainty was reduced in the 4th Process Step to $\varphi_{EXP,C45/55} = 1.04$, see [4]. For the C100/115 column, the uncertainty improved the $\varphi_{EXP,C100/115}$ from 1.23 to 1.06 in the 4th Process Step. Consequently, the optimized 4th Round-Robin ATENA 3D NLFEM model from the University of Natural Resources and Life Sciences (BOKU) was used for the following probabilistic analyses.

4.8.3. Probabilistic NLFEM-Modeling

The probabilistic modeling based on the BOKU ATENA 3D NLFEM model and the stochastic information of the selected random variables according to Tables 4 and 5 were

carried out with the Structural Analysis and Reliability Assessment (SARA) program package developed in the project “Safety and Reliability Assessment of Structure” [36,37] in which the Latin Hyper Cube Sampling (LHS) method with a sample number of $n = 305$ was used for the development of the input sampling sizes. The significantly increased number of samples compared to the previously described analytical probabilistic analysis results from the fracture processes that occur during the loading process and the clearly pronounced physical and material non-linearities that are also taken into account in the NLFEM analysis. A corresponding convergence analysis in the statistical structure responses already shows correspondingly stable results with an LHS sample number of 105, however, the number of samples was increased to 305 due to the trustworthiness of the results. In total, around 1450 simulations were carried out for all deterministic and probabilistic considerations on the cross-sectional level and on the structural level for the materials C45/55 and C100/115.

The N - M structural response curves from the 305 NLFEM probabilistic analyses are shown in Figure 12a with the maximum values indicated by pink dots.

As can be seen from this bundle of results and the associated maximum values (pink points in Figure 12a, the P-NLFEM results in terms of axial forces are well above the experimental blue values which can also be seen in the corresponding PDF shown in Figure 12a on the right. These P-NLFEM results, which lie above the experimental results, are to be classified as dangerous because the P-NLFEM results lie above the real N -load of the experimental results and, as shown in the previous sections, the experimental failure points. Similar to the analytical predictions based on the interaction diagrams, the NLFEM failure points are also clearly located within interaction curves, and as can be seen in Figure 12a on the right, the NLFEM results are even below the experimental moment lines for some modeling groups. In addition to the probabilistic modeling based on the BOKU ATENA 3D NLFEM model, the probabilistic analyses were also carried out based on the findings of the LHS simulations on the BOKU model and the models from:

STUBA: Slovak University of Technology in Bratislava, Bratislava, Slovakia.

UNIZG-FCE: University of Zagreb Faculty of Civil Engineering, Department of Structural Engineering.

U-MINHO: University of Minho, Institute for Sustainability and Innovation in Structural Engineering (ISISE).

It can be seen from the trend of the mean values (Figure 12b–d) that the maximum values of the normal force from STUBA, UNIZG-FCE and U-MINHO are above the experimental values. The STUBA analyses (PDF) with regard to the moments associated with the normal forces show, as for BOKU, a failure well before the $I-D_m$ on the mean level, see Figure 12b on the right. Such an underestimation of moment capacity was not seen in the simulations of the partners UNIZG-FCE and U-MINHO, see Figure 12c,d. Therefore, we can conclude that BOKU, UNIZG-FCE and U-MINHO came to completely different results for moment distribution. The probabilistic analyses of most of the partners showed that the calculated normal force mean values are significantly higher than the experimentally determined ones, as can be seen from the box whisker plots (P-NLFEM results in pink; experimental results in blue) and the histograms of Figure 12. In these histograms of the normal forces it can also be seen that these differences are smaller in the lower fractile ranges.

By considering a model uncertainty of 1.10, an agreement between the normal force mean values of the P-NLFEM and the experiments can be found, see the graphs in the middle column of Figure 12. Consequently, the lower P-NLFEM fractile values shift below the experimental ones, which is on the safe side. Since these deviations appeared in all simulations of the partners and errors can be excluded in the experiments due to the high quality controls, it is important to clarify which effects in the NLFEM lead to this overestimation of the column performance.

Considering the normal force maxima of the P-NLFEM and the experiments, see Figure 12a–d, it can be seen that the distance in the corresponding moments (at half column

height) to moments of the EN1992-1 interaction diagram ($I-D$) at the mean value level are significant.

These experimental and P-NLFEM detected column collapses in front of or to the left of the $I-D_{\text{mean}}$ according to EN1992-1 indicate a possible defect and possibly safety problems in the $I-D$ formulations too, in particular for the examined columns geometry.

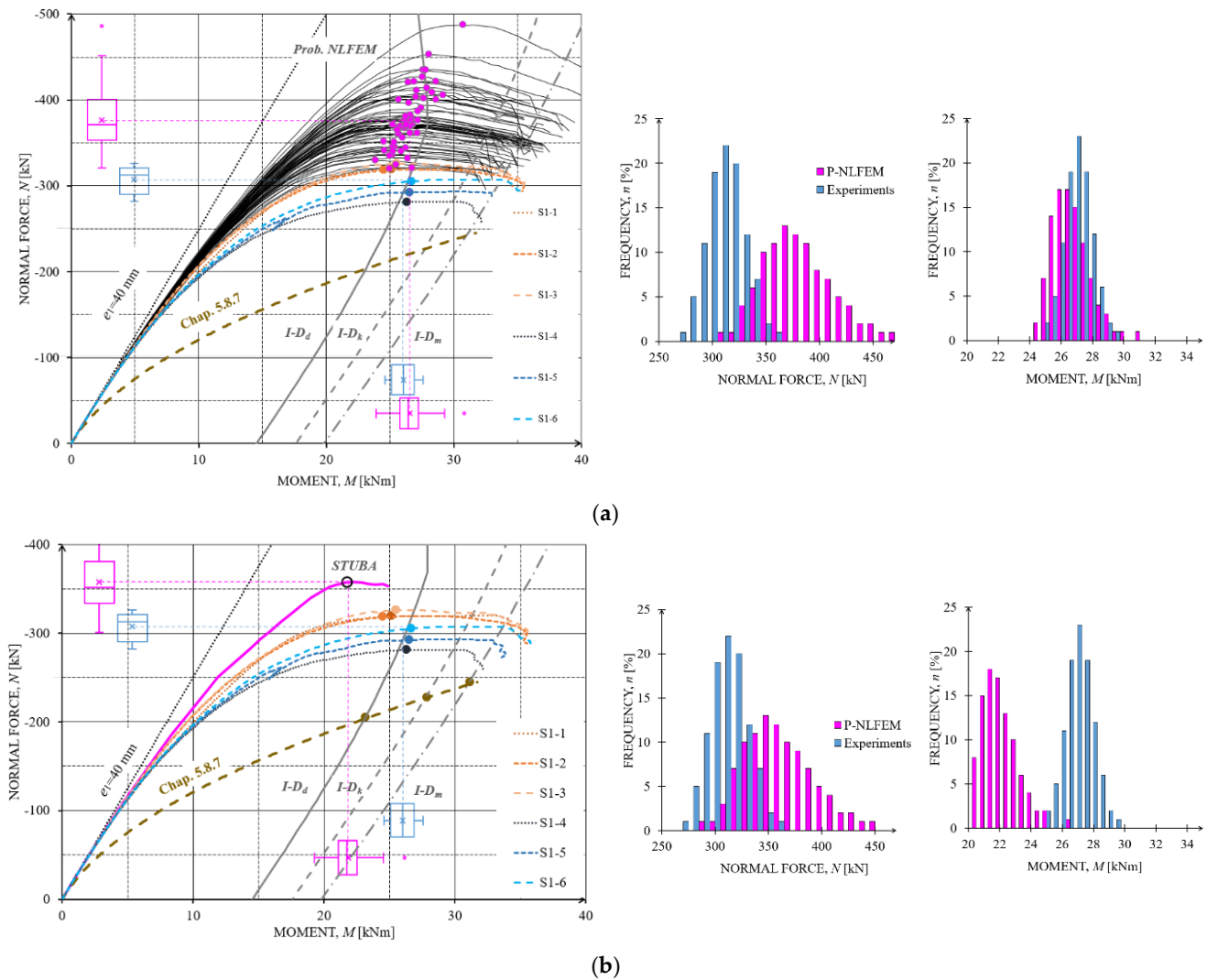


Figure 12. Cont.

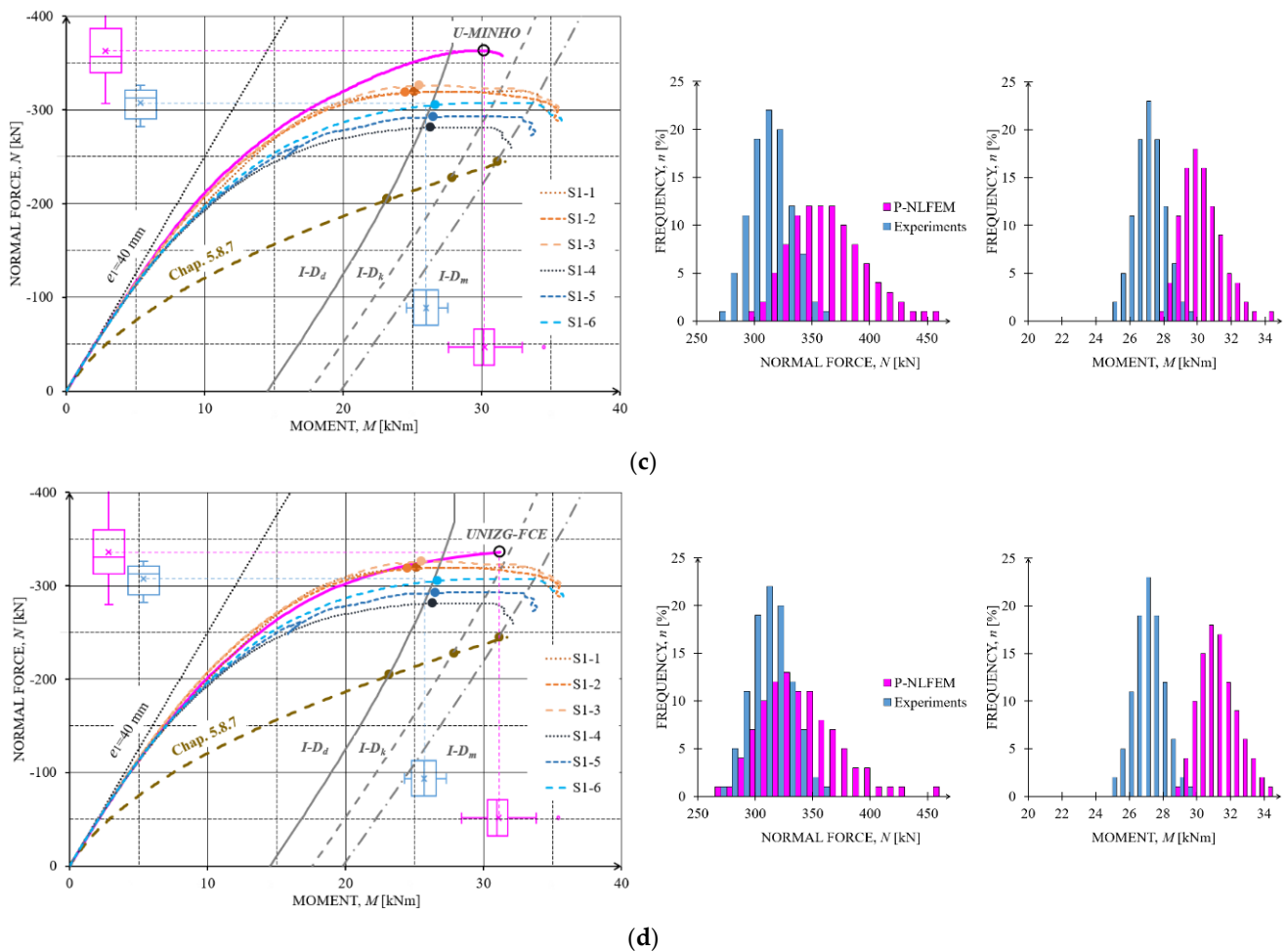


Figure 12. Statistical structural responses and PDFs obtained according to EN1992-1 non-linear finite element analyses: (a) BOKU Group: University of Natural Resources and Life Sciences Vienna, Institute of Structural Engineering, (b) STUBA Group: Slovak University of Technology in Bratislava, Department of Concrete Structures and Bridges, (c) U-MINHO Group: University of Minho, Institute for Sustainability and Innovation in Structural Engineering (ISISE) and (d) UNIZG-FCE Group: University of Zagreb Faculty of Civil Engineering, Department of Structural Engineering.

4.9. ECOV Analyses

According to the ECOV format detailed in Section 2.2, the global resistance factor and the design resistance value for the normal force and moment of the slender columns are computed considering two safety levels characterized by target reliability indexes of 3.8 and 4.2 (see Table 6). These reliability levels have been selected due to the assumption of moderate ($\beta = 3.8$) and low ($\beta = 4.2$) relative costs of safety measures and great consequences of failure for a considered classical public building and a reference period of 50 years according to EN 1990.

Furthermore, two model uncertainty factors were considered for NLFEM. For the nominal stiffness method and the NLFEM, a model uncertainty factor equal to 1.10 was first considered since such models are considered here as high uncertainties given the fact that the NLFEM results have shown poor agreement with the experimental results. Nevertheless, the Model Code [27] recommends a model uncertainty factor of 1.06 for refined numerical analysis such as non-linear finite element analysis since such modeling approaches are regarded as low uncertainties models. Accordingly, calculations considering the low model uncertainty factor for NLFEM are also presented for the purpose of benchmarking.

Table 6. Global resistance factor and design resistance according to ECOV format.

Safety Level		$\beta = 3.8$				$\beta = 4.2$			
		γ_{RN}	N_d (kN)	γ_{RM}	M_d (kNm)	γ_{RN}	N_d (kN)	γ_{RM}	M_d (kNm)
Stiffness Method		1.28	170.27	1.28	21.64	1.32	165.88	1.32	21.08
NLFEM $\gamma_{Rd} = 1.1$	BOKU	1.37	246.33	1.32	17.87	1.41	238.36	1.36	17.35
	STUBA	1.41	228.90	1.24	16.11	1.46	220.81	1.27	15.75
	U-MINHO	1.41	232.15	1.32	20.96	1.46	223.93	1.36	20.35
	UNIZG-FCE	1.32	226.80	1.24	22.70	1.36	220.23	1.27	22.18
NLFEM $\gamma_{Rd} = 1.06$	BOKU	1.37	255.67	1.32	18.54	1.32	247.30	1.32	18.00
	STUBA	1.41	237.49	1.24	16.71	1.41	229.10	1.36	16.33
	U-MINHO	1.41	240.91	1.32	21.75	1.46	232.34	1.27	21.12
	UNIZG-FCE	1.32	235.38	1.24	23.55	1.46	228.51	1.36	23.02
Experiments		1.24	235.41	1.28	20.91	1.23	230.07	1.32	20.37

For exceptional cases when models are validated through assessment of an existing structure and no uncertainties are observed, a model uncertainty factor of 1.10 is recommended. This could be the case for the experimental campaign. Nonetheless, given deviations in the results provided by the experimental campaign, a low model uncertainty factor was considered when applying the ECOV format to the outputs of the experiments.

The ECOV format results are displayed in Table 6 and the model uncertainty factor is of crucial importance. Employing the ECOV method as suggested by the Model Code, and considering a model uncertainty factor of 1.06 and a target safety index of 3.8, leads to an overestimation of the slender column axial capacity for most of the developed NLFEM, except for the model developed by the UNIZG-FCE where the design normal force is below the design value obtained from the experimental campaign results (i.e., 235.41 kN). For the same target safety level when considering a model uncertainty factor of 1.1, the overestimation of the normal force is only observed for the model developed by BOKU. Concerning the higher safety index, i.e., 4.2, the design value overestimation was observed only for the BOKU prediction for high uncertainty models ($\gamma_{Rd} = 1.1$). For low uncertainty models ($\gamma_{Rd} = 1.06$), the overestimation is observed for the U-MINHO and BOKU NLFEM. As previously stated, the nominal stiffness method provides results that are too conservative, with a design normal force representing approximately 70% of the design normal force provided by the experimental campaign results.

According to such findings, higher model uncertainty factors (i.e., $\gamma_{Rd} > 1.1$) are recommended for the design and safety assessment of slender columns using standard NLFEM. Further research is also suggested to investigate more sophisticated numerical models for the prediction of the carrying capacity of slender columns.

5. Conclusions

The work described in this paper was able to show that the geometrical and mathematical non-linear design of slender members, such as columns in the ultimate limit state, is still a matter of controversy because of the known inconsistencies in the design concepts.

The analyses which were carried out show that the stability failure of the investigated compressed slender concrete columns calculated by non-linear numerical format occur before reaching the material capacity in the critical cross-section and hence failure occurs before the scattering Interactions Diagrams (*I-D*) according to EN 1992-1. In addition, the probabilistic non-linear finite element analyses (P-NLFEM), based on an advanced Latin Hyper Cube Sampling technique, indicate that the computed structural responses in terms of axial forces are higher than those derived from experiments, which can be evaluated as a failure to meet the required safety level.

The modeling uncertainties used for this study came from the previous modeling for NLFEM models and were 1.04 for the C45/55 columns and 1.06 for the C100/115 columns. In the following global resistance factor studies, model uncertainties of 1.06 and 1.10 were taken into account.

The global resistance factors determined using the “Estimation of the Coefficient of Variation” (ECOV) and the resulting slender column axial capacity showed, as expected when using a model uncertainty factor of 1.10, an overestimation of the axial capacity for the majority of the columns. According to such findings, higher model uncertainty factors (i.e., $\gamma_{Rd} > 1.10$) are recommended for the design and safety assessment of slender columns using standard NLFEM.

From the sensitivity studies at the cross-sectional level in the middle height of the column on one side and the sensitivity studies of the whole column on the other side, it can be seen that the sensitivities behave very differently in relation to the normal force and the horizontal force. The concrete modulus of elasticity is most significant in relation to the normal force at the cross-sectional level compared to the component level, but its importance diminishes with increasing load. For the horizontal deformations, the sensitivity analyses showed that in addition to the concrete’s modulus of elasticity, they are also influenced by the compressive strength, the tensile strength and the fracture energy of the concrete. It is also of great interest that the effective influences of these material parameters change significantly with increasing load as well as change their relative positions with regard to levels of influence.

The knowledge gained from this paper permits the conclusions that it is of great importance for the NLFEM and the P_NLFEM to determine the model uncertainty appropriately and that there is a need to adjust the safety formats for the non-linear modeling.

All in all, the probabilistic studies of the non-linear modeling and analyses of the safety format of slender columns investigated in this article show that the present Eurocode provisions for some column geometries can result in not acceptable uncertainties and premature failures. It is therefore recommended to supplement the Eurocode provisions associated with the non-linear numerical analyses formats with additional system safety factors, as it is already the case in some national EN documents.

Author Contributions: Conceptualization, A.S., A.M.I. and A.O.; methodology, A.S., A.M.I. and A.O.; formal analysis, B.T., M.H., N.G., J.D. and D.S.; writing—original draft preparation, A.S.; J.M. and N.G. writing—review and editing, A.S., A.M.I., K.N. and A.O.; Resources, R.W.-W.; Visualization, B.T.; supervision, V.B.; All authors have read and agreed to the published version of the manuscript.

Funding: This research received no explicit external funding.

Institutional Review Board Statement: Not applicable.

Informed Consent Statement: Not applicable.

Data Availability Statement: Data to support the reported results can be found at the University of Natural Resources and Life Sciences, Vienna, Austria; Alfred.strauss@boku.ac.at, University of Zagreb, Faculty of Civil Engineering, Zagreb, Croatia; ana.mandic.ivankovic@grad.unizg.hr.

Acknowledgments: This paper describes work mainly carried out during IABSE activities. The authors would like to acknowledge IABSE Commission 1 for supporting this project, the authors acknowledge the financial support provided by the Interreg project ATCZ190 SAFE BRIDGE. The authors also gratefully acknowledge Scientific Grant Agency of the Ministry of Education. This work was supported by the Slovak Research and Development Agency under the contract No. APVV-15-0658. The authors also would like to express their thanks for the support provided from the Czech Science Foundation project MUFRAS No. 19-09491S. In addition, this work was partly financed by: (1) national funds through the Foundation for Science and Technology (FCT) under Grant No. PD/BD/143003/2018 attributed to the seventh author; and (2) FCT/MCTES through national funds (PIDDAC) under the R&D Unit Institute for Sustainability and Innovation in Structural Engineering (ISISE), under Reference UIDB/04029/2020.

Conflicts of Interest: The authors declare no conflict of interest.

References

1. JCSS. JCSS Probabilistic Model Code. Available online: <https://www.jcss-lc.org/jcss-probabilistic-model-code/> (accessed on 18 August 2021).
2. Faber, M. *Statistics and Probability Theory*; Springer: Berlin, Germany, 2012.
3. Benko, V. Nichtlineare Berechnung von Stahlbetondruckglieder. (Nonlinear analysis of reinforced concrete compression members). *Innov. Betonbau* **2001**, *27*, 9–12.
4. Strauss, A.; Ivanković, A.M.; Benko, V.; Matos, J.; Marchand, P.; Wan-Wendner, R.; Galvão, N.; Orcesi, A.; Dobrý, J.; Diab, M.E.H.; et al. Round-Robin Modelling of the Load-bearing Capacity of Slender Columns by Using Classical and Advanced Non-linear Numerical and Analytical Prediction Tools. *Struct. Eng. Int.* **2021**, *31*, 118–135. [\[CrossRef\]](#)
5. Benko, V.; Gúcky, T.; Valašík, A. The reliability of slender concrete columns subjected to a loss of stability. In *Advances and Trends in Engineering Sciences and Technologies II, Proceedings of the 2nd International Conference on Engineering Sciences and Technologies, ESaT 2016, Vysoké Tatry, Slovak Republic, 29 June–1 July 2016*; Taylor & Francis: London, UK, 2017. [\[CrossRef\]](#)
6. Benko, V.; Dobrý, J.; Čuhák, M. Failure of Slender Concrete Columns Due to a Loss of Stability. *Slovak J. Civ. Eng.* **2019**, *27*, 45–51. [\[CrossRef\]](#)
7. CEB-FIP. *Practitioners' Guide to Finite Element Modelling of Reinforced Concrete Structures*; Fib Fédération Internationale du Béton: Lausanne, Switzerland, 2008.
8. EN 1992-1-1. *Eurocode 2: Design of Concrete Structures—Part 1-1: General Rules and Rules for Buildings*; European Standard: Brussels, Belgium, 2004; Volume 1.
9. Shlune, H.; Gylltoft, K.; Plos, M. Safety format for non-linear analysis of concrete structures. *Mag. Concr. Res.* **2012**, *64*, 563–574. [\[CrossRef\]](#)
10. Holický, M. Global resistance factors for reinforced concrete members. In *Proceedings of the 1st International Symposium on Uncertainty Modelling in Engineering*, Prague, Czech Republic, 2–3 May 2011.
11. Cervenka, V. Global Safety formats in Fib Model Code 2010 for Design of Concrete Structures. In *Proceedings of the 11th Probabilistic Workshop*, Brno, Czech Republic, 6–8 November 2013.
12. Cervenka, V. Reliability-based non-linear analysis according to Model Code 2010. *Struct. Concr.* **2013**, *14*, 19–28. [\[CrossRef\]](#)
13. Caspeele, R.; Steenbergen, R.; Sykora, M. *Partial Factor Methods for Existing Concrete Structures*; FIB Bulletin No. 80; FIB: Lausanne, Switzerland, 2016; ISBN 978-2-88394-120-5. [\[CrossRef\]](#)
14. Engen, M.; Hendriks, M.; Köhler, J.; Øverli, J.; Åldtstedt, E. A quantification of modelling uncertainty for non-linear finite element analysis of large concrete structures. *Struct. Saf.* **2017**, *64*, 1–8. [\[CrossRef\]](#)
15. Castaldo, P.; Gino, D.; Bertagnoli, G.; Mancini, G. Partial safety factor for resistance model uncertainties in 2D non-linear analysis of reinforced concrete structures. *Eng. Struct.* **2018**, *176*, 746–762. [\[CrossRef\]](#)
16. Moccia, F.; Yu, Q.; Ruiz, M.F.; Muttoni, A. Concrete compressive strength: From material characterization to a structural value. *Struct. Concr.* **2021**, *22*, E655–E682. [\[CrossRef\]](#)
17. Momeni, M.; Bedon, C. Uncertainty Assessment for the Buckling Analysis of Glass Columns with Random Parameters. *Int. J. Struct. Glass Adv. Mater. Res.* **2020**, *4*, 254–275.
18. Mehmél, A.; Schwarz, H.; Karperek, K.; Makovi, J. *Tragverhalten Ausmittig Beanspruchter Stahlbetondruckglieder*; Institut Für Baustatik, EHT, Deutscher Ausschuss für Stahlbeton, Heft. 204; DafStb: Berlin, Germany, 1969.
19. Foster, S.; Attard, M. Experimental tests on eccentrically loaded high strength concrete columns. *Struct. J.* **1997**, *94*, 295–303.
20. Allaix, D.; Carbone, V.; Mancini, G. Global safety format for non-linear analysis of reinforced concrete structures. *Struct. Concr.* **2013**, *14*, 29–42. [\[CrossRef\]](#)
21. Cervenka, V.; Cervenka, J.; Kadlek, L. Model uncertainties in numerical simulations of reinforced concrete structures. *Struct. Concr.* **2018**, *19*, 2004–2016. [\[CrossRef\]](#)
22. Gino, D.; Castaldo, P.; Giordano, L.; Mancini, G. Model uncertainty in non-linear numerical analyses of slender reinforced concrete members. *Struct. Concr.* **2021**, *22*, 845–870. [\[CrossRef\]](#)
23. Ditlevsen, O.; Madsen, H. *Structural Reliability Methods*; John Wiley & Sons Ltd.: Chichester, Denmark, 1996.
24. Ang, A.H.; Tang, W.H. *Probability Concepts in Engineering Planning*, 2nd ed.; John Wiley & Sons, Inc.: Hoboken, NJ, USA, 2007.
25. Hendriks, M.A.N.; de Boer, A.; Belletti, B. *Guidelines for Nonlinear Finite Element Analysis of Concrete Structures: Girder Members*; Report RTD:1016:2012; Rijkswaterstaat Ministry of Infrastructure and Water Management: The Hague, The Netherlands, 2012.
26. European Committee for Standardization (CEN). *EN 1990, Eurocode 0: Basis of Structural Design*; CEN: European Standard: Brussels, Belgium, 2005.
27. International Federation for Structural Concrete (FIB). *Model Code for Concrete Structures*; Ernst & Sohn: Lausanne, Switzerland, 2010.
28. Novák, D.; Vořechovský, M.; Teplý, B. FReET: Software for the statistical and reliability analysis of engineering problems and FReET-D: Degradation module. *Adv. Eng. Softw. Adv. Eng. Softw.* **2014**, *72*, 179–192. [\[CrossRef\]](#)
29. Beletti, B.; Vecchi, F.; Cosma, M.P.; Strauss, A. Non linear structural analyses of prestressed concrete girder: Tools and safety formats. In *Life-Cycle Analysis and Assessment in Civil Engineering. Towards an Integrated Vision, Proceedings of the Sixth International Symposium on Life-Cycle Civil Engineering, Ghent, Belgium, 28–31 October 2008*; Caspeele, R., Taerwe, L., Frangopol, D.M., Eds.; Taylor & Francis Group: London, UK, 2018.
30. Achenbach, M.; Gernay, T.; Morgenthal, G. Quantification of model uncertainties for reinforced concrete columns subjected to fire. *Fire Saf. J.* **2019**, *108*, 102832. [\[CrossRef\]](#)

31. Zimmermann, T.; Lehký, D.; Strauss, A. Correlation among selected fracture-mechanical parameters of concrete obtained from experiments and inverse analyses. *Struct. Concr.* **2016**, *17*, 1094–1103. [[CrossRef](#)]
32. Strauss, A.; Krug, B.; Slowik, O.; Novak, D. Combined shear and flexure performance of prestressing concrete T-shaped beams: Experiment and deterministic modeling. *Struct. Concr.* **2018**, *19*, 16–35. [[CrossRef](#)]
33. Strauss, A.; Benko, V.; Taubling, B.; Valasik, A.; Cuhak, M. Reliability of slender columns. *Beton-Stahlbetonbau* **2017**, *112*, 392–401. [[CrossRef](#)]
34. Červenka, V.; Jendele, L.; Červenka, J. *Atena Program Documentation—Part 1: Theory*; Cervenka Consulting: Prague, Czech Republic, 2007.
35. Tau, K.; Agresti, A. *Analysis of Ordinal Categorical Data*, 2nd ed.; John Wiley & Sons: New York, NY, USA, 2010.
36. Strauss, A.; Novák, D.; Lehký, D.; Vořechovský, M.; Teplý, B.; Pukl, R.; Červenka, V.; Eichinger-Vill, E.M.; Santa, U. Safety analysis and reliability assessment of engineering structures—The success story of SARA. *Ce/Papers* **2019**, *3*, 38–47. [[CrossRef](#)]
37. Strauss, A.; Wan-Wendner, R.; Vidovic, A.; Zambon, I.; Yu, Q.; Frangopol, D.M.; Bergmeister, K. Gamma prediction models for long-term creep deformations of prestressed concrete bridges. *J. Civ. Eng. Manag.* **2017**, *23*, 681–698. [[CrossRef](#)]



Application of quality control plan to existing bridges

Edward A. Baron^a , Neryvaldo Galvão^a , Marija Docevska^b , Jose C. Matos^a  and Goran Markovski^b

^aISISE, Department of Civil Engineering, University of Minho, Guimarães, Portugal; ^bFaculty of Civil Engineering, University “Ss. Cyril and Methodius”, Skopje, Republic of North Macedonia

ABSTRACT

The long-term quality assurance of bridges demands an adequate quality control plan detailing the main required activities and assessment tools. This paper presents the application of a quality control plan on two existing reinforced concrete bridges located in Portugal and North Macedonia. Based on the available results from visual inspections and non-destructive tests, defects and corresponding damage processes were identified. The structural safety of the case studies was assessed by means of a reliability index considering the identified damages. The reliability index computation was supported by a nonlinear finite element analysis. The computed reliability index that reflects the actual ('today') bridge condition was used as the base information in the preparation of possible maintenance scenarios. Three different maintenance scenarios were considered, namely, the improvement (corrective scenario), reduction (do nothing and rebuilt scenario), or delay in the reduction (preventative scenario) of the performance of the structure. By comparison of normalised net present values of the key performance indicators (reliability, safety, availability and costs), the most appropriate scenarios are found.

ARTICLE HISTORY

Received 30 May 2021

Revised 15 July 2021

Accepted 15 July 2021

KEYWORDS

Quality control plan; reliability index; maintenance; bridge assessment; degradation; non-linear structural analysis; uncertainties; key performance indicators

1. Introduction

The transport network is extremely important for the socio-economic development of a country. In particular, there is a broad consensus regarding the benefits of road infrastructures. The European Commission has envisioned the need to overcome current and foreseen societal issues such as rising traffic demand, congestion, energy supply security, climate change, among others. Nevertheless, the complexity in the quantification of the economic benefit of road infrastructure remains a present-day issue. Some authors estimated the benefits to be between 4% (Firestine, 2015) and 10% (Kurte & Kurte, 2008; Powers et al., 2018) of Gross Domestic Product (GDP). Besides the moderate economic benefits, road infrastructures enable the users to be involved in various activities that yield private, public and social benefits (Frischmann, 2012).

Bridges are critical components of the road network infrastructure as their full or partial failure can lead to detours or even complete inaccessibility to a region, leading sometimes to moderate or even disastrous economic impacts. Therefore, there is an increasing need for the development of strategies to ensure the long-term quality performance of bridges. A quality control plan (QCP) should specify all activities and tools necessary to guarantee safety. Furthermore, a QCP should define the extent and the interval of inspections or interventions and the data necessary to estimate key performance indicators (KPI) and forecast their future development (Pakrashi et al., 2019). Thereby, evident choices as KPIs for existing bridges would be safety and serviceability related indicators. Nonetheless,

some other sources suggest the combination of serviceability with durability into a performance category called 'Structural Condition', as well as a combination of safety with stability into a category named 'Structural Integrity' (Brown, Gomez, Hammer, & Hooks, 2014; Dette & Sigrist, 2011). Other performance categories often included in the QCPs are 'Costs' (including agency and users costs as delay, detour and accidents) and 'Functionality' (including ride quality, load ratings, clearances and restrictions on use).

Recently, a methodology for quality control of existing bridges was established within the COST Action TU1406 – *Quality specifications for roadway bridges, standardisation at a European level* within its working package 3 (WG3) dedicated to the 'Establishment of a Quality Control Plan' (Hajdin et al., 2018). This methodology provides a broad and holistic approach for the assessment of bridges – an approach that current element-oriented QCPs are lacking. The recommendations and guidelines for implementation of this methodology are suggestive and therefore allow to be implemented in various ways. In terms of KPIs, the WG3 framework is based on the Dutch RAMSSHEEP approach as indicated in Figure 1 (Rijkswaterstaat, 2012). In (Kifokeris, Matos, Xenidis, & Braganca, 2018) the authors outline the initial framework methodological steps from TU1406 and present its application on a real reinforced concrete overpass. Recently, some important aspects of the latest developed version of the methodology are reported in detail in Casas and Matos (2021).

This paper intends to demonstrate the applicability of the developed QCP through two real case studies – arch

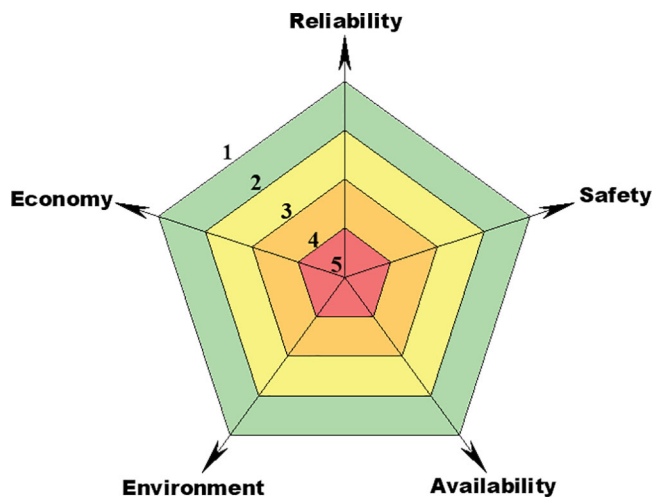


Figure 1. "Spider net" diagram of KPIs based on (Rijkswaterstaat, 2012).

reinforced concrete bridges, one located in Portugal and the other in North Macedonia. The TU1406 QC framework was recently demonstrated on an arch masonry bridge in Portugal (Amado & Costa, 2020) where all KPIs are evaluated in a qualitative manner. In this paper, however, an additional attempt was made to employ a quantitative, instead of a qualitative approach, to appraise the evolution of one of the governing key performance indicators of the bridges, i.e., their structural reliability. This quantitative approach is beyond the requirements of the proposed methodology; however, it provides more accurate information about the case studies. Nevertheless, due to the computational costs, such an approach is not recommended when a network is concerned. The ultimate aim of the paper is to show the application feasibility of application of the methodology proposed by WG3 of the COST TU1406 Action in cases where a quantitative approach for the governing KPI (Reliability) is selected. One should be mentioned that the aim of the paper is not to evaluate the plausibility of the maintenance scenarios applied. In the following sections, a detailed step-by-step explanation of the framework will be outlined along with the results from its application on two existing bridges.

2. QCP framework

The QCP framework proposed by Hajdin et al.,(2018) has two stages – static and dynamic. In general, the first one comprises preparatory works, on-site inspection tasks and snapshot assessment of the KPIs. The second one implies the forecast of the evolution of the KPIs according to the identified damage processes and the definition of possible maintenance scenarios aiming at the identification of the optimal one (Hajdin et al., 2018).

The following steps are necessary for the implementation of the static QCP (Hajdin et al., 2018):

- Collection of general bridge data (original drawings, construction year and method, inspection/intervention year,

bridge location, importance of the roadway of the bridge, obstacle type, exposure, etc.).

- Studying of the visual inspection's information and (if any) non-destructive tests (NDT).

Definition of the actual structural system and related vulnerable zones.

- Estimation of prior virgin reliability (i.e., a 'damage free' scenario).
- Documentation of the damages and their causes.
- Assessment of the resistance reduction according to the observed damages.

While the dynamic steps of the QCP are the following (Hajdin et al., 2018):

- Modelling of the damage processes and estimation of the reduced reliability at the time of bridge inspection.

Definition of various maintenance scenarios.

- Evolution over time of all KPIs: Reliability, Safety, Availability and Cost.
- Comparison of the benefits of each scenario and identification of the optimal one.

All these steps will be presented in this work through their implementation in two existing reinforced concrete bridges.

3. Case studies – overall description

The first case study is a reinforced concrete arch bridge located over the Cró river in Guarda district, Portugal (bridge A) (Figure 2a). The bridge carries the national road EN324 and has two traffic lanes (each with 2.53 m and 2.51 m), two roadsides (each with 0.45 m and 0.51 m) and two sidewalks of 1 m each. The case study was constructed in 1940 and repaired in 2010. The data used for the numerical analysis and implementation of the QCP are based on the design project and two inspection reports (one from 2007 and the other from 2015) provided by Infraestruturas de Portugal, i.e., the national manager agency of the roadway and railway infrastructures.

The bridge A is an open-spandrel deck arch bridge with a total length of 24 m. Its geometric information is displayed in Figure 3. In the design project, it was indicated that the deck is supported by a two-hinged arch. For this case study, the results from NDTs of concrete strength are available in Table 1.

The second case study is a slab-type arch reinforced concrete bridge located in North Macedonia (bridge B), as detailed in Figure 2b. The bridge carries the national road M-1 (E-75) on the Katlanovo-Veles and its overall width is 9.20 m ($2 \times 3.80\text{m} + 2 \times 0.60\text{m} + 2 \times 0.20\text{m}$). It was built in 1963 and strengthened in 2007. The design

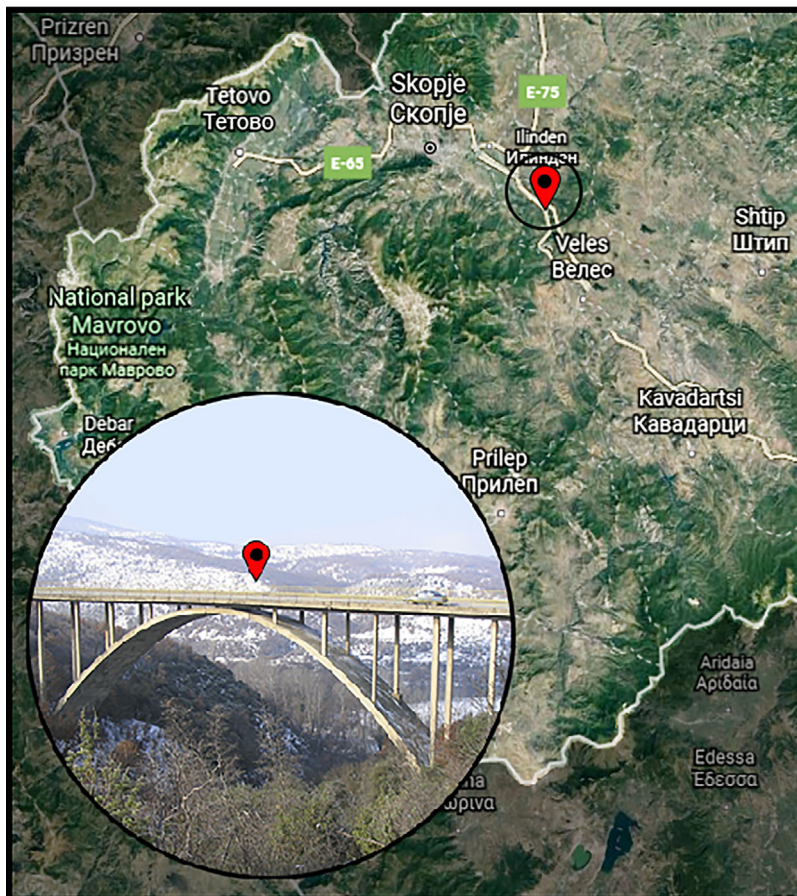


Figure 2. Location plan. (a) Bridge A, Cró river, Guarda, Portugal. (b) Bridge B, Katlanovo-Veles, North Macedonia.

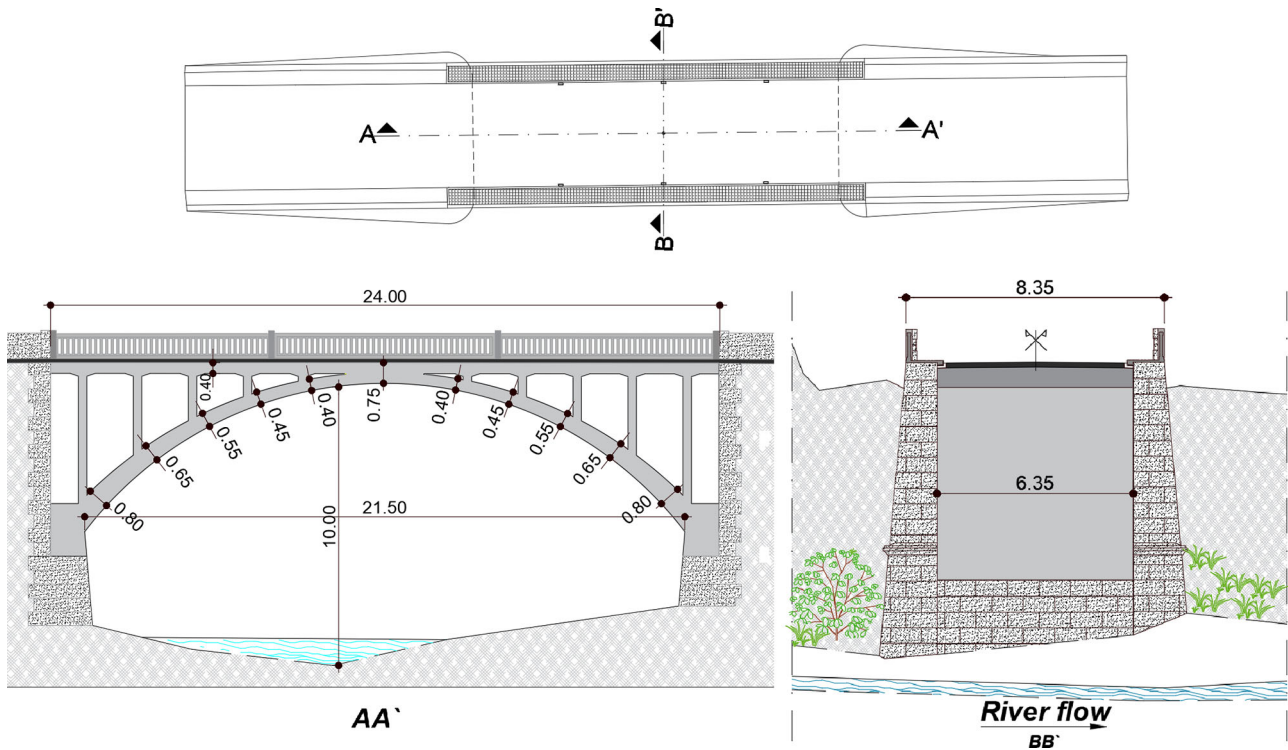


Figure 3. Bridge A blueprints.

Table 1. Compressive strength results from NDTs of bridge A.

Spec. no	f_c [MPa]	$f_{c,avg}$ [MPa]
2	43.9	
3	50	
4	42.5	
5	41	
1	38.3	43.14

documentation of the bridge was not available; thus, construction drawings were considered.

The bridge B is shaped by a fixed-end slab-type arch with a span of 54 m, whose approaching structures comprise three spans on one side and five spans on the other, each with approximately 6 m, shaping a bridge with an overall length of 102.65 m (see Figure 4). For this case study, the following results from testing were available: concrete compressive strength from the extracted concrete cores and tensile strength from 'pull-off' tests (see Table 2).

3.1. Vulnerable zones identification

The case studies structural systems are defined according to the WG3 Report (Hajdin et al., 2018) of the COST Action TU1406 recommendations and structural analysis best practices. After defining the actual static condition of the structural system and its structural elements, vulnerable zones were carefully identified. These vulnerable zones are segments and/or elements of a bridge where the damages have the largest impact on structural safety and serviceability. Such zones can be related to several failure modes (Hajdin et al., 2018). One need not say that they are case study dependent.

Since both bridges have similar structural systems, common vulnerable zones considering the load-bearing elements are defined, namely: high moment regions HMR (critical sections of the arch and the deck), high compression regions HCR (support of the arch and piers/walls) and high deflection regions HDR (crown of the arch and mid-span of the deck). The case studies' vulnerable zones are acknowledged in Figure 5. Later on, such zones were carefully inspected, and the identified defects were taken into account for structural analysis.

3.2. Identification of ongoing damage processes

The information concerning damage processes is essential for the further implementation of the QCP. This information helps to assess the actual (at the time of inspection) and predict the future bridge performance, allowing to plan maintenance and eventual rehabilitation works. Both subject bridges were built quite some time ago, so the deterioration processes have already been initiated in the past. Figures 6 and 7 present the most important defects observed during the performed inspections in the previously defined vulnerable zones.

In the bridge A (Figure 6), the following defects were observed: concrete spalling (f,g,k), hairline cracks (b,h), calcium leaching (b,f,j), brown spots (a,g,i), direct wetting of concrete (b,c,e), steel corrosion (f,g) and drainage inadequacy (c,e).

A considerable number of defects were also observed in the bridge B (Figure 7): construction error (d, h), inappropriate water drainage (a), very heavy damages due to advanced corrosion of concrete and steel reinforcement of the deck slab (b, g) and the longitudinal girders (b),

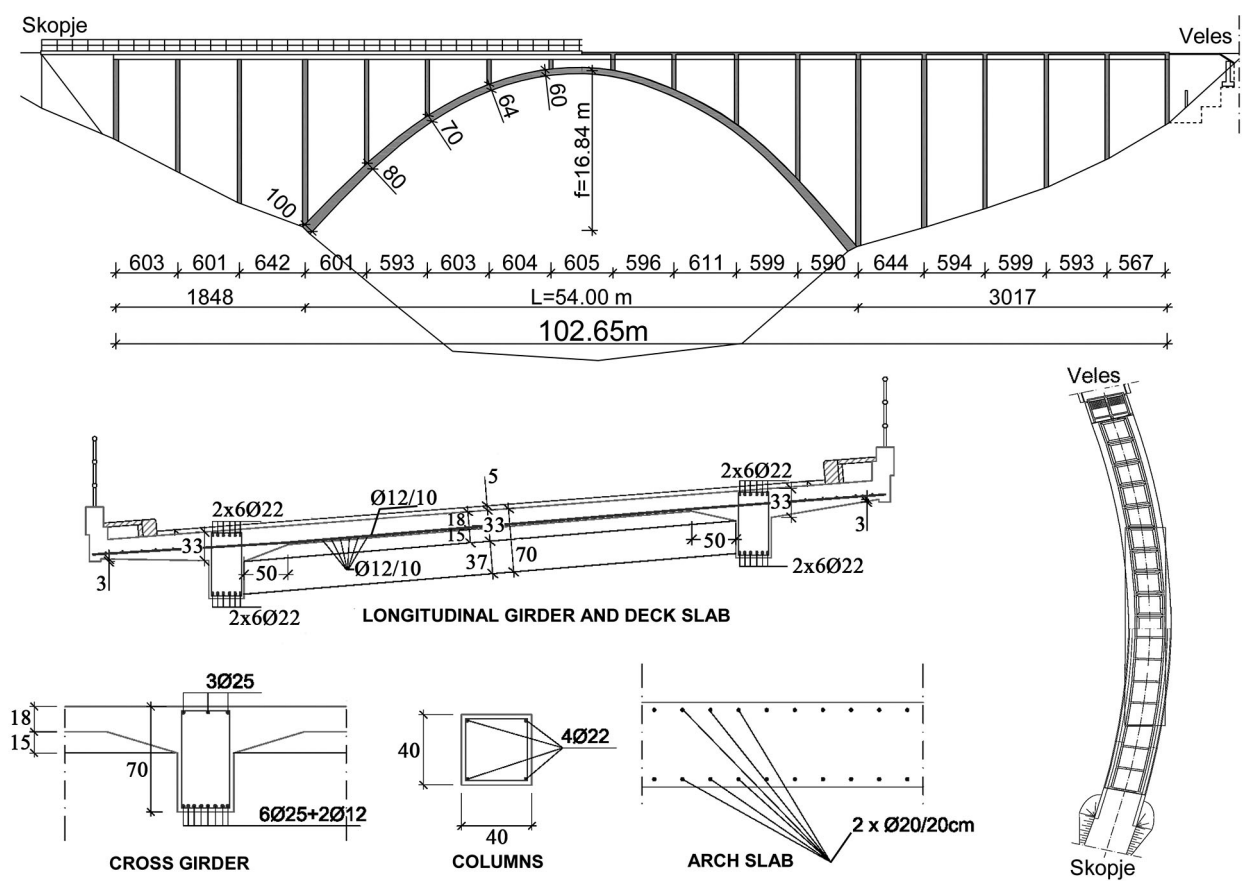


Figure 4. Bridge B blueprints.

Table 2. Compressive and tensile strength results from NDTs of bridge B.

Spec. no	f_c [MPa]	$f_{c,avg}$ [MPa]	Spec. No	f_t [MPa]	$f_{t,avg}$ [MPa]
1	51.93	40.96	1	2.5	2.4
2	31.05		2	3.1	
3	50.13		3	1.6	
4	40.89				
5	30.79				

expressed process of carbonation on entire deck slab (a), insufficient or spalled concrete cover (b, d, f, g), cracks at the connection with the column (c), improper expansion joint (i), visible reinforcement due to missing parts of concrete on the railing parapets (j) and inappropriate concreting and segregation (d, f, h).

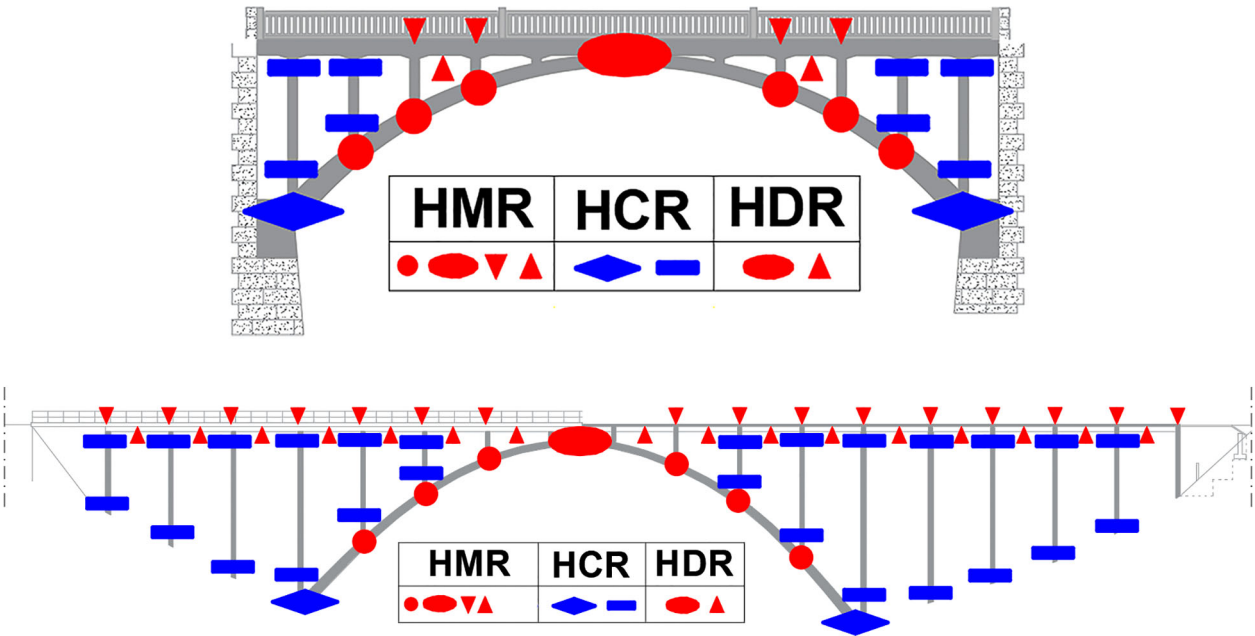


Figure 5. Vulnerable zones. (a) Bridge A. (b) Bridge B.

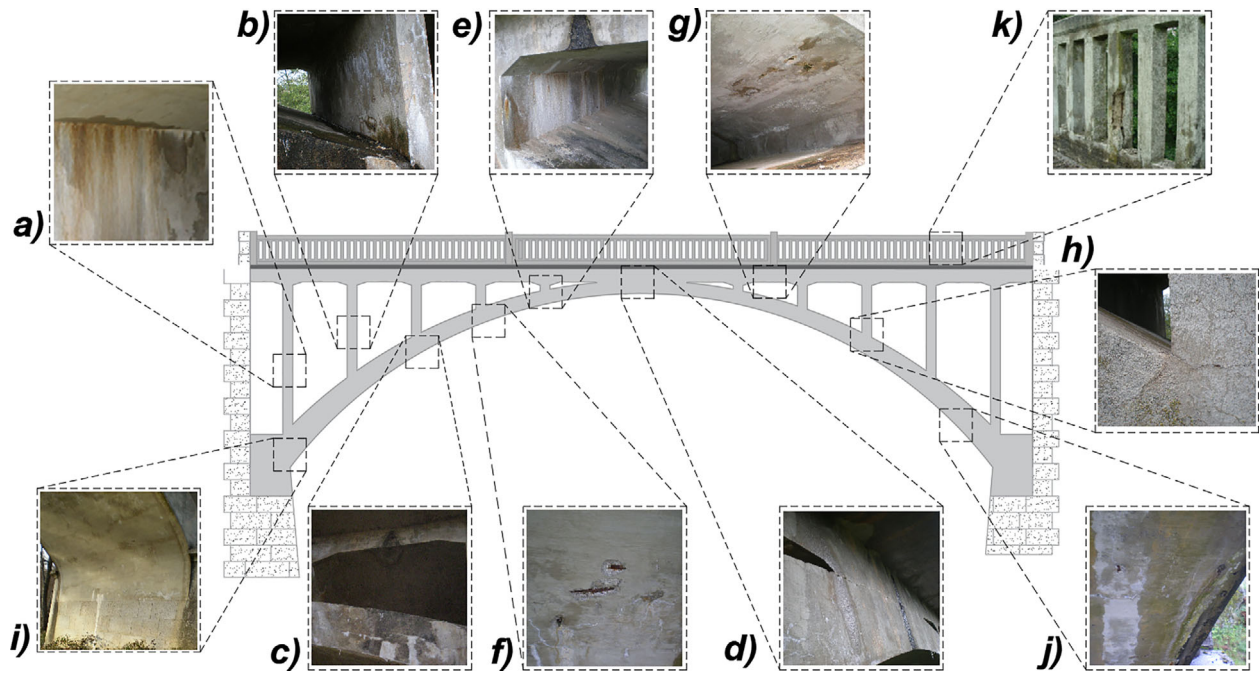


Figure 6. Main observations from the visual inspection in the vulnerable zones (bridge A).

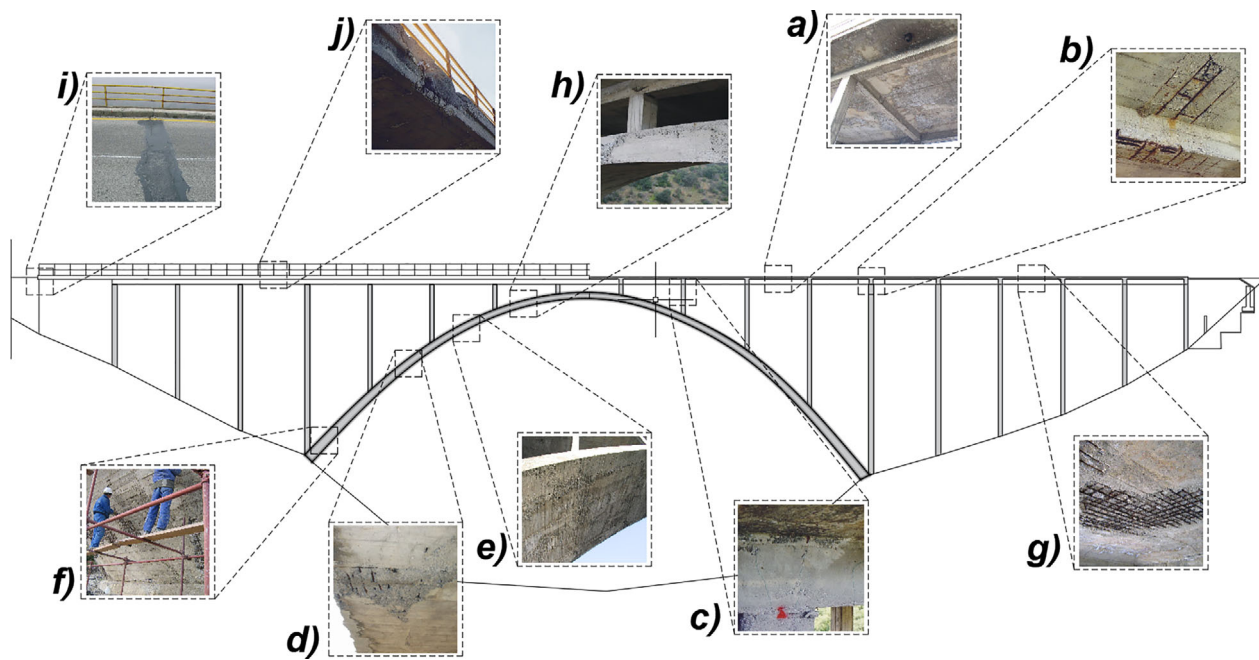


Figure 7. Main observations from the visual inspection in the vulnerable zones (bridge B).

To estimate the safety level (i.e., reliability index) at the time of the inspection, it is required the identification of the governing degradation processes of the bridge, according to the observed damages, aiming at a scenario-based safety assessment. Therefore, according to the extent and severity of the damages, the following damage scenarios, considering the provided mean values and coefficients of variation (CoVs), were considered:

- Scenario 1: Reinforcement cross-section area reduction due to corrosion - global reduction of the mean value in 20% (bridge A) and 30% (bridge B), considering a CoV of 5%.
- Scenario 2: Concrete degradation - global reduction of the mean value of the Young modulus in 20%, considering a CoV of 5%.
- Scenario 3: Combination of scenario 1 and scenario 2.

According to the information gathered by the inspection, the NDT and the destructive tests, a degradation of the Young modulus was observed. Therefore, scenario 2 was established according to such information. Concerning scenario 1, an estimation of the advancement of the corrosion, by removal of the steel rust (steel oxides) was attempted. The carbonation depth information was also considered.

The estimations provided in the scenarios are a rough appraisal of what was observed and inferred. Nevertheless, a detailed investigation, using more sophisticated techniques to assess the progress of corrosion, the consideration of deterioration models for corrosion, as well as the evaluation of bond loss between the concrete element and the reinforcement should be carried out. Elaborated work on such matter can be found in (Cavaco, Neves, & Casas, 2017; Stewart & Al-Harthy, 2008).

4. Safety assessment

Efficient techniques for both, nonlinear numerical analysis and probabilistic methods coupled with finite element models (FEM) were implemented to set an advanced tool for the assessment of the real performance of the bridges. Considering such numerical techniques, the structural safety levels of the case studies were assessed for the damage-free and damage included scenarios. Accordingly, the virgin reliability index was at first estimated for both bridges. Such safety level corresponds to the performance of the bridges at the time of their commissioning. Here, design and construction errors are disregarded.

4.1. Fem nonlinear analysis

In order to compute the reliability index of the case studies, the load-bearing capacities of the structures must be known. For such purpose, non-linear analysis considering non-linear elasticity of the concrete, according to (CEN 2004) stress-strain curve, was performed in DIANA FEA software (TNO Diana, 2016b). A two-dimensional (2D) FEM was built using plane stress finite elements for concrete (namely, a four-node quadrilateral isoperimetric element, see Figure 8) and embedded bonded truss elements for longitudinal reinforcement. Only bending reinforcements were considered according to as build blueprints (TNO DIANA, 2016a) to build the overall numerical models (see Figure 9).

The concrete nonlinear behaviour is simulated with a total strain rotating crack model. The reinforcement steel is modelled by an elastic-plastic stress-strain curve. To reduce the computational cost for the non-linear analysis, three degrees of freedom per node were considered. Mechanical properties obtained through NDTs were used as inputs (see Tables 1 and 2).

The load-bearing capacity of the systems was verified only for permanent (self-weight and additional dead loads) and live loads. Other loads that are usually considered at a designing stage (earthquake, temperature, creep and shrinkage, wind, etc.) were not considered in this analysis. Regarding the live loads, traffic load model 1 (LM1) of CEN (2003) was considered. The governing live load case considered for the assessment of the bridges was an equivalent uniformly distributed load of 38 kN/m and a two-axle load of 401 kN spaced in 1.2 m, applied to the deck at a section located at 1/4th of the arch span (Chajes et al., 2002; Onstein, 2013) (Figure 9). The applied live load is equivalent to the mean value of LM1 considering that the provided

characteristic loads of LM1 in (CEN 2003) correspond to the 95th percentile of a normal probabilistic function with 15% of CoV, according to (Matos et al., 2019). A 50-year reference period was considered.

The load-bearing capacity of the structure (without any damage) was determined through an incremental-iterative loading procedure that allows the tracking of the non-linear behaviour of the structure until its failure. The numerical results are analysed in terms of the load-displacement curve and cracking pattern showed during failure (see Figure 10). The system failure occurs as a progressive failure taking into account the defined vulnerable zones. The failure is triggered initially by the failure of the deck due to concrete crushing after the yielding of the reinforcement, then the HCR located in the columns present excessive stresses leading to the failure of the arch due to the high induced moment.

4.2. Sensitivity analysis

A probabilistic assessment is typically preceded by a sensitive analysis seeking at decreasing the number of random variables primarily chosen according to expert appraisal (Galvão, Matos, Oliveira, & Hajdin, 2021). Thereby, an important reduction of the computational cost and the optimisation of the procedure due to the selection of parameters with high influence on the bridge resistance is achieved. The importance of each random variable can be computed according to:

$$b_k = CV * \sum_{i=1}^n \left(\frac{\Delta y_k}{y_m} \right) / \left(\frac{\Delta x_k}{x_m} \right) [\%] \quad (1)$$

where b_k the importance measure of parameter k , Δy_k the variation in the output parameter due to a deviation of the input parameter Δx_k concerning the mean value of the input parameter x_m , y_m the average response and n is the number of generated parameters. Thus, specific uncertainties (random variables) concerning the geometry and material properties of the structures were initially taken into account as shown in Table 3. Such random variables are characterised by a normal probabilistic distribution function (PDF), and the proposed mean values and CoV were obtained from the Joint Committee on Structural Safety (Joint Committee on Structural Safety, 2000) and (Wiśniewski, Cruz, Henriques, & Simões, 2012).

The computed importance measure of each random variable is graphically displayed in Figure 11. A threshold value of 20% is used to classify the random variables as being essential or nonessential for the probabilistic analysis (Matos et al., 2019). Therefore, the following random variables were considered for further investigation: i) yielding stress and strength of the conventional reinforcement (f_{sy} e f_p); (ii) reinforcement cross-section area (A_s); and (iii) C40/50 concrete compressive strength (f_{cm}).

The random variable with the highest importance measure was the yielding stress of the reinforcement in both case studies, as reported in (Galvão et al., 2021), (Wiśniewski et al., 2012), (Matos et al., 2019) and (Nowak, Yamani, & Tabsh, 1994) for ductile structures.

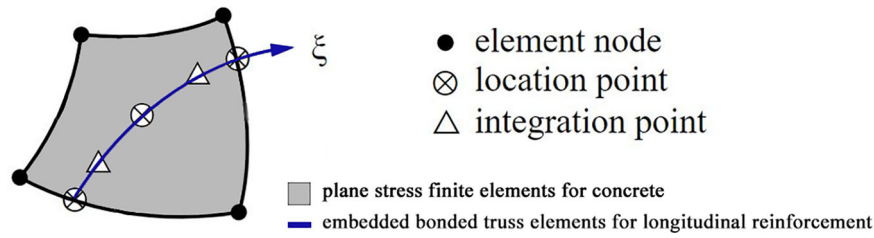


Figure 8. Plane stress element with its embedded reinforcement.

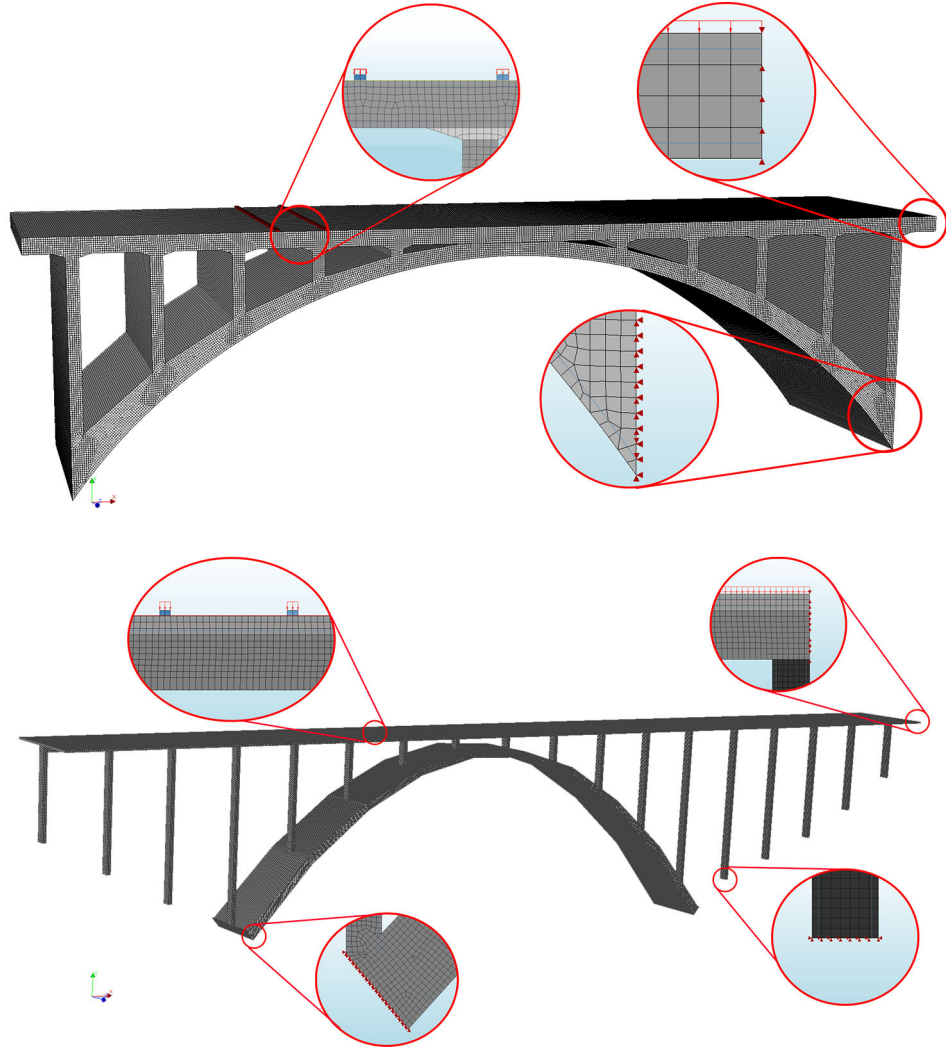


Figure 9. FEM in DIANA Software using plane stress finite elements (extrude view). (a) Bridge A. (b) Bridge B.

4.3. Probabilistic analysis

Once the deterministic analysis and the sensitivity analysis have been performed, a probabilistic assessment followed. At first, the probability of failure and reliability of the bridges in their virgin states were computed. In order to achieve the characterisation of the mean and the CoV coefficient of variation of the PDF of the resistance curve (R), the Latin hypercube sampling technique was implemented according to Olsson, Sandberg, and Dahlblom (2003). The number of samples generated through the Latin Hypercube Sampling technique was only used to approximate the mean and the CoV of the PDF of the resistance curve. It was not used to directly compute the probability of failure or the

reliability index of the system, which by the way, even using the LHS technique would require way more samples. To approximate the mean and the standard deviation of the resistance curve, as well as its PDF, 200 FEM samples considering the selected random variables were considered. For each generated sample, a non-linear analysis was performed to quantify their load-bearing capacity. Doing so, the PDF of the load-carrying capacity of the case studies were obtained (see Figure 12).

Considering the obtained information concerning the structural system resistance and loading uncertainty, the reliability index of the case studies can be computed using the formulation in Equation (2) (CEN 2002), valid if the resistance and the load are approximated by a normal

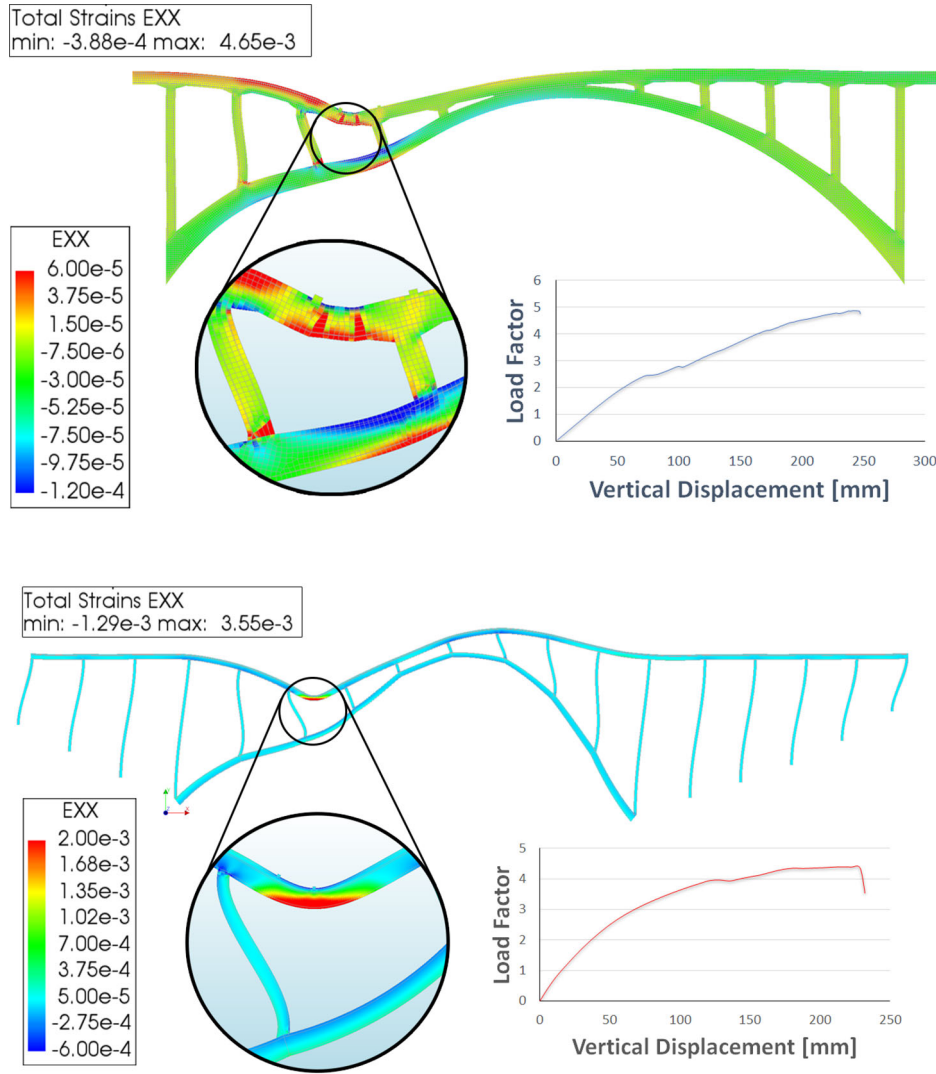


Figure 10. Structural non-linear results in DIANA. (a) Bridge A. (b) Bridge B.

Table 3. Random variables considered for material and geometry probabilistic characterisation.

	Description	Random variables	Notation	Mean values	CoV
Bridge A	C35/45	Compressive strength	f_{cm}	43 MPa	12%
		Concrete self-weight	γ_c	24 kN/m ³	8%
		Poisson's ratio	ν	0.2	10%
		Modulus of elasticity	E_{cm}	35 GPa	8%
	S500	Yielding and ultimate strength	f_{sy} e f_p	560 MPa	5%
Bridge B		Reinforcement cross-section area	A_s	–	2%
	C40/50	Compressive strength	f_{cm}	40.96 MPa	12%
		Concrete self-weight	γ_c	24 kN/m ³	8%
		Poisson's ratio	ν	0.2	10%
		Modulus of elasticity	E_{cm}	35 GPa	8%
	GA 240/360	Yielding and ultimate strength	f_{sy} e f_p	240 MPa	5%
		Reinforcement cross-section area	A_s	–	2%

probabilistic distribution function (PDF). The reliability index and consequently the probability of failure are estimated according to based on Equation (2) should provide similar results to FORM (First Order Reliability Method) if the problem is reduced to $G(X)=R-S$ and R and S are characterised by a normal PDF:

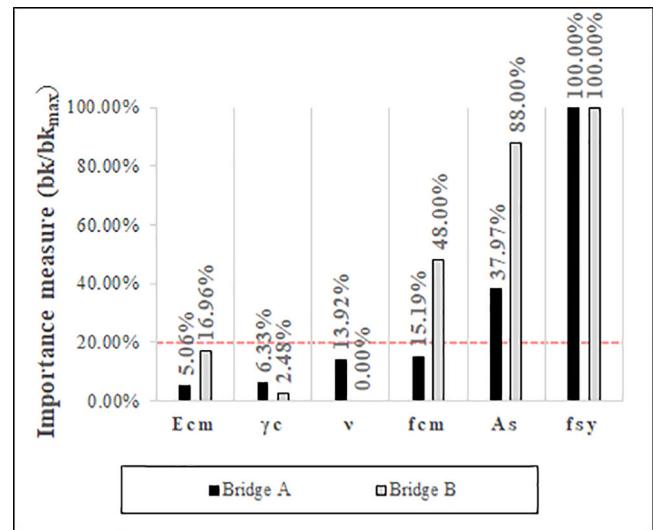


Figure 11. Random variables importance measure.

$$\beta = \frac{\mu_R - \mu_S}{\sqrt{\sigma_R^2 + \sigma_S^2}} \quad (2)$$

where, μ_R and σ_R represent the mean value and the

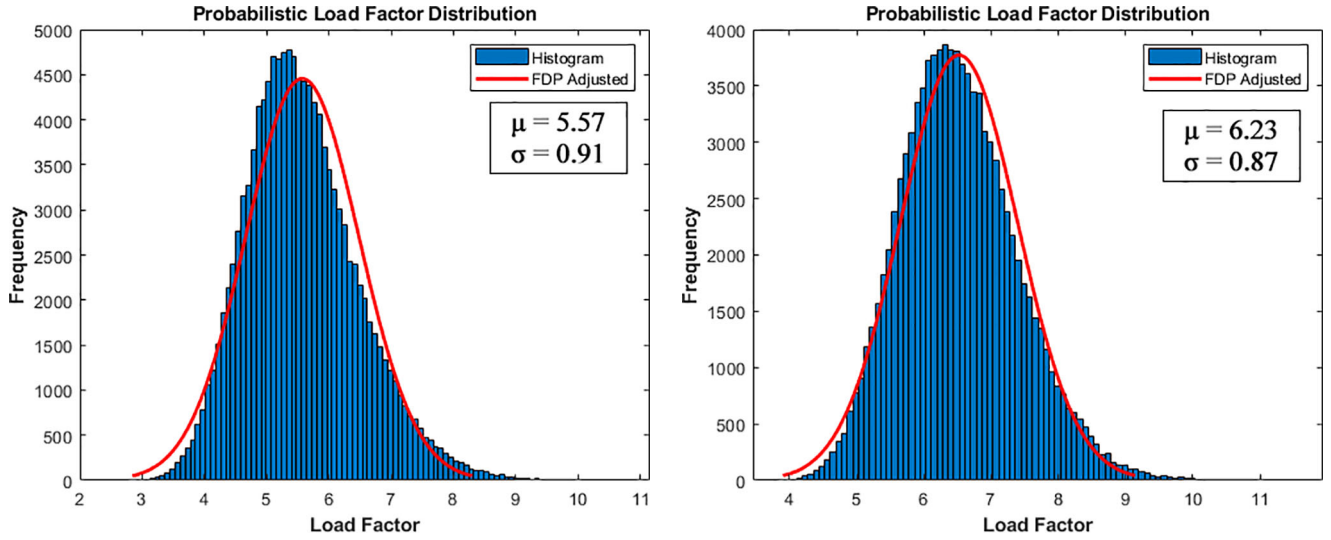


Figure 12. PDF of the load-bearing capacity of (a) Bridge A and (b) Bridge B.

standard deviation of the resistance curve, and μ_s and σ_s the mean value and the standard deviation of the load curve, respectively.

Nonetheless, far more sophisticated reliability methods that would provide a more accurate estimation of the reliability index are available in the literature. Such methods can be found in Guimarães, Matos, and Henriques (2018), Marelli and Sudret (2018) and Teixeira, Nogal, and O'Connor (2021). Having said that, one needs to say that those are beyond the scope of this work since a more simplistic approach was deemed reasonable for the aim of this paper.

Aiming the consideration of the uncertainty of the model itself in the prediction of the real behaviour of the bridges, numerical model uncertainty concerning the structure's resistance capacity were considered. Such model uncertainty is the result of simplifications or negligence of the mathematical relations (e.g., 3D effects, inhomogeneities, interactions, boundary effects, simplification of connection behaviour, imperfections, among others). The model uncertainty was modelled by a lognormal PDF with a mean value of 1.2 and a CoV of 0.15 according to (Joint Committee on Structural Safety, 2000). Such values are recommended for standard structural finite element models.

The characterisation of the previously determined structural system resistance is directly associated with the applied live load, in other words, it is the result of the maximum applied load factor relative to the LM1. Thus, the resistance curve is a multiplier of the mean value of the PDF describing the live load, where its CoV depends on the random variables that influence the resistance. Thereby, the mean value of the loading PDF shall be defined as a unitary load factor. The associated CoV is 15%, as recommended by (Matos et al., 2019). Nevertheless, ideally, the uncertainty concerning the live load should be assessed through monitoring data obtained, for instance, by weight in motion systems.

The obtained indexes (see Table 4) for both bridges are higher than the target reliability index ($\beta_{\text{target}}=4.3$) for

Table 4. Obtained reliability indexes for the considered damaged scenarios.

Scenario	Bridge A			Bridge B		
	β	μ	σ	β	μ	σ
No damage	4.96	5.57	0.91	6.23	6.52	0.87
Scenario 1	4.68	5.15	0.87	5.35	5.24	0.78
Scenario 2	4.61	4.24	0.69	6.05	6.24	0.85
Scenario 3	3.89	3.97	0.75	4.92	4.86	0.78

ultimate limit state established according to CEN (2002) and Sykora, Diamantidis, Holicky, and Jung (2017) for a structural system, considering a 50-year reference period. The relatively high values can be explained by the fact that the performed analysis considers the overall structural behaviour taking into account the moment redistribution through the system. The values are often of lower order when the analysis is performed at the cross-sectional or element level (Galvão et al., 2021).

4.4. Reliability index considering damage processes

The main goal of the probabilistic analysis considering the previously mentioned damage scenarios (see section 3.2) was to obtain the reliability indexes that represent the actual condition of the bridges at the time of their inspection. Table 4 presents the obtained reliability indexes for the considered damage scenarios. The results from the third scenario will be used further as a starting point in the preparation of maintenance scenarios.

5. Maintenance scenarios models

Making decisions on the maintenance of existing bridges strongly depends on the effect of interventions on structural reliability and their costs (Neves & Frangopol, 2005). In this paper, different maintenance scenarios were considered, in which the maintenance interventions are actions that either improve/increase the reliability, delay the degradation of the reliability or reduce the reliability deterioration rate. The costs for the interventions are strongly dependent on the

state of the structure before their application. However, here, for the sake of simplicity, the costs are roughly estimated and considered to be independent of the structure state. In this paper, linear time-dependent reliability profiles under no maintenance and considering the effect of maintenance actions are simulated using the model proposed by (Frangopol, Kong, & Gharaibeh, 2001). The applied deterioration models for the reliability index are explained briefly in the following sections.

5.1. Model under no maintenance

For the model where no maintenance is considered, the reliability index decreases over time as a result of deterioration. Initially, the performance level is maintained constant after the bridge construction until damage initiation. Hence, the reliability profile under no maintenance is described in Equation (3) by the following three variables: initial reliability index β_0 , initiation time of the deterioration t_I and deterioration rate of the reliability index α (Frangopol et al., 2001):

$$\beta(t) = \begin{cases} \beta_0, & 0 \leq t \leq t_I \\ \beta_0 - (t - t_I)\alpha, & t > t_I \end{cases} \quad (3)$$

5.2. Model under maintenance

Maintenance actions can have one, several or all of the following effects: (i) increase in the reliability index at the time of application, (ii) delay of the deterioration process of the reliability index during a certain period, and (iii) reduction of the deterioration rate of the reliability index during a certain period.

The effect of each maintenance action can be modelled through the following parameters: (a) increase in reliability index immediately after an application of an action γ , (b) duration of maintenance effect on bridge reliability t_{PD} , (c) reliability deterioration rate during maintenance effect θ , (d) time of first application of the action t_{PI} and (e) interval between subsequent applications t_p . The reliability profile under maintenance can be modelled using (Frangopol et al., 2001):

$$\beta(t) = \begin{cases} \beta_0, & \text{if } 0 \leq t < t_I \\ \beta_0 - (t - t_I)\alpha, & \text{if } t_I \leq t < t_{PI} \\ \beta_1 - (t - t_{PI})\theta, & \text{if } t_{PI} \leq t < t_{PI} + t_{PD} \\ \beta_1' - [t - (t_{PI} + t_{PD})]\alpha, & \text{if } t_{PI} + t_{PD} \leq t < t_{PI} + t_p \\ \beta_n - \{t - [t_{PI} + (n-1)t_p]\}\theta, & \text{if } t_{PI} + (n-1)t_p \leq t < t_{PI} + (n-1)t_p + t_{PD} \\ \beta_n' - \{t - [t_{PI} + (n-1)t_p + t_{PD}]\}\alpha, & \text{if } t_{PI} + (n-1)t_p + t_{PD} \leq t < t_{PI} + nt_p \end{cases} \quad (4)$$

6. Possible maintenance scenarios

Three different maintenance scenarios were considered for 100 years horizon, namely: (1) 'Do nothing and rebuild', (2) Corrective and (3) Preventative scenario. In all of them, no

need for urgent intervention after the inspection ($t = 0$) was recognised, since both bridges have reliability indexes that, according to Table 5, correspond to good performance levels (reliability level 2 for bridge A and reliability level 1 for bridge B).

In the first scenario, initiated deterioration is allowed to continue until failure and afterwards, the bridge is replaced by a new one (i.e., a significant increase of the structural reliability). This scenario is considered a reference. The second scenario comprises a set of identical corrective actions that, when compared with the first one, increases the structural reliability less significantly. The last scenario consists of frequently applied preventative actions that do not influence the reliability but delay its degradation. The parameters defining each scenario are chosen based on the recommendations in the literature (Frangopol et al., 2001).

For each scenario, the time-dependent reliability index was quantitatively assessed using the simple linear maintenance models described in the previous section (see Figure 13). Then, they were transformed on the scale from 1 (best) to 5 (worst) respecting the proposed correlation between the quantitative and qualitative reliability scale (see Table 5) defined within the COST Action TU1406 (Hajdin et al., 2018).

Scales for the other KPIs (i.e., Availability and Safety) were elaborated within the COST Action TU1406 (Hajdin et al., 2018), but only qualitatively, expressing them on a scale from 1 to 5 (see Table 5). The costs for interventions are roughly estimated and only this KPI has a monetised scale. Within the proposed QC framework (Hajdin et al., 2018), each KPI refers to:

- Reliability: the probability of structural failure (safety), operational failure (serviceability) or any other failure mode.
- Availability: the amount of time a system is in a functioning condition.
- Safety: user safety during the service life of a bridge (related to non-structural elements).
- Cost: long-term costs for maintenance activities over the service life of a bridge.

6.1. Do nothing and rebuild scenario – lack of management

The scenario 'Do nothing and rebuild' (in Figures 14 and 15 with the black lines) allows the deterioration of the reliability index to continue until reaching the inadmissible level i.e., Level 5. At such a point in time, replacement of the whole structure with an identical new one was assumed. This action restores the reliability index of the case studies to their virgin reliability index (i.e., $\beta_0 = 4.96$ -Bridge A and $\beta_0 = 6.23$ -Bridge B), consequently, also leading to a delay in the initiation of the deterioration ($t_i = 8$ years). Such a delay corresponds to the period required for damage initiation in a new structure (e.g., initiation of reinforcement corrosion, among other phenomenons).

Table 5. Scale for KPIs (reliability, availability and safety) (Hajdin et al., 2018).

Scale	Reliability		Safety		Availability
	Quantitative scale (β)	Urgency of intervention	Quantitative scale	Qualitative scale	Qualitative scale
1	>4.00	Regular inspection	Injury return period > 100 years	No danger	No restrictions to traffic
2	3.25-4.00	Reassessment should be performed to update the period between inspections	Injury return period ~ 75 years	It is very unlikely that a person could get injured.	Weight, speed, and lane restrictions for heavy trucks
3	2.50-3.25	Reassessment should be performed to plan an optimal time of an intervention	Injury return period ~ 50 years	It is unlikely that a person could get injured.	Closure except for cars and regular lorries. Possible lane restrictions for regular lorries
4	2.00-2.50	Reassessment and possible intervention shall be performed shortly after an inspection	Injury return period ~ 20 years	It is likely that a person could get injured.	Closure except for cars. Possible lane restrictions for cars
5	<2.00	Immediate action/intervention is required	Injury return period < 10 years	Immediate danger	Complete closure

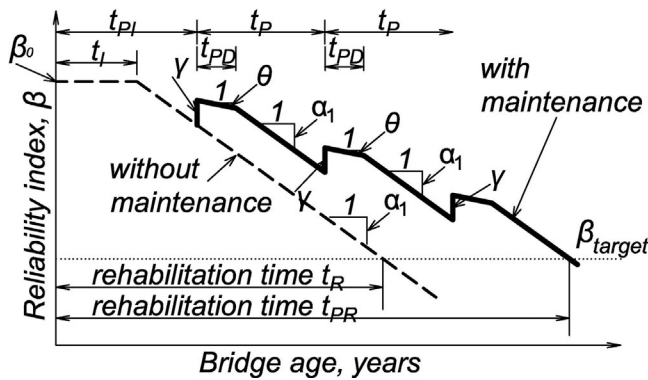


Figure 13. Reliability profile under no (dashed) and under maintenance (solid line) (Frangopol et al., 2001).

After the initiation period, the deterioration rate was assumed to be the same as the one before the bridge replacement ($\alpha = 0.08/\text{year}$). This action has the highest impact on reliability, but also the highest cost per action. The assumed costs are 2 mil. EUR based on the COST Action TU1406 recommendations (Hajdin et al., 2018).

Lack of any accessories repair is also assumed. Therefore, a decrease in the KPI 'safety' was proposed considering a higher deterioration rate than the one considered for structural reliability. For both case studies, a deterioration of the pavement, anchoring failure of the railings and/or disintegration of the expansion joints can be reasons for user safety reduction.

During the replacement, the KPI availability has dropped to a level 5 which corresponds to the complete closure of the bridges. After the replacement, the KPIs 'Availability', 'Reliability', as well as user 'Safety', are restored to a level 1 (best). Nevertheless, due to lack of maintenance, the availability starts to decrease again after a certain period. The reason may be a speed restriction due to poor riding conditions or restriction for heavy trucks due to reduced bridge reliability.

6.2. Corrective scenario

In this scenario, a set of identical corrective actions were assumed to be applied periodically with 15 years time

interval. Each action produces both, an increase in the reliability index and a decrease in the reliability deterioration rate. This scenario is defined in a way that, within the considered time horizon of 100 years, the reliability index would never down-cross the reliability level 5. This scenario simulates the effects of some of the maintenance actions on existing bridges. As corrective actions, rehabilitation of the deteriorated components of the bridges (arch slab and pier walls in bridge A, and deck's slab, girders and arch piers in bridge B) are considered.

It is assumed that each of the action improves the reliability index in 0.40-0.50 units and decrease the reliability deterioration rate to 0.07/years during an effective period of 7 years. After that, the reliability index continues to decrease with the same deterioration rate assumed before the action implementation ($\alpha = 0.08/\text{year}$). In this scenario, the first corrective maintenance action was employed while the bridges were still in overall good condition (reliability level 3).

A continuous decrease in availability was considered over time as a result of decreasing quality of riding conditions. During the application of the corrective action, the availability is reduced due to partial useability of the bridge (e.g., closure of one lane), while immediately after the actions, a small temporary improvement was assumed. Moderate costs were established for the corrective actions (250 000 EUR) based on the COST Action TU1406 (Hajdin et al., 2018). Bridge and accessories repairs are considered to be applied at the same time. Furthermore, user safety was considered to decrease over time with a small improvement after the performed maintenance action.

6.3. Preventative scenario

The last scenario considers preventative bridge maintenance through many relatively small repairs and activities to keep the bridge in a good condition and thereby avoiding large expenses in major rehabilitation. Minor concrete and reinforcement repairs were considered for both bridges: cleaning and sealing of the localised areas with damaged

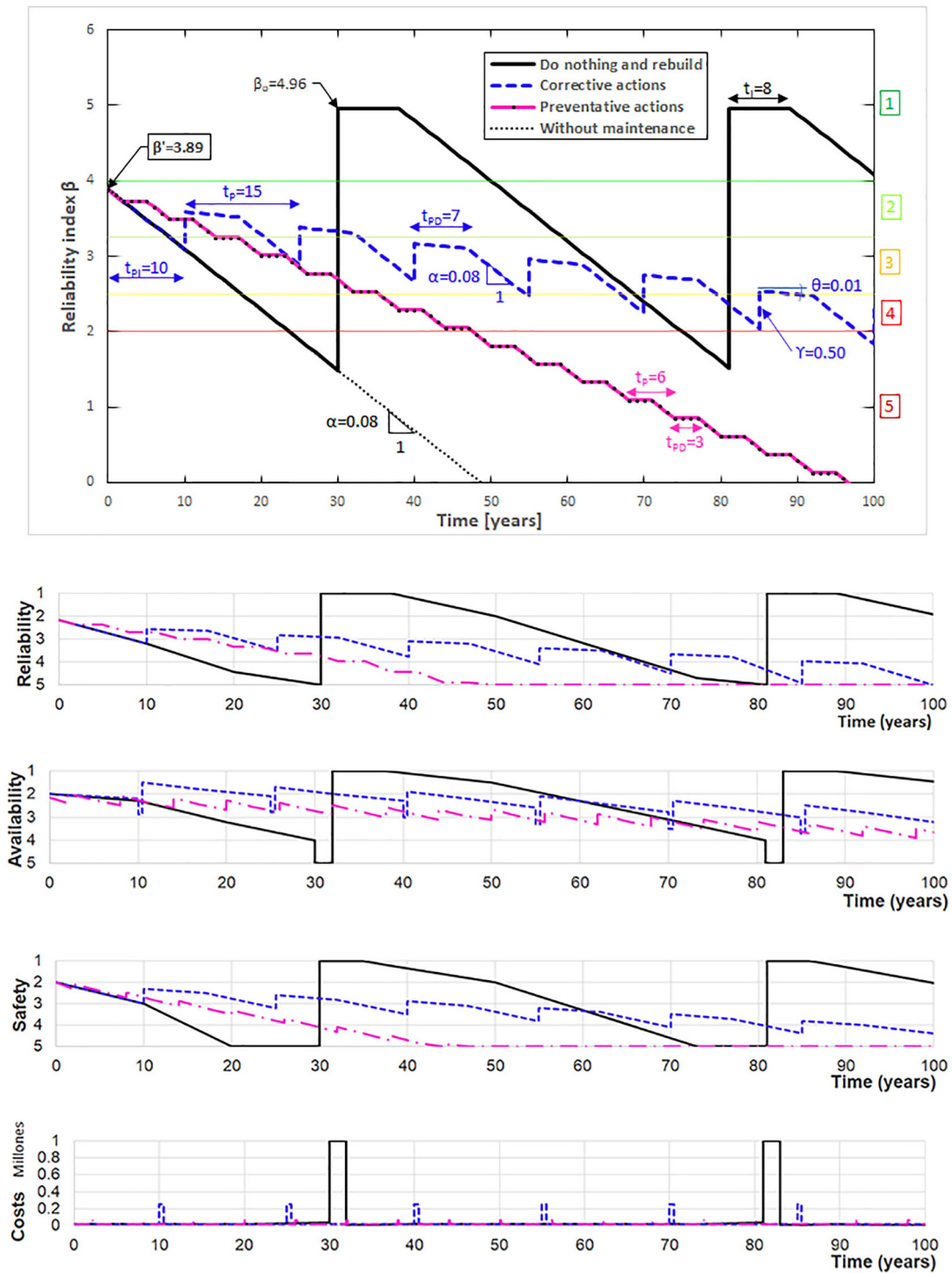


Figure 14. Evolution of KPIs: Reliability, Availability, Safety and Cost (Bridge A).

concrete and cleaning and protection of the corroded reinforcement. These actions cause no improvement in the reliability index but produce a delay in the deterioration rate (magenta coloured line in Figures 14 and 15). Here, the preventative actions were assumed to be taken over 6 years, delaying the degradation of the reliability for 3 years.

No reduction in availability during the performance of these actions was considered since they do not require traffic interruption. In this scenario, the availability was

continuously decreasing over time with a small temporary improvement after the preventative action. Minimum costs for these actions were considered (60 000EUR) based on the COST Action TU1406 (Hajdin et al., 2018).

6.4. Comparison

To be able to compare the results from all considered scenarios, 'the average' or net present value (NPV) of KPIs

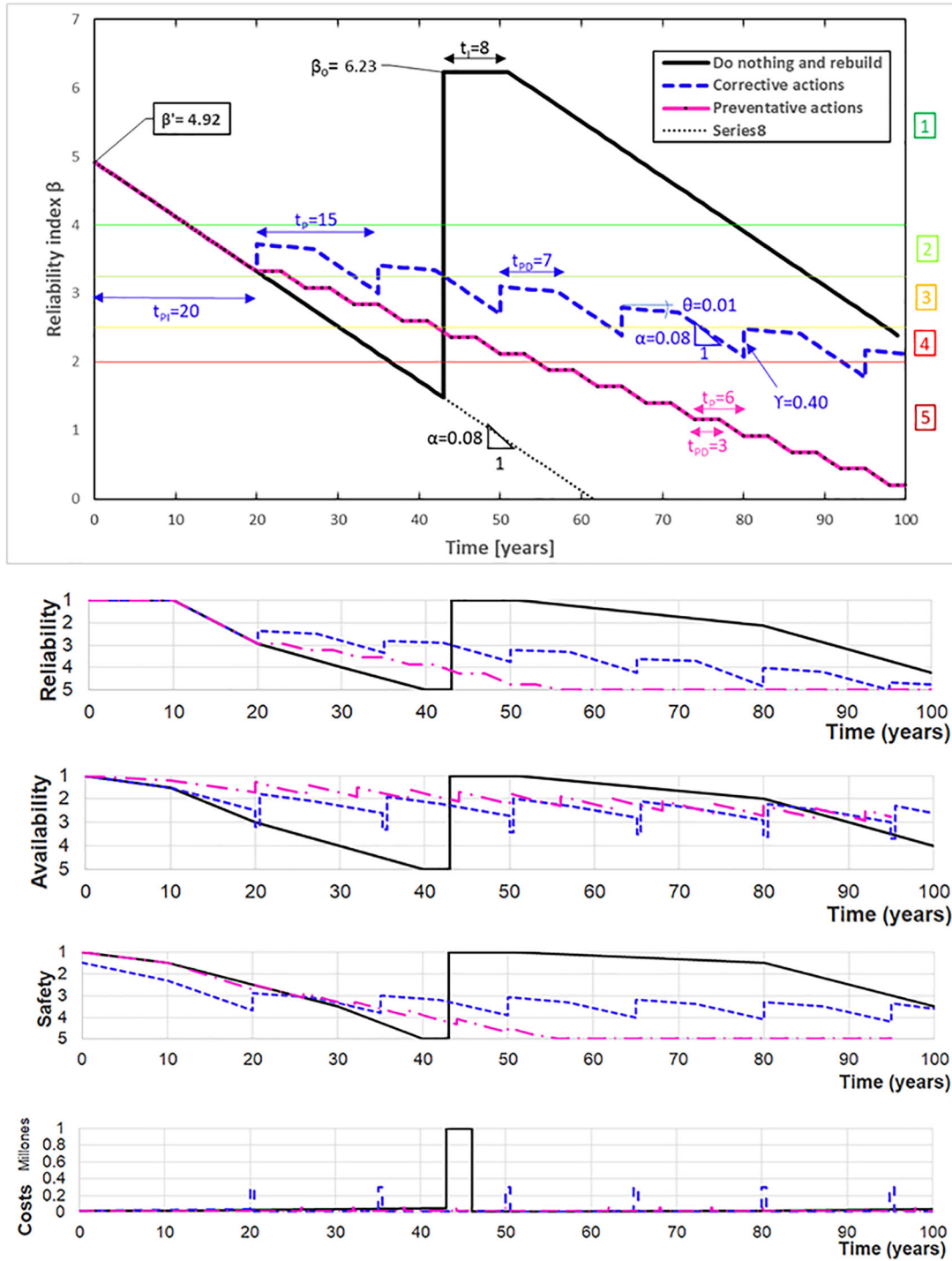


Figure 15. Evolution of KPIs: Reliability, Availability, Safety and Cost (Bridge B).

should be found and normalisation has to be performed to the values presented in Figures 14 and 15 based on Equations (5) (6) (7) and (8). In order to estimate the NPV as established in Hajdin et al. (2018), a procedure following Equation (9) is implemented:

$$R_N = 6 - (5 - (R - 1)) \quad (5)$$

$$A_N = 6 - \left(\left(\frac{-4}{3} \right) \cdot (A - 1) + 5 \right) \quad (6)$$

$$S_N = 6 - (6 - S) \quad (7)$$

$$C_N = 6 - \frac{4 - 4C}{C_{max} + 1} \quad (8)$$

where R_N is the normalised values of the reliability levels R , A_N is the normalised values of the availability levels A , S_N is the normalised values of the safety levels S and C_N is the assigned costs normalised by maximum yearly cost C_{max} of all considered cost scenarios C :

$$NPV_{KPI} = \frac{\{[r \cdot (t_i - t_{i-1}) - 1] \cdot KPI_i + KPI_{i-1}\} \cdot e^{-r \cdot t_i} + \{[r \cdot (t_{i-1} - t_i) - 1] \cdot KPI_{i-1} + KPI_i\} \cdot e^{-r \cdot t_{i-1}}}{r^2 \cdot (t_i - t_{i-1})} \quad (9)$$

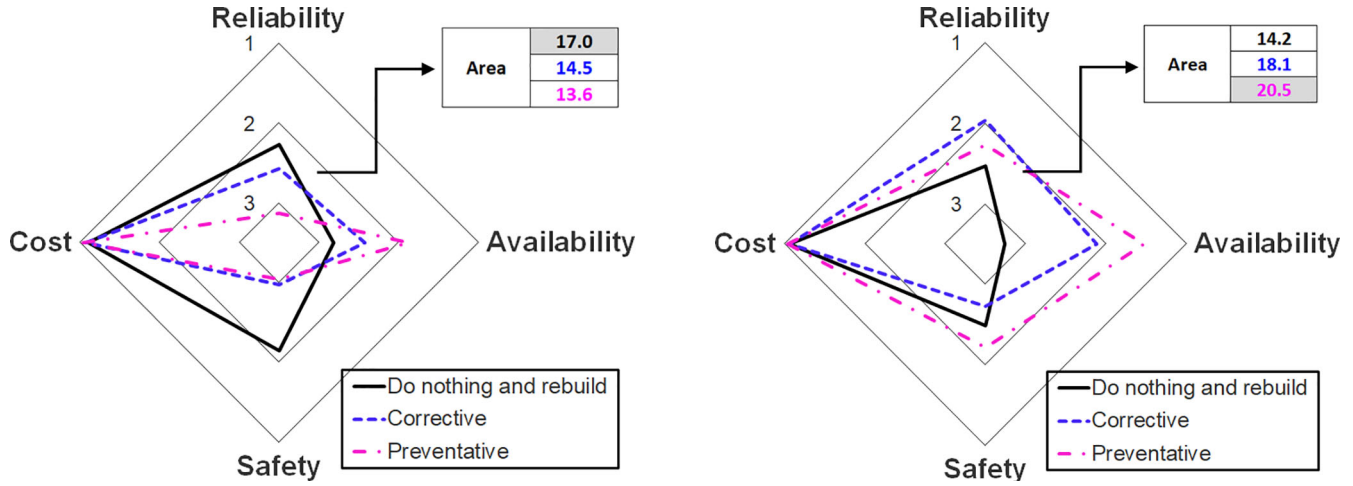


Figure 16. Four-leg spider diagram for the Bridge B. (a) 100-years period. (b) 43-years period.

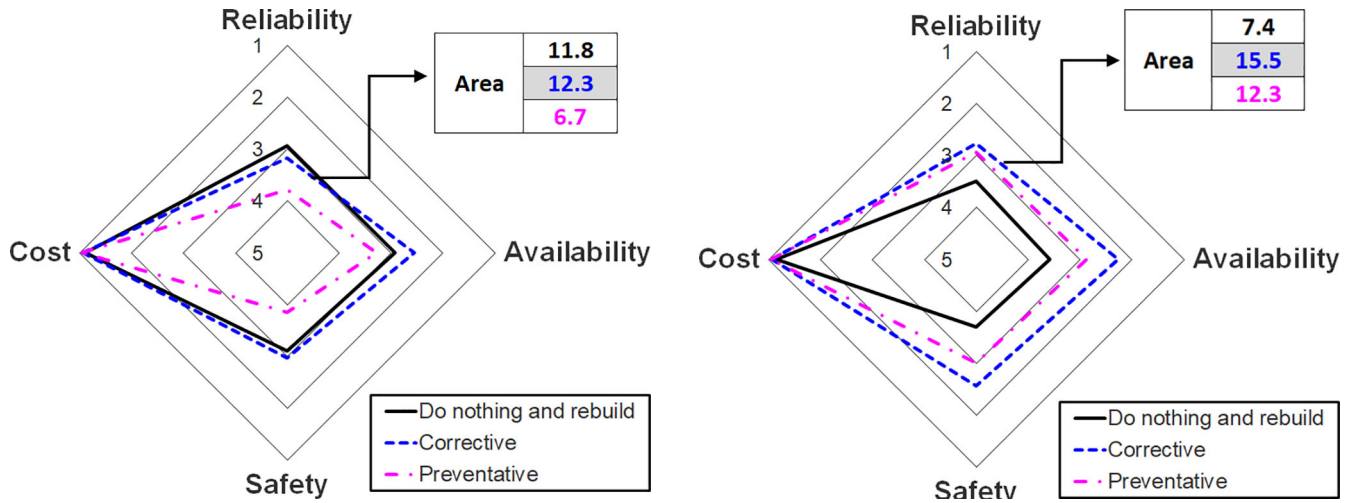


Figure 17. Four-leg spider diagram for the Bridge A. (a) 100-years period. (b) 32-years period.

where r is the discount rate, and the values KPI_i and KPI_{i-1} are the normalised KPIs related to the beginning and the end of a time interval (i.e., t_i and t_{i-1}), respectively. The KPI Cost is normalised by the maximum yearly costs of all considered scenarios. The net present KPIs are presented in Figures 16 and 17 in a form of a four-leg spider diagram, obtained using the 'Spidertool' established within the Action TU1406 (Hajdin et al., 2018). However, it is important to highlight that the four-leg spider diagram aims to compute the generated area of normalised KPIs to find the most suitable scenario for each case study.

For a general overview of the considered scenarios, different periods are examined. Therefore, the comparison is made here at two points in time, namely, at the end of the considered time horizon (100 years in both case studies) and right after the replacement of the structure by a new one

according to the reference scenario (32 years in the bridge A and 43 years in the bridge B).

The larger the spider diagram area, the higher the bridge performance under certain maintenance scenarios. Following this, for a period of 100 years, bridge B shows the highest performance under the scenario based on do nothing and rebuild actions ($A_{\text{spider}}=17\text{units}^2$) with a significant effect on reliability (comparing with the corrective scenario) but applied less frequently. On the other hand, for a period of 43 years (right after the replacement of the structure), the reference scenario provides the lowest performance of the bridge ($A_{\text{spider}}=14.2\text{units}^2$), while the preventative scenario is the most suitable one ($A_{\text{spider}}=20.5\text{units}^2$). For bridge A, the performance of the bridge is being kept higher with the corrective scenario for both considered periods. For clarification purposes, one needs to state that 'Costs' are

comparable for the different scenarios due to the performed normalisation based on a discounting rate of 2%.

7. Conclusions

This paper aims to present the implementation of a QCP based on the COST Action TU1406 framework through two illustrative examples i.e., two existing arch concrete bridges, one in Portugal and the other in North Macedonia. A probabilistic approach combined with a FEM nonlinear analysis was used to estimate the bridges' reliability index in their damaged state. Knowing the actual reliability at the time of the bridges inspection, three possible maintenance scenarios were considered: 'Do-nothing and rebuild', corrective, and preventative bridge maintenance. Comparing the normalised, net present values of each KPI in the form of a spider diagram, the following conclusions can be drawn:

- For a period of 100 years, bridge A shows the highest performance under maintenance with a set of corrective actions that improve the reliability index and decrease the deterioration rate during the action implementation period. On the other hand, bridge B has the best performance under the 'do nothing and rebuilt' scenario, allowing the deterioration of the structure over time. However, in terms of decision making, a hybrid scenario presenting a combination of different types of maintenances, would be a better solution for further optimisation.
- Other scenarios, like preventative maintenance in the case of bridge B, can be more appropriate if the comparison of NPV of the KPIs is performed for different periods (i.e., 43 years).
- Due to the performance over time of bridge A, it is notable that corrective maintenance offers a better solution to accomplish quality specifications standardised in COST Action TU1406 at a European level.
- More reliable results from this implementation can be obtained by a more accurate quantification of the evolution of the KPI 'Availability', as well as by employing a precise estimation of the maintenance costs and their dependency on the condition state of the structure when the actions are undertaken.

Disclosure statement

No potential conflict of interest was reported by the authors.

Funding

This research was developed at the University of Minho in close cooperation with the following entities: Portuguese Infrastructures, Ss. Cyril and Methodius University, COST Action TU 1406. This work was partly financed by: (i) national funds through FCT - Foundation for Science and Technology, under grant agreement 'PD/BD/143142/2019' and 'PD/BD/143003/2018' attributed to the 1st and 2nd author, respectively; and (ii) FCT/MCTES through national funds (PIDDAC) under the R&D Unit Institute for Sustainability and Innovation in Structural Engineering (ISISE), under reference UIDB/04029/2020.

ORCID

Edward A. Baron  <http://orcid.org/0000-0003-3270-9367>
 Neryvaldo Galvão  <http://orcid.org/0000-0002-9405-5445>
 Marija Docevska  <http://orcid.org/0000-0002-3256-747X>
 Jose C. Matos  <http://orcid.org/0000-0002-1536-2149>

References

- Amado, J., & Costa, C. (2020). Application of the COST TU1406 quality control framework to a stone arch bridge in Portugal. In *Proceedings of 9th International Conference on Arch Bridges* (Vol. 11). Springer. doi:10.1007/978-3-030-29227-0_97
- Brown, M. C., Gomez, J. P., Hammer, M. L., & Hooks, J. M. (2014). *Long-term bridge performance high priority bridge performance issues*. United States: Federal Highway Administration. Office of Infrastructure Research and Development.
- Casas, J. R., & Matos, J. C. (2021). Quality specifications for roadway bridges in Europe: Overview of COST action TU1406. In H. Yokota & Dan M. Frangopol (Eds.), *Bridge maintenance, safety, management, life-cycle sustainability and innovations*. YLondon: CRC Press. doi:10.1201/9780429279119-270
- Cavaco, E., Neves, L. A. C., & Casas, J. R. (2017). Reliability-based approach to the robustness of corroded reinforced concrete structures. *Structural Concrete*, 18(2), 316–325. doi:10.1002/suco.201600084
- Chajes, M., Hall, D., Taylor, W. L., Lewis, J., Wolfe, S., & Taylor, R. (2002). Load rating of arch bridges.
- Detle, G., & Sigrist, V. (2011). Performance indicators for concrete bridges. *Proceedings of Fib Symposium "Concrete Engineering for Excellence and Efficiency"*. doi:10.1002/suco.201190012
- European Committee for Standardization (2002). EN 1990, Eurocode 0: Basis of structural design. Brussels, Belgium.
- European Committee for Standardization (2003). EN 1991-2, Eurocode 1: Actions on structures - Part 2: Traffic loads on bridges. Brussels, Belgium.
- European Committee for Standardization (2004). EN 1992-1-2, Eurocode 2: Design of concrete structures - Part 1-2: General rules Structural fire design. Brussels, Belgium.
- Frangopol, D. M., Kong, J. S., & Gharaibeh, E. S. (2001). Reliability-based life-cycle management of highway bridges. *Journal of Computing in Civil Engineering*, 15(1), 27–34. doi:10.1061/(ASCE)0887-3801(2001)15:1(27)
- Frischmann, B. M. (2012). *Infrastructure: The social value of shared resources*. Oxford/New York: Oxford University Press.
- Galvão, N., Matos, J. C., Oliveira, D. V., & Hajdin, R. (2021). Human error impact in structural safety of a reinforced concrete bridge. *Structure and Infrastructure Engineering*, 0(0), 1–15. doi:10.1080/15732479.2021.1876105
- Hajdin, R., Kusar, M., Masovic, S., Linneberg, P., Amado, J., & Tanasić, N. (2018). Establishment of quality control plan - Cost action TU1406: WG. doi:10.13140/RG.2.2.28730.03526
- Guimarães, H., Matos, J. C., & Henriques, A. A. (2018). An innovative adaptive sparse response surface method for structural reliability analysis. *Structural Safety*, 73, 12–28. doi:10.1016/j.strusafe.2018.02.001
- Joint Committee on Structural Safety (2000). *Probabilistic model code - part 3: Material properties*. doi:10.1093/jicru/ndm007
- Kifokeris, D., Matos, J. C., Xenidis, Y., & Braganca, L. (2018). Bridge quality appraisal methodology: Application in a reinforced concrete overpass roadway bridge. *Journal of Infrastructure Systems*, 24(4), 04018034. ASCE doi:10.1061/(ASCE)IS.1943-555X.0000455
- Kurte, J., & Esser, K. (2008). Benefit of road traffic (Nutzen des Straßenverkehrs). In: *ADAC study on mobility (in German)*. Munich: ADAC (Ed.).
- Marelli, S., & Sudret, B. (2018). An active-learning algorithm that combines sparse polynomial chaos expansions and bootstrap for structural reliability analysis. *Structural Safety*, 75, 67–74. doi:10.1016/j.strusafe.2018.06.003

- Matos, J. C., Moreira, V. N., Valente, I. B., Cruz, P. J. S., Neves, L. C., & Galvão, N. (2019). Probabilistic-based assessment of existing steel-concrete composite bridges – Application to Sousa River Bridge. *Engineering Structures*, 181, 95–110. doi:10.1016/j.engstruct.2018.12.006
- Neves, L. C., & Frangopol, D. M. (2005). Condition, safety and cost profiles for deteriorating structures with emphasis on bridges. *Reliability Engineering and System Safety*, 89(2), 185–198. doi:10.1016/j.res.2004.08.018
- Nowak, A. S., Yamani, A. S., & Tabsh, S. W. (1994). Probabilistic models for resistance of concrete bridge. *ACI Structural Journal*, 91(3), 269–276. doi:10.14359/4354
- Olsson, A., Sandberg, G., & Dahlblom, O. (2003). On Latin hypercube sampling for structural reliability analysis. *Structural Safety*, 25(1), 47–68. doi:10.1016/S0167-4730(02)00039-5
- Onstein, R. (2013). *Arches, Nonlinear? Investigating the geometrically nonlinear behaviour of arches in 2D*. Delft, Netherlands: Delft University of Technology. Retrieved from <http://resolver.tudelft.nl/uuid:4bec56a9-de9c-4862-8d0e-affec6d0d035>.
- Pakrashi, V., Wenzel, H., Matos, J., Casas, J. R., Strauss, A., Stipanovic, I., ... Skaric, S. (2019). WG5 - Drafting of guideline/recommendations of cost action TU1406. Retrieved from <https://www.tu1406.eu/wp-content/uploads/2019/03/tu1406-wg5-report-final.pdf>.
- Powers, N., Frangopol, D. M., Al-Mahaidi, R., & Caprani, C. (2018). Maintenance, safety, risk, management and life-cycle performance of bridges. In *Proceedings of the Ninth International Conference on Bridge Maintenance, Safety and Management (IABMAS 2018)*, 9-13 Melbourne, Australia. CRC Press.
- Rijkswaterstaat. (2012). Leidraad RAMS—sturen op prestaties van systemen [RAMS guideline — managing the performance of systems]. Retrieved from https://puc.overheid.nl/doc/PUC_136293_31/1.
- Stewart, M. G., & Al-Harthy, A. (2008). Pitting corrosion and structural reliability of corroding RC structures: Experimental data and probabilistic analysis. *Reliability Engineering & System Safety*, 93(3), 373–382. doi:10.1016/j.res.2006.12.013
- Sykora, M., Diamantidis, D., Holicky, M., & Jung, K. (2017). Target reliability for existing structures considering economic and societal aspects. *Structure and Infrastructure Engineering*, 13(1), 181–194. doi:10.1080/15732479.2016.1198394
- Teixeira, R., Nogal, M., & O'Connor, A. (2021). Adaptive approaches in metamodel-based reliability analysis: A review. *Structural Safety*, 89, 102019. doi:10.1016/j.strusafe.2020.102019
- TNO DIANA (2016a). *User's manual - element library*. Delft, The Netherlands: TNO DIANA bv.
- TNO DIANA (2016b). *User's manual analysis procedures* (1st ed.). Delft, The Netherlands: TNO DIANA bv.
- Firestone, T. (2016). *Industry snapshots: Uses of transportation: 2015* (U.S. Department of Transportation. Bureau of Transportation Statistics, Ed.). Washington D.C. doi:10.21949/1501603
- Wiśniewski, D. F., Cruz, P. J. S., Henriques, A. A. R., & Simões, R. A. D. (2012). Probabilistic models for mechanical properties of concrete, reinforcing steel and pre-stressing steel. *Structure and Infrastructure Engineering*, 8(2), 111–123. doi:10.1080/15732470903363164



Article

Risk Assessment of Terrestrial Transportation Infrastructures Exposed to Extreme Events

Unni Eidsvig ^{1,*} , Monica Santamaría ², Neryvaldo Galvão ², Nikola Tanasic ³, Luca Piciullo ¹, Rade Hajdin ³, Farrokh Nadim ¹, Hélder S. Sousa ² and José Matos ²

¹ Natural Hazards Division, Norwegian Geotechnical Institute (NGI), N-0806 Oslo, Norway; Luca.Piciullo@ngi.no (L.P.); Farrokh.Nadim@ngi.no (F.N.)

² Department of Civil Engineering, Institute for Sustainability and Innovation in Structural Engineering (ISISE), University of Minho, 4800-058 Guimarães, Portugal; id8021@alunos.uminho.pt (M.S.); id8023@alunos.uminho.pt (N.G.); hssousa@civil.uminho.pt (H.S.S.); jmatos@civil.uminho.pt (J.M.)

³ Infrastructure Management Consultants GmbH (IMC), 8008 Zürich, Switzerland; nikola.tanasic@imc-de.com (N.T.); rade.hajdin@imc-ch.com (R.H.)

* Correspondence: uke@ngi.no

Abstract: Keeping transport links open in adverse conditions and being able to restore connections quickly after extreme events are important and demanding tasks for infrastructure owners/operators. This paper is developed within the H2020 project SAFEWAY, whose main goal is to increase the resilience of terrestrial transportation infrastructure. Risk-based approaches are excellent tools to aid in the decision-making process of planning maintenance and implementation of risk mitigation measures with the ultimate goal of reducing risk and increasing resilience. This paper presents a framework for quantitative risk assessment which guides an integrated assessment of the risk components: hazard, exposure, vulnerability and consequences of a malfunctioning transportation infrastructure. The paper guides the identification of failure modes for transportation infrastructure exposed to extreme events (natural and human-made) and provides models for and examples of hazard, vulnerability and risk assessment. Each assessment step must be made in coherence with the other risk components as an integral part of the risk assessment.

Keywords: risk assessment; natural hazards; extreme events; terrestrial transportation infrastructures; vulnerability; resilience



Citation: Eidsvig, U.; Santamaría, M.; Galvão, N.; Tanasic, N.; Piciullo, L.; Hajdin, R.; Nadim, F.; Sousa, H.S.; Matos, J. Risk Assessment of Terrestrial Transportation Infrastructures Exposed to Extreme Events. *Infrastructures* **2021**, *6*, 163. <https://doi.org/10.3390/infrastructures6110163>

Academic Editor: Belen Riveiro

Received: 22 October 2021

Accepted: 12 November 2021

Published: 17 November 2021

Publisher's Note: MDPI stays neutral with regard to jurisdictional claims in published maps and institutional affiliations.



Copyright: © 2021 by the authors. Licensee MDPI, Basel, Switzerland. This article is an open access article distributed under the terms and conditions of the Creative Commons Attribution (CC BY) license (<https://creativecommons.org/licenses/by/4.0/>).

1. Introduction

Efficient and secure transport networks are essential to the modern society. They ensure transportation of goods and people as well as access to employment and to essential services such as education, health care and emergency services. Keeping transport links open in adverse conditions and being able to restore connections quickly after extreme events are important and demanding tasks [1]. Many different types of adverse weather conditions challenge transportation networks such as intense precipitation [2], extreme temperatures [3], storms [4], floods [5], erosion, landslides [6–8], avalanches [9] and forest fires [10]. Climate change is anticipated to lead to an escalation of natural extreme events, both in frequency and magnitude [11,12]. In addition, human-made extreme events such as collisions [13,14], explosions [15], suicides on transportation lines, arson and terrorist attacks [16] pose a threat to transportation networks. Consequences of extreme events include accidents, damage to infrastructure assets, delays and malfunctioning of the transportation network, resulting in socio-economic losses and adverse environmental impacts [17–19]. The available funds for operation, maintenance and climate adaptation measures are limited, and it is important to make well-founded priorities. Thus, risk-based approaches are increasingly being applied to aid in the decision-making process of planning maintenance and prioritizing risk mitigation measures [20–22]. Here, the main tasks are to

identify the most vulnerable assets and prioritize measures and resources according to the available budget. Despite the implementation of state-of-the-art maintenance programs and risk mitigation measures, failures of infrastructure may still occur. Thus, it is necessary to also prepare for the recovery phase after failure.

1.1. Risk Assessment of Terrestrial Transportation Infrastructures in the Literature

The ISO framework [23] describes risk identification (i.e., adverse events that may occur and what may trigger them) as the first step in a risk management process. This assessment step is however scarcely described in risk assessment examples of terrestrial transportation infrastructures in the literature. Application examples usually start with a risk assessment of a specific adverse event, e.g., [2]—omitting the screening of all threats. There is a lack of studies that describe the identification of risk scenarios as part of the risk assessment framework, in a similar way that [22] describes holistic methods for risk evaluation of bridges. Existing overviews of adverse events for transportation infrastructure leading to structural damage and/or service disruptions consist of detailed lists [11,17,24]. However, these overviews are not exhaustive, and their use is also not presented as a part of the risk assessment. There is therefore a need to take a step back and present the identification of the risk scenarios in a more general way—to support the definition of the scope of the risk assessment.

General risk assessment frameworks (e.g., [23,25]) comprise assessing the hazard and vulnerability/fragility of the exposed elements/assets. However, practical challenges with concretization and conceptualization of the risk assessment steps arise when adopting these frameworks to specific applications. For instance, the Italian guidelines on risk classification and management of existing bridges group bridges into risk classes for prioritization of detailed assessment and funds allocation. Nevertheless, the application of the framework to real road networks has been found to provide conservative results and do not enable the ranking of bridges belonging to the same class given their qualitative nature [21]. Other risk assessment literature considers transport infrastructure specifically but treats the risk semi-quantitatively (e.g., [6,26]) and is focused on a specific hazard type (e.g., [27]) and/or a specific asset (e.g., [20]). Research efforts have been conducted in recent years to formulate methodologies capable of integrating all risk components effectively and reliably. A predominant part of this research has focused on the development of methodologies for risk quantification of bridge networks subjected to seismic ground motion [28,29]. Some work has been done for other types of natural hazards such as flooding and flood-induced scour [22,30]. Impacts of climate change on the intensity and frequency of the extreme events have also received attention and have been integrated into the hydrological modelling step within risk assessment frameworks [20,31].

In addition, given the possibility of infrastructure systems to experience multiple hazards, research interest has emerged towards the development of risk assessment methodologies to investigate the effect of interacting hazards such as rainfall-induced floods and mudflows [2] and earthquake-induced tsunami [32,33]. However, for other types of multi-hazard interactions, only the performance of bridges under these events have been studied since the risk analysis at the transportation system level requires spatial and temporal modelling of complex phenomena. Moreover, vulnerability models for other types of infrastructure assets such as road segments, pavements, tunnels, retaining walls, embankments and slopes are rather limited [34]. Thus, most risk assessment methodologies are demonstrated with real transportation networks yet select few bridges as primary vulnerable elements and neglect the damage to other network components.

Fragility functions have been widely applied in probabilistic risk and vulnerability assessment for buildings, in particular for earthquake risk (Hazus n.d.), but recently also for landslide risk assessment. Fragility functions have also been used for assessment of probability of damage to transportation infrastructure assets and service disruptions caused by landslides, debris-earth flow and flooding and for assessment of the combined effects of scouring and earthquakes for bridges, e.g., in [2,5,7,8,35–40]. An overview of the content

of these (and other vulnerability functions) is provided in Section 2.3.2. However, these functions only cover a subset of assets, failure modes and extreme events.

1.2. Scope of the Paper

The research presented in this paper was done within the H2020 project SAFEWAY, whose main goal is to increase the resilience of terrestrial transport infrastructure while minimizing long-term costs associated with maintenance and rehabilitation of the infrastructure. SAFEWAY aims to design and implement holistic methods, strategies, tools and technical interventions to strengthen terrestrial transportation network systems that are exposed to extreme events (natural and human-made). The project addresses reduction of vulnerabilities within:

- Preparation: by improving risk estimation and prediction and by developing better monitoring and decision tools;
- Response and recovery: by optimizing emergency plans and real-time communication with operators and end users;
- Mitigation: by introducing new construction systems and smart materials and by assessing consequences of different scenarios and mitigation solutions for selection of the optimal mitigation strategy.

The scope of this paper is to propose a framework for quantitative risk assessment of terrestrial transport infrastructures, integrating results from detailed analyses, application of existing models in the literature and external data sources, valid for:

1. Different levels of detail (regarding accuracy and complexity) and analysis scale (e.g., at asset level, within a transportation link or at network level);
2. Different types of infrastructure assets;
3. Natural extreme events (with focus on weather-related hazards) and unintentional human-made extreme events; (i.e., potentially disastrous events or disorders caused by human activity. Human errors [41] related to technical human activities are not included);
4. Assessment of structural damage and loss of mobility. The safety of the users is not considered directly, i.e., cases where road or railway users are directly injured by an extreme event are not considered, and the focus is on the infrastructure assets.

The proposed framework aims to bridge the gap between general risk assessment frameworks and specific risk assessments of terrestrial transportation infrastructures in literature (that focuses on specific risk component, on specific hazard types and/or specific assets).

The paper is organized in the following sections: Section 2 presents the development and conceptualization of the quantitative risk assessment framework, and application examples are provided in Section 3. Section 4 discusses limitations in the work done and the need for further work. Section 5 provides concluding remarks for the work.

2. Risk Assessment of Terrestrial Transportation Systems—Conceptualization of the Assessment Steps

The ISO 31000:2018 [23] represents a globally accepted standard for risk management, where risk assessment includes: risk identification, risk analysis and risk evaluation, and is followed by risk treatment (decision-making and execution of measures aimed at risk reduction). Risk assessment basically consists of finding answers to the following questions [25]:

1. What can cause harm? (Potential threats and adverse events are identified.)
2. How often may the identified adverse event occur? (What is the frequency of occurrence?)
3. What can go wrong? (Which are the exposed elements and what are the consequences?)

4. If it goes wrong, how severe are the consequences? (The severity will depend on the robustness/resistance of the exposed elements/assets and the intensity of the hazard.)

If the assessed risk is considered intolerable or unacceptable, the next question would be: What should be done to reduce the risk to an acceptable level?

This section outlines a framework for the risk assessment for terrestrial transportation systems by answering these basic questions. The focus is on the quantitative assessment of the risk, expressing each of the risk components and their combination into risk quantitatively.

2.1. What Can Cause Harm?

The first step in the risk assessment is to specify the scope of the analysis, and a key question is “What can cause harm”? This question will consist of identifying risk scenarios encompassing plausible descriptions of how a structural damage of the infrastructure assets and/or a service disruption may occur (i.e., failure mode), as well as description of the triggering event. Identification of risk scenarios should be based on experiences from the past, but other plausible extreme events (natural and human-made hazards) and failure modes should also be considered.

Table 1 is provided as an element for a screening process for selection of hazard types and failure modes to be considered in the risk assessment regarding the scope specification. The focus was on the weather-related natural hazards and on the unintentional human-made hazards. The selection of risk scenario(s) for further assessment can be made based on the most predominant hazard type in the study area and/or based on particularly vulnerable assets. Each of the failure modes in the table must be assessed separately following the steps in the risk assessment framework.

This paper suggests the arrangement of the failure modes/modes of malfunctioning into the following categories: (1) structural damage of transportation line assets, (2) material or obstacles (e.g., water, debris, objects) on the transportation line, (3) failure of supporting systems (signal system for trains, etc.) and (4) dangerous driving conditions, including precautionary closure (e.g., wind on bridges, forest fires, potential landslide hazard).

There could also be a chain of events over time that make the structure more prone to a certain failure mode or preconditioning events, which increases the probability of one or more of the failure modes listed in Table 1. For example: loss of vegetation (e.g., due to fire or drought) may lead to a decrease in slope stability and over time lead to slope failure. Other examples could be advanced deterioration or other slow hazards that over time causes failure.

Table 1. Overview of failure modes/modes of malfunctioning triggered by extreme events, classified into main categories (n.a. = not applicable).

Failure Modes/Modes of Malfunctioning				
Extreme Events	Structural Damage of Assets	Material or Obstacles on the Transportation Line	Failure in Supporting Systems	Other Dangerous Driving Conditions (Including Precautionary Closure)
Heat waves	Road: damage to pavement Railway: rail buckling	n.a.	Overheating of equipment	n.a.
Forest fires	Damages and deformations due to heat	n.a.	Overheating of equipment	Reduced visibility
Heavy precipitation	Damage to slope or embankment due to mass transport by surface water	n.a.	n.a.	Reduced visibility and reduced road surface friction
Flooding (urban, river, flash floods, storm surge)	Erosion of embankment, damage to bridge supports (e.g., scour)	Water on transportation line and in underground transport system	n.a.	Reduced road surface friction
Gravitational mass movements (Landslides, rock-falls, etc.)	Damage to road/rail sections, damages to bridges, embankments, etc.	Blocking of transportation line by soil/rock masses	Failure of signal systems	Load posting or line closure due to increase in occurrence probability of mass movements
Fog	n.a.	n.a.	n.a.	Reduced visibility
Storms (thunderstorms, hail, blizzards, i.e., strong wind gusts, intense snowfall)	n.a.	Unavailability of transportation line due to snow or obstacles on the transportation lines (e.g., falling trees)	Damage to support systems (e.g., owing to falling trees)	Reduced visibility and surface friction; strong wind gusts, especially on bridges, may lead to overturning of vehicles
Cold spells	“Thermal fatigue”; frost heave; asphalt of pavement Cracking, contractions of components	n.a.	Malfunction of signaling due to low temperatures	Technical failure of vehiclesReduced surface friction
Surface motions from, e.g., subsidence, sinkholes, uplift and swelling	Damage to road/rail sections, damages to bridges, tunnels, etc.	n.a.	Failure of signal systems	Load/speed posting or line closure (to prevent potential hazard trigger or reduce potential consequences to users)
Ship and vehicle collisions against bridges (or other assets)	Buckling of piers, deck overturning, failure of supports, etc.	Interruption of the underpass and/or overpass	n.a.	Vibrations and/or large deflections
Highway-railway grade-crossing accidents/incidents	Damage to the rail track or pavement	Obstacles on the transportation lines (e.g., damaged vehicles, injured people)	Damage to support systems (e.g., rail safety-guards, traffic lights)	Vibrations and/or large deflections
Explosion (i.e., gas explosion and vehicles on fire)	Damage to assets (resistance reduction due to high temperatures, dynamic loads)	Interruption caused by debris from the explosion or fire	Damage to support systems (e.g., rail safety-guards, traffic lights)	Reduced visibility caused by smoke

2.2. How Often May the Identified Adverse Event Occur?

This question is related to both the frequency or the temporal probability of the triggering extreme event and the conditional probability of structural damage of infrastructure assets and/or a service disruption (i.e., failure mode) in case of an extreme event.

Let:

- FM be the failure mode of interest. The failure mode describes the severity of structural damage and/or functional loss, due to an extreme event;
- EE_i be the extreme event of interest that could trigger the failure mode;
- i represent the intensity of the extreme event EE_i . The intensity is a single or a composite parameter expressing a damaging potential/action of the extreme event at asset(s) location;
- $P_{temporal}$ denote the temporal probability, e.g., annual probability expressing the occurrence probability per year.

The temporal probability of FM when considering a specific intensity value is the product of $P_{temporal}(EE_i)$ and $P(FM|EE_i)$. For assessment of the temporal probability of the failure mode, all intensity values need to be considered and their contributions summed:

$$P_{temporal}(FM) = \sum_{\text{All } i} P_{temporal}(EE_i) \cdot P(FM|EE_i) \quad (1)$$

The term $P_{temporal}(EE_i)$ expresses the temporal probability (typically the annual probability) of the extreme event, with a certain intensity, which is referred to as the hazard. For a specific geographical position, the hazard can be represented as a curve, i.e., as a mathematical function of the relationship between intensity and return period of the hazard (e.g. as described in Section 3.1.2). However, for practical design, the hazard curve is assessed at discrete return periods specified in the design code. Hazard assessment for an area would then comprise hazard zoning or hazard mapping, visualizing the spatial intensity distribution of the hazard on maps.

In general, the probability of an event might be estimated using three main strategies, separately, or in combination: (i) statistical analysis of historical events, e.g., by the use of extreme event analysis such as Gumbel, to analyze meteorological, geological, hydrological, agricultural, environmental and epidemiological data statistically in natural hazards assessment [42]; (ii) models expressing the occurrence of the event, considering also the uncertainty in the model parameters, e.g., by use of a geotechnical model in probabilistic slope stability analysis for slope-specific precipitation-induced landslide hazard assessment; and (iii) use of expert judgment, relating the probability to the degree-of-belief based on knowledge and intuition, e.g., by use of heuristic models for regional landslide hazard assessment [43].

The term $P(FM|EE_i)$ expresses the probability of FM in case of an extreme event with intensity i . For the different failure modes described in Table 1, this term would typically express the probability of:

- Structural damage to the asset, e.g., a partial failure or an asset collapse;
- Material or obstacles on the transportation line leading to service disruption, e.g., in terms of capacity reductions (e.g., a % of total capacity at an analyzed road section), speed reductions or load postings (e.g., a bridge is closed for freight traffic);
- Failure of supporting systems, where the definition of failure is contained within the detailed failure mode description;
- Dangerous driving conditions leading to restrictions, usually defined as thresholds on intensity parameters.

These probabilities will be assessed by using mathematical models for vulnerability assessment addressed in Section 2.3.2.

2.3. What Can Go Wrong?

In this step, the exposed elements and potential consequences are identified. Following the conceptualization of Section 2.2, the exposed elements are the assets or parts of the infrastructure, for which $i > 0$. The exposure assessment is a prerequisite to define the possible simultaneous failures of assets and other combinations of failures in the network. Bridges and tunnels are key assets in a terrestrial transport network. Their non-availability will directly lead to a service disruption on the transportation line. For other assets, the structural asset damage would not cause a service disruption, e.g., damages to the pavement.

2.3.1. Assessment of Exposure

For natural hazards, the exposed infrastructure assets can be identified as the geographical coincidence between the hazard and the location of the asset (Figure 1).

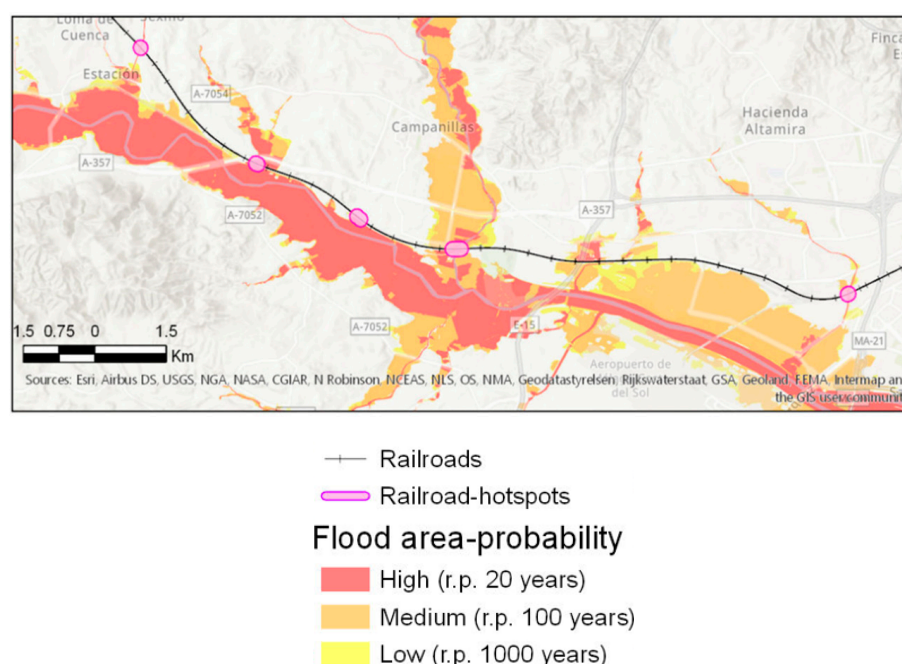


Figure 1. Exposure of railway track to floods for different flood return periods (20-years, 100-years and 1000-years) within the Málaga region, Spain. The exposed parts of the railway are indicated with pink ellipses. (Source: [44]).

Users, economic activity and the environment can be indirectly exposed to the event due to failures of related infrastructure assets, something accounted for in the consequence assessment (Section 2.4).

For unintentional human-made hazards, exposure maps as shown in Figure 1 are difficult to develop because it is unfeasible to predict spatial distribution of human-made events. However, one might identify locations with a higher likelihood for occurrence of such events, e.g., points more prone to collision (i.e., bridge crossing a river or seaway of high traffic) or other accidents.

The unintentional vehicle collision hazard is usually characterized by its intensity (in terms of collision force) and temporal probability [13]. An equivalent static design force of 2670 kN when a resistance design is concerned is suggested by [45]. Nonetheless, if the annual probability of collision occurrence concerning heavy vehicles is lower than 1.0×10^{-4} for critical bridges and 1.0×10^{-3} for typical bridges, resistance design for vehicle collision is not required. The annual probability for a bridge pier to be struck by a heavy vehicle depends on the expected average daily traffic, the share of heavy vehicles and characteristics of the road where the investigated bridge is located.

2.3.2. Assessing the Conditional Probability of Failure Modes

The potential consequences are described through the failure modes. Mathematical models for vulnerability assessment allow estimation of both direct and indirect consequences for a range of hazard intensities, through the definition of failure modes [46]. In estimation of direct material consequences, e.g., potential damage(s) to physical assets, damage or loss functions are often applied, describing the structural damage or functional loss of the asset (e.g., a bridge is closed until the inspection/repairs are finished). These functions take into account the hazard intensity and the structural resistance of asset(s) to the loads resulting from the related hazard action [47–49]. The structural damage is often described as the degree of loss on a dimensionless 0–1 scale.

Alternatives to damage and loss functions are fragility functions, which also express the uncertainty in the damage or functional loss. These functions describe the probability of exceeding different damage states for various hazard intensities [50]. The probability of damage or thresholds in a hazard intensity for different damage levels could also be described in terms of tables that specify the failure probability for different load conditions. Such tables represent discrete points on a fragility curve.

The probability $P(FM|EE_i)$ from Equation (1) could be found directly from fragility functions or fragility tables, if such models are available for the failure mode FM (e.g., as developed in Section 3.2. If damage functions are applied, the following strategy for calculation of $P(FM|EE_i)$ may be applied:

Let:

- $SD(FM)$ be the degree of structural damage of the asset(s) in the failure mode;
- SD_{calc} be the structural damage estimated from the damage functions.

For failure modes involving structural damage, Equation (2) yields:

$$P(FM|EE_i) = \begin{cases} 1, & \text{if } SD_{calc} \geq SD(FM) \\ 0, & \text{if } SD_{calc} < SD(FM) \end{cases} \quad (2)$$

Similarly, for failure modes, where dangerous driving conditions are defined by the intensity exceeding a threshold T , Equation (3) yields:

$$P(FM|EE_i) = \begin{cases} 1, & \text{if } i \geq T \\ 0, & \text{if } i < T \end{cases} \quad (3)$$

A review of existing damage, loss and fragility functions has been conducted for both natural and human-made hazards. As the availability of such functions is limited in literature, the reviewed extreme events and related failure modes/modes of malfunctioning cover a subset of all the aspects from Table 1. Table 2 provides a summary of the review.

Table 2. Damage, loss and fragility models from the literature for different extreme events and failure modes/modes of malfunctioning (n.a. = not available).

Overview of Available Damage, Loss and Fragility Models			
Extreme Event	Structural Damage of Assets	Material or Obstacles on the Transportation Line	Dangerous Driving Conditions (Including Precautionary Closure)
Heat waves	Temperature threshold models for rail buckling: [3,51–53]	n.a.	Probability of adverse events for different threshold values of temperature: [54]
Flooding (urban, river, flash floods, storm surge)	Bridge scour leading to bridge failure: [35–37,55] Ballast scour and failure: [38] Roadway embankment scour: [39] Material damage to roads: [56]	Vehicle speed as function of floodwater depth: [5] Functional capacity loss functions as a function of inundation depth: [2,7]	Thresholds for vehicle stability in floods: [57]

Table 2. Cont.

Overview of Available Damage, Loss and Fragility Models			
Extreme Event	Structural Damage of Assets	Material or Obstacles on the Transportation Line	Dangerous Driving Conditions (Including Precautionary Closure)
Landslides	Material damage to roads: [9,56]	Malfunctioning due to debris on roads as a function of landslide volume: [8]	n.a.
Storms	n.a.	Probability of adverse events for different threshold values of wind speed: [54]	Threshold models for wind speed on bridges: [53]
Ship and vehicle collisions against bridges	Vehicle collision with bridge piers: [58] Vehicle collision with bridge piers: A state-of-the-art review: [13] Nonlinear finite element analysis of barge collision with a single bridge pier: [14] A comprehensive assessment of the existing accident and hazard prediction models for the highway-rail grade crossings in the state of Florida: [59].	n.a.	n.a.
Highway-rail grade-crossing accidents/incidents	Vulnerability of bridges to fire: [16] Analysis of a bridge failure due to fire using computational fluid dynamics and finite element models: [60]	n.a.	n.a.
Explosion (i.e., gas explosion), bombing and vehicles on fire	Analysis of a bridge collapsed by accidental blast loads: [15]	n.a.	n.a.

2.3.3. Recommendations for Development/Adaptation of Structural and Functional Vulnerability Functions

The review of vulnerability functions summarized in Table 2 indicates a lack of vulnerability functions in literature for several failure modes and extreme events. Nonetheless, existing vulnerability functions should also be used with caution. Significant variabilities for assets exist across different countries, and different classes of assets are encountered depending on the classification of the transport system [34]. Prior to the vulnerability assessment, one of the following steps should be accomplished:

1. Verification of existing fragility functions to site-specific conditions, i.e., by examining if the available fragility function appropriately represents the behavior of the asset types representative of the study area.
2. Adaptation of existing fragility functions to site-specific conditions, i.e., by calibrating the existing fragility function to observational data or by combining an existing fragility curve with observational data through Bayesian updating.
3. Development of new fragility functions based on recommended intensity parameters in Table 3 and using one of the four main approaches to develop vulnerability models [49]:
 - Judgmental: based on expert opinion or engineering judgement.
 - Empirical: based on observations.
 - Analytical: based on analytical or numerical solution methods.
 - Hybrid approach: combining one or more of above approaches.

For development of fragility curves for assets, analytical approaches validated by experimental data and observations from recent events have become more popular. According to [49], the analytical approach is the most commonly encountered in the peer-reviewed literature. This approach could be applied to different structure types and geographical regions, where damage records are insufficient. Functions describing degree of loss are mainly based on empirical data collected in the field in the aftermath of an event and are consequently specific to the exposed elements in the area where the data have been collected [50].

Table 3. Summary of the main parameters for vulnerability and risk analysis.

Extreme Event/Hazard		Asset	
Type	Modelling Variable	Type	Failure Mode
Flooding	Water discharge	Bridge	Bridge scour leading to bridge failure
Flooding	Water discharge	Culvert	Failure of culvert leading to water overtopping and material damage to road/rail
Flooding	Water discharge	Embankment	Failure of embankment caused by erosion
Flooding	Water discharge	Roadway or rail track	Wash-out of roadway/rail track
Rainfall/urban flooding	Water depth	Roadway	Speed and capacity reductions/service disruption due to water on road
			Speed and capacity reductions/service disruption due to debris on road/track after flooding
Flooding	Volume of debris	Roadway or rail track	Speed and capacity reductions/service disruption due to landslide masses on road/track
Landslide	Volume of landslides	Roadway or rail track	Speed reductions of trains to avoid buckling of tracks
Heatwave	Temperature	Rail track	Closed bridges due to strong wind gusts
Wind	Wind speed perpendicular to the bridge	Bridge	Failure, collapse, damaged element
Ship and vehicle collisions against bridges	Impact force	Bridge	Closed or traffic reduction/failure, collapse, damaged element
Highway-rail grade-crossing accidents/incidents	Down time and restricted lanes	Roadway or rail track	Closed or traffic reduction/failure, collapse, damaged element
Explosion (i.e., gas explosion and vehicles on fire)	Pressure-impulse	All types of assets	Closed or traffic reduction/failure, collapse, damaged element

Table 3 summarizes the failure modes for different asset types and extreme events with suggested main modelling variable for the vulnerability assessment.

2.4. If It Goes Wrong: How Severe Are the Consequences?

Economic consequences of extreme events on transportation infrastructure encompass direct consequences (e.g., structural damage, loss of life and limb e.g., [61]) as well as indirect consequences, which stem from the interruption of the transportation service (e.g., user costs due to additional travel time, socio-economic consequences due to the service disruption). The consequences could further be classified as associated to market values or not [19]. In the following, only consequences associated with market values are considered. Let:

- $C(FM)$, $C_{direct}(FM)$ and $C_{indirect}(FM)$ denote the consequences, the direct consequences and the indirect consequences respectively associated with a failure mode FM , considering the full range of plausible intensities of EE_i .
- RC be the full repair and reconstruction costs of the asset.
- CS be the costs of service disruption per hour.
- $D(FM)$ be the duration of the service disruption in hours associated with a failure mode FM .

Then:

$$C(FM) = C_{direct}(FM) + C_{indirect}(FM) \quad (4)$$

To calculate the probability of a failure mode and related consequences caused by different natural hazards, it is suggested to use event trees or a Bayesian network. Guidance for such analyses is provided as an example in Section 3.3.

2.4.1. Assessment of Direct Consequences

The damage, loss and fragility functions connects directly the intensity of a hazard with a failure mode, described in quantitative terms (e.g., damage degree of an asset, number of failed elements). This further enables monetization by including the value of affected assets. If $SD(FM)$ is expressed on a scale 0–1, and the direct consequences refer to the costs for repair and reconstruction related to extreme events, Equation (5) yields:

$$C_{direct}(FM) = SD(FM) \cdot RC \quad (5)$$

Fragility functions can be converted into damage functions using a damage-to-loss model, i.e., relation between a damage state/failure mode and the corresponding damage degree [62].

The consequence assessment could be performed for each asset individually or on a portfolio of assets. Assessment at the level of the individual assets is challenging as it requires development of a series of structural vulnerability functions as well as access to detailed data about the assets. Thus, for regional scale analyses, it is proposed to work on the portfolio level, classifying the assets into homogeneous classes. The idea is to identify the key parameters for a group of assets, which can be readily applied in development of the series of fragility functions. For example, to cluster similar bridges, features that govern the resistance to extreme events are identified. Such features might be intrinsic such as bridge material, mileage, or span count, or extrinsic such as local weather conditions or traffic. Further steps in the portfolio assessment encompass estimation of number of assets within each class in the study area and relating the failure mode to an intensity parameter of a hazard process. The total direct consequences are found by an aggregation of the monetized structural damage to all the assets in the flooded area [27,56,63].

In the evaluation of direct consequences to infrastructure due to natural hazards, some simplifications can be adopted. For example, drainage systems and roads are usually designed based on a specific return period of flooding or rainfall. In these and similar cases, it is a valid assumption to adopt neglectable damages for flooding events with return periods below the design rainfall/flooding event. Such approximation is demonstrated in Section 3.3.

2.4.2. Assessment of Indirect Consequences

In estimation of indirect consequences of extreme events on transportation systems, assessment of disruption of the related transportation service(s) is the key task. For such assessments, functional vulnerability functions are useful, expressing directly the probability of service disruption as a function of event intensity instead of probability of structural damage states [2,40]. Functional vulnerability functions are feasible for quantitative vulnerability assessment at a network level, describing the functionality loss (e.g., reduction of a traffic capacity) due to a given hazard intensity.

A service disruption would leave the travelers with several options: postpone or cancel the trip, change mode of transport or travel destination, or take a detour [64]. The severity of the indirect consequences is influenced by the failure mode (e.g., full/partial closure), the duration of the service disruption, the quality and capacity of the alternative transportation routes or alternative modes of transportation as well as the traffic volume and traffic composition in the affected network. The main portion of indirect costs to users stems from additional travel time, which is commonly used in calculations (e.g., the total time delay in [65]). Besides additional travel time, if sufficient input data on traffic are available, other consequences can be included as well: those due to the increased travel distances (via fuel consumption) and accident costs (e.g., [66]), increased air pollution and increased noise [67]. Further, indirect consequences can also encompass costs related to work time lost, and loss of income due to perishable goods spoiling. Long-term indirect effects of a repeatedly malfunctioning infrastructure could also comprise change in travel patterns affection, e.g., tourism and businesses depending on the transportation line.

Meyer et al. [19] gave a broad review of assessment of indirect costs of natural hazards affecting infrastructure. The review encompasses methods such as event analysis, econometric approaches, input–output analysis, computable general equilibrium analysis, intermediate models, public finance analysis and idealized models.

Network analysis is used to determine the flow of vehicles through a transport network. Network analysis could be based on:

- Graph theory and topological properties of the transport network. Such approaches consider networks as a collection of vertices (or nodes) that are connected by arcs (or links) and consider the importance of different links, cascading failures and interdependencies between different networks. Graph-theoretical concepts are useful for the description of transport network characteristics and its connectivity [18].
- Understanding of the dynamic behavior exhibited on networks (e.g., traffic flow) using transportation system models, modelling demand and supply side of the transport system and travelers' responses to disturbances and disruptions. Most risk frameworks account for traffic-related consequences using a macroscopic model with static user-equilibrium flow formulation. This traffic assignment model presents strong assumptions such as steady traffic conditions during the time of investigation, constant demand, and user's complete knowledge of the traffic conditions. The traffic flow could be modelled, e.g., considering the traffic as a fluid and using models based on fluid dynamics equations [68]. However, it has been found that traffic demands and changes in travel patterns, i.e., in destination and mode choice, may be significantly altered after the occurrence of hazardous events [4]. Users' response represents the main capability of the system to adapt to changes when any disruptive event occurs. Recent research has investigated the stochastic user's behavior in disrupted networks to provide a more realistic mobility pattern [69].

The modelling could encompass behavioral responses of the travelers to network disruptions or other changes in the supply side of the transport system. The travelers' behavior would affect the demand side of the transport system. Important mathematical and statistical aspects of the disposition and behavior of road traffic are considered by [70].

The failure modes provided in Table 1, involve a different course of events from a malfunctioning of infrastructure back to its normal operation and result in different durations of service disruptions. It should be noted that resourcefulness (i.e., availability of adequate human, machinery, funding resources) and duration of procedures preceding the restoration activities (elaborating project documentation, tenders) can also impact the duration of service disruption.

Failure modes involving structural damage and functional failure of assets can be related from a short (hours/days) to a long duration (months/years), depending on the extent and complexity of repair/restoration activities (or a replacement of failed assets). The same goes for failure modes involving failure of supporting systems (e.g., gas, electricity). The severity of service disruption caused by material or debris on the transportation line would depend on volume of material on the roadway/track to be removed and available resources to act on a short notice. For the failure modes involving dangerous driving conditions and precautionary closure due to exceedance of a weather parameter threshold, these solely depend on natural conditions and generally relate to a short duration (e.g., hours) of service disruption. A simplified way to calculate the indirect consequences is presented in Equation (6).

$$C_{indirect}(FM) = CS \cdot D(FM) \quad (6)$$

2.5. Proposed Framework for Risk Assessment of Terrestrial Transportation Systems

Following the risk assessment steps and the conceptualization in Sections 2.2–2.4, the risk assessment encompasses identification of risk scenarios and selection of analysis scope (FM and extreme event EE), assessment of hazard ($P_{temporal}(EE_i)$), exposure (assets where $i > 1$), vulnerability ($P(FM|EE_i)$ and structural damage, SD) and consequences ($C(FM)$).

These steps are illustrated in Figure 2. The risk associated with one failure mode, $R(FM)$, could be expressed as:

$$R(FM) = P_{temporal}(FM) \cdot C(FM) \quad (7)$$

The steps necessary for assessment of risk posed by natural and human-made hazard events on transportation systems are illustrated in Figure 2.

It is worth noting that the implementation of the proposed framework is based upon the assumption that an inventory of the infrastructure assets is provided by the infrastructure owner. However, the unavailability of high-quality inventory data is an issue shared by many countries. One of the main drivers of this problem is the lack of a systematic data collection procedure. Thus, some efforts have been made to propose protocolled taxonomy and methods for data collection, aiming at unifying databases into a functional structure ready to be used in risk assessment frameworks (e.g., [21,22]).

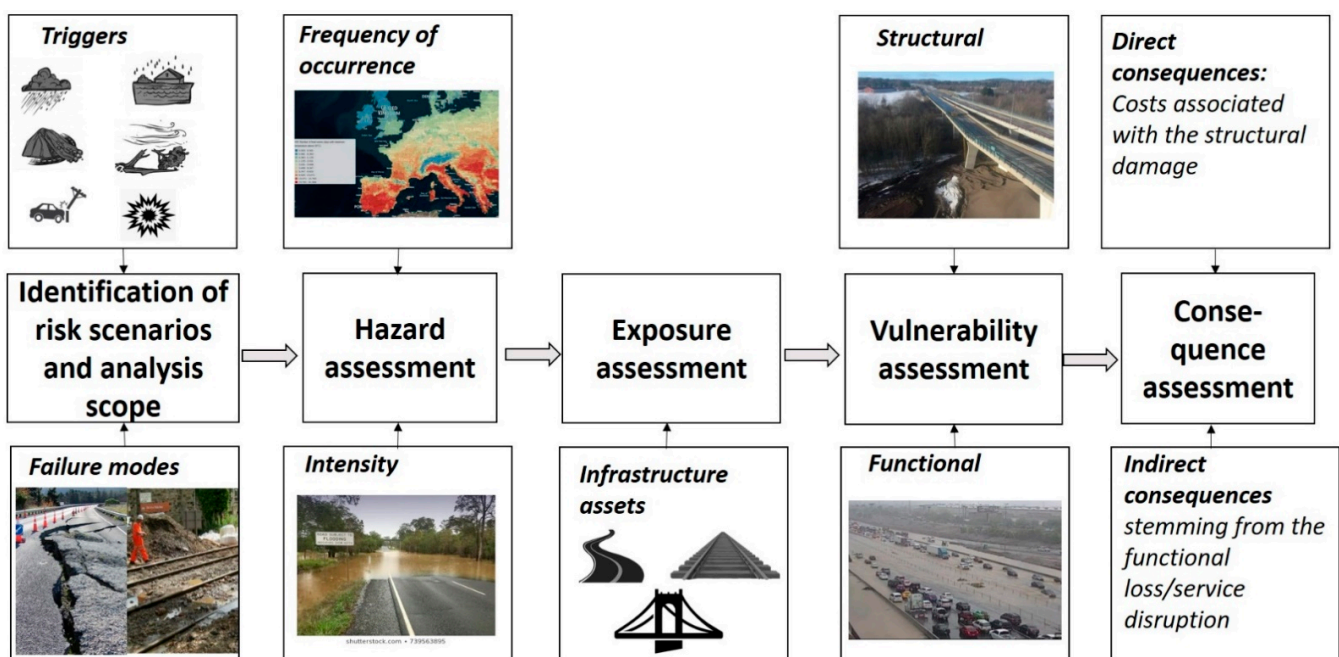


Figure 2. Framework for assessment of risk associated with extreme events on transportation systems.

3. Application Examples

The next subsections provide examples of assessment of hazard, vulnerability and risk. The hazard assessment examples (Section 3.1) demonstrate assessment of the temporal probabilities from Equation (1)

- $P_{temporal}(FM)$, for the failure mode failure of bridge caused by human-made hazard (Section 3.1.1);
- $P_{temporal}(EE_i)$, for the extreme event flooding, for a range of flooding intensities i (Section 3.1.2);
- $P_{temporal}(EE_i)$ of natural hazards from available data bases and data sources (Section 3.1.3).

Addressing the lack of vulnerability functions, a vulnerability assessment example is provided, demonstrating the development of a fragility curve for the failure mode bridge failure caused by flooding-induced bridge scour. The fragility curve expresses $P(FM | EE_i)$ for a range of flooding intensities (Section 3.2).

The risk assessment example demonstrates the assessment of $R(FM)$ for the failure mode service disruption of road caused by flooding and exceeded culvert capacity (Section 3.3).

3.1. Hazard Assessment Examples

3.1.1. Use of Bridge Failure Data for a Temporal Probability Assessment

Table 4 describes the rate of failure of existing bridges from 1966 to 2020 based on a worldwide bridge failure database [71]. The content of this table is limited to existing bridges, therefore disregarding failure during the construction phase. Accordingly, the main causes of failure were grouped in two main groups (Figure 3), natural hazards (NHs) and artificial hazards. This last one has been subdivided into three subgroups, namely, human-made hazards (HMHs), human error (i.e., design and construction errors (D&CEs) and operational errors (OEs)). A more detailed discussion on the proposed classification concerning the causes of failure can be found in [72].

Table 4. Rate of failure of existing bridges (data extracted from: [71]).

Period	Recorded Failures	Percentage	Failure Frequency *			
			NHs	HMHs	D & CEs	OEs
1966–1970	10	1.5%				
1971–1975	18	2.7%				
1976–1980	38	5.8%				
1981–1985	13	2.0%				
1986–1990	20	3.0%				
1991–1995	16	2.4%				
1996–2000	21	3.2%				
2001–2005	65	9.9%				
2006–2010	108	16.4%				
2011–2015	157	23.9%				
2016–2020	191	29.1%	1.92×10^{-5}	1.86×10^{-5}	2.79×10^{-6}	1.40×10^{-5}
Total	657	100% **				

Total Bridge Stock: 3.225.047 [73]

* NH: natural hazards; HMH: human-made hazards; D&CE: design and construction errors; OE: operational errors. ** Due to rounding error, the sum of the percentages shown in the table is not exactly 100%.

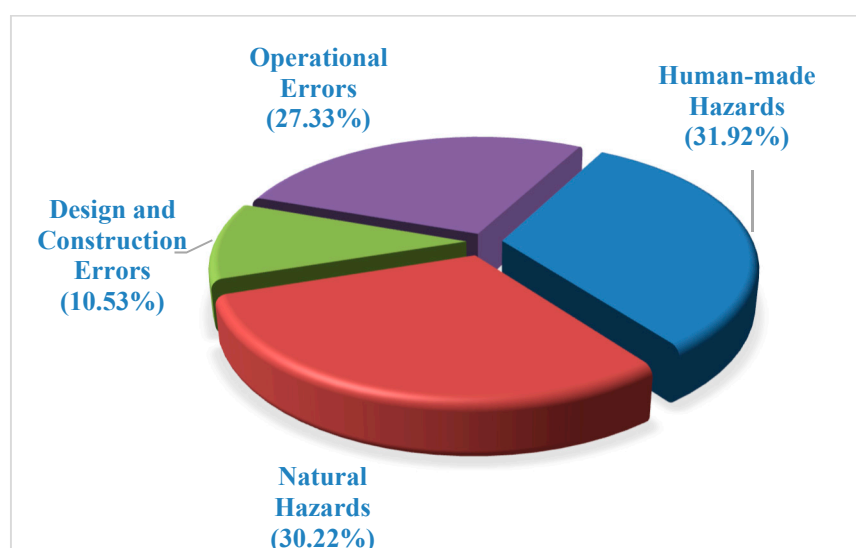


Figure 3. Main causes of failure of existing bridges (1966–2020).

By tracking the recorded number of failures since 1966, an increasing trend is observed. Although the causes behind this trend are unknown, one can speculate that information from more recent failures is easier to obtain, e.g., through social media. Nonetheless, the ageing of the bridge stock, increasing traffic load, climate change and the growth of the built environment, as society evolves, are also variables that must be considered.

The total number of bridge stock around the globe is roughly estimated to be 3,225,047 according to [73]. Using such number and according to the number of failures recorded between 2016 and 2020 and the main cause of failure, the failure frequency for each main cause is estimated. NHs and HMHs are the main causes of failure. The total frequency of failure is estimated to be around 5.46×10^{-5} for a five-year period, which corresponds to an average annual failure frequency around 1.09×10^{-5} . Similar numbers were presented in [73] for some bridge failure databases analyzed under the scope of the developed work. Curiously, the annual target failure probability for ultimate limit state proposed in [74] is 1.0×10^{-6} ($\beta = 4.7$) for a structure of reliability class two (RC2). Nevertheless, when factoring the cost of safety and consequence of failure, considering normal cost of safety and moderate consequences (something expected from typical bridges according to ISO 2394:2015), an annual target probability of failure around 1.0×10^{-5} ($\beta = 4.2$) is suggested [75].

The average annual bridge-failure probability due human-made hazards is in the same way estimated as 3.72×10^{-6} . This number represents mostly the failure of bridges triggered by unintentional human-made hazards (ship and vehicle collisions, and overloading caused by users).

3.1.2. Flood Hazard Assessment on a Local Level

One of the most widespread approaches for assessing the flood hazard consists of estimating the extreme discharge for a given exceedance probability by fitting of a probability distribution function to a record of annual maximum discharges. This method, frequently referred to as flood frequency analysis (FFA), has been standardized in different manuals such as in the Flood Estimation Handbook in the UK [76] and the Bulletin 17C in the US [77].

A flood frequency curve was derived for the Tagus River in Portugal at Tramagal river gauge location. Data are available for 26 years of records approximately.

Despite that there is no standardization proposed at the Portuguese level, a Gumbel distribution is assumed to represent more appropriately the peak discharges as suggested by the Management Plan of the Tagus Hydrographic Region [78]. The L-moments method was used to estimate the parameters of the Gumbel distribution. Gumbel probability plots and Chi-squared goodness of fit tests showed that the peak annual discharge can be reasonably well modelled by a Gumbel probability distribution function (see Figure 4).

It is acknowledged that the obtained flood frequency curve is not an exact approximation, as the record of annual peak flows at a given location is a random sample of the underlying population of annual peaks. Then, to quantify the confidence of this approximation, an interval which contains the population frequency curve is commonly constructed (usually 95% of confidence is used) [77]. In this manner, the uncertainty in the flood event intensity due to sampling variability is considered, yet conditional on the choice of a particular distribution.

It can be observed from Figure 4 that for smaller, i.e., more frequent events, the reliability of the discharge estimation is greater than for larger events (very wide confidence intervals). This is expected as the database of past events is sparse, i.e., only 25 years of records are available. Thus, there are significant uncertainties in the estimated river discharges obtained through this statistical approach. As more data become available, it is expected that the estimates improve and consequently the confidence intervals narrowed.

Despite the wide applicability of the method, it should be kept in mind that the accuracy of the estimated flood frequency curve depends on many factors, such as the records sample size, its representativeness, errors in the measured annual peak discharges and the underlined assumptions, namely the appropriateness of the chosen distribution and the hydrologic stationarity [77,79]. Research efforts are being conducted with the overall aim of reducing all these sources of epistemic and aleatory uncertainties in the estimation of flood frequency analysis.

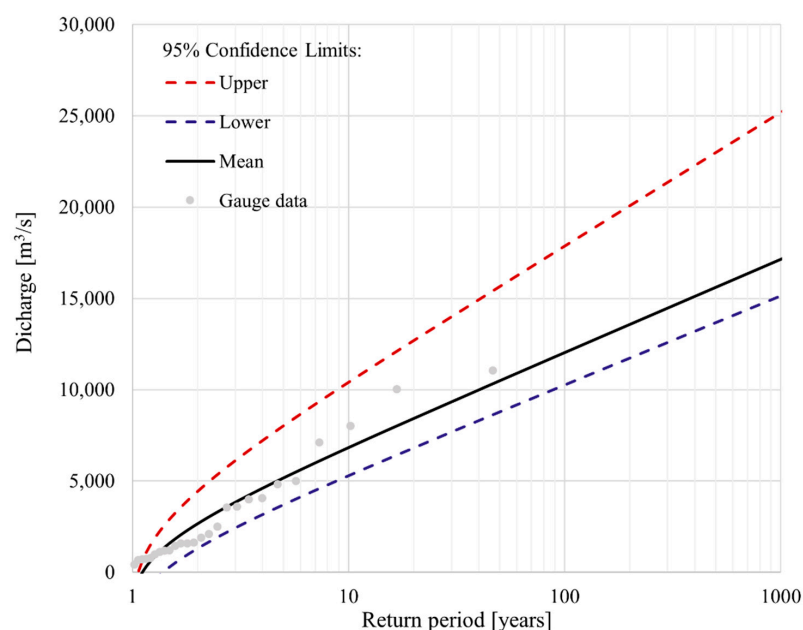


Figure 4. Flood frequency curve for the Tagus River at Tramagal river gauge.

Figure 4 expresses the relationship between return period of flooding and flooding intensity (i.e., discharge). To assess the temporal probability of flooding, equation 8 could be applied, where the discharge represents the intensity i .

$$P_{temporal}(EE_i) = \frac{1}{\text{Return period for } i} \quad (8)$$

3.1.3. Natural Hazards at Regional Level

$P(EE_i)$ may also be found from already existing hazard data. Freely available data sources on natural hazards at the European level compatible with GIS include: flood hazard maps and catalogues, wildfire catalogues, hazard maps related to wind and temperature (heat), landslide hazard maps, earthquake hazard maps and catalogues and rainfall catalogue and forecast analyses. An overview of available inventories, databases and GIS maps of natural hazards at the European level is provided by [80].

Hazard maps for natural events may represent past, current or future hazard situations, where the latter typically would account for climate changes. For projections of future hazard situations or assessment of changes in the hazard situation due to climate change, a time span and representative concentration pathway need to be selected. An overview of effect of climate change on a variety of natural hazards for different time spans and emission scenarios is provided by [11].

3.2. Vulnerability Assessment Example of an Asset-Specific Assessment of a Fragility Curve—A Case of a Bridge Scour in Portugal

In most approaches found in the literature, failure of bridges on shallow foundations is assumed to occur when the predicted local scour depth reaches the foundation base, which has been demonstrated to be a conservative assumption for multiple span RC girder bridges [37] as well as for masonry arch bridges [81]. Consequently, it is important to identify the maximum scour depth and extent (i.e., the geometry of the scour cavity) beneath the foundation level that the soil-bridge structure may withstand before collapse [81,82].

Masonry arch bridges (MAB) have been recognized as particularly vulnerable to local scour due to their rigid behavior and the fact they are often built on shallow footings [83]. In this respect, a fragility analysis of a four-span masonry arch bridge under flood-induced scour was conducted (Figure 5). The bridge considered is located at the Santarém district, Portugal, and presents a total length of approximately 30 m, with arch spans of 4.80 m. The

bridge piers are wall-type sections (1.0×7.0 m) with round-nose shape and 1.85 m height. The pier footings are 1.20 m thick, and 2.55 m length. The foundation soil corresponds to an alluvial deposit that is mostly granular, with coarse sands loosely cohesive, which renders the bridge susceptible to scour.

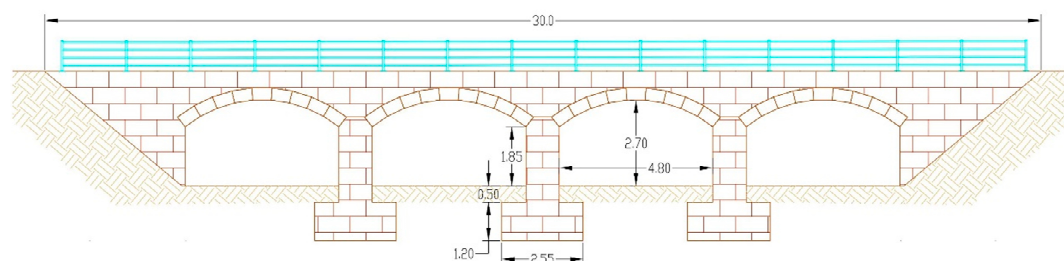


Figure 5. Masonry arch bridge under study (dimensions in meters).

Based on the shape of the local scour cavity at the foundation, MAB can exhibit different failure modes such as fragmentation of piers/abutments, out-of-plane failures, and symmetrical or non-symmetrical in-plane failures [46]. Due to the squat piers in the transversal direction to the flow, an out-of-plane failure mechanism is not expected. Conversely, depending on the inclination of the water flow, a symmetrical or non-symmetrical in-plane failure mechanism can develop. It is assumed for the MAB under analysis that the water flow is aligned to the piers and that the scour is acting at the base of the central pier, while the other piers did not significantly experience this phenomenon.

All random variables associated with the soil-bridge resistance, load effects, and model uncertainties were considered in the analysis. The probability density function (PDF) of peak flow discharges for the waterway where the bridge is located is estimated from flow regionalization curves provided by the Management Plan of the Tagus Hydrographic Region [78]. Since there are no available data to estimate flood hydrographs, a peak flood duration of 48 h is assumed. The Gauckler–Manning–Strickler formula is considered for the hydraulic analysis under the assumption of uniform flow conditions. Probability distributions for the hydraulic parameters, i.e., Manning roughness coefficient and channel slope, are adopted from [84] (Table 5). Based on the hydraulic loads and the soil characteristics on the site, local scour at a bridge pier was investigated as the most probable cause of a failure in a flooding event.

Table 5. Statistical properties of variables.

	Parameters	Mean ¹ [Units]	COV	Distribution	Reference ²
Local scour action	Peak discharge	74.6 [m ³ /s]	0.70	Gumbel	[78]
	Peak flood duration	48 [h]	-	-	Assumed
	Channel width	30 [m]	0.05	Normal	Assumed
	Channel bed slope	0.002 [m/m]	0.10	Normal	Assumed
	Manning roughness coefficient	0.035 [s/m ^{1/3}]	0.015	Lognormal	[84]
Soil properties	Riverbed mean size diameter	20 [mm]	0.1	Lognormal	Assumed
	Scour model error	0.80	0.20	Normal	[84]
	Angle of friction	35 [°]	0.05	Normal	[85]
	Saturated unit weight	19 [kN/m ³]	0.05	Normal	[75]
	Pier width	1.0 [m]	-	-	Assumed
Bridge properties	Masonry unit weight	25 [kN/m ³]	0.05	Normal	[75]
	Masonry compressive strength	3000 [kN/m ²]	0.15	Normal	[86]
	Masonry joints friction coefficient	0.60	0.15	Normal	[86]
	Backfill angle of friction	35 [°]	0.10	Normal	[86]
	Backfill cohesion	30 [kN/m ²]	0.15	Normal	[86]
Computational model uncertainty	Backfill unit weight	17 [kN/m ³]	0.05	Normal	[75]
	Computational model uncertainty factor	1.0	0.15	Normal	[75]

¹ Assumed except as otherwise indicated. ² Regarding to the COV value and the distribution type selection.

The local scour depth was estimated following the FDOT methodology with the Melville-Sheppard (M-S) equation to account for the temporal scour evolution [87]. The epistemic uncertainty associated with the accuracy of the FDOT method to predict scour has been considered through the application of a normally distributed model error with mean value equal to a bias factor and a coefficient of variation (COV) (Table 5), obtained from the ratio of observed scour with predicted scour as suggested by [84].

Discontinuity layout optimization (DLO), which is a numerical limit analysis technique, is used herein to estimate the collapse load of the structure [88]. Masonry units were modelled using a rigid material model, and masonry joints were modelled using a Mohr–Coulomb model with zero cohesion and an angle of friction derived from the coefficient of friction. A Mohr–Coulomb model was also considered for the backfill and the foundation soil, as well as for interface elements used to model the interface between the bridge elements and the soil. All material properties used in the analysis together with the probability distributions selected to describe each variable are shown in Table 5. Masonry units were modelled using a rigid material model, and masonry joints were modelled using a Mohr–Coulomb model with zero cohesion and an angle of friction derived from the coefficient of friction. A Mohr–Coulomb model was also considered for the backfill and the foundation soil, as well as for interface elements used to model the interface between the bridge elements and the soil. The material properties used in the analysis, i.e., masonry compressive strength, unit weights for each material, and internal friction angles, together with the probability distributions selected to describe each variable, are shown in Table 5.

The scour effect was modelled by the removal of soil around and under the foundation, assuming that the scour cavity slope along the direction perpendicular to the flow is equal to $5/6 \cdot \phi$ (soil friction angle,) as proposed by [83]. Figure 6 shows the masonry arch bridge modelled in LimitState:GEO [89] for the no-scour condition (Figure 6a) and for different scour depth configurations, i.e., 1.30 m of scour depth (Figure 6b), and 1.85 m of scour depth leading to soil underneath the pier foundation being eroded (Figure 6c). It should be noted that a symmetrical in-plane failure mode was assumed, as the water flow is aligned with respect to the pier plan orientation (if skewed, the expected failure mode would be non-symmetrical).

The flood discharge, Q , was considered as the intensity measure for the fragility functions. An adequacy factor, which is defined as the factor by which specified loads must be increased in order for the system to reach a collapse state, was obtained in LimitState:GEO by modelling the corresponding loading conditions, i.e., the scour cavity and hydrodynamic pressure for different Q s, namely discharges associated to 5-, 20-, 50-, 100-, 500- and 1000-year floods. The collapse load factors from 150 DLO models generated through Latin Hypercube Sampling were used to define the soil-bridge resistance distribution, R . The load distribution, S , was defined by a curve with a mean value equal to one and a standard deviation of 0.05 since the resistance is quantified as a function of the self-weight [75]. The limit state equation is then defined as $G = R - S = 0$, where the failure of the system takes place for $R < S$ or $G < 0$ [72]. Subsequently, the reliability analysis was performed for each Q using the first-order reliability method (FORM). Finally, the estimation of the parameters of the fragility curve was achieved by performing a generalized linear model (GLM) regression over the set of data points at the selected Q s, to describe the fragility function as a lognormal probability distribution function [90].

The fragility analysis was performed for two different scenarios, one assuming that the equilibrium scour depth is attained for the given discharge and the other considering a time-dependent scour depth given a flood duration of 48 h. The obtained fragility curves are shown in Figure 7. For the former case, the probability of bridge scour leading to failure given a flooding with discharge $300 \text{ m}^3/\text{s}$, i.e., $P(FM | Q = 300 \text{ m}^3/\text{s})$, is equal to 0.043, while for the latter case it corresponds to 0.017. These results highlight that the assumption of attainment of the equilibrium scour which is often made for assessing bridge vulnerability may be overconservative. Thus, it is important to investigate the event durations within

scour fragility analysis. The bridge functionality associated to the damage levels that were analyzed corresponds to 100% loss of service.

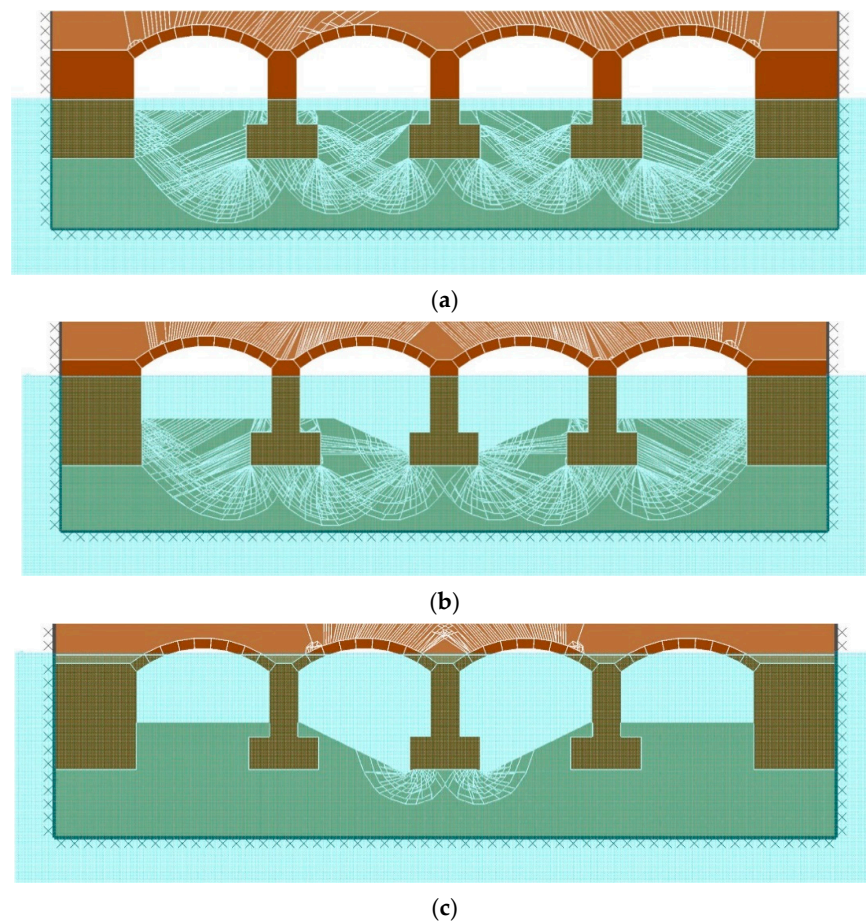


Figure 6. DLO model of the masonry arch bridge in LimitState:GEO [89]: (a) no scour condition, (b) 1.30 m of scour depth, (c) 1.85 m of scour depth.

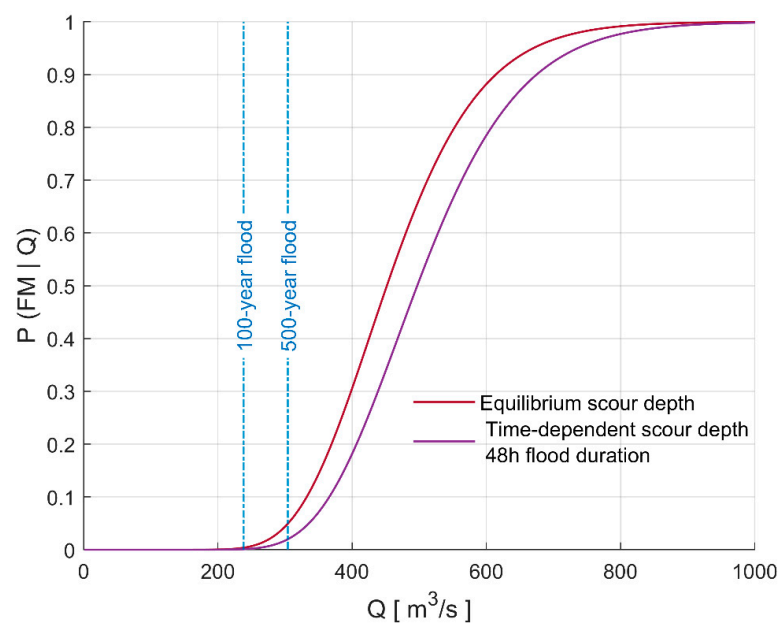


Figure 7. Flood fragility function for the MAB under study.

3.3. Risk Assessment Example: Asset Failure and Related Service Disruption

This section demonstrates assessment of service disruption caused by a structural asset failure for a generic road link, considering flooding of roadway due to exceeded culvert capacity. The context of this analysis could be that the analyzed road link is of high importance for the road network and that the culvert considered is the most critical asset at this road link. The assessment is done following the steps of the risk assessment framework (Figure 2). An overview of data and models needed for the assessment is given in Table 6.

Table 6. Data and models needed for the assessment.

Step in Risk Framework	Data, Models and Considerations Necessary for Defining Events and Assessment of Event Probabilities
Identification of risk scenarios	Selection of analysis object, hazard type and failure modes for this case: The analysis object (asset) is a road link over a culvert, and the hazard to be considered is flooding. The failure modes encompass flooding of roadway leading to different degrees of capacity reductions (from insignificant reductions to full closure). Exceedance of culvert capacity and structural damage to the roadway are also considered as part of the assessment.
Hazard assessment	Data needed for assessment of $P_{temporal}(EE_i)$: flood hazard maps for selected return periods, showing water depth and velocity, i.e., flood intensity values to be applied in the vulnerability assessment.
Exposure	Data needed: flood hazard maps and maps of the road. The road link in study is assumed to be in a flood-prone area. Tool for assessment of $P(FM EE_i)$:
Vulnerability	FM: service disruption of the road: functional vulnerability providing vehicle speed as a function of flood depth of road, adopted from [5]. FM: structural damage of roadway: structural vulnerability relations for roadway/pavement exposed to flooding [56].
Consequence	This example encompasses failure modes represented by several sequences of events leading to different consequences. The severity of the consequences is determined by the degree of capacity reductions (e.g., if the road is only partly closed or the traffic is possible with reduced speed) and the duration of the service disruption. Four consequence severity classes are adopted (Table 7). Only capacity reduction below the demand will represent a failure mode. The demand expresses the transport needs, usually expressed in AADT (annual average daily traffic).

Table 7. Adopted consequence severity classes.

Consequence Severity Class	Description
Very high	Closed road for long duration (weeks–months)
High	Closed road for days or severe capacity reduction for weeks
Moderate	Moderate capacity reductions with limited durations (hours–days)
Low	Insignificant delays or capacity reduction with duration less than a few hours

The assessment is conducted by use of Event Tree Analysis [91]. Event tree analysis (ETA) is a logical modelling technique that shows all possible outcomes resulting from an initiating event, considering further events and factors that affect the performance of the system, e.g., whether installed safety barriers are functioning or not. The analysis considers the sequence of events that could lead to failure by asking “what can happen if?” at every step. ETA may be used for assessing hazard and consequences, assessing probabilities of the outcomes and overall system analysis. It is applicable for qualitative as well as quantitative assessment.

The steps considered in ETA are as follows (if a flooding event occurs):

- What is the return period of the flooding event that may pose a threat?
- Is the culvert capacity exceeded?
- Will flooding of the road cause full service disruption?
- Will flooding cause material damage?
- Is the capacity reduced below demand?

- How severe are the consequences?

Figure 8 illustrates the event tree constructed from the assessment steps above as well as event probabilities (at the branch prior to an event). Each sequence of events will lead to a different consequence in terms of severity and duration of service disruption. The probability of each sequence of events is found by multiplying the probabilities along the branch. The value is shown next to the consequence severity class. The following simplifications are made when assessing the severity of the consequences:

- Very high consequences: A flood depth higher than 30 cm, velocity of the flooding water high enough to cause material damage to the roadway.
- High consequences: A flood depth higher than 30 cm, velocity of the flooding water not high enough to cause material damage to the roadway.
- Moderate consequences: A flood depth less than 30 cm. The capacity of the roadway is reduced to less than the demand.
- Low consequences: A flood depth less than 30 cm. The capacity of the roadway is larger than the demand (including the case where the culvert capacity is not exceeded).

Table 8 indicates which considerations should be done and the reasoning behind the choice of event probabilities in Figure 8.

Table 8. Definition of events and considerations for assessment of event probabilities.

Assessment Steps	Example of Assessment (Explanation of the Choice of Probabilities in the Event Tree in Figure 8)
What is the return period of the flooding event?	The event tree in Figure 8 is for the 60–300-year flooding event (represented by/applying data for the 200-year flooding event, Table 9). $p = 1/60\text{yr} - 1/300\text{yr} = 0.013/\text{yr}$
Is the culvert capacity exceeded?	The culvert is designed for the 200-year flood, but we assume there is a long time since the last inspection and the capacity may have been reduced due to debris deposition, $P(\text{exceeded culvert capacity}) = 0.5$.
Does the flooding cause full service disruption? (Is the flood depth at the roadway above a threshold for full service disruption?)	A threshold of 30 cm is chosen in accordance with the curve from [5], corresponding to full service disruption.
Does the flooding cause material damage? (Is the intensity of the flooding high enough to cause material damage?)	Probability of a flood depth larger than 30 cm could be estimated considering different degrees of culvert capacity reduction. We assume that the critical level of clogging for the circumstances considered in this case occurs in 20% of the cases, i.e., $P(\text{flood depth} > 30 \text{ cm}) = 0.2$.
Is the capacity reduced below demand?	The intensity of the flooding is compared to flood intensity thresholds for structural damage from [56]. We assume that the flooding intensity is close to the threshold and consequently that $P(\text{flood intensity} \geq \text{threshold}) = 0.5$.
What are the consequences?	We assume that application of the functional vulnerability model from [5] indicates that the probability of reducing the capacity below demand is 60% for flood depths below 30 cm. Dependent on the sequence of events, the consequences could be very high, high, moderate or low. The probability of one consequence severity class encompasses the probabilities of all sequences of events leading to that consequence class.

Table 9. Return period classes and flood scenarios used in the assessment.

Return Period Range	Representative Flood Scenario Used in Analyses
<10 years	No loss
10–60 years	50-year
>60–300 years	200-year
>300 years	500-year

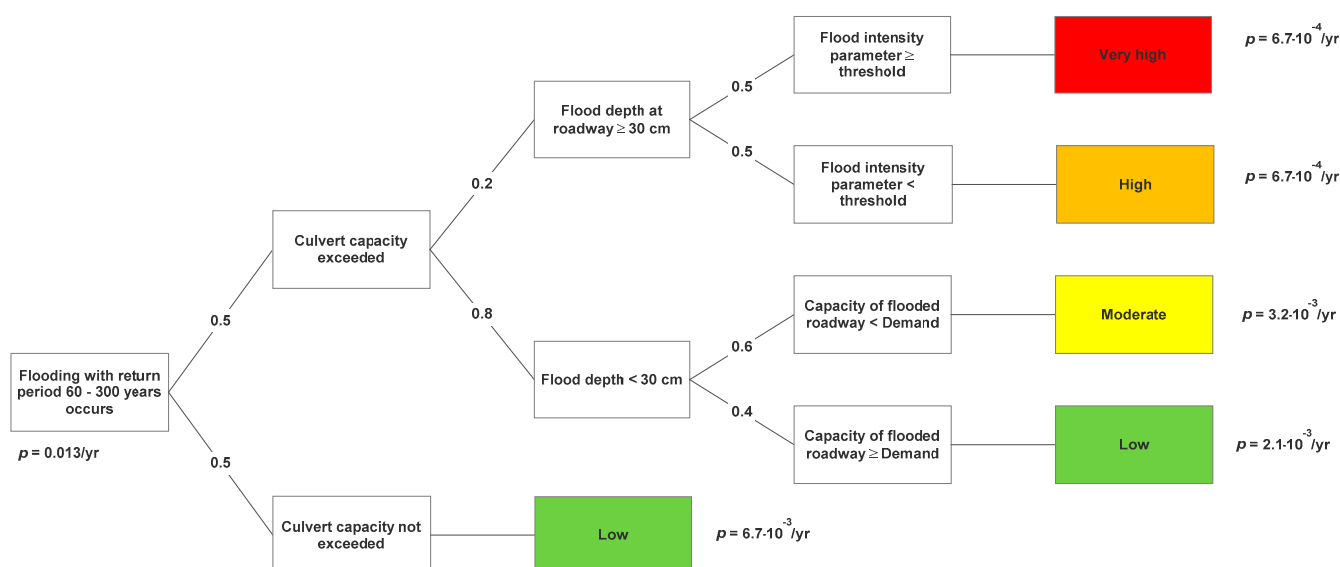


Figure 8. Quantitative assessment of the probability for different consequence classes.

In accordance with Equation (1), the full range of plausible intensities of EE_i should be accounted for and their contributions summed. Table 9 outlines four different flood scenarios to be applied in the assessment, as well as the range of probabilities covered by each scenario.

Figure 8 demonstrates the assessment for the 200-year flood scenario (representing return periods of 60–300 years as indicated in Table 9). The structure in Figure 8 is applied for assessments of the scenarios representing return periods <60 years and higher than 300 years, but with different event probabilities. The summation of the contribution from each of the return period ranges is presented in Table 10. The result of the assessment is that the annual probability is 0.987 for low consequences, $8.1 \cdot 10^{-3}$ for moderate consequences and $2.3 \cdot 10^{-3}$ for high consequences and for very high consequences. The risk can be further quantified by calculating the costs associated with each consequence severity class.

Table 10. Results of risk assessment, based on assessment of all the scenarios.

Consequence Class	Contributions from Each of the Return Period Ranges				Aggregated Probability from All the Assessments
	<10 Years	10–60 Years	60–300 Years	>300 Years	
Low	0.9/yr	0.078/yr	0.0088/yr	0.0006/yr	0.987/yr
Moderate	≈0	0.0045/yr	0.0032/yr	0.0004/yr	$8.1 \cdot 10^{-3}$ /yr
High	≈0	0.0004/yr	0.0007/yr	0.0012/yr	$2.3 \cdot 10^{-3}$ /yr
Very high	≈0	0.0004/yr	0.0007/yr	0.0012/yr	$2.3 \cdot 10^{-3}$ /yr
Sum	0.9/yr	0.083/yr	0.013/yr	0.003/yr	1/yr

The provided example demonstrates analysis of a malfunctioning asset that could lead to a service disruption. In the given example, the duration of the service disruption (i.e., the recovery time) is linked only to the efforts required after an event to return from a malfunctioning infrastructure to normal operation. However, the recovery time depends also on the resourcefulness of the operator, affecting how the situation is managed.

Another simplification in the example is that the severity of the consequences is defined from the severity and duration of the service disruption only. This would be a good approach if there is no redundancy in the transportation infrastructure, i.e., if no diversion roads exist, if possible diversion roads are flooded as well, or if the diversion roads imply a very long detour. If proper diversion roads exist, the severity of the consequences would be lower than in this example and Table 10 would need to be modified.

4. Discussion

The main tasks of infrastructure engineers are to identify the most vulnerable assets in networks with respect to oncoming threats and prioritize maintenance measures and resources accordingly to the available budget. Here, risk-based approaches applied for terrestrial transportation systems aid the decision-making process of planning and implementation of risk mitigation measures and identification of the most cost-effective mitigation measures. Mitigation measures can encompass more robust design of exposed assets, building of protective structures that can reduce hazards intensities (e.g., landslide and flood protection) or measures to reduce consequences of failure(s). On most occasions, the optimal measure is the one that has an effect on mitigation of a predefined failure mode. Here, the fragility functions pertinent to a failure mode need to be elaborated to cover the range of extreme event intensities and the resistance of the investigated asset in cases with and without applied maintenance measure.

Nevertheless, future work is needed to understand the influence of certain assumptions often made for the quantification of risks in transportation systems. The comprehensive evaluation of quantitative risk of infrastructure failures can be complex as well as being computationally expensive. It requires the simulation of different interrelated processes involving epistemic and aleatory uncertainties. The proposed framework and conceptualization of the risk assessment should be extended to incorporate a quantification of the uncertainties associated with each of the risk components. The risk formulations in this paper are expressed using both deterministic and probabilistic quantities. Uncertainties associated with the vulnerability of the exposed assets are included when fragility curves are applied. In addition, the framework should incorporate uncertainties in the spatial extent and intensity of extreme events, as well as uncertainties associated with the direct and indirect consequences. Uncertainties associated with the indirect consequences are mainly aleatory.

The past applied models usually focused on either evaluation of consequences of failures via traffic macrosimulation [64,66] or analyzing scenarios of multiple object failures, e.g., as in [92]. There are not many methodologies that link infrastructure performance to transport network operations, e.g., as in [93]. Consequently, infrastructure owners are reluctant to implement state-of-the-art approaches as the sensible prioritization of investments requires all transportation modes and multiple critical assets to be considered as part of the risk assessment methodology.

Research efforts are needed to link modelling of user's behavior in disrupted transportation systems [69] to spatial and temporal modelling of both hazard and network vulnerability, similarly to [94]. However, as the accuracy of the traffic modelling increases, the computational costs of each simulation increase significantly. For this reason, current risk assessment approaches for transportation networks have limited the analysis to few deterministic scenarios which do not appropriately account for all the uncertainties. Strategies such as importance sampling techniques have been adopted within simulation frameworks aiming to reduce the computational effort [29]. A trade-off between sophisticated models and computational cost is necessary and should depend on results from sensitivity analysis to specify which components of the risk assessment should be analyzed in more detail.

Despite proper risk assessment of the infrastructure, failures and service disruptions may still occur. It is necessary to be prepared for a recovery and to ensure a resilient infrastructure by establishing plans for keeping the functionality of the transportation system under adverse conditions and for a quick restoration of the transportation service after a service disruption induced by an extreme event.

5. Conclusions

This paper aims to bridge the gap between general risk assessment frameworks and specific risk assessments of terrestrial transportation infrastructures by proposing a framework that is flexible enough to accommodate different failure modes, asset types and extreme events. The proposed approach improves the identification of risk scenarios

by providing a comprehensive overview of extreme events and failure modes/modes of malfunctioning. The paper describes and conceptualizes the content of the necessary steps in a quantitative risk assessment of transport infrastructures. The framework is envisioned as a support for practical risk assessment, which is demonstrated through practical examples for assessment of separate risk components. The paper discusses strategies and tools for a quantification of risk components by applying models in literature and using available data sources. Finally, the paper guides and formulates explicitly the integration of the risk components into a risk estimate. The guidance is supported by a risk assessment case study considering flooding of a roadway demonstrating the combination of several assessment steps.

This paper also provides recommendations for the choice of intensity parameters for different extreme events when developing damage, loss and fragility functions. The derivation of a fragility curve for a masonry arch bridge subjected to local foundation scour during river flooding is described in detail as well as all the challenges that were encountered in establishing this curve.

The results from the application of the proposed framework serve as a basic input for a risk-based decision making on preventative maintenance of infrastructure in the face of sudden extreme events. Future work can be directed towards evaluation of competing risk mitigation actions, based on predefined risk acceptance criteria and a cost-benefit analysis, in order to select the optimal maintenance activities on assets in transportation networks.

Author Contributions: Conceptualization, U.E.; software, M.S.; formal analysis, U.E., M.S., N.G., N.T., L.P., R.H.; investigation, N.G.; data curation, N.G.; writing—original draft preparation, U.E., M.S., N.G., N.T., L.P., R.H.; writing—review and editing, U.E., M.S., N.G., N.T., L.P., R.H., F.N., H.S.S., J.M.; visualization, L.P., U.E., M.S., N.G.; supervision, H.S.S., J.M. All authors have read and agreed to the published version of the manuscript.

Funding: The research leading to the results in this paper has received funding from the European Community’s H2020 Program MG-7-1-2017, Resilience to extreme (natural and human-made) events, under Grant Agreement number: 769255—“GIS-based infrastructure management system for optimized response to extreme events of terrestrial transport networks (SAFEWAY)”. The support is gratefully acknowledged.

Institutional Review Board Statement: Not applicable.

Informed Consent Statement: Not applicable.

Data Availability Statement: Not applicable.

Conflicts of Interest: The authors declare no conflict of interest.

Disclaimer: The sole responsibility for the content of this publication lies with the authors. It does not necessarily reflect the opinion of the European Union. Neither the Innovation and Networks Executive Agency (INEA) nor the European Commission are responsible for any use that may be made of the information contained herein.

References

1. Mattsson, L.G.; Jenelius, E. Vulnerability and resilience of transport systems—A discussion of recent research. *Transp. Res. Part A* **2015**, *81*, 16–34. [\[CrossRef\]](#)
2. Hackl, J.; Lam, J.C.; Heitzler, M.; Adey, B.; Hurni, L. Estimating network related risks, A methodology and an application in the transport sector. *Nat. Hazards Earth Syst. Sci.* **2018**, *18*, 2273–2293. [\[CrossRef\]](#)
3. Dobney, K.; Baker, C.J.; Quinn, A.D.; Chapman, L. Quantifying the effects of high summer temperatures due to climate change on buckling and rail related delays in south-east United Kingdom. *Meteorol. Appl.* **2009**, *16*, 245–251. [\[CrossRef\]](#)
4. Kontou, E.; Murray-Tuite, P.; Wernstedt, K. Duration of commute travel changes in the aftermath of Hurricane Sandy using accelerated failure time modeling. *Transport. Res. A Policy Pract.* **2017**, *100*, 170–181. [\[CrossRef\]](#)
5. Pregnotato, M.; Ford, A.; Wilkinson, S.M.; Dawson, R.J. The impact of flooding on road transport, A depth-disruption function. *Transp. Res. Part D* **2017**, *55*, 67–81. [\[CrossRef\]](#)
6. Eidsvig, U.; Kristensen, K.; Vangelsten, B.V. Assessing the risk posed by natural hazards to infrastructures. *Nat. Hazards Earth Syst. Sci.* **2017**, *17*, 481–504. [\[CrossRef\]](#)

7. Lam, J.C.; Adey, B.T.; Heitzler, M.; Hackl, J.; Gehl, P.; van Erp, N.; D'Ayala, D.; van Gelder, P.; Hurni, L. Stress tests for a road network using fragility functions and functional capacity loss functions. *Reliab. Eng. Syst. Saf.* **2018**, *173*, 78–93. [CrossRef]
8. Winter, M.G.; Smith, J.T.; Fotopoulou, S.; Pitolakis, K.; Mavrouli, O.; Corominas, J.; Argyroudis, S. An expert judgement approach to determining the physical vulnerability of roads to debris flow. *Bull. Eng. Geol. Environ.* **2014**, *73*, 291–305. [CrossRef]
9. Oberndorfer, S.; Sander, P.; Fuchs, S. Multi-hazard risk assessment for roads, probabilistic versus deterministic approaches. *Nat. Hazards Earth Syst. Sci.* **2020**, *20*, 3135–3160. [CrossRef]
10. Mitsakis, E.; Stamos, I.; Papanikolaou, A.; Aifadopoulou, G.; Kontoes, H. Assessment of extreme weather events on transport networks, case study of the 2007 wildfires in Peloponnesus. *Nat. Hazards* **2014**, *72*, 87–107. [CrossRef]
11. EEA. *Climate Change, Impacts and Vulnerability in Europe 2016, An Indicator-Based Report*; European Environment Agency (EEA), 2017. Available online: www.eea.europa.eu (accessed on 19 September 2018).
12. WMO; UNISDR. Disaster Risk and Resilience, UN System Task Team on the Post-2015 UN Development Agenda. 2012. Available online: https://www.un.org/en/development/desa/policy/untaskteam_undf/thinkpieces/3_disaster_risk_resilience.pdf (accessed on 6 June 2021).
13. Chen, L.; Wu, H.; Liu, T. Vehicle collision with bridge piers, A state-of the-art review. *Adv. Struct. Eng.* **2021**, *24*, 385–400. [CrossRef]
14. Sha, Y.; Hao, H. Nonlinear finite element analysis of barge collision with a single bridge pier. *Eng. Struct.* **2012**, *41*, 63–76. [CrossRef]
15. Wang, W.; Liu, R.; Wu, B. Analysis of a bridge collapsed by an accidental blast loads. *Eng. Fail. Anal.* **2014**, *36*, 353–361. [CrossRef]
16. Giuliani, L.; Crosti, C.; Gentili, F. Vulnerability of Bridges to Fire. Bridge Maintenance, Safety, Management, Resilience and Sustainability. In Proceedings of the Sixth International Conference on Bridge Maintenance, Safety and Management, Stresa, Lake Maggiore, Italy, 8–12 July 2012.
17. VTT. Extreme Weather Impacts on Transport Systems. VTT Working Papers 168, EWENT Project Deliverable D1. 2011. Available online: <http://www.vtt.fi/publications/index.jsp> (accessed on 20 September 2018).
18. Erath, A.L. Vulnerability Assessment of Road Transport Infrastructure. Ph.D. Thesis, ETH, Zürich, Switzerland, 2011. Available online: www.research-collection.ethz.ch/handle/20.500.11850/153072 (accessed on 30 October 2019).
19. Meyer, V.; Becker, N.; Markantonis, V.; Schwarze, R.; van den Bergh, J.C.J.M.; Bouwer, L.M.; Bubeck, P.; Ciavola, P.; Genovese, E.; Green, C.; et al. Review article, Assessing the costs of natural hazards—state of the art and knowledge gaps. *Nat. Hazards Earth Syst. Sci.* **2013**, *13*, 1351–1373. [CrossRef]
20. Liu, L.; Yang, D.Y.; Frangopol, D.M. Network-level risk-based framework for optimal bridge adaptation management considering scour and climate change. *J. Infrastruct. Syst.* **2020**, *26*, 516. [CrossRef]
21. Santarsiero, G.; Masi, A.; Digrisolo, V.; Picciano, A. The Italian Guidelines on Risk Classification and Management of Bridges, Applications and Remarks on Large Scale Risk Assessments. *Infrastructures* **2021**, *6*, 111. [CrossRef]
22. Pregnotato, M. Bridge safety is not for granted—A novel approach to bridge management. *Eng. Struct.* **2019**, *196*, 35. [CrossRef]
23. Technical Committee ISO/TC 262, Risk Management. In *ISO 31000:2018 Risk Management—Guidelines*; ISO (The International Organization for Standardization): Geneva, Switzerland, 2018. Available online: <https://www.iso.org/standard/65694.html> (accessed on 7 July 2021).
24. Snelder, M.; Calvert, S. Quantifying the impact of adverse weather conditions on road network performance. *Eur. J. Transp. Infrastruct. Res.* **2016**, *1*, 128–149.
25. Düzgün, H.S.B.; Lacasse, S. Vulnerability and Acceptable Risk in Integrated Risk Assessment Framework. In *Landslide Risk Management*; A.A. Balkema Publishers: Vancouver, BC, Canada, 2005.
26. Falermo, S.; Blied, L.; Danielsson, P. *Guideline-Part C, GIS-Aided Vulnerability Assessment for Roads—Existing Methods and New Suggestions*; Roadapt Report; SGI: Linköping, Sweden, 2015.
27. Koks, E.E.; Bockarjova, M.; de Moel, H.; Aerts, J.C.J.H. Integrated Direct and Indirect Flood Risk Modeling, Development and Sensitivity Analysis. *Risk Anal.* **2014**, *35*, 882–900. [CrossRef] [PubMed]
28. Kilanitis, I.; Sextos, A. Integrated seismic risk and resilience assessment of roadway networks in earthquake prone areas. *Bull. Earthq. Eng.* **2019**, *17*, 181–210. [CrossRef]
29. Messore, M.M.; Capacci, L.; Biondini, F. Life-cycle cost-based risk assessment of aging bridge networks. *Struct. Infrastruct. Eng.* **2020**, *17*, 515–533. [CrossRef]
30. Pregnotato, M.; Winter, A.O.; Mascarenas, D.; Sen, A.D.; Bates, P.; Motley, M.R. Assessing flooding impact to riverine bridges, an integrated analysis. *Nat. Hazards Earth Syst. Sci. Discuss.* **2020**. preprint. [CrossRef]
31. Yang, D.Y.; Frangopol, D.M. Physics-based assessment of climate change impact on long-term regional bridge scour risk using hydrologic modeling, Application to Lehigh River watershed. *J. Bridge. Eng.* **2019**, *24*, 13. [CrossRef]
32. Akiyama, M.; Frangopol, D.M.; Ishibashi, H. Toward lifecycle reliability-, risk- and resilience-based design and assessment of bridges and bridge networks under independent and interacting hazards, emphasis on earthquake, tsunami and corrosion. *Struct. Infrastruct. Eng.* **2019**, *16*, 26–50. [CrossRef]
33. Ishibashi, H.; Akiyama, M.; Frangopol, D.M.; Koshimura, S.; Kojima, T.; Nanami, K. Framework for estimating the risk and resilience of road networks with bridges and embankments under both seismic and tsunami hazards. *Struct. Infrastruct. Eng.* **2020**, *17*, 494–514. [CrossRef]

34. Argyroudis, S.A.; Mitoulis, S.A.; Winter, M.G.; Kaynia, A.M. Fragility of transport assets exposed to multiple hazards, State-of-the-art review toward infrastructural resilience. *Reliab. Eng. Syst. Saf.* **2019**, *191*, 22. [CrossRef]
35. Kim, H.; Sim, S.H.; Lee, J.; Lee, Y.J.; Kim, J.M. Flood fragility analysis for bridges with multiple failure modes. *Adv. Mech. Eng.* **2017**, *9*, 1687814017696415. [CrossRef]
36. Lamb, R.; Aspinall, W.; Odbert, H.; Wagener, T. Vulnerability of bridges to scour, insights from an international expert elicitation workshop. *Nat. Hazards Earth Syst. Sci.* **2017**, *17*, 1393–1409. [CrossRef]
37. Tanasic, N. Vulnerability of Reinforced Concrete Bridges Exposed to Local Scour in Bridge Management. Ph.D. Thesis, University of Belgrade, Belgrade, Serbia, 2015.
38. Tsubaki, R.; Bricker, J.D.; Ichii, K.; Kawahara, Y. Development of fragility curves for railway embankment and ballast scour due to overtopping flood flow. *Nat. Hazards Earth. Syst. Sci.* **2016**, *16*, 2455–2472. [CrossRef]
39. McKenna, G.; Argyroudis, S.A.; Winter, M.G.; Mitoulis, S.A. Multiple hazard fragility analysis for granular highway embankments, Moisture ingress and scour. *Transp. Geotech.* **2021**, *26*, 1143. [CrossRef]
40. Gehl, P.; D'Ayala, D. System loss assessment of bridge networks accounting for multi-hazard interactions. *Struct. Infrastruct. Eng.* **2018**, *14*, 1355–1371. [CrossRef]
41. Starossek, U.; Haberland, M. Disproportionate collapse: Terminology and procedures. *J. Perform. Constr. Facil.* **2010**, *24*, 519–528. [CrossRef]
42. Van Westen, C.J.; Castellanos Abella, E.A.; Sekhar, L.K. Spatial data for landslide susceptibility, hazards and vulnerability assessment, an overview. *Eng. Geol.* **2008**, *102*, 112–131. [CrossRef]
43. Nadim, F. *Risk Assessment and Management for Geohazards, Keynote Lecture*, 2nd ed.; Symposium on Geotechnical Safety & Risk; CRC Press/Balkema: Gifu, Japan, 2009; pp. 13–26.
44. Ministerio Para la Transición Ecológica. Available online: <https://www.miteco.gob.es/es/agua/temas/gestion-de-los-riesgos-de-inundacion/mapa-peligrosidad-riesgo-inundacion/> (accessed on 5 April 2019).
45. AASHTO. *LRFD Bridge. Design Specifications*; American Association of State Highway and Transportation Officials (AASHTO): Washington, DC, USA, 2012.
46. Hajdin, R.; Kušar, M.; Mašović, S.; Linneberg, P.; Amado, J.; Tanasić, N. WG3 Technical Report, Establishment of a Quality Control Plan. COST TU 1406. 2018. Available online: https://www.tu1406.eu/wp-content/uploads/2018/09/tu1406_wg3_digital_vf.pdf (accessed on 31 October 2018).
47. Li, Z.; Nadim, F.; Huang, H.; Uzielli, M.; Lacasse, S. Quantitative vulnerability estimation for scenario based landslide hazards. *Landslides* **2010**, *7*, 125–134. [CrossRef]
48. Cardona, O.D.; van Aalst, M.K.; Birkmann, J.; Fordham, M.; McGregor, G.; Perez, R.; Pulwarty, R.S.; Schipper, E.L.F.; Sinh, B.T. Determinants of risk, exposure and vulnerability. In *Managing the Risks of Extreme Events and Disasters to Advance Climate Change Adaptation*. In *A Special Report of Working Groups I and II of the Intergovernmental Panel on Climate Change (IPCC)*; Cambridge University Press: London, UK, 2012; pp. 65–108.
49. Schultz, M.T.; Gouldby, B.P.; Simm, J.D.; Wibowo, J.L. *Beyond the Factor of Safety, Developing Fragility Curves to Characterize System Reliability*; Army Corps of Engineers: Washington, DC, USA, 2010.
50. Schneiderbauer, S.; Calliari, E.; Eidsvig, U.; Hagenlocher, M. The most recent view of vulnerability. In *Science for Disaster Risk Management 2017, Knowing Better and Losing Less*; Publications Office of the European Union: Luxembourg, 2017; pp. 70–84.
51. Chapman, L.; Thornes, J.E.; Huang, Y.; Cai, X.; Sanderson, V.L.; White, S.P. Modelling of rail surface temperatures, a preliminary study. *Theor. Appl. Climatol.* **2008**, *92*, 121–131. [CrossRef]
52. Dobney, K.; Baker, C.J.; Chapman, L.; Quinn, A.D. The future cost to the United Kingdom's railway network of heat-related delays and buckles caused by the predicted increase in high summer temperatures owing to climate change. *Proc. Inst. Mech. Eng. Part F* **2009**, *224*, 25–34. [CrossRef]
53. NetworkRail. *Route Weather Resilience and Climate Change Adaptation Plans, London North. West.*; NetworkRail: London, UK, 2014.
54. Vajda, A.; Tuomenvirta, H.; Juga, I.; Nurmi, P.; Jokinen, P.; Rauhala, J. Severe weather affecting European transport systems, the identification, classification and frequencies of events. *Nat. Hazards* **2014**, *72*, 169–188. [CrossRef]
55. Argyroudis, S.A.; Mitoulis, S.A. Vulnerability of bridges to individual and multiple hazards-floods and earthquakes. *Reliab. Eng. Syst. Saf.* **2010**, *210*, 107564. [CrossRef]
56. ASTRA. *Naturgefahren auf den Nationalstrassen, Risikokonzept. Dokumentation ASTRA 89001, Guidelines*; Swiss Federal Roads Office (Bundesamt für Strassen): Bern, Switzerland, 2012.
57. UNSW. *Vehicle Stability Testing for Flood Flows*; WRL Technical Report 2017/07; Water Research Laboratory, University of New South Wales: New South Wales, Australia, 2017.
58. El-Tawil, S.; Severino, E. Vehicle Collision with Bridge Piers. *J. Bridge. Eng.* **2005**, *10*, 637–640. [CrossRef]
59. Pasha, J.; Dulebenets, M.A.; Abioye, O.F.; Kavoosi, M.; Moses, R.; Sobanjo, J.; Ozguven, E.E. A comprehensive assessment of the existing accident and hazard prediction models for the highway-rail grade crossings in the state of Florida. *Sustainability* **2020**, *12*, 4291. [CrossRef]
60. Alos-Moya, J.; Paya-Zaforteza, I.; Garlock, M.E.M.; Loma-Ossorio, E.; Schiffner, D.; Hospitaler, A. Analysis of a bridge failure due to fire using computational fluid dynamics and finite element models. *Eng. Struct.* **2014**, *68*, 96–110. [CrossRef]
61. Lange, D.; Sjöström, J.; Honfi, D. Losses and Consequences of Large Scale Incidents with Cascading Effects. In *EU FP 7 Project CascEff Modelling of Dependencies and Cascading Effects for Emergency*; CascEff Project: Vienna, Austria, 2015.

62. Martins, L.; Silva, V. Development of a fragility and vulnerability model for global seismic risk analyses. *Bull. Earthq. Eng.* **2020**, *7*, 8851. [\[CrossRef\]](#)
63. Papathoma-Köhle, M.; Kappes, M.; Keiler, M.; Glade, T. Physical vulnerability assessment for alpine hazards, state of the art and future needs. *Nat. Hazards* **2011**, *58*, 645–680. [\[CrossRef\]](#)
64. Erath, A.; Birdsall, J.; Axhausen, K.W.; Hajdin, R. Vulnerability assessment of the Swiss road network. *Transp. Res. Rec.* **2009**, 2137, 118–128. [\[CrossRef\]](#)
65. Pregnotato, M.; Ford, A.; Robson, C.; Glenis, V.; Barr, S.; Dawson, R. Assessing urban strategies for reducing the impacts of extreme weather on infrastructure networks. *R. Soc. Open Sci.* **2016**, *3*, 160023. [\[CrossRef\]](#) [\[PubMed\]](#)
66. Tanasic, N.; Ilic, V.; Hajdin, R. Vulnerability assessment of bridges exposed to scour. *Transp. Res. Rec. J. Transp. Res. Board* **2013**, 2360, 36–44. [\[CrossRef\]](#)
67. Santamaria, M.; Arango, E.; Jafari, F.; Sousa, H. SAFEWAY consortium. In *Dynamic Risk-Based Predictive Models*; SAFEWAY Deliverable 5.1; SAFEWAY Project: Vigo, Spain, 2021.
68. Hoogendoorn, S.; Knoop, V. Traffic flow theory and modelling. In *The Transport System and Transport Policy*; Edward Elgar Publishing: Cheltenham, UK, 2012; pp. 125–159.
69. Nogal, M.; Honfi, D. Assessment of road traffic resilience assuming stochastic user behaviour. *Reliab. Eng. Syst. Saf.* **2019**, *185*, 72–83. [\[CrossRef\]](#)
70. Wardrop, J.G. Some theoretical aspects of road traffic research. *Road Eng. Div. Meet. Road Pap.* **1952**, *36*, 325–378. [\[CrossRef\]](#)
71. Syrkov, A.; Høj, N.P. Bridge failures analysis as a risk mitigating tool. In *IABSE Symposium, Towards a Resilient Built Environment -Risk and Asset*; IABSE: Guimarães, Portugal, 2019; pp. 304–310.
72. Galvão, N.; Matos, J.; Oliveira, D.V. Human Errors induced risk in reinforced concrete bridge engineering. *J. Perform. Constr. Facil.* **2021**, *35*, 4.
73. Proske, D. *Bridge. Collapse Frequencies versus Failure Probabilities*; Springer International Publishing: Cham, Switzerland, 2018.
74. CEN. *EN 1990, Eurocode 0, Basis of Structural Design*; European Committee for Standardization (CEN): Brussels, Belgium, 2002.
75. Joint Committee on Structural Safety. Probabilistic Model. Code—Part. 1, Basis of Design. 2001. Available online: <https://www.jcss-lc.org/jcss-probabilistic-model-code/> (accessed on 3 September 2020).
76. Centre for Ecology and Hydrology. *Flood Estimation Handbook*; Centre for Ecology and Hydrology (Formerly the Institute of Hydrology): Wallingford, UK, 1999.
77. England, J.F.; Cohn, T.A.; Faber, B.A.; Stedinger, J.R.; Thomas, W.O.; Veilleux, A.G.; Kiang, J.E.; Mason, R.R. Guidelines for determining flood flow frequency—Bulletin 17C (ver. 1.1, May 2019). *USA Geol. Surv. Tech. Methods* **2019**, *5*, 148. [\[CrossRef\]](#)
78. Tejo, A.R.H. *Plano de Gestão da Região Hidrográfica do Tejo Relatório Técnico*; Agência Portuguesa do Ambiente (APA): Amadora, Portugal, 2012.
79. Parkes, B.; Demeritt, D. Defining the hundred year flood, A Bayesian approach for using historic data to reduce uncertainty in flood frequency estimates. *J. Hydrol.* **2016**, *540*, 1189–1208. [\[CrossRef\]](#)
80. Eidsvig, U.; Piciullo, L.; Ekseth, K.; Ekeheien, C. SAFEWAY consortium. European critical hazards (natural), GIS Map and identification of hot spots of sudden extreme natural hazard events, including database with impact and return periods. In *SAFEWAY Deliverable D2.1*; SAFEWAY Project: Vigo, Spain, 2019.
81. Zampieri, P.; Zanini, M.A.; Faleschini, F.; Hofer, L.; Pellegrino, C. Failure analysis of masonry arch bridges subject to local pier scour. *Eng. Fail. Anal.* **2017**, *79*, 371–384. [\[CrossRef\]](#)
82. Tanasic, N.; Hajdin, R. Management of RC bridges with shallow foundation exposed to local scour. *J. Struct. Infrastruct. Eng.* **2017**, *14*, 468–476. [\[CrossRef\]](#)
83. Scozzese, F.; Ragni, L.; Tubaldi, E.; Gara, F. Modal properties variation and collapse assessment of masonry arch bridges under scour action. *Eng. Struct.* **2019**, *199*, 109665. [\[CrossRef\]](#)
84. Lagasse, P.F.; Ghosn, M.; Johnson, P.A.; Zevenbergen, L.W.; Clopper, P.E. *Risk-Based Approach for Bridge Scour Prediction*; National Cooperative Highway Research Program Transportation Research Board National Research Council: Washington, DC, USA, 2013.
85. Uzielli, M.; Lacasse, S.; Nadim, F.; Phoon, K.K. Soil variability analysis for geotechnical practice. *Charact. Eng. Prop. Nat. Soils* **2007**, *22*, 1653–1754. [\[CrossRef\]](#)
86. Conde, B.; Matos, J.; Oliveira, D.; Riveiro, B. Probabilistic-based structural assessment of a historic stone arch bridge. *Struct. Infrastruct. Eng.* **2020**, *17*, 379–391. [\[CrossRef\]](#)
87. Sheppard, D.M.; Renna, R. *Bridge. Scour Manual*; State of Florida Department of Transportation: Tallahassee, FL, USA, 2010.
88. Smith, C.; Gilbert, M. Application of discontinuity layout optimization to plane plasticity problems. *Proc. R. Soc. A* **2007**, *463*, 2461–2484. [\[CrossRef\]](#)
89. LimitState. Geotechnical Analysis Software. 2019. Available online: <https://www.limitstate.com/geo> (accessed on 30 January 2021).
90. Ioannou, I.; Rossetto, T.; Grant, D.N. Use of Regression Analysis for the Construction of Empirical Fragility Curves. In *Proceedings of the Fifteenth World Conference on Earthquake Engineering*, Lisbon, Portugal, 24–28 September 2012.
91. ISO. IEC 31010:2019 Risk Management—Risk Assessment Techniques. Technical Committee, ISO/TC 262 Risk Management. 2019. Available online: <https://www.iso.org/standard/72140.html> (accessed on 7 July 2021).

-
92. Adey, B.; Birdsall, J.; Hajdin, R. Methodology to Estimate Risk Related to Road Links, due to Latent Processes. In Proceedings of the 5th International Conference on Bridge Maintenance, Safety and Management IABMAS, Philadelphia, PA, USA, 11–14 July 2010.
 93. Hajdin, R.; Lindenmann, H. Algorithm for the Planning of Optimum Highway Work Zones. *J. Infrastruct. Syst.* **2007**, *13*, 202–214. [[CrossRef](#)]
 94. Pyatkova, K.; Chen, A.S.; Butler, D.; Vojinović, Z.; Djordjević, S. Assessing the knock-on effects of flooding on road transportation. *J. Environ. Manag.* **2019**, *244*, 48–60. [[CrossRef](#)] [[PubMed](#)]